The University of Maine
DigitalCommons@UMaine

Electronic Theses and Dissertations | Fogler Library

5-2006

Dynamics of Forest Structure under Different Silvicultural Regimes in the Acadian Forest

Michael R. Saunders

Follow this and additional works at: http://digitalcommons.library.umaine.edu/etd

 Part of the Forest Biology Commons, and the Forest Management Commons

Recommended Citation

Saunders, Michael R., "Dynamics of Forest Structure under Different Silvicultural Regimes in the Acadian Forest" (2006). *Electronic Theses and Dissertations*. 420.
http://digitalcommons.library.umaine.edu/etd/420

This Open-Access Dissertation is brought to you for free and open access by DigitalCommons@UMaine. It has been accepted for inclusion in Electronic Theses and Dissertations by an authorized administrator of DigitalCommons@UMaine.

DYNAMICS OF FOREST STRUCTURE UNDER DIFFERENT SILVICULTURAL REGIMES IN THE ACADIAN FOREST

By

Michael R. Saunders

B.S. Iowa State University, 1994

B.S. Iowa State University, 1994

M.S. University of Minnesota, 1998

A THESIS

Submitted in Partial Fulfillment of the

Requirements of the Degree of

Doctor of Philosophy

(in Forest Resources)

The Graduate School

University of Maine

May 2006

Advisory Committee:

Robert G. Wagner, Henry A. Saunders Distiguished Professor in Forestry, Advisor

Robert S. Seymour, Curtis Hutchins Professor of Forest Resources

Malcolm L. Hunter, Jr., Libra Professor of Conservation Biology

Jeremy A. Wilson, Irving Chair for Forest Ecosystem Management

John C. Brissette, Research Forester and Project Leader, Northeastern Research Station, USDA Forest Service

DYNAMICS OF FOREST STRUCTURE UNDER DIFFERENT SILVICULTURAL REGIMES IN THE ACADIAN FOREST

By

Michael R. Saunders

B.S. Iowa State University, 1994

B.S. Iowa State University, 1994

M.S. University of Minnesota, 1998

A THESIS

Submitted in Partial Fulfillment of the

Requirements of the Degree of

Doctor of Philosophy

(in Forest Resources)

The Graduate School

University of Maine

May 2006

Advisory Committee:

Robert G. Wagner, Henry A. Saunders Distiguished Professor in Forestry, Advisor

Robert S. Seymour, Curtis Hutchins Professor of Forest Resources

Malcolm L. Hunter, Jr., Libra Professor of Conservation Biology

Jeremy A. Wilson, Irving Chair for Forest Ecosystem Management

John C. Brissette, Research Forester and Project Leader, Northeastern Research Station, USDA Forest Service

LIBRARY RIGHTS STATEMENT

In presenting this thesis in partial fulfillment of the requirements for an advanced degree at The University of Maine, I agree that the Library shall make it freely available for inspection. I further agree that permission for "fair use" copying of this thesis for scholarly purposes may be granted by the Librarian. It is understood that any copying or publication of this thesis for financial gain shall not be allowed without my written permission.

Signature:

Date:

DYNAMICS OF FOREST STRUCTURE UNDER DIFFERENT SILVICULTURAL REGIMES IN THE ACADIAN FOREST

By Michael R. Saunders

Thesis Advisor: Dr. Robert G. Wagner

An Abstract of the Thesis Presented
in Partial Fulfillment of the Requirements for the
Degree of Doctor of Philosophy
(in Forest Resources)
May, 2006

Research plots in many long-term studies of forest ecosystems often cannot be used for spatial modeling because of their small scale and nested inventory design. This has been unfortunate as these plots represent some of the best records of structural development as affected by forest management. I developed methodologies to reconstruct both tree height growth and spatial pattern in these types of plots from historical inventory records and stem-mapped data, and then retrospectively investigated 3-dimensional structural development as affected by five silvicultural and harvesting treatments (unmanaged natural area, commercial clearcut, fixed-diameter limit, 5-year selection, and 3-stage shelterwood— with and without precommercial thinning) in a long-term, USDA Forest Service study in Bradley, ME. In order to capture site variation and account for the hierarchical inventory design, mixed-effects, nonlinear height-diameter models were developed for the nine most common tree species in 50 stem-mapped plots: *Abies balsamea* (L.) Mill., *Acer rubrum* L., *Betula papyrifera* Marsh., *B. populifolia* Marsh., *Picea rubens* Sarg., *P. mariana* (Mill.) B.S.P., *Pinus strobus* L.,

Populus tremuloides Michx., and *Tsuga canadensis* (L.) Carr. Height-diameter models for the remaining species were fit with generalized nonlinear least squares. A morphing algorithmn was developed and then tested on both simulated and actual point patterns, to scale the spatial pattern from nested, sapling subplots (0.020 ha) to the scale of the larger tree plots (0.081 ha). Differences in spatial pattern, species mingling, height differentiation, and relative stand complexity index (*rSCI*) were compared among treatments. Regeneration events, whether induced through natural stand breakup or by harvesting, increased aggregation in spatial pattern and reduced species mingling. This pattern was heightened when treatments shifted species composition more towards hardwood species. Variation in height differentiation and *rSCI* was generally highest in the natural areas and 5-year selection compartments, intermediate in commercial clearcut and fixed diameter-limit compartments, and lowest in 3-stage shelterwood compartments. Divergence in spatial structure between the two natural areas reflects natural stand development within this forest and is an appropriate benchmark for management. The reconstruction model developed here can be applied to other long-term studies where the lengthy temporal scale can substitute for small spatial scale.

DYNAMICS OF FOREST STRUCTURE UNDER DIFFERENT SILVICULTURAL REGIMES IN THE ACADIAN FOREST

By Michael R. Saunders

Thesis Advisor: Dr. Robert G. Wagner

An Abstract of the Thesis Presented
in Partial Fulfillment of the Requirements for the
Degree of Doctor of Philosophy
(in Forest Resources)
May, 2006

Research plots in many long-term studies of forest ecosystems often cannot be used for spatial modeling because of their small scale and nested inventory design. This has been unfortunate as these plots represent some of the best records of structural development as affected by forest management. I developed methodologies to reconstruct both tree height growth and spatial pattern in these types of plots from historical inventory records and stem-mapped data, and then retrospectively investigated 3-dimensional structural development as affected by five silvicultural and harvesting treatments (unmanaged natural area, commercial clearcut, fixed-diameter limit, 5-year selection, and 3-stage shelterwood— with and without precommercial thinning) in a long-term, USDA Forest Service study in Bradley, ME. In order to capture site variation and account for the hierarchical inventory design, mixed-effects, nonlinear height-diameter models were developed for the nine most common tree species in 50 stem-mapped plots: *Abies balsamea* (L.) Mill., *Acer rubrum* L., *Betula papyrifera* Marsh., *B. populifolia* Marsh., *Picea rubens* Sarg., *P. mariana* (Mill.) B.S.P., *Pinus strobus* L.,

Populus tremuloides Michx., and *Tsuga canadensis* (L.) Carr. Height-diameter models for the remaining species were fit with generalized nonlinear least squares. A morphing algorithmn was developed and then tested on both simulated and actual point patterns, to scale the spatial pattern from nested, sapling subplots (0.020 ha) to the scale of the larger tree plots (0.081 ha). Differences in spatial pattern, species mingling, height differentiation, and relative stand complexity index (*rSCI*) were compared among treatments. Regeneration events, whether induced through natural stand breakup or by harvesting, increased aggregation in spatial pattern and reduced species mingling. This pattern was heightened when treatments shifted species composition more towards hardwood species. Variation in height differentiation and *rSCI* was generally highest in the natural areas and 5-year selection compartments, intermediate in commercial clearcut and fixed diameter-limit compartments, and lowest in 3-stage shelterwood compartments. Divergence in spatial structure between the two natural areas reflects natural stand development within this forest and is an appropriate benchmark for management. The reconstruction model developed here can be applied to other long-term studies where the lengthy temporal scale can substitute for small spatial scale.

DYNAMICS OF FOREST STRUCTURE UNDER DIFFERENT SILVICULTURAL REGIMES IN THE ACADIAN FOREST

By Michael R. Saunders

Thesis Advisor: Dr. Robert G. Wagner

An Abstract of the Thesis Presented
in Partial Fulfillment of the Requirements for the
Degree of Doctor of Philosophy
(in Forest Resources)
May, 2006

Research plots in many long-term studies of forest ecosystems often cannot be used for spatial modeling because of their small scale and nested inventory design. This has been unfortunate as these plots represent some of the best records of structural development as affected by forest management. I developed methodologies to reconstruct both tree height growth and spatial pattern in these types of plots from historical inventory records and stem-mapped data, and then retrospectively investigated 3-dimensional structural development as affected by five silvicultural and harvesting treatments (unmanaged natural area, commercial clearcut, fixed-diameter limit, 5-year selection, and 3-stage shelterwood— with and without precommercial thinning) in a long-term, USDA Forest Service study in Bradley, ME. In order to capture site variation and account for the hierarchical inventory design, mixed-effects, nonlinear height-diameter models were developed for the nine most common tree species in 50 stem-mapped plots: *Abies balsamea* (L.) Mill., *Acer rubrum* L., *Betula papyrifera* Marsh., *B. populifolia* Marsh., *Picea rubens* Sarg., *P. mariana* (Mill.) B.S.P., *Pinus strobus* L.,

Populus tremuloides Michx., and *Tsuga canadensis* (L.) Carr. Height-diameter models for the remaining species were fit with generalized nonlinear least squares. A morphing algorithmn was developed and then tested on both simulated and actual point patterns, to scale the spatial pattern from nested, sapling subplots (0.020 ha) to the scale of the larger tree plots (0.081 ha). Differences in spatial pattern, species mingling, height differentiation, and relative stand complexity index (*rSCI*) were compared among treatments. Regeneration events, whether induced through natural stand breakup or by harvesting, increased aggregation in spatial pattern and reduced species mingling. This pattern was heightened when treatments shifted species composition more towards hardwood species. Variation in height differentiation and *rSCI* was generally highest in the natural areas and 5-year selection compartments, intermediate in commercial clearcut and fixed diameter-limit compartments, and lowest in 3-stage shelterwood compartments. Divergence in spatial structure between the two natural areas reflects natural stand development within this forest and is an appropriate benchmark for management. The reconstruction model developed here can be applied to other long-term studies where the lengthy temporal scale can substitute for small spatial scale.

DEDICATION

D and Zy:

To the two most important girls in my life, you will always have my gratitude and love.

ACKNOWLEDGEMENTS

I would like to first thank my advisor, Dr. Robert Wagner, for help in honing my research skills and mentoring me throughout my residency here at the University of Maine. I also would like to thank my committee members, Drs. John Brissette, Malcolm Hunter, Jr., Robert Seymour, Jeremy Wilson and the late Raymond O'Connor for their reviews and guidance. Lastly, I would like to again thank John Brissette and the USDA Forest Service at the Penobscot Experimental Forest, Rick Dionne and Tim Stone, for use of field sites and access to their long-term datasets.

Without Spencer Meyer, Sally Gilbert, Jennifer Becker, Matt Labelle, Blanka Peridot, Matt Pettengill, Dan Rosso, and Maggie Burke, I never would have gotten all the data collection done. Without Darci Schofield, Keith Kanoti and Matt Olson, I would have never gotten to see my family as I tried to juggle this dissertation and my FERP duties. Without Micah Pace, I may have drowned in or gotten run over by another boat in my rookie year of the Keneduskeg Stream Race. And without Dena and Zylee, I would not have had smiling faces to come home to.

For those I have not listed, thank you. I think almost everyone in Nutting Hall helped me in one way or the other through the last few years.

This work was supported by the Maine Agricultural and Forest Research Station at the University of Maine (MAFES # 2795) and USDA National Research Initiative (Project # ME0-2000-0700).

...and I didn't fiddle with the numbers either.

Dave Struble

TABLE OF CONTENTS

LIST OF TABLES

LIST OF FIGURES

PROLOGUE

Forest structure is a broadly defined term, relating to the physical arrangement, intermixing and composition, and size distribution of trees and other components within a stand. Forest structure is fundamentally linked to ecological function and processes which both affect and react to forest structure (McElhinney et al. 2005). For example, the spatial arrangement of forest canopies affects both seed rain and understory light, interception which in turn influences the germination and subsequent growth rates of tree regeneration that ultimately determines future forest composition. Increased amounts of forest structure generally increase the array of habitats and niches available, thereby increasing the alpha biodiversity of the stand (MacArthur and MacArthur 1961, Willson 1974, Kimmins 1997, Brokaw and Lent 1999, Lähde et al. 1999, Zenner 2005). Lastly, forest structure is often an indication of the history of a stand, either through management and cutting practices (Montes et al. 2005, Stamatellos and Panourgias 2005) or natural disturbance events like fire (Fúle and Covington 1998).

Forest management affects forest structure by manipulating its components through silvicultural activities to achieve goals determined by the land manager or owner. Silvicultural practices have often simplified forest structure, turning relatively complex and highly variable natural structures into more uniform structures (O'Hara and Gersonde 2004), with a goal of providing a sustainable wood supply (Hawley and Hawes 1925, Smith 1962). This approach has often been based on the false assumption that these managed structures mimic those created by the natural disturbances (Lindenmayer and Franklin 2002). Even-aged silvicultural methods have been modeled after large-scale, stand-replacing disturbance events, but often ignore differences in the spatial and

temporal variability of stand structure between harvested and naturally disturbed forests (Seymour and Hunter 1999, Seymour et al. 2002). These methods also may not provide sufficient amounts of deadwood that are common after most stand-replacing disturbances and essential to ecological function (McComb and Lindenmayer 1999). Uneven-aged selection systems, that are touted as maintaining a high level of structural diversity compared to even-aged systems, are for most part quite artificial (O'Hara 2001) and rarely explicitly retain decadent trees, snags or logs (Lindenmayer and Franklin 2002), or replicate the more irregular aged-structures that are commonly found in remaining old-growth stands within the Northeast and elsewhere (Fraver and White 2005, Kenefic et al. 2005b). Many of these concerns have lead to the development of "close-to-nature" or "disturbance-based" silvicultural systems that try to more closely link silvicultural prescriptions to natural disturbance regimes and structures within a given region (Schütz 1999, Seymour and Hunter 1999, Saunders and Wagner 2005, Keeton 2005).

The structural dynamics (i.e., the changes in forest structure over time) of unmanaged stands have commonly been used as references or benchmarks for determining the success of forest management activities (Solomon and Gove 1999). In unmanaged, even-aged, single-species stands, structural dynamics can be relatively straightforward; stands progress through predictable developmental stages (e.g., stand initiation, stem exclusion, stand re-initiation and old growth phases, sensu Oliver and Larson [1996]) that are akin to the structural development of the stand. For example, regardless of the structural variables used, forest structure usually remains relatively "low" in these forests until the stand re-initiation phase of development. In stands other than even-aged, single-species, structural development can be exceedingly complex. For

example, even-aged stands with several species of varying growth rates can form even-aged stratified mixtures that, by its structural features, appear "uneven-aged" in appearance (Toumey 1928, Smith 1962). In contrast, uneven-aged stands containing a mixture of intermediate and shade tolerant tree species can appear quite "even-aged" in its structural characteristics during certain times of its development (pers. observation). Watt (1947) suggested that natural, nearly pure, all-aged beech forests operated as a mosaic of uneven-sized, single-aged patches that were temporally asynchronous; this work was the foundation of the gap-phase dynamics model for structural development in uneven-aged stands (Picket and White 1985, Barnes et al. 1998, Gratzer et al. 2002). Regardless, dynamics of structural development in more complex stand structures can appear almost "chaotic" in that future states are inherently sensitive to the initial conditions (e.g., tree densities, tree age structure, species composition, and spatial patterns) and the timing and strength of processes that operate across different scales (e.g., interspecific competition vs. natural disturbance patterns).

These perceptions have led some researchers to abandon the patch- or gap-based models of forest dynamics in complex stands, and develop spatially explicit individual tree-based models of structural development. Advances in spatial ecology allow researchers to focus on neighborhood interactions among trees, explicitly quantifying how the competitive influences among individuals change with distance and tree size, and then incorporate these effects into stand development models (Pacala et al. 1996). However, significant challenges still remain in parameterizing these models and using them to investigate forest dynamics. These challenges include (Gratzer et al. 2004): 1) describing vegetative development and spatial structures across a range of forest types; 2)

identifying relevant ecological processes that generate these structures; and 3) understanding the consequences of the generated structures for community dynamics. Empirical studies of spatial pattern and process, and development and parameterization of these spatially-explicit models are integral parts of any research effort into forest stand dynamics (Gratzer et al. 2004).

However, there are challenges to obtaining the data necessary to quantify spatial relationships and parameterizing spatially explicit models. Three approaches have been used (Gratzer et al. 2002, Montes et al. 2005): chronosequences, retrospective studies and permanent sample plots.. Chronosequences, or temporary plots used to sample several forest developmental stages, have been used to access the changes in structure due to management (e.g., Zenner 2004), but they require similar sites and stand histories that often differ significantly among sampled stands. Retrospective studies use a variety of historical evidence (e.g., photos, land-use records, pollen analysis, dendrochonological reconstructions) to describe development (e.g., Montes et al. 2005), but do not necessarily lend themselves to causal descriptions of changes in pattern from an ecological process. Permanent sample plots are, by far, the most desirable for two reasons. First, the process can be directly measured through repeated samples, e.g., rates of colonization can be estimated from seed trap collections. Second, permanent plots are the only reliable method to validate model results (Gratzer et al. 2004). Unfortunately, few spatially explicit plots exist that are sufficiently large (> 0.1 ha) and span more than 20 years (e.g., Peterson and Squiers 1995). Instead, most permanent plots are associated with forest growth and yield inventory systems (e.g., USDA Forest Service's Forest Inventory and Analysis plots) which are often too small and measure different

subpopulations of trees at different scales. As a result, the use of growth and yield plots for spatial structural analysis of forest structure; research to adapt spatial statistical analyses to these plots is needed since growth and yield plots offer some of the longest-running, spatially explicit datasets available.

The work presented in this thesis reconstructs and models the spatially explicit structure of stands that were manipulated by five silvicultural and harvesting treatments using a longitudinal dataset from the USDA Forest Service study at the Penobscot Experimental Forest (PEF) in Bradley, ME. I had two objectives. First, I developed methodology to overcome the limitations of growth and yield inventories in spatial analyses; methodology that should be useful for both calibrating and validating spatially explicit, individual-tree models with growth and yield plot data and for visualizing structural development. The long-term dataset from these sites were typical of most growth-and-yield inventory designs, using small-scale (<0.1 ha), nested plot arrays to estimate changes in forest structure using such parameters as changes in basal area, diameter distributions and species composition. Height data were lacking and different subpopulations of trees were sampled on different sized plots, making straightforward analysis of spatial pattern using established methodology difficult, if not impossible. Second, I compared spatial parameters over time among the five silvicultural and harvesting treatments to access the effects of management on the structural development of forest stands. This work should be useful to managers in determining which silvicultural systems come closest to emulating natural structural development in the Northeast.

This thesis is divided into three main chapters and a concluding epilogue. Chapter 1 outlines the development of mixed-effect, height-diameter models for nine tree species, using allometric data collected from 6,146 trees (between 136 and 2,615 trees per species) across 50 plots within 10 structurally diverse management compartments on the PEF. This approach allows estimates of past tree height to be calibrated to specific compartments and plots, thereby reducing potential irregularities in the reconstruction model. Chapter 2 introduces and tests, using both computer simulation and application to real data, a technique called "morphing" which can be used to scale up the spatial pattern in nested subplots to that of the larger sample plot. Chapter 3 describes the development of the reconstruction model using the results and techniques from Chapters 1 and 2. Chapter 43 then summarizes the changes in spatial pattern, species mingling (i.e., intermixing), height differentiation, and stand complexity index (SCI; Zenner and Hibbs 2000) over time across the ten management compartments treated by one of five silvicultural and harvesting treatments (unmanaged natural area, commercial clearcut, fixed-diameter limit, 5-year selection, and 3-stage shelterwood— with and without precommercial thinning).

Chapter 1

ALLOMETRIC RELATIONSHIPS FOR TREE SPECIES OF CENTRAL MAINE: HEIGHT-DIAMETER MODELS WITH RANDOM COEFFICIENTS AND SITE VARIABLES

1.1. ABSTRACT

Height-diameter models were developed for nine common northeastern tree species: *Abies balsamea* (L.) Mill., *Acer rubrum* L., *Betula papyrifera* Marsh., *B. populifolia* Marsh., *Picea rubens* Sarg., *P. mariana* (Mill.) B.S.P., *Pinus strobus* L., *Populus tremuloides* Michx., and *Tsuga canadensis* (L.) Carr. Data were collected from 6,146 trees (between 136 and 2,615 trees per species) on 50 plots within 10 structurally diverse stands created by a long-term silviculture study at the Penobscot Experimental Forest in central Maine. Models were fitted using both generalized nonlinear least squares (GNLS) and multi-level, mixed-effects approaches. Site variables (tree density and plot basal area) were included in mixed-effects models to help account for variability in the random coefficients. While a mixed-effects approach was superior to a GNLS approach, the inclusion of site covariates in the mixed-effect model led to significant, but not large improvements in model fit for each species. Analysis of the plot-level parameter estimates suggested that differences in stand structure (even-aged vs. uneven-aged silvicultural practices) had significant influences on the height-diameter relationship. Calibration of these models to other stands should include a number of trees across the range of size classes, not just the largest or dominant trees in a stand as other studies have suggested.

1.2. INTRODUCTION

The allometric relationship between tree diameter and total tree height is commonly used to estimate tree volume and thus is a fundamental component of many growth and yield, functional, and forest planning models (Meyer 1940, Yuancai and Parresol 2001). This relationship is highly site-dependent and not constant over time, even in the same stand (Curtis 1967). Traditionally, height-diameter models had to be developed specific to very localized regions, site fertility classes, and/or structural stand types (e.g., even-aged plantations), or include site and regional parameters that defined these variables within the model itself (e.g, Ek et al. 1984). Furthermore, height-diameter models were often sensitive to forest management practices that changed competitive relationships among neighboring trees (Fang et al. 2001, Daggett 2003). These limitations required foresters and researchers to develop site-specific diameter-height models, rather than using broader, regional models that were far less accurate or precise.

Earlier modeling efforts focused only on describing the mean parameter values of the height-diameter relationship and centered on functional model forms that were both biologically meaningful and statistically flexible (Curtis 1967, Huang et al. 1992, Fang and Bailey 1998, Peng et al. 2001). Recently, focus has shifted towards understanding the variability in parameter estimates over the spectrum of stand conditions. Although other techniques have been used, most current modeling efforts have used mixed-effects models that simultaneously include both fixed coefficients to explain population-wide average response and random coefficients that explain variability in the response in a given sampling unit (e.g., study, stand, or plot; Pinheiro and Bates 2000, Calama and Montero 2004).

Mixed-effects models offer several benefits over ordinary linear (OLS), generalized nonlinear least squares (GNLS), and other approaches. First and foremost, mixed-effect models can incorporate the hierarchical structure of data collection in analysis and reduce interdependence among measurements from the same sample unit by specifically defining a covariance matrix among random parameters within and among sampling levels (Calama and Montero 2004, Demidenko 2004). This approach can reduce dependence on site-index curves for growth and yield modeling (Lappi and Bailey 1988, Hall and Bailey 2001). Second, mixed-effect models are statistically efficient. Mixed-effects models are compromises between OLS and GNLS models that ignore sample unit variability and fully parameterized models that fit each sample unit separately (Pinheiro and Bates 2000). For example, a nonlinear model with three parameters estimated over 20 stands would have 3 x 20 = 60 parameters when fully-parameterized, while a single-level, nonlinear mixed-effects model would have 9 – 15 parameters, depending on the structure of the covariance matrix and assuming all three fixed parameters each had an associated random parameter. Third, because the variation in the parameter estimates is known at each level of the hierarchical sampling structure, mixed-effect models provide unbiased estimation of model parameters for sample units with very small sample sizes. Lastly, mixed-effects models can be calibrated for new, unsampled plots or stands quickly and effectively (Mehtätalo 2004), particularly if values of the random parameters can be predicted from covariates. Some height-diameter mixed-effects models can be calibrated with as few as 4-10 tree heights per sample unit with minimal introduction of bias (Calama and Montero 2004, Lynch et al. 2005).

The NE-TWIGS variant of the individual-tree growth model Forest Vegetation Simulator (FVS; Bush 1995) includes one of few height-diameter models for the northeast region. While accurate enough for some species and regions, height estimates from NE-TWIGS have been largely imprecise when applied to mixed-conifer stands in northern New England, often requiring the development of site-specific functions (i.e., Daggett 2003). This has occurred for two related reasons. First, NE-TWIGS uses a Chapman-Richards model that is largely unadapted from Ek et al.'s (1981, 1984) study of Lake States species; geographical differences in stand history, silvicultural treatment and soil properties between the Lake States and the Northeast likely change the allometric relationship between height and diameter. Second, the NE-TWIGS model includes site index and basal area as covariates. These adjustments give the function additional adaptability, but can make it difficult to apply to the mixed species, uneven-aged stands—that are common to this region—where site indices cannot be determined by traditional approaches. Mixed-effects modeling may be an alternative approach since site differences would be captured by the random parameters.

Therefore, this study develops height-diameter models for nine tree species found throughout northern New England using both GNLS and mixed-effects modeling approaches. Equations were developed for balsam fir (*Abies balsamea* (L.) Mill.), red (*Picea rubens* Sarg.) and black spruce (*P. mariana* (Mill.) B.S.P.), eastern hemlock (*Tsuga canadensis* (L.) Carr.), eastern white pine (*Pinus strobus* L.), red maple (*Acer rubrum* L.), gray (*Betula populifolia* Marsh.) and paper birch (*B. papyrifera* Marsh.), and quaking aspen(*Populus tremuloides* Michx.). Data came from a nested plot design that included highly variable structural stand conditions that were created by different

silvicultural treatments. I hypothesized that: 1) models fit with random coefficients would outperform those fit only with fixed coefficients; 2) height-diameter relationships would differ by silvicultural treatment, and 3) additional plot-level covariants, specifically tree density or plot basal area, would further improve model fits and simplify model structure by explaining the variability that was captured by the random coefficients in the original model.

1.3. METHODS

1.3.1. Study Area and Field Measurements

The data used in this study came from the Penobscot Experimental Forest near the town of Bradley, Maine (44° 52' N, 68° 38' W). This 1,550 ha area lies on soil types derived from glacial till and ranging from well-drained loams and sandy loams on glacial till ridges to poorly and very poorly drained loams and silt loams in flat areas between the ridges (Brissette 1996, Brissette et al. 1999, Brissette and Kenefic 2000). Cover types are dominated by Acadian Region softwoods including red, white (*P. glauca* (Moench) Voss) and black spruce, balsam fir, eastern white pine, eastern hemlock, and northern white cedar (*Thuja occidentalis* L.). Common hardwoods in these types include red maple, paper and gray birch, and quaking and bigtooth aspen (*P. grandidentata* Michx.). Natural stand structures in this region are typically uneven-aged and diverse with windstorms and insect epidemics as the major disturbance events. Stand replacing fires are thought to occur less than once per 1,000 years in these types (Lorimer 1977).

The dataset was obtained from measurements on a subset of long-term plots established in 1952 by the USDA Forest Service (USFS) to monitor the effects of five silvicultural and three exploitative harvest systems on stand growth, yield, and structure

within the Acadian Forest region. Beginning in June 2001 and continuing through August 2002, 7,938 trees were measured and stem-mapped on 50 plots of the study—10 plots each in unregulated commercial clearcut (CC), fixed diameter limit (DL), 5-year selection (5S), 3-stage shelterwood (SW), both with and without spacing treatments, and unharvested natural area control treatments (NA). Marking prescriptions and harvesting techniques and timings for each treatment are described extensively in Sendak et al. (2003). Plots were nested with all trees >11.45 cm (4.5 in) diameter at breast height (DBH) measured within a 0.081 ha (0.20 ac) plot and trees >1.27 cm DBH (0.5 in) measured on a smaller, interior 0.020 ha (0.05 ac) plot. Heights were measured to the nearest 0.1 m either directly, using 10 and 15 m telescoping height poles, or as an average of 2-4 readings from a Haglöf hypsometer (Haglöf 2002).

With the full dataset, basal area and density were calculated for each plot (Figure 1.1). The dataset was then trimmed of all cull, dying and leaning trees. Of the 26 species recorded, only 9 species—balsam fir, red maple, paper and gray birch, red and black spruce, white pine, trembling aspen, and eastern hemlock—occurred in high numbers ($n > 100$) and across a majority of the stands and plots. Red and black spruce hybridize extensively within the PEF and were grouped together for this analysis. Summary statistics for each species are given in Table 1.1.

1.3.2. Statistical Analysis

Several nonlinear functional forms have been used to model height-diameter relationships (Huang et al. 1992, Peng et al. 2001). Although other mixed-modeling efforts have used functional forms that could be linearized and/or exponential (Calama and Montero 2004, Mehtätalo 2004, Nanos et al. 2004), sigmoid models are more

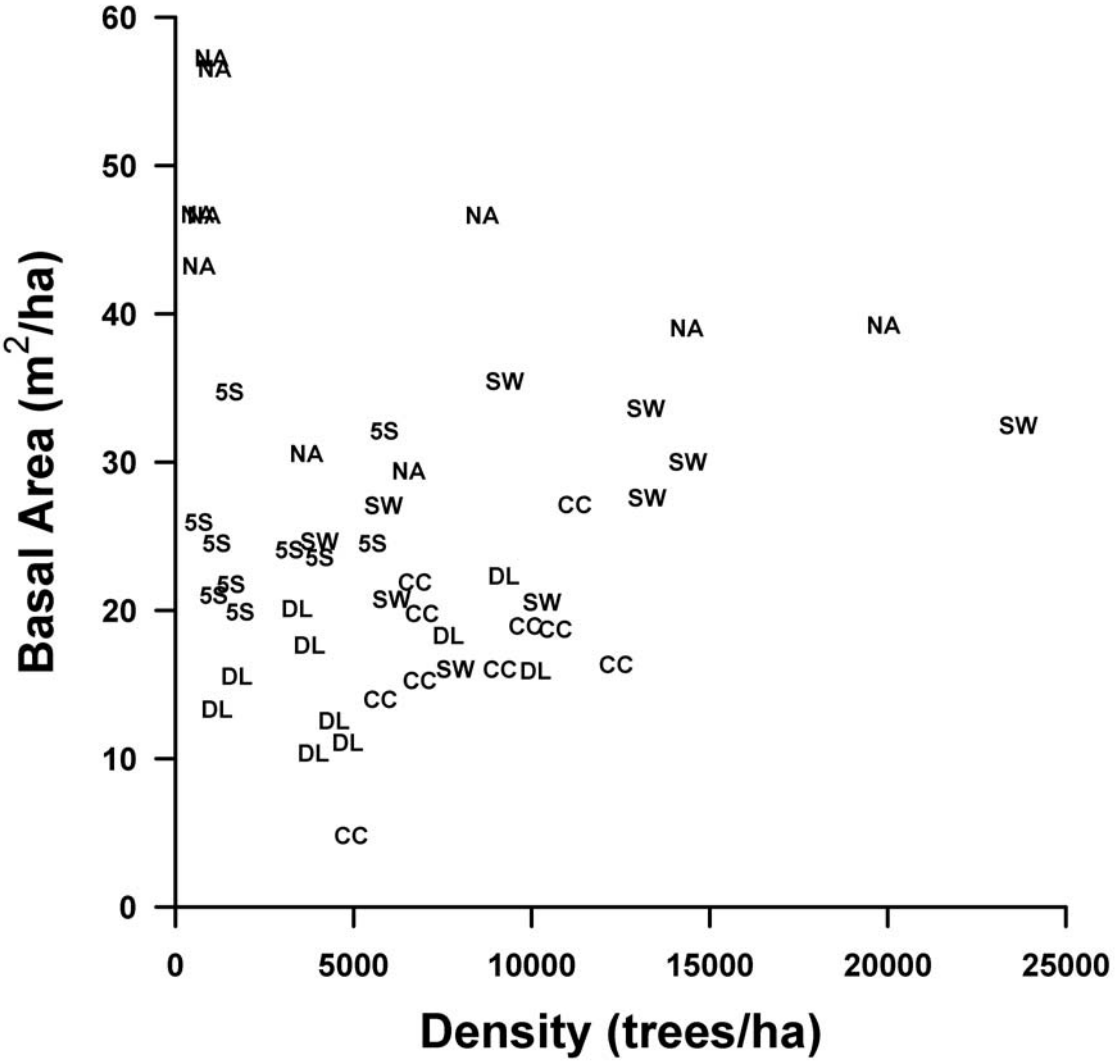

Figure 1.1. Density and basal area distribution of sample plots as they vary by silvicultural treatment (NA = unharvested natural area control, CC = unregulated commercial clearcut, DL = fixed diameter limit, 5S = 5-year selection system, and SW = 3-stage shelterwood).

Table 1.1. Summary statistics of the diameter at breast height (DBH) and height of trees by species. Total sample size (N), the number of stands and plots that the species was observed in is also given.

Species	N	Stands	Plots	DBH (cm)			Height (m)		
				Mean	S.D.	Range	Mean	S.D.	Range
Balsam fir	2615	10	47	5.7	4.9	1.3 – 29.2	5.35	3.34	1.65 – 20.25
Red & black spruce	1415	10	43	7.1	6.9	1.3 – 47.2	6.05	4.00	1.70 – 27.00
Eastern hemlock	831	10	41	12.0	12.5	1.3 – 67.8	8.55	6.46	1.98 – 27.90
Eastern white pine	181	10	26	21.8	19.2	1.4 – 81.5	13.32	9.44	2.26 – 33.73
Red maple	547	10	45	9.1	8.2	1.3 – 43.5	9.50	5.42	2.01 – 24.65
Gray birch	238	6	21	4.4	2.3	1.3 – 13.0	6.82	2.31	2.06 – 12.22
Paper birch	183	9	29	5.8	6.0	1.3 – 30.1	6.91	4.25	2.37 – 23.70
Quaking aspen	136	6	15	9.3	8.8	1.3 – 45.4	10.16	4.38	2.80 – 24.50

biologically appropriate for height-diameter relationships (Yuancai and Parresol 2001). In a preliminary study using weighted OLS, fits of the data with a 3-parameter form of the Chapman-Richards function (Richards 1959) were slightly better and converged more often than 3-parameter Weibull (Weibull 1951), modified logistic (Ratowsky and Reedy 1986), or exponential (Ratowsky 1983) functions. In this study, the Chapman-Richards function was parameterized as (here after referred to as Model I):

$$HT = 1.35 + a_0\left[1 - \mathrm{e}^{(b_0 \cdot DBH)}\right]^{c_0} + \varepsilon \qquad [1.1]$$

where HT is tree height (m), DBH is tree diameter at breast height (cm), a_0, b_0, and c_0 are estimated, fixed (population-wide) parameters, and $\varepsilon \sim N(0, \phi)$. In a multi-level, mixed-effects model, random coefficients can be assigned to each parameter at each level (stand and plot in this study), and have a complex variance-covariance structure that varies

among parameters and levels. However, as Hall and Bailey (2001) suggest, this complexity can lead to nonidentifiability and ill-conditioning, with convergence becoming computationally intensive and difficult. Trial analyses with random coefficients at both stand and plot levels for all three fixed parameters only converged with large sample sizes (n > 1000). In these runs, random coefficients for b_0 and c_0 were highly correlated, therefore I simplified the full random model to (Model II):

$$HT = 1.35 + \left(a_0 + \upsilon_S + \upsilon_P\right)\left[1 - \mathrm{e}^{\left(b_0 \cdot DBH\right)}\right]^{\left(c_0 + \omega_S + \omega_P\right)} + \varepsilon \qquad [1.2]$$

where υ_S, υ_P, ω_S and ω_P are random coefficients at the stand (S) and plot (P) levels for a_0 and c_0, respectively, and b_0 was not allowed to vary randomly. I also found that complex variance-covariance structures prevented convergence when sample sizes were less than 500, so I simplified the variance-covariance structure to assume that the random coefficients were independent at each level or:

$$\Psi_S = \begin{pmatrix} \sigma^2_{\upsilon_S} & 0 \\ 0 & \sigma^2_{\omega_S} \end{pmatrix} \text{ and } \Psi_P = \begin{pmatrix} \sigma^2_{\upsilon_P} & 0 \\ 0 & \sigma^2_{\omega_P} \end{pmatrix}$$

where:

$$\begin{pmatrix} \upsilon_S \\ \omega_S \end{pmatrix} \sim N\left(0, \phi\Psi_S\right), \begin{pmatrix} \upsilon_P \\ \omega_P \end{pmatrix} \sim N\left(0, \phi\Psi_P\right), \ \varepsilon \sim N\left(0, \phi\right). \qquad [1.3]$$

These simplifications in model structure are not ideal as it limits the flexibility of the random model to capture variability and interdependence among residuals at each level; however, I wanted to maintain parallelism in analyses among the species within this study.

The next phase in developing a mixed-effect model is determining whether covariates can help explain or potentially eliminate random coefficients from a model

(Pinero and Bates 2000, Nanos et al. 2004). I tested the inclusion of the natural logarithm of plot-level tree density (ln[trees/ha]; Model III) and total basal area (m^2/ha; Model IV) as fixed parameters to help explain variability. These two covariates were chosen because they could be reliably calculated from the historical records for the USFS study and have been found to be correlated with height growth (Ek et al. 1984, Zhang et al. 1997). Other authors have suggested dominant height and/or some index of the dispersion of the diameter or height distribution as potential covariates (Fang and Bailey 1998, Calama and Montero 2004), but it is not clear if these covariates have been applied when the data source is obtained from a mix of normally distributed, even-aged and non-normally distributed, two- or uneven-aged stands. The original fixed parameters a_0, b_0 and c_0 where assumed to depend linearly on the covariates (*COV*). The model form was:

$$HT = 1.35 + \left(a_0 + a_1 \cdot COV + \upsilon_S + \upsilon_P\right)\left[1 - \mathrm{e}^{-(b_0 + b_1 \cdot COV)\cdot DBH}\right]^{(c_0 + c_1 \cdot COV + \omega_S + \omega_P)} + \varepsilon \qquad [1.4]$$

where a_1, b_1 and c_1 are estimated parameters for the covariate, and with a variance-covariance structure identical to Model II [1.3]. I tested the inclusion of an interaction term between tree density and basal area, but the interaction was not significant ($p > 0.05$) for many of the species and often caused the model to not converge, often due to the high correlation between density and basal area (Figure 1.1).

Model I was fit with generalized nonlinear least-squares (the *gnls* function) and Models II-IV were fit with pseudo-likelihood approach for nonlinear mixed-effect models (the *nlme* function) within the *nlme* package for the R programming language (Pinheiro et al. 2005, R Development Team 2005). Details on the algorithms can be found in Pinheiro and Bates (2000, Chapters 5 and 7). Heteroscedasticity was commonly observed in the plot-level residuals for all models during initial runs. Therefore, I used

the *varPower* function to weight the variance of the residuals by a power of the diameter or:

$$Var(\varepsilon_{ijk}) = \sigma^2 \left| DBH_{ijk} \right|^{2\Delta} \quad [1.5]$$

where DBH_{ijk} are the i tree diameters in plot j of stand k, and Δ is the power of the variance covariate.

Models were simplified by removing terms stepwise and assessing significance of the parameter (fixed or random) by likelihood ratio tests between the original and reduced models. Models were compared using both the Akaike Information Criterion (AIC) and Bayesian Information Criterion (BIC), a conservative approach suggested by Kuha (2004). These two criteria differ only slightly in computation, but have different properties for model selection with BIC imposing a greater penalty for additional parameters than AIC. They were calculated as (Pinheiro and Bates 2000):

$$AIC = -2\text{logLik} + 2n_{par}$$

$$BIC = -2\text{logLik} + n_{par}\log(N) \quad [1.6]$$

where n_{par} is the number of parameters used to fit the model and N is sample size. For both criterion, the smaller the value of either AIC or BIC, the better the model fit the data.

1.4. RESULTS

Without exception, the mixed-effects modeling approach (Model II) outperformed a generalized least squares approach (Model I; Table 1.2). There were large and significant ($p \ll 0.001$) improvements in both AIC and BIC for all species by including random coefficients in the model. An example of the difference in fits between the two

Table 1.2. Weighting power (Δ), model parameters, variance components for the random effects, residual mean squared error (φ), and fit statistics for the four models described in the text. All parameters are significant at $\alpha = 0.05$ unless noted by "n.s." Fit statistics include the Akaike Information Criterion (AIC), the Baysian Criterion (BIC), and the log-likelihood (LL).

Species	Model	Δ	Fixed Effects					
			a_0	a_1	b_0	b_1	c_0	c_1
Balsam fir	I	1.13	14.05	-	0.105	-	1.438	-
	II	1.03	13.27	-	0.114	-	1.527	-
	III	1.02	25.76	-1.45	0.115	n.s.	3.187	-0.190
	IV	1.04	9.96	0.13	0.114	n.s.	1.522	n.s.
Red & black spruce	I	1.23	23.13	-	0.038	-	1.038	-
	II	0.86	15.99	-	0.094	-	1.465	-
	III	0.89	35.00	-2.25	-0.093	0.023	1.480	n.s.
	IV	0.88	16.35	n.s.	0.042	0.002	1.077	0.015
Eastern hemlock	I	0.58	30.11	-	0.025	-	0.941	-
	II	0.63	22.04	-	0.032	-	0.899	-
	III	0.65	42.22	-2.73	0.038	n.s	1.657	-0.088
	IV	0.61	25.41	n.s.	0.009	0.001	0.692	0.009
Eastern white pine*	I	-**	39.97	-	0.026	-	1.312	-
	II	0.98	21.56	-	0.030	-	0.741	-
	III	0.96	20.97	n.s.	0.087	-0.006	0.746	-
Red Maple	I	0.92	24.16	-	0.049	-	0.935	-
	II	0.61	17.17	-	0.094	-	1.016	-
	III	0.61	27.48	-1.24	0.096	n.s.	1.025	n.s.
	IV	0.61	10.02	0.26	0.136	-0.001	1.057	n.s.
Gray birch	I	0.58	10.16	-	0.276	-	1.514	-
	II	0.63	9.04	-	0.287	-	1.463	-
	III	0.65	30.58	-2.33	-0.998	0.140	1.417	n.s.
	IV	0.61	14.91	-0.22	0.065	0.010	1.227	n.s.
Paper birch	I	1.03	23.21	-	0.049	-	0.917	-
	II	0.61	14.91	-	0.126	-	1.048	-
	III	0.68	15.18	n.s.	0.125	n.s.	2.760	-0.190
	IV	0.63	9.76	0.19	0.125	n.s.	1.178	-0.007
Quaking aspen	I	0.65	19.87	-	0.079	-	0.994	-
	II	0.66	18.03	-	0.076	-	0.957	-
	III	0.73	14.77	n.s.	1.142	-0.109	8.191	0.752
	IV	0.65	6.46	0.31	0.394	-0.009	2.441	-0.044

* Model IV was not significant.

** Model would not converge with variance weighting by varPower().

Table 1.2. Continued.

Species	Model	Random Effects				φ	Fit Statistics		
		σ_{ν_S}	σ_{ν_P}	σ_{ϖ_S}	σ_{ϖ_P}		AIC	BIC	LL
Balsam fir	I	-	-	-	-	0.1191	5277	5307	-2634
	II	1.721	0.112	0.992	0.114	0.1163	4562	4615	-2272
	III	1.250	n.s.	0.809	0.106	0.1185	4524	4584	-2253
	IV	0.898	0.106	0.954	0.108	0.1155	4551	4611	-2266
Red & black spruce	I	-	-	-	-	0.1080	3471	3497	-1731
	II	3.927	0.221	0.795	0.053	0.1531	2863	2910	-1422
	III	3.921	0.211	0.585	0.061	0.1455	2834	2891	-1405
	IV	3.263	0.220	0.412	0.049	0.1494	2850	2908	-1414
Eastern hemlock	I	-	-	-	-	0.1005	2488	2512	-1239
	II	3.829	0.079	1.665	0.020	0.1291	2266	2309	-1124
	III	2.193	0.068	1.723	n.s.	0.1281	2253	2300	-1116
	IV	n.s.	0.187	1.730	n.s.	0.1284	2243	2286	-1113
Eastern white pine*	I	-	-	-	-	2.8363	896	909	-444
	II	8.663	0.233	0.564	n.s.	0.0999	614	639	-299
	III	7.948	0.235	n.s.	n.s.	0.1044	606	632	-295
Red maple	I	-	-	-	-	0.1860	1830	1852	-910
	II	2.708	0.090	1.260	n.s.	0.2767	1662	1696	-823
	III	2.112	0.085	1.217	n.s.	0.2752	1658	1697	-820
	IV	1.543	0.072	1.176	n.s.	0.2762	1644	1687	-816
Gray birch	I	-	-	-	-	0.2570	603	620	-296
	II	1.172	0.250	0.548	n.s.	0.2115	555	583	-269
	III	0.857	0.113	0.474	n.s.	0.2039	544	578	-262
	IV	0.886	n.s.	n.s.	0.091	0.2232	550	581	-266
Paper birch	I	-	-	-	-	0.1322	464	480	-227
	II	3.037	0.075	1.302	n.s.	0.1904	395	420	-189
	III	3.085	0.083	0.992	n.s.	0.1673	389	418	-186
	IV	1.899	n.s.	1.020	n.s.	0.1832	379	408	-180
Quaking aspen	I	-	-	-	-	0.3266	484	499	-237
	II	2.569	0.116	n.s.	n.s.	0.2389	434	455	-210
	III	2.971	n.s.	n.s.	n.s.	0.2007	433	456	-209
	IV	2.750	n.s.	n.s.	n.s.	0.2323	426	453	-204

approaches is shown for red and black spruce in Figure 1.2. Visually, Model II did a much better job at fitting the data specific to each stand, even when there were very few data points (e.g., the commercial clearcut stands in Figure 1.2). Furthermore, Model II captured a far wider range of behavior in the height-diameter relationship than Model I. Model II was, however, sensitive to a restricted data range within any given plot or stand (e.g., the shelterwood stands in Figure 1.2). This is common problem for many sigmoid functional forms of the height-diameter relationship, regardless of the fitting procedure, and perhaps a reason why some exponential forms continue to be used. Therefore, calibration of Model II to any other stand should capture a broad range of tree sizes observed, and not just a few of the largest trees (but see Calama and Montero 2004). Both stand and plot level random coefficients were significant for many of the species, although the random effects associated with the "shape" of the height-diameter relationship (i.e., the c_0 parameter and associated σ_{ϖ_S} and σ_{ϖ_P} variance components) were less commonly found to be significant, particularly for hardwood species. Not surprisingly, the variance components associated with the stand-level random effects (σ_{ν_S} and σ_{ϖ_S}) were several times greater than those associated with the plot-level random effects (σ_{ν_P} and σ_{ϖ_P}). Some of this increased variability was clearly caused by restricted data ranges associated with the silvicultural treatments, but some of the variability may indicate differences among sites in quality. However, when I fit models including a site quality covariate that was derived from soil drainage classes of the mapped soil profiles of the PEF (Briggs 1994, Briggs and Lemin 1994), site quality was not significant for any species.

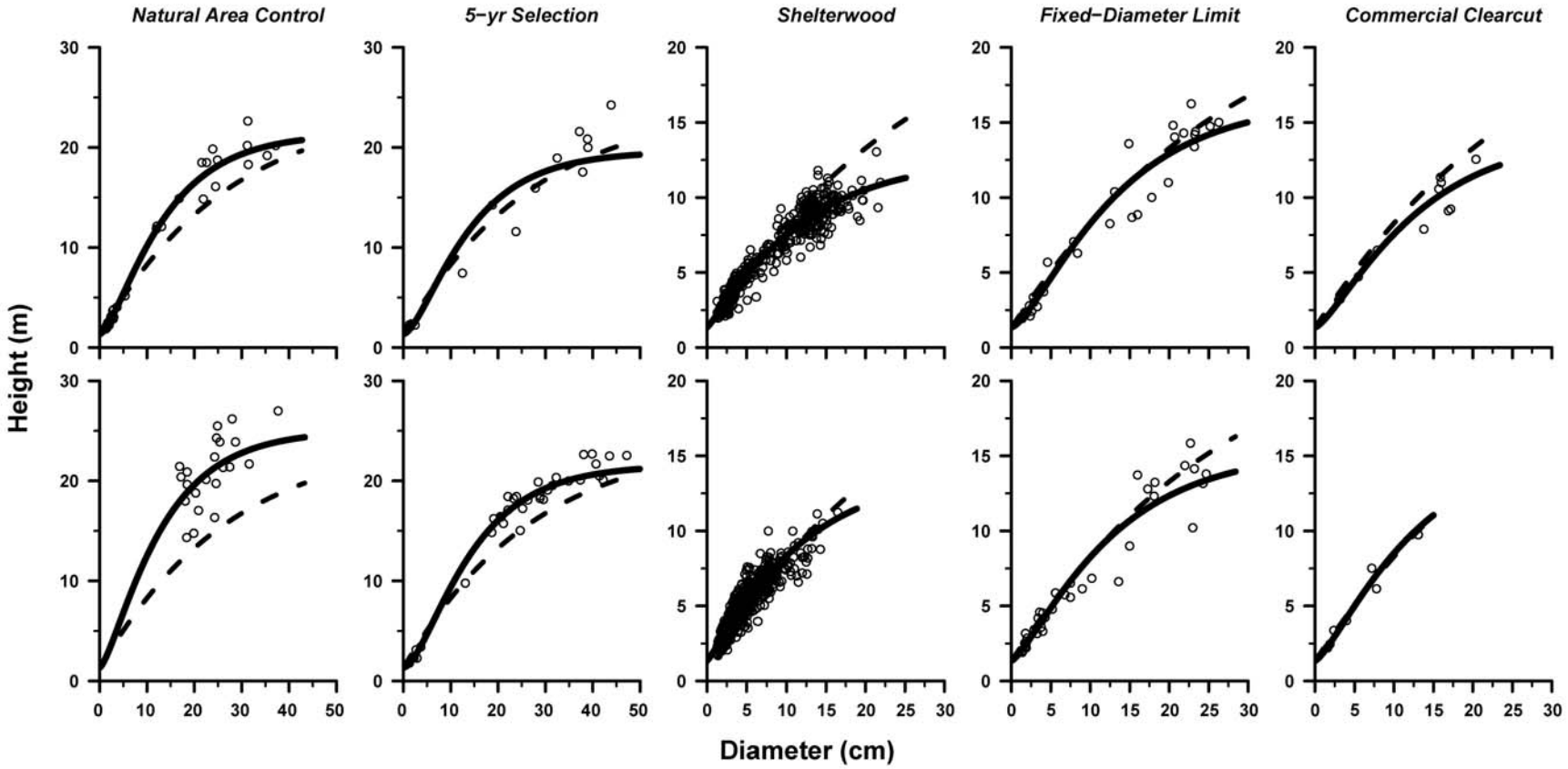

Figure 1.2. Mixed-effect models (solid line) and a population-wide general least squares model (dashed line) for the relationship between height and diameter at breast height for red and black spruce as measured across the two replicates (top and bottom rows) of each of the five treatments. These fits include only the stand-level random coefficients within Model II.

Therefore, the broad differences in structure and competitive conditions among the stands could be driving the height-diameter relationships for most species. A graph of the estimated plot-level coefficients of Model II suggests that plots with uneven-aged structures (i.e., NA and 5S) occupy different areas of parameter space than plots with even-aged (i.e., SW) or highly irregular (i.e., CC and DL) structures (Figure 1.3). For conifers and red maple, the height models have both higher asymptotes (the *a* parameter) more sigmoid shapes (the *c* parameter) in uneven-aged structures than other structures. Eastern white pine, in particular, showed a very strong difference in the height-diameter relationships between uneven-aged structures and the shelterwood treatment; this difference may be driven by slower height growth from attacks by white-pine weevil (*Pissodes strobi* Peck.) which are more prevalent in open stands (Wilkinson 1983). For early-successional hardwoods, there is no discernable pattern in the coefficients. Unfortunately small sample sizes, site differences, and the restricted diameter distributions within individual sample units confound statistical tests for specific silvicultural treatment effects on the height-diameter relationship (Figure 1.2). It would likely require a longitudinal data set across many more plots within these stands to conclusively test for a treatment effect.

Addition of density (Model III) and basal area (Model IV) plot-level covariates to the mixed-model significantly improved model fits for all species (Table 1.2). However, improvements were not dramatic and the additional covariate generally only partially described the variation captured by random coefficients in Model II. Model III was superior to Model IV for only three species—balsam fir, red and black spruce, and grey birch. With some obvious exceptions, increasing plot density within Model III negatively

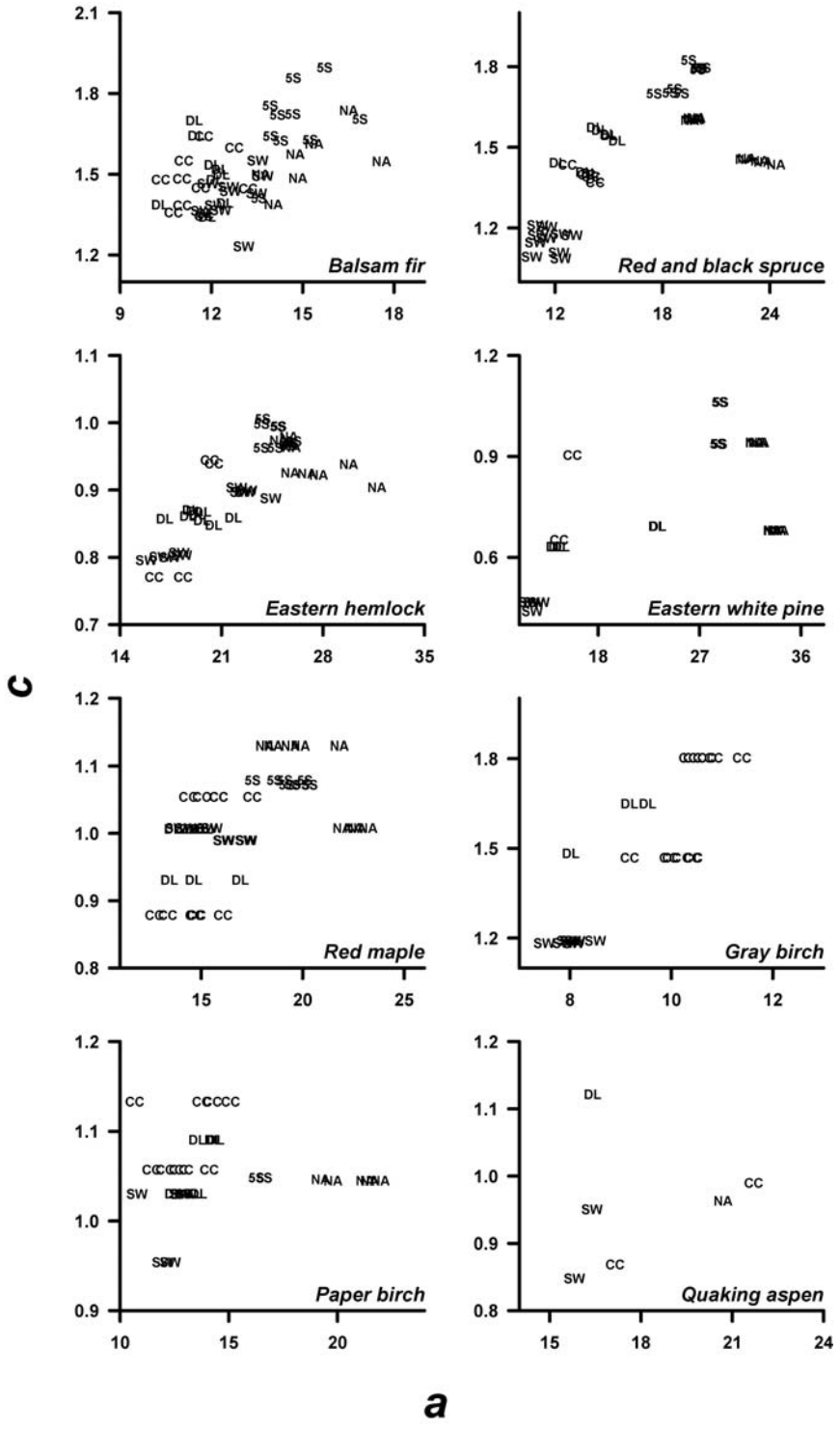

Figure 1.3. Comparison of plot-level estimates of *a* and *c* parameters from Model II as they vary by silvicultural treatment (CC = unregulated commercial clearcut, DL = fixed diameter limit, 5S = 5-year selection system, SW = 3-stage shelterwood, and NA = unharvested natural area control) for nine tree species.

adjusted inflated base parameters (a_0, b_0, and c_0) for most covariate parameters (a_1, b_1, and c_1) that were significant (Table 1.2). Basal area effects were not as prevalent or consistent in Model IV, although for five of the species a_1 was a positive adjustment to a reduced estimated asymptote (a_0) from Model II. Lastly, both Models III and IV were sensitive to the range of the covariate used for species with smaller sample sizes. For example, Model IV for quaking aspen gave realistical heights only within a diameter range of approximately 2-30 cm and a basal area range of approximately 20-40 m^2/ha.

1.5. DISCUSSION

Within this study, a mixed-effects approach to modeling the height-diameter relationship was superior to a GNLS approach using only fixed effects. While it can be argued that the increased complexity of a mixed model is unnecessary given the small gain in precision, these gains in precision multiply rapidly when calculating average plot or stand volumes (Bragg 2001). Furthermore, although GNLS models are not biased across the entire dataset, accuracy often will diminish at stand- or plot-levels if the model is not parameterized to include covariates specific to describe variation at all levels. For example, Model I in this study consistently underestimated red and black spruce height within both natural area controls (Figure 1.2). Mixed-effects models avoid this behavior by incorporating that stand- and plot-level variability into the model form (Lappi and Bailey 1988, Hall and Bailey 2001) and then using covariates to explain the variability captured by the random effects (Pinheiro and Bates 2000).

A mixed-effects approach is also attractive when stand- and plot-level covariates are not always obvious (Nanos et al. 2004). Both tree density and basal area were obvious plot-level covariates that influence the height-diameter relationship (Parresol

1992, Zhang et al. 1997, Daggett 2003). For example, this study generally agrees with Ek et al. (1984) who found that total tree height increased with basal area (Table 1.2). However, other potential covariates were not apparent, particularly since the dataset was collected from mixed-species stands that included a broad array of structural types. For example, dominant height, although obviously correlated with site quality by Eichorn's rule (Assmann 1970) and used in a mixed-effects model by Calama and Montero (2004), was not used as a covariate in this study because canopy position is a function of both growth potential and a cumulated history of suppression by older cohorts in multiaged stands (Oliver and Larsen 1996). Spatially explicit indices of plot structure (e.g., Clark-Evans statistic [Clark and Evans 1954]) could prove useful as covariates in modeling height-diameter relationships from multi-aged stands.

However, this study also highlights the more intense data requirements of mixed-effects approaches to modeling height-diameter relationships. First, multi-level, mixed-effects models with more than two random parameters and/or with complex variance-covariance structures may have difficulty converging unless sample sizes are quite large and well dispersed among all sampling units and sampling levels. Most published mixed-effects models have used fitting datasets of >1000 trees, with at least 10-20 trees within the intermost sampling unit (Calama and Montero 2004). Longitudinal models are commonly fit with fewer trees per sampling unit, but the multiple measurements per tree increase the sample size considerably (Lappi and Bailey 1988, Lappi and Malinen 1994). During trial fits in this study, only balsam fir was numerous enough and distributed broadly enough across sample units (Table 1.1) for a more complicated version of Model

II, with all three parameters as random and an unrestricted variance-covariance matrix, to converge.

Second, a mixed-effects modeling approach can be quite sensitive to the range of tree sizes used to develop the model. This same concern is apparent when modeling with OLS or GNLS approaches, but for the mixed-effect approach, the concern should be considerable since the ranges of data in each individual sample unit can influence the variance components associated with each random effect. In this study, young even-aged stands had quite different parameter estimates than uneven-aged stands (Figure 1.2 and 1.3) suggesting that some type of structural covariate should be included as a fixed effect in any broader modeling effort. Choice of a different functional model form may help reduce this sensitivity.

Although the models in this study were developed primarily for descriptive purposes, they can be calibrated to new stands quite easily using the methods of Lappi (1991). As suggested earlier, calibration data for these models should include a broader range of diameters and more individuals than that recommended by Calama and Montero (2004). The broader range of stand ages and structural classes used within this study should give these models wider applicability than many other height-diameter models used for tree species in the Northeast.

Chapter 2

APPLICATION OF MORPHING TO COMMON FOREST INVENTORY PLOTS FOR SPATIAL POINT PATTERN ANALYSIS

2.1. ABSTRACT

Spatial analyses of trees within forest inventory plots have often been avoided due to small plot sizes, and nested or clustered plot design. Instead, most studies of spatial relationships among tree stems have relied on a single, large (≥0.5 ha) plot. This disparity has been unfortunate as forest inventory plots provide some of the longest-running, repeatedly measured, spatially explicit datasets. I assessed Williams et al.'s (2001, 2003) morphing algorithm as a tool for spatial analysis of forest inventory plots. Two simulation experiments were used to test the sensitivity of the Clark-Evans (CE) nearest neighbor index and the $\hat{L}(d)$ function, a transformation of Ripley's $\hat{K}(d)$, to the effects of morphing used as either an edge-correction technique or scaling tool. Specifically, population-level estimates were compared to sample plot-level estimates, both with and without morphing, of CE and $\hat{L}(d)$. Comparisons were made for clustered, random and regular point patterns over a range of point densities. For these experiments, several approaches to edge-correction and scaling were tested.

Results suggested that the morphing algorithm introduced some bias into both CE and $\hat{L}(d)$, mostly in the form of regularity at a scale near the plot radius. Bias was most pronounced in clustered populations and with low point densities. With morphing, plots were not classifed as clustered, random, or regular patterns as consistently as the more established Donnelly (1978) and Ripley (1976) edge-correction techniques for CE and

$\hat{L}(d)$, respectively. As such, the morphing algorithm had limited use as an edge correction tool. However, morphing demonstrated significant promise as a scaling tool for nested plot/subplot designs, particularly if different subplots within the same stratum or stand were used for torodial wrapping within the algorithm. In this case, morphing performed nearly as well as unscaled control plots of twice the original plot size in estimating population level CE or $\hat{L}(d)$ and during classification of plots into clustered, random or regular patterns.

When applied to actual forest inventory data, the morphing algorithm did not significantly change CE estimates (p = 0.442) and was unbiased up to 2.5 m for the $\hat{L}(d)$ function. Plots with spatial patterns greatly different from other plots within the same stand showed the most pronounced changes in CE or $\hat{L}(d)$ in response to morphing. Therefore, if assessing variation among plots is the primary study objective, individual plots should be used for torodial wrapping within the morphing algorithm.

2.2. INTRODUCTION

Over the past several decades, spatial point pattern analyses have increasingly been used to study forest stand structure and function. This research has generally been descriptive, often focusing on the horizontal structural patterns within the forest, i.e., quantification of tree stems as having an aggregated, uniform, or random spatial distribution (Pretzsch 1997, Larson and Bliss 1998, Kint et al. 2001, Antos and Parish 2002, Aguirre et al. 2003). In these cases, spatial point pattern analysis is useful for hypothesis development (Moeur 1993, Thomson et al. 1996) or developing management prescriptions (Harrod et al. 1999, Zenner 2000). Less commonly, spatial pattern is used

to explain ecological function. Laessle (1965), for example, used nearest neighbor indices to show that trees were often either aggregated or randomly distributed early in stand development, and more uniformly spaced later in development. Kenkel (1988) later attributed this shift in spatial pattern to differential mortality involving two distinct competitive phases: 1) an early "scramble phase" where two-sided competition for soil nutrients and water reduced the density of individuals in dense patches, and 2) a later "contest phase" where one-sided competition for light would differentiate a stand reducing clumpiness and density even further. In another example, Ferrari (1999) found that the availability of soil N in an old-growth eastern hemlock (*Tsuga canadensis* (L.) Carr.) – northern hardwood forest was highly influenced by the locations and identities of individual trees. Ferrari suggested that soil N created a positive feedback switch that maintained the canopy species patchiness over time. Finally, spatial point pattern analysis can be used to improve or validate model results. Ménard et al. (2002), for instance, used one commonly used spatial metric, the $\hat{K}(d)$ function, to validate the use of the spatially explicit SORTIE forest succession model (Pacala et al. 1996) for small-scale disturbance dynamics and impacts.

While immensely useful, spatial point pattern analyses have data requirements that can be limiting. Clearly, these statistics require precise and accurate tree locations within sample plots. For example, Freeman and Ford (2002) reported that although the $\hat{K}(d)$ function was generally robust to data management errors such as transcription errors and misidentification, it was sensitive to errors inherent to the measurement technique and shifted spatial patterns to larger scales. They argued that $\hat{K}(d)$ may not be able to accurately identify spatial inhibition, particularly at fine scales. Likewise, most

spatial point pattern statistics compel use of relatively large, compactly-shaped plots (e.g., rectangles or circles) for two reasons. First, all second- and higher-order spatial statistics are designed to test for local patterns among the points, not trends across an entire study area or extent (Bailey and Gatrell 1995). Analyses are generally robust with sample sizes of greater than 100 locations and for scales of less than 25-50% of the minimum dimension of an extent or study area, although this "rule of thumb" varies with the individual spatial metric being used. Plot sizes, therefore, should be much greater than the scale of interest and ideally contain a minimum of a several dozen individuals.

Second, most point pattern statistics are sensitive to edge effects where unobserved events outside the sample plot influence or interact with events within the sampled plot (Diggle 2003). While some spatial indices have straightforward, mathematical corrections for edge effects, many do not or the simple corrections only can work on regularly shaped plots (e.g., Donnelly [1978] correction for the Clark-Evans statistic). Weighting algorithms can be used that reduce the contribution of a point to the value of the spatial statistic, usually based on some function of the distance of the point to the edge relative to the scale of interest (Upton and Fingleton 1985, Diggle 2003). Another method to adjust for edge bias creates a buffer zone along the outer plot edges, effectively reducing the analyzed plot area (e.g., Woodall and Graham 2004). Individuals within the buffer zone are used only for the calculations for points within the reduced, inner subplot, with the width of the buffers determining the greatest scale of interest (Williams et al. 2001). As a result, buffers are generally inefficient when the scale of interest is large relative to the extent (Diggle 2003). For example, if one wanted to

determine the spatial patterns of trees on scales ≤10 m in a 400 m^2 square plot, buffers would require mapping trees in an additional 1,114 m^2 around that plot.

Many studies employ toroidal edge correction as a way to reduce edge effects. Toroidal edge correction essentially uses the entire plot itself as a buffer by using points on the opposite side of the plot to correct for edge effects on any particular side. This process maps the plot into continuous space as a torus, or more simply as a 3 x 3 array of replicates of the sample plot point pattern (Upton and Fingleton 1985). Not surprisingly, this technique has only been applied to square or rectangular plots. However, Williams et al. (2001, 2003) showed that toroidal edge correction could be applied to circular plots through a "morphing" algorithm with minimal introduction of bias for tree canopy cover estimation and also suggested that it could be used for other spatial indices. Williams et al. (2001, 2003) did not, however, investigate whether this technique would introduce bias in local, second-order spatial properties, such as those measured by the Clark-Evans statistic (CE) or the $\hat{K}(d)$ function.

In most long-term forest inventories that track growth and yield, e.g., the U.S. Forest Service FIA plots (Tillman 2004), plots are circular and usually nested, with larger plots up to 0.05 - 0.2 ha for larger, overstory trees, 0.01 - 0.05 ha for saplings, and plots as small as 0.0004 ha for regeneration. This design is used to maximize sampling efficiency; small trees occur in large numbers but do not contribute as much biomass or yield to a stand as larger trees. Typically, mapped tree locations within plots have had little value for point pattern analyses. Instead, plot averages for some variable were used to study patterns across a landscape or larger extent. Even when overstory plots are large enough (> 0.1 ha), a nested design precludes investigation of pattern interactions between

the tree classes measured at different plot scales. Often the size of the smaller nested plot will not contain enough individuals of the larger tree class to draw any statistically significant conclusions about the interaction between tree locations of the two classes. This situation has been unfortunate, as growth-and-yield plots constitute some of the oldest, most continuously monitored, spatially explicit datasets available.

Williams' et al. (2001, 2003) morphing algorithm could prove advantageous in applying spatial statistical methods to tree positions in relatively small, circular, and nested, forest inventory plots. At the plot level, morphing could allow unbiased estimates of second-order spatial properties and, if one assumes a homogenous extent as often is done within each sampling stratum of a forest inventory, all second-order spatial tests could be summarized across numerous plots, thereby shifting inference to the experimental design and away from a stochastic model (Diggle 2003). In addition, the use of multiple, smaller plots captures the average or range of conditions within a sample stratum more effectively than one large plot. Granted, this multi-plot approach would reduce the maximum scale of inference since each individual plot is smaller; however, it could be argued that by using other plots in the stratum to toroidally wrap within the morphing algorithm, not the same plot itself, one could investigate at scales that approach the plot radius. Similarly, at the subplot level, morphing could provide a means to increase the scale of smaller nested plots to the scale of the larger plot, again by either using the smaller nested plot itself or its conspecifics in the stratum to toroidally wrap. This approach is much easier than trying to identify the point pattern of each smaller, nested plot using a Markov, Matern or other point processes, and then simulate those processes over the larger plot (Williams et al. 2001). Furthermore, this approach should

provide a better estimate of the true spatial pattern than the predetermined patterns often used for scaling within simulation/visualization programs (e.g., the Stand Visualization System [McGaughey 2004]). However, it is unlikely that spatial relationships between points measured on different scales would be maintained without some type of "adjustment" to positions during the morphing procedure to account for interpoint attraction or repulsion.

If the morphing technique is to be applied in the aforementioned manner, then the sensitivity of spatial metrics to the effects of morphing needs to be quantified. This study investigated two metrics commonly used in spatial analysis of tree populations, the CE statistic (Clark and Evans 1954) and the univariate $\hat{L}(d)$ function (Besag 1977), a square-root transformation of the $\hat{K}(d)$ function (Ripley 1976, 1977). Two hypotheses were tested: 1) morphing as an edge correction technique does not bias estimates of the CE statistic or $\hat{L}(d)$ function as averaged across several plots; and 2) morphing used as scaling tool does not bias estimates of the CE statistic or the univariate $\hat{L}(d)$ function. These hypotheses were tested using multiple Monte-Carlo type simulation experiments, factoring both on known, simulated point distributions (i.e, clustered, random and regular patterns) and on a targeted sample size. Comparisons were made with both population level estimates of these metrics and with estimates derived from equivalent controls (e.g., plots of twice the area on the original scale to compare with plots scaled up to twice their original size with the morphing algorithm). Examples using actual forest inventory data also are presented.

2.3. BACKGROUND

2.3.1. Morphing

The morphing algorithm of Williams et al. (2001, 2003) remaps the trees within a circular Euclidean space *C* with the origin at the plot center and a radius of ρ (formally defined by $C = \{(x_1, y_1): x_1^2 + y_1^2 \le \rho^2\}$), to a square space *D* of equal area and a side length of $\rho\pi^{0.5}$ (formally defined by $D = \{(x_2, y_2): |x_2| \le 0.5\rho\pi^{0.5}, |y_2| \le 0.5\rho\pi^{0.5}\}$). The equations to transform or "morph" the coordinates from *C* to *D* are (from Williams et al. 2001, 2003):

$$\begin{aligned} x_2 = {} & \left[\mathrm{I}_{\left(0,\frac{3\pi}{4}\right]}(\theta) + \mathrm{I}_{\left(\frac{7\pi}{4},2\pi\right]}(\theta) - \mathrm{I}_{\left(\frac{3\pi}{4},\frac{7\pi}{4}\right]}(\theta) \right] \left(\frac{s}{2}\right) \\ & - \mathrm{I}_{\left(\frac{\pi}{4},\frac{3\pi}{4}\right]}(\theta) \left[\frac{2s\left(\theta - \pi/4\right)}{\pi} \right] + \mathrm{I}_{\left(\frac{5\pi}{4},\frac{7\pi}{4}\right]}(\theta) \left[\frac{2s\left(\theta - 5\pi/4\right)}{\pi} \right], \end{aligned} \qquad [2.1]$$

$$\begin{aligned} y_2 = {} & \left[\mathrm{I}_{\left(\frac{\pi}{4},\frac{5\pi}{4}\right]}(\theta) - \mathrm{I}_{\left(\frac{5\pi}{4},2\pi\right]}(\theta) \right] \left(\frac{s}{2}\right) + \mathrm{I}_{\left(0,\frac{\pi}{4}\right]}(\theta) \left(\frac{2s\theta}{\pi}\right) \\ & - \mathrm{I}_{\left(\frac{3\pi}{4},\frac{5\pi}{4}\right]}(\theta) \left[\frac{2s\left(\theta - 3\pi/4\right)}{\pi} \right] + \mathrm{I}_{\left(\frac{7\pi}{4},2\pi\right]}(\theta) \left[\frac{2s\left(\theta - 7\pi/4\right)}{\pi} \right], \end{aligned} \qquad [2.2]$$

where $\mathrm{I}_{(a,b]}(c)$ is one for $a < c \le b$, zero otherwise,

$$s = \sqrt{\pi\left(x_1^2 + y_1^2\right)} \qquad [2.3]$$

and

$$\begin{aligned} \theta = {} & \left[\tan^{-1}\frac{y_1}{x_1} + \pi \cdot \mathrm{I}_{(-\infty,0)}(x_1) \right] \left[1 - \mathrm{I}_{(0,\infty)}(x_1) \cdot \mathrm{I}_{(-\infty,0)}(y_1) \right] \\ & + \left[\tan^{-1}\frac{y_1}{x_1} + 2\pi \right] \cdot \mathrm{I}_{(0,\infty)}(x_1) \cdot \mathrm{I}_{(-\infty,0)}(y_1) \end{aligned} \qquad [2.4]$$

where θ is in radians. These transformations preserve the density of process across the two spaces (Williams et al. 2001, Appendix) and the membership of each quadrant by any given point (Williams et al. 2003).

After morphing the coordinates to space *D*, the now-square plot can be toroidal edge corrected with replicates of the same morphed plot, or potentially from other morphed plots drawn from the same point process. The 3 x 3 array of morphed plots can then be "demorphed" back to a circle of radius 3ρ using the following system of equations (modified from Williams et al. [2001, 2003] to avoid undefined values of γ through division by 0):

$$r = \left| \frac{2x_2}{\sqrt{\pi}} \left(\mathrm{I}_{\left(0,\frac{\pi}{4}\right]}(\varphi) + \mathrm{I}_{\left(\frac{3\pi}{4},\frac{5\pi}{4}\right]}(\varphi) + \mathrm{I}_{\left(\frac{7\pi}{4},2\pi\right]}(\varphi) \right) \right| + \left| \frac{2y_2}{\sqrt{\pi}} \left(\mathrm{I}_{\left(\frac{\pi}{4},\frac{3\pi}{4}\right]}(\varphi) + \mathrm{I}_{\left(\frac{5\pi}{4},\frac{7\pi}{4}\right]}(\varphi) \right) \right| \qquad [2.5]$$

$$\gamma_{(x_2=0,y_2=0)} = 0$$

$$\gamma_{(x_2\neq 0,y_2=0)} = \pi \cdot \mathrm{I}_{\left(\frac{3\pi}{4},\frac{5\pi}{4}\right]}(\varphi)$$

$$\gamma_{(x_2=0,y_2\neq 0)} = \frac{\pi}{2} \cdot \mathrm{I}_{\left(\frac{\pi}{4},\frac{3\pi}{4}\right]}(\varphi) + \frac{3\pi}{2} \cdot \mathrm{I}_{\left(\frac{5\pi}{4},\frac{7\pi}{4}\right]}(\varphi)$$

$$\gamma_{(x_2\neq 0,y_2\neq 0)} = \frac{\pi y_2}{4x_2}\left[\mathrm{I}_{\left(0,\frac{\pi}{4}\right]}(\varphi) + \mathrm{I}_{\left(\frac{7\pi}{4},2\pi\right]}(\varphi) \right] + \frac{\pi}{2}\left(1 - \frac{x_2}{2y_2} \right)\left[\mathrm{I}_{\left(\frac{\pi}{4},\frac{3\pi}{4}\right]}(\varphi) \right] + \pi\left(1 + \frac{y_2}{4x_2} \right)\left[\mathrm{I}_{\left(\frac{3\pi}{4},\frac{5\pi}{4}\right]}(\varphi) \right] + \frac{3\pi}{2}\left(1 - \frac{x_2}{6y_2} \right)\left[\mathrm{I}_{\left(\frac{5\pi}{4},\frac{7\pi}{4}\right]}(\varphi) \right] \qquad [2.6]$$

with φ as the angular displacement of the morphed coordinates (x_2, y_2),

$$x_1 = r\cos\gamma \qquad [2.7]$$

and

$$y_1 = r\sin\gamma\,. \qquad [2.8]$$

The larger "demorphed" plot now can be trimmed to any size radius between ρ and 3ρ, and then used for edge corrections for any standard spatial analyses conducted on the original plot (Williams et al. 2003), or potentially as a scaling tool to simulate the original plot across a larger extent (this study).

2.3.2. Spatial Metrics

2.3.2.1. Clark-Evans Nearest Neighbor Index

There are numerous metrics available to investigate spatial point pattern. For this study, two metrics commonly used in the study of the spatial dynamics of plant populations were chosen. The Clark-Evans nearest neighbor index (CE; Clark and Evans 1954) relates the mean nearest neighbor distances in any spatial pattern (r_A) to that mean distance (r_E) expected under complete spatial randomness (*csr*). It was calculated as:

$$CE = \frac{r_A}{r_E} = \frac{\frac{1}{\mathrm{N}}\sum_{i=1}^{N} r_i}{0.5\left(\frac{N}{A}\right)^{-1/2}} \qquad [2.9]$$

where r_i is the distance between tree i and its nearest neighbor, N is the total number of points in the pattern, and A is the area. In this form, CE will be biased from edge effects as points near the perimeter of the plot having longer nearest neighbor distances than would be expected. Donnelly (1978) provided a correction to r_E that reduces this bias in compactly-shaped plots:

$$r_E = 0.5\left(\frac{A}{N}\right)^{1/2} + 0.0514\frac{P}{N} + 0.041\frac{P}{N^{3/2}} \qquad [2.10]$$

where P is the perimeter of the plot. CE ranges from 0 for completely aggregated points to 1 for *csr* to 2.1491 for perfectly regular hexagonally distributed points (Clark and

Evans 1954, Kint et al. 2003). Significances of departure of CE from *csr* are tested with a standard, normal variate defined as:

$$c = \frac{r_A - r_E}{\sigma_{r_E}} \text{ where } \sigma_{r_E} = \frac{0.26136}{\sqrt{N \cdot \lambda}} \quad [2.11]$$

where λ is the density of the point pattern (Clark and Evans 1954).

2.3.2.2. *K(d)* Function

Unlike CE, which summarizes overall spatial pattern in a single statistic, the $\hat{K}(d)$ function describes the spatial pattern as it relates to distance within the extent (Ripley 1976, 1977). Basically, *K(d)* is the expected number of points within distance *d* of an event, relative to the overall density (λ) of the point process. *K(d)* is estimated from the distances (d_{ij}) between all points in the extent (Moeur 1993, Diggle 2003):

$$\hat{K}(d) = \frac{A}{N(N-1)} \sum_{\substack{i=1 \\ i \neq j}}^{N} \sum_{j=1}^{N} I(d_{ij}) \quad [2.12]$$

where

$$I(d_{ij}) = \begin{cases} 1 \text{ if } d_{ij} \leq d \\ 0 \text{ if } d_{ij} > d \end{cases}$$

for $d > 0$. Like CE, $\hat{K}(d)$ is strongly biased by edge effects. For point patterns that have an exclusively defined buffer, $\hat{K}(d)$ is modified to:

$$\hat{K}(d) = \frac{A}{N(N-1)} \sum_{\substack{i=1 \\ i \neq j}}^{N+} \sum_{j=1}^{N} I(d_{ij}) \quad [2.13]$$

where *N*+ is the number of points in *A* and the surrounding buffer (i.e., d_{ij}'s are calculated between all points in *A* and only from the buffer points to those in *A*; Cressie

1993). For areas without a buffer, Ripley (1976, as modified by Diggle 2003) suggested the following form:

$$\hat{K}(d) = \frac{A}{N(N-1)} \sum_{\substack{i=1 \\ i \neq j}}^{N} \sum_{j=1}^{N} w_{ij}^{-1} \cdot I(d_{ij}) \qquad [2.14]$$

where w_{ij} is the proportion of the circumference of a circle centered on point i and passing through point j that is inside A. $\hat{K}(d)$ is typically calculated for evenly spaced d between 0 to one-half of the length shortest boundary or of the radius of A, at steps that are greater than the measurement error of the points (Freeman and Ford 2002).

Many studies use the square root transformation of $\hat{K}(d)$, defined as (Besag 1977):

$$\hat{L}(d) = \sqrt{\frac{\hat{K}(d)}{\pi}} - d \qquad [2.15]$$

instead of $\hat{K}(d)$. $\hat{L}(d)$ linearizes $\hat{K}(d)$, stabilizes its variance and has an expected value of approximately zero at all d under *csr*. Furthermore, $\hat{L}(d)$ is much easier to interpret than $\hat{K}(d)$, with positive values indicating clustering in the point pattern and negative values indicating regularity (Moeur 1993, Freeman and Ford 2002).

Significance for $\hat{K}(d)$, and subsequently $\hat{L}(d)$, is estimated via Monte Carlo procedures as the sampling distribution for $\hat{K}(d)$ is analytically intractable for all but the homogeneous Poisson process (Goreaud and Pélissier 2000, Diggle 2003). Confidence envelopes are generated by simulating several realizations (η) of a benchmark point process that conforms to the null hypothesis, e.g., a homogenous Poisson process to test for *csr*, and calculating $\hat{K}(d)$ for each realization. These simulations are generally

conducted with the same intensity and lag distances, and across the same extent as the observed point pattern. For a given α, local confidence envelopes are built from $\eta_{[\alpha/2]}$ and $\eta_{[1-\alpha/2]}$, sorted at each *d* (Goreaud and Pélissier 2000). Although many studies have set $\eta = 1 - \alpha^{-1}$ (Kenkel 1988, Harrod et al. 1999, Antos and Parish 2002), Martens et al. (1997) suggest that these Monte Carlo confidence envelopes have low validity when $\eta \cdot \alpha < 5$.

Studies of replicated point patterns, such as in this one, require a modification to the normal calculation of $\hat{K}(d)$. Since $\hat{K}(d)$ is scaled by the estimated density $\hat{\lambda}$, and $\hat{\lambda}$ would naturally vary across replicates of an underlying point process with the same λ, Diggle (2003) suggested that $\hat{K}(d)$ should not be calculated as a simple arithmetic average of the $\hat{K}_i(d)$'s. Instead, he suggested that

$$\hat{K}(d) = \sum_{i=1}^{r} n_i \hat{K}_i(d) \Big/ \sum_{i=1}^{r} n_i \qquad [2.16]$$

where r is the replicate and $\hat{K}_i(d)$ is calculated on each r with either [2.12], [2.13] or [2.14] from above. The standard deviation is calculated as:

$$sd_{\hat{K}(d)} = \sum_{i=1}^{r} n_i \left[\hat{K}_i(d) - \hat{K}(d)\right]^2 \Big/ \sum_{i=1}^{r} n_i \qquad [2.17]$$

Standard errors and parameteric confidence intervals can then be calculated normally. Diggle (2003) explains that significance of $\hat{K}(d)$ for unknown point distributions can also be assessed nonparametrically by calculating a bootstrapped estimate of its sampling variance; this approach was not taken in this study since the properties of the underlying point population were known. If Monte Carlo envelopes are required to determine a

departure of $\hat{K}(d)$ from *csr*, they should incorporate the variability in $\hat{\lambda}$ as it varies across the replicates and, if replicate-level $\hat{K}_i(d)$ is also of interest, be corrected for experimentwise Type I error using the bonferroni adjustment to α (Kuehl 1994).

2.4. METHODS

2.4.1. Experiment I: Edge Correction of Circular Plots

The first two of the three simulation experiments were conducted to investigate the potential of the morphing algorithm as both an edge-correction and scaling tool on univariate data. Williams et al. (2001) suggested that the morphing algorithm could be used to create a buffer of points for edge correction for attributes of the original plot; subsequently CE and $\hat{L}(d)$ could be calculated using equations [2.9] and [2.13], respectively. Experiment I was designed to test the hypothesis that use of the morphing algorithm in this manner did not bias sample plot-level estimates of either the CE or the $\hat{L}(d)$ function, either as compared to those calculated 1) from the entire population or extent (i.e., CE_{popl} and $\hat{L}_{popl}(d)$), or 2) using either the Donnelly [2.10] or Ripley [2.14] edge-correction techniques on the unmorphed sample plots. For CE, one-way and paired t-tests were used to test these two intermediate hypotheses, respectively, at each point pattern and targeted sample size (N_{tar}) combination (see below). For the $\hat{L}(d)$ function, the difference between $\hat{L}_{popl}(d)$ and the weighted mean sample-plot $\hat{L}(d)$ [2.16] was plotted for each of the two edge-correction techniques as applied to the concurrent set of sample plots. Distances at which the 95% confidence interval (as calculated using [2.17]) for this difference did not contain 0 indicated potential bias in either edge-correction

technique. L-function comparisons were tested at scales up to one-half of the sample plot radius (0.5·*rad*).

Classification errors for individual plots were also calculated to investigate differences between the edge-correction techniques in detection of clustering or regularity from the sample plots. Ideally, classification of plots, either correctly or incorrectly, between the Donnelly and morphing edge-corrections for CE or between the Ripley and morphing edge-corrections for $\hat{L}(d)$, should not differ; e.g., all plots from which the CE using Donnelly correction was significant should also be significant using the morphing correction, and visa versa. In the best case, there should be no plots where one technique detected significance and the other did not; i.e., marginal detection rates would equal zero. However, the marginal detection rates often vary from 0, but if there is no difference in detection the rates should be identical for both techniques. The McNemar test (Zar 1999) was used to test for this homogeneous marginality between the different edge-correction methods for both CE and $\hat{L}(d)$.

2.4.2. Experiment II: Scaling of Circular Plots

Experiment II was designed to test the hypothesis that the morphing algorithm could be used to scale univariate point processes within the sample plot; i.e., estimates of average CE or $\hat{L}(d)$ as calculated from morphed plots scaled up from smaller plots should not differ significantly from 1) population level estimates or 2) those calculated from unmorphed, control plots of the same scale (2·*rad*; CONT). There are at least three ways to approach scaling with plots from a forest inventory. First, the same sample plot could be used for toroidal wrapping within the morphing algorithm. Although

straightforward, this SAME approach would likely introduce bias into the CE and $\hat{L}(d)$ statistics, manifested as inhibition at the scale near *rad* (Upton and Fingleton 1985). Therefore, most inferences about spatial pattern would still probably only be valid at scales <0.5·*rad*. Another approach would use a random selection of 8 different sample plots within the same sampling stratum for toroidal wrapping (DIFF approach). The DIFF approach assumes a homogenous, isotropic process across the entire stratum, i.e., all plots represent the same process, but this is the primary assumption when defining a sampling stratum. Furthermore, this approach might reduce the amount of inhibition bias introduced into the pattern. A third approach, common in many visualization systems, is to scale plots up using a predetermined point process, often random allocation, within the expansion area (i.e., the RAND approach). Unfortunately, this technique ignores the spatial pattern of the original plot and may mute unique spatial characteristics, particularly if the predetermined process is quite different from the observed pattern. All three approaches were tested using the same set of sample plots to scale plots to twice the original radius (2·*rad*). The Donnelly [2.10] and the Ripley [2.14] corrections were used to calculate CE and $\hat{L}(d)$, respectively, for both the control sample plots and the three scaling approaches.

Analysis for Experiment II was similar to that for Experiment I. One-way t-tests were used to test the difference between CE_{popl} and mean sample plot CE for the control and each of the three scaling options. Multiple comparisons among the control and the three scaling options for mean CE were tested using a Tukey HSD test at a familywise $\alpha = 0.05$. For $\hat{L}(d)$, 95% confidence intervals for the difference between $\hat{L}_{popl}(d)$ and mean sample plot $\hat{L}(d)$ for each option were calculated for lag distances up to *rad*.

Differences in classification proportions were tested using the Cochran's Q test, which is an extension of the McNemar test when the number of repeated-measures or categories in a dichtomous dataset is greater than 2 (Zar 1999). Pairwise comparisons among the control and the three scaling approaches were tested using a nonparametric form of the Scheffé test (Marascuilo and McSweeney 1967, as cited in Zar 1999).

2.4.3. Point Pattern Generation

Simulations in Experiments I and II were conducted with three different point patterns—clustered, random, and regular, and with three different mean sample sizes (N)—25, 50, and 100. This set of sample sizes covers much of the range found in plots of many forest inventories; plot sizes are generally increased if sample sizes in individual plots fall below 20-30 and generally decreased when much above 100. Point patterns were created as follows:

1. Clustered: This point pattern was generated using the Thomas process, which is a special case of the Neyman-Scott process (Baddeley and Turner 2004). "Parent" points of intensity β_p were generated from a homogeneous Poisson process. About each parent point, a Poisson distributed number (μ) of "offspring" points are independently placed with isotropic Gaussian displacements that have a standard deviation of σ from the parent point. Parent points are then subsequently deleted, leaving only offspring points as the realization of the process. For this study, well-distributed, relatively strong clustering was desired, so parameters were set at $\lambda_p = 0.1$, $\mu = 11$, and $\sigma = 3.16$. To maintain a constant intensity (λ) across all simulated patterns, the offspring points were randomly thinned to $\lambda = 1.0$.

2. Random: This point pattern was generated with a homogeneous Poisson point process of $\lambda = 1.0$.
3. Regular: This point pattern was generated with a Strauss hardcore inhibition process using the Metropolis-Hastings algorithm (Baddeley and Turner 2004). The Strauss process has several parameters that control the radii of total (i.e., hardcore) inhibition between points (r_{hard}), the radii of some (i.e., softcore) inhibition between points (r_{soft}), and the strength of the softcore inhibition (γ_s), with $\gamma_s = 0$ effectively as hardcore inhibition and $\gamma_s = 1$ effectively as no inhibition between points closer r_{soft}, but farther apart than r_{hard} (Isham 1984). In this study, relatively strong inhibition was desired, so $r_{hard} = 0.5$, $r_{soft} = 0.75$, and $\gamma_s = 0.75$. Spatial point "birth" and point "death" routines within the Metropolis-Hastings algorithm were turned off; this allowed the model to be conditioned on $\lambda = 1.0$, identical to the other two point patterns, and points to only be shifted in location iteratively in accordance with r_{hard}, r_{soft} and γ_s (Baddeley and Turner 2004).

These point patterns were simulated across a 125 x 125 extent, with the outer 12.5 ring serving as a buffer area, thus eliminating the need to toroidal wrap during sample plot selection. Point maps and the population-level $\hat{L}_{popl}(d)$ are shown in Figure 2.1. The population-level Clark-Evans statistic for the clustered, random, and regular patterns were 0.872, 0.995, and 1.363, respectively. For each pattern by size combination, 1,000

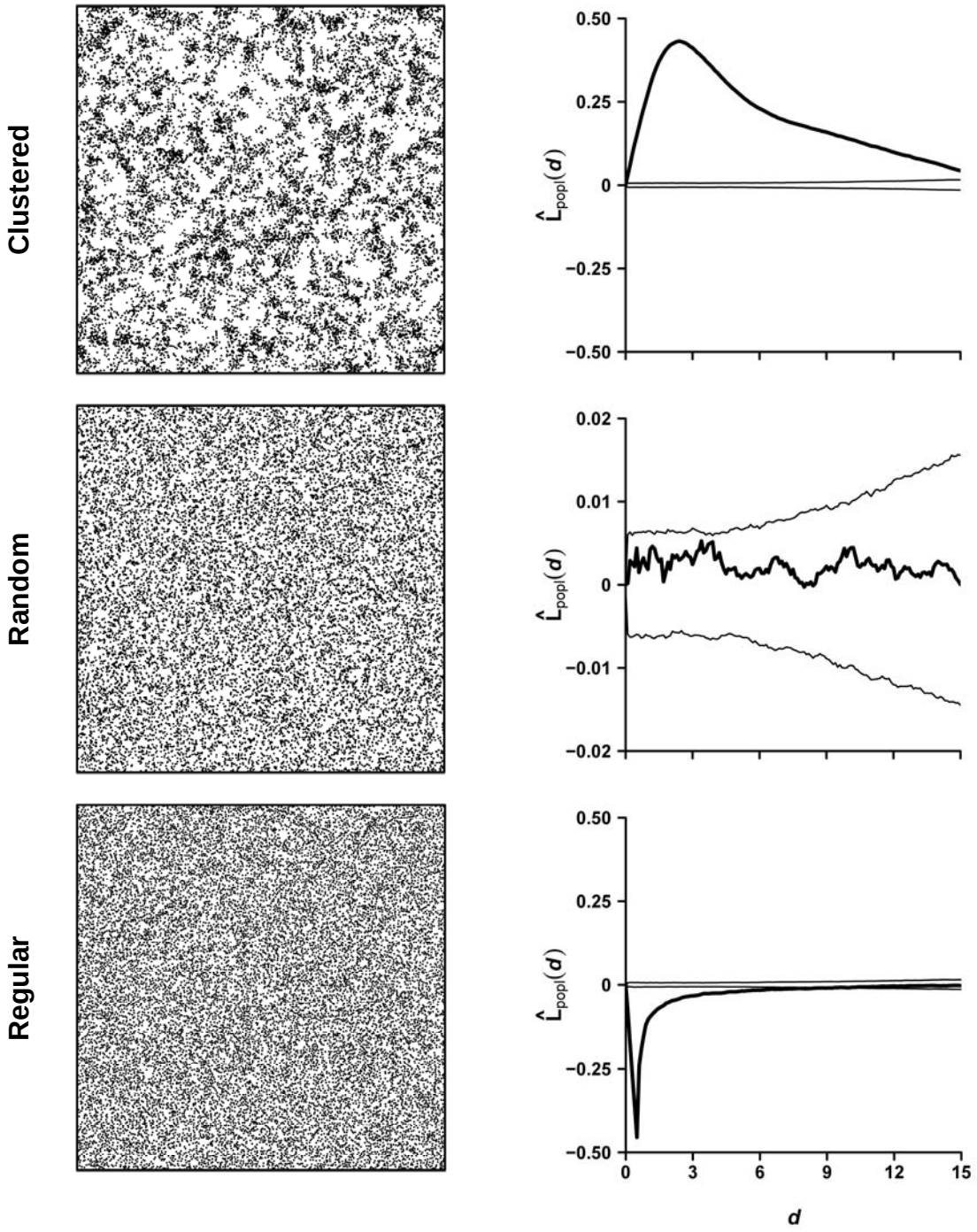

Figure 2.1. Point maps and the population-level $\hat{L}_{popl}(d)$ with increasing lag distance (d) for the three simulated point patterns used in both simulation experiments. Monte Carlo 95% confidence envelopes for $\hat{L}_{popl}(d)$ are shown by the light lines.

circular plots of *rad* 2.82, 3.98, 5.64 for N of 25, 50, and 100, respectively, and were then randomly located within the interior 100 x 100 area. Data for Experiments I and II were collected concurrently from the same sample plots and across the three simulated point patterns. All statistical tests and pattern generation was coded in R (R Development Core Team 2005) using both the splancs (Rowlingson et al. 2005) and spatstat (Baddeley et al. 2004) packages. The R code used for this analysis can be found in Appendix A.

2.5. RESULTS & DISCUSSION

2.5.1. Experiment I: Edge Correction of Circular Plots

Use of the Donnelly edge correction for estimating the Clark-Evans statistic (CE_{don}) provided a slightly better approximation of the population-level CE (CE_{popl}) than did the morphing algorithm (CE_{mor}), but neither estimated CE_{popl} for most point pattern and sample size combinations adequately (Table 2.1). Both edge-correction methods yielded significant overestimates of CE_{popl}, with the CE_{mor} consistently and significantly greater than CE_{don}. As expected, the absolute difference between CE_{don} or CE_{mor} and CE_{popl} was least when the targeted sample size was greatest. Likewise, the differences between CE_{don} and CE_{mor} were reduced as sample size increased (Table 2.1), suggesting that the two edge-correction techniques may converge on CE_{popl} with higher sample sizes.

At the sample plot level, both the Donnelly edge correction and the morphing algorithm performed poorly for aggregated point patterns, with significant clustering detected in only 1.1-8.0% and 0.4-5.0% for the Donnelly and morphing edge corrections, respectively (Table 2.2). This result was not surprising; several authors have reported the shortcomings of CE in clustered stands (Kint et al. 2003). For the random and regular

Table 2.1. Results for one-way and paired t-tests for the 1,000 sample-plot estimates of the Clark-Evan statistic using the Donnelly (1977) and morphed edge correction techniques (CE_{don} and CE_{mor}, respectively) against the population-level CE statistic (CE_{popl}), and the mean difference (diff) between the two edge correction estimates for each of the 9 point pattern by target sample size (N_{tar}) combinations. The mean of the actual plot-level sample size is given by n_{sp}.

Pattern	N_{tar}	CE_{popl}	n_{sp}	H_0: $CE_{don} = CE_{popl}$			H_0: $CE_{mor} = CE_{popl}$			H_0: $CE_{mor} - CE_{don} = 0$		
				CE_{don}	t	p	CE_{mor}	t	p	diff	t	p
Clustered	25	0.872	26.5	0.903	7.12	<0.001	0.914	10.15	<0.001	0.0106	4.98	<0.001
Clustered	50	0.872	49.4	0.883	3.01	0.002	0.886	4.22	<0.001	0.0033	2.15	0.031
Clustered	100	0.872	96.6	0.876	1.50	0.135	0.877	2.21	0.027	0.0016	1.83	0.067
Random	25	0.995	25.0	1.001	2.94	0.003	1.013	5.23	<0.001	0.0073	3.80	<0.001
Random	50	0.995	49.8	1.003	3.72	<0.001	1.007	5.41	<0.001	0.0033	2.79	0.005
Random	100	0.995	100.1	1.006	7.17	<0.001	1.009	8.78	<0.001	0.0021	2.99	0.003
Regular	25	1.363	25.0	1.323	-14.30	<0.001	1.336	-11.79	<0.001	0.0087	4.20	<0.001
Regular	50	1.363	50.1	1.339	-15.01	<0.001	1.343	-13.24	<0.001	0.0039	3.15	0.002
Regular	100	1.363	99.9	1.345	-16.32	<0.001	1.349	-13.70	<0.001	0.0033	4.63	<0.001

Table 2.2. Number of sample plots out of 1,000 that showed significant CEs or $\hat{L}(d)$ values (at any lag distance) for the morphing and Donnelly or Ripley, respectively, edge-corrections for each of the point pattern by target sample size (N_{tar}) combinations. Significant differences in classification between the two methods were tested with the McNemar test (M) for each pattern by N_{tar} combination. $\hat{L}(d)$ incorrectly classified some clustered patterns as regular over at least one lag distance; the total number of plots for which this occurred is given in the parentheses. During classification, significance values were Bonferroni-corrected; for $\hat{L}(d)$ these were obtained from the $\eta_{[5]}$ and $\eta_{[199,995]}$ ranked values from 200,000 Monte Carlo simulations of *csr* with mean sample size N_{tar} drawn from a random Poisson distribution.

Pattern	N_{tar}	CE			$\hat{L}(d)$		
		Donnelly	Morphed	M	Ripley	Morphed	M
Clustered	25	11	4	4.0*	84 (2)	15 (0)	67.0**
Clustered	50	31	9	18.4**	400 (2)	246 (4)	150.1**
Clustered	100	80	50	17.5**	782 (6)	693 (5)	83.3**
Random	25	0	0	0.0	0	0	0.0
Random	50	0	0	0.0	0	0	0.0
Random	100	0	0	0.0	0	0	0.0
Regular	25	249	153	48.0**	0	0	0.0
Regular	50	849	802	15.0**	998	903	93.0**
Regular	100	999	998	0.0	1000	1000	0.0

* $p < 0.05$

** $p < 0.01$

point patterns, both approaches performed similarly. McNemar tests of each pattern by sample size combination suggests that use of the Donnelly edge correction leads to higher detection rates of both significant clustered and regular patterns (Table 2.2); the overall odds ratio across all point pattern and sample size combinations was 2.95 ($p < 0.001$) and the McNemar statistic was 99.28 ($p < 0.001$).

Results for the $\hat{L}(d)$ function were similar. Neither the Ripley nor the morphing corrections yielded mean $\hat{L}(d)$ values equal to or at all distances equivalent to those observed in the population (Figure 2.2). This effect was particularly pronounced for the clustered pattern where both corrections significantly underestimated $\hat{L}_{popl}(d)$ across all distances for all sample sizes (Figure 2.2); this was somewhat expected since the clustered pattern showed a peak in $\hat{L}_{popl}(d)$ beyond the scale of the plots (Figure 2.1). Nevertheless, the Ripley correction performed slightly better for this pattern as it better approximated $\hat{L}_{popl}(d)$ than the morphing correction, regardless of sample size (Figure 2.3). The morphing algorithm also significantly overestimated $\hat{L}_{popl}(d)$ for the regular pattern at smaller sample sizes; the Ripley correction did not. For the regular pattern, both corrections did yield significant peaks in their mean $\hat{L}(d)$ that corresponded to approximately the same lag distances as the population; the morphing correction tended to significantly overestimate $\hat{L}_{popl}(d)$ at this point (Figure 2.2).

At the sample plot level, it was obvious that $\hat{L}(d)$ was more powerful than CE at detecting clustering or regularity (Table 2.2). However, $\hat{L}(d)$ still did not detect differences from *csr* with sample sizes of 25, and it performed relatively poorly for the

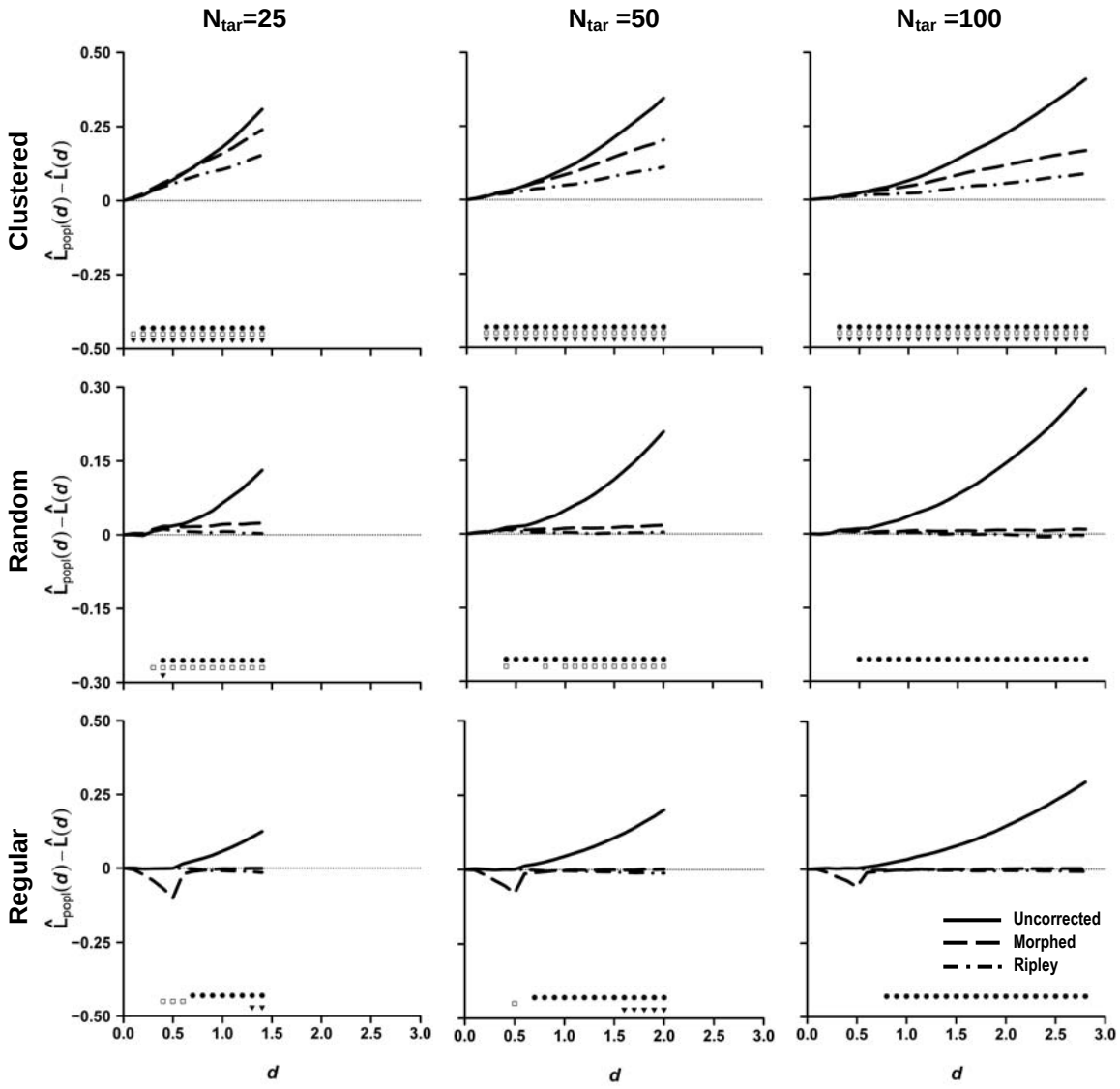

Figure 2.2. Difference between population-level $\hat{L}_{popl}(d)$ and mean sample plot $\hat{L}(d)$ functions with increasing lag distances (d) and using the morphing and Ripley edge-correction algorithms ([2.14] and [2.13], respectively), as calculated from 1,000 plots of targeted sample size (N_{tar}) for clustered, random, and regular point patterns. The uncorrected $\hat{L}(d)$ function [2.12] is shown for comparative purposes. The symbols at the bottom of each plot indicate over which range the uncorrected (filled circle), the morphing (open square), and Ripley (filled triangle) $\hat{L}(d)$ functions were not significantly different from $\hat{L}_{popl}(d)$.

clustered point pattern with either the Ripley or the morphing corrections (Table 2.2). Larger sample sizes did increase detection and use of the Ripley correction detected significant departure from *csr* more readily (McNemar statistic = 399.12, $p < 0.001$), from 7-15% more plots depending on pattern and sample size.

In summary, when used as an edge-correction technique as Williams et al (2003) suggested, the morphing algorithmn generally introduced some bias into the CE or $\hat{L}(d)$ statistics, likely through the introduction of regularity into the edge-corrections. For regular or random point patterns, this effect would probably be negligble for either classification of plots or in identifying the scale of pattern, but for clustered patterns it could be significant enough to reduce detection rates with many second-order spatial metrics (Figure 2.2). Although the Donnelly and Ripley corrections did not adequately approximate the clustered population's CE and $\hat{L}(d)$, respectively, both corrections provided better estimates than the morphing algorithmn. Cressie (1993) calculated several edge corrections of $\hat{L}(d)$ for the spatial analysis of longleaf pines (*Pinus palustris*). Edge-corrected estimates of $\hat{L}(d)$ using morphing algorithmn would likely fall somewhere between those based on toroidal distances and those with a guard area for most point patterns (Cressie 1993, Figure 8.15). This statement would likely apply to CE estimates as well. Based on these results, there probably is no reason to select the morphing algorithmn over either the Donnelly or Ripley techniques for edge correction of CE or $\hat{L}(d)$ on circular sample plots.

2.5.2. Experiment II: Scaling of Circular Plots

Scaling small circular sample plots upwards to larger-sized plots using the morphing algorithmn was the focus of Experiment II. Morphing using either the same (SAME) or different (DIFF) sample plots did not provide a good approximation of CE_{popl}. However, neither did the random approach (RAND) nor even the large control plots approximate CE_{popl} adequately. For example, across the nine point pattern by targeted sample size combinations, one-way t-tests of no difference between CE_{popl} and mean sample plot CE were nonsignificant ($p > 0.05$) only 4 times—once for CONT, once for DIFF and twice for RAND (Table 2.3). However, assuming that the CONT estimate would be the best approximation for CE_{popl} one could expect within an analysis from sample plots, the mean CEs of DIFF and SAME did not differ greatly from the mean CE of CONT for most point pattern by sample size combinations (Table 2.3). The most notable exception to this trend was for regular point patterns, where the mean CEs for the CONT were significantly greater. As expected, the RAND approach eliminated any significant pattern that could be detected with CE (Table 2.3).

Classification rates for the control and three scaling options were significantly different for all patterns by sample size combinations (Table 2.4). All approaches except RAND, generally classified plots correctly for the random and regular. For clustered patterns, CE did not detect clustering well in sample plots regardless of the approach even with sample size approaching 200 points. Furthermore, the regularity that the SAME approach incorporates into the edge corrections caused a small number of random patterns to be classified as regular. Overall, the CONT and DIFF generally had the same rates of correct classification, followed by SAME and finally RAND (Table 2.4).

Table 2.3. Average sample size (n), and mean and standard deviation of the Clark-Evans statistic (CE) for the control and the three scaling options listed in the text, as calculated from 1,000 sample plots across the nine point pattern by target sample size (N_{tar}) combinations. Except for the control, all three options scaled plots upward from a sample size of $N_{tar}/4$. One-way T-tests of CE against CE_{popl} were performed for all sample plot CEs; those CEs that were not significantly different from CE_{popl} at α=0.05 are italicized. Means with the same superscript letter within a row are not significantly differently different from one another as determined with the Tukey HSD test at a familywise α=0.05.

Pattern	N_{tar}	CE_{popl}	Control		Same		Different		Random	
			n	CE (sd)	n	CE (sd)	n	CE (sd)	n	CE (sd)
Clustered	100	0.872	102.4	0.885 (0.067)^{a}	105.9	0.920 (0.121)^{c}	105.3	0.906 (0.063)^{b}	105.9	0.968 (0.060)^{d}
Clustered	200	0.872	197.3	0.877 (0.050)^{a}	197.7	0.887 (0.098)^{b}	197.9	0.881 (0.046)^{ab}	197.7	0.966 (0.043)^{c}
Clustered	400	0.872	392.2	*0.873 (0.035)*^{ab}	386.4	0.878 (0.069)^{b}	386.2	*0.872 (0.037)*^{a}	386.4	0.965 (0.030)^{c}
Random	100	0.995	100.2	1.002 (0.054)^{a}	100.2	1.012 (0.100)^{b}	100.1	1.011 (0.057)^{b}	100.2	*0.994 (0.055)*^{a}
Random	200	0.995	200.5	1.004 (0.037)^{b}	199.4	1.005 (0.068)^{b}	200.1	1.003 (0.038)^{b}	199.4	*0.996 (0.038)*^{a}
Random	400	0.995	400.0	1.003 (0.027)^{b}	400.3	1.007 (0.047)^{c}	399.6	1.005 (0.026)^{bc}	400.3	0.997 (0.027)^{a}
Regular	100	1.363	100.1	1.347 (0.036)^{c}	100.1	1.278 (0.068)^{b}	99.7	1.278 (0.042)^{b}	100.1	1.071 (0.052)^{a}
Regular	200	1.363	200.2	1.351 (0.024)^{c}	200.3	1.287 (0.044)^{b}	199.9	1.289 (0.028)^{b}	200.3	1.077 (0.037)^{a}
Regular	400	1.363	400.9	1.356 (0.017)^{c}	399.6	1.294 (0.030)^{b}	399.3	1.294 (0.019)^{b}	399.6	1.082 (0.025)^{a}

Table 2.4. Number of sample plots out of 1,000 that showed significant CEs or $\hat{L}(d)$'s (at any lag distance) for the control and the three scaling options listed in the text for each of the point pattern by target sample size (N_{tar}) combinations. Both CE and $\hat{L}(d)$ incorrectly classified some clustered patterns as regular, or regular as clustered, over at least one lag distance; the total number of plots for which this occurred is given in the parentheses. During classification, significance values were Bonferroni-corrected; for $\hat{L}(d)$ these were obtained from the $\eta_{[5]}$ and $\eta_{[199,995]}$ ranked values from 200,000 Monte Carlo simulations of *csr* with mean sample size N_{tar} drawn from a random Poisson distribution. Differences in classification proportions among all four options were tested with the Cochran's Q test (Q) for each pattern by N_{tar} combination. Letters within the same row indicate no significant difference in proportions as tested using pairwise comparison tests at a familywise α=0.05.

Pattern	N_{tar}	Number of Significant Plots				Q*
		Control	Same	Different	Random	
		CE				
Clustered	100	55^{b} (0)	135^{c} (3)	41^{b} (0)	3^{a} (0)	181.4
Clustered	200	296^{bc} (0)	315^{c} (1)	254^{b} (0)	0^{a} (0)	413.7
Clustered	400	745^{c} (0)	559^{b} (0)	720^{c} (0)	2^{a} (0)	1377.4
Random	100	0^{a}	30^{b}	1^{a}	0^{a}	85.3
Random	200	1^{a}	30^{b}	0^{a}	0^{a}	87.1
Random	400	0^{a}	29^{b}	0^{a}	0^{a}	87.0
Regular	100	1000^{c} (0)	840^{b} (0)	955^{c} (0)	9^{a} (0)	2490.5
Regular	200	1000^{b} (0)	998^{b} (0)	1000^{b} (0)	36^{a} (0)	2886.0
Regular	400	1000^{b} (0)	1000^{b} (0)	1000^{b} (0)	192^{a} (0)	2424.0
		$\hat{L}(d)$				
Clustered	100	755^{d} (0)	308^{b} (83)	419^{c} (0)	49^{a} (9)	1137.8
Clustered	200	989^{c} (0)	725^{b} (161)	971^{c} (2)	241^{a} (20)	1697.0
Clustered	400	1000^{b} (3)	967^{b} (193)	1000^{b} (2)	613^{a} (7)	1071.2
Random	100	0^{a}	121^{b}	3^{a}	5^{a}	318.0
Random	200	2^{a}	137^{b}	2^{a}	3^{a}	375.4
Random	400	1^{a}	136^{c}	3^{a}	25^{a}	298.8
Regular	100	1000^{b} (0)	949^{b} (0)	990^{b} (0)	3^{a} (1)	2822.3
Regular	200	1000^{b} (0)	1000^{b} (0)	1000^{b} (0)	24^{a} (2)	2928.0
Regular	400	1000^{b} (0)	1000^{b} (0)	1000^{b} (0)	120^{a} (9)	2610.0

* $Q \sim \chi_{0.05,3} = 7.815$

Mean sample plot $\hat{L}(d)$ calculated with the control or any scaling approach significantly underestimated $\hat{L}_{popl}(d)$ across most distances for the aggregated point pattern, regardless of the target sample size (Figure 2.3). Interestingly, peaks in mean $\hat{L}(d)$ for the CONT and the SAME and DIFF approaches all occurred between lag distances of 1.5 and 2.0 regardless of sample size; $\hat{L}(d)$ calculated using the SAME approach usually peaked at the shortest lag distances within this range with DIFF and CONT peaking at successively longer distances. For the random point patterns, $\hat{L}(d)$ of both CONT and DIFF was not significantly different from $\hat{L}_{popl}(d)$ across all lag distances and for all target sample sizes; SAME and RAND significantly underestimated and overestimated $\hat{L}_{popl}(d)$, respectively, across all lag distances (Figure 2.3). For the SAME approach, in particular, this was likely due to the same regularity introduced into the pattern that was also seen in the CE results. Woodall and Graham (2004), in a similar study that studied spatial relationships across trimmed, torodial wrapped, FIA subplots, also reported misleading $\hat{K}(d)$ results. Diggle (2003) notes that a common weakness with normal toroidal wrapping is that it incorporates regularity at scales approaching the dimensions of a plot and aggregation for points near the edge of the plot. For the regular point patterns, $\hat{L}(d)$ using any of the three scaling approaches significantly overestimated $\hat{L}_{popl}(d)$ across the scales of inhibition found in the population (d = 0.3 – 0.9). Beyond this range, $\hat{L}(d)$ calculated using either the SAME or DIFF approaches was not significantly different from $\hat{L}_{popl}(d)$. The CONT was never different from $\hat{L}_{popl}(d)$ for any lag distance or sample size (Figure 2.3).

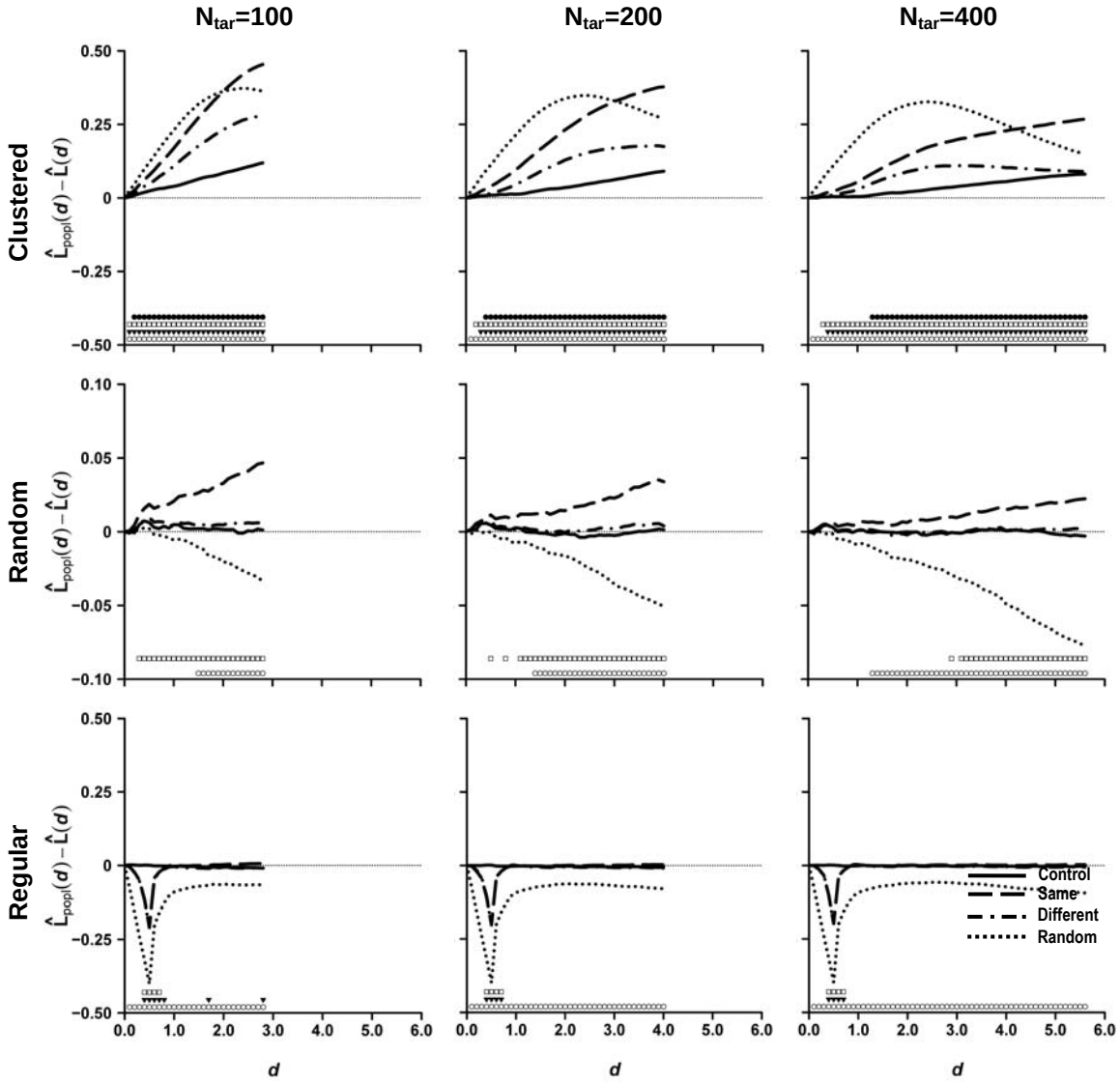

Figure 2.3. Difference between population-level $\hat{L}_{popl}(d)$ and mean sample plot $\hat{L}(d)$ functions with increasing lag distance (*d*) for the control and the three scaling options listed in the text, as calculated from 1,000 plots of targeted sample size N for clustered, random, and regular point patterns. The Ripley edge correction [3.13] was used for all plots. The symbols at the bottom of each plot indicate over which range the control (filled circle), morphing with same (open square), morphing with different (filled triangle), and random (open circle) $\hat{L}(d)$ functions were not significantly different from $\hat{L}_{popl}(d)$.

Classification rates of plots as showing clustering or regularity using $\hat{L}(d)$ differed significantly by approach for all pattern by target sample size combinations (Table 2.4). Like for CE, $\hat{L}(d)$ using the RAND approach generally could not detect clustering or regularity unless the target sample size was 200-400, and even then the classification rate was low. The SAME approach worked adequately, but again the regularity introduced during the edge correction caused several sample plots in the clustered and random patterns to be classified as regular. The $\hat{L}(d)$ with DIFF approach correctly identified aggregation or regularity in the point patterns, and was not significantly different ($p > 0.05$) from the CONT for 8 of the 9 pattern by sample size combinations (Table 2.4).

Although the morphing algorithm was not a panacea for scaling point processes, it did appear to offer a large improvement over use of random allocation of points during plot expansion (the RAND approach). Even with regularity "injected" into the point pattern by morphing, our results suggest that many spatial patterns can still be detected. Furthermore, additional improvements can be made by using multiple stem-mapped plots within each sampling stratum to bootstrap spatial metric estimates and get better estimates of variability across plots. However, it cannot be overlooked that the significance of clustered spatial patterns are muted and sometimes lost after using the morphing algorithm (Figure 2.3, Table 2.4).

2.6. APPLICATION

Many growth and yield studies that were initiated by the USDA Forest Service in the 1950s and 1960s were not designed to examine spatial relationships among trees

within a sample plot. Any spatial data collected was generally an afterthought and intended only to relocate trees in later surveys (Woodall and Graham 2004). As such, many of these studies use nested plots or clustered plots to increase sampling efficiency. The morphing algorithm is a tool that can help link data among nested sample plots of various scales, particularly for visualization purposes and for preliminary investigation of spatial patterns among trees. This capacity can be very important when comparing long-term patterns in stand structural development among stands subjected to different silvicultural treatments, particularly among treatments resulting in vastly different stand ages and tree sizes. For example, structural development of an uneven-aged, selection system would be driven by larger trees that are usually sampled at a much broader scale than the trees driving the structural development within a young, even-aged, shelterwood system. These differences would persist for an extended period of time, often 20 years or more, making spatial comparisons awkward or difficult during this time span.

Therefore, I tested the utility of the morphing algorithm to scale up nested sample plot data from a long-term forest inventory. Data from a USDA Forest Service long-term silviculture study at the Penobscot Experimental Forest (PEF) near Bradley, Maine (44° 52' N, 68° 38' W) were used. The PEF is predominantly an uneven-aged forest with stands dominated by eastern hemlock (*Tsuga canadensis* (L.) Carr.), balsam fir (*Abies balsamea* (L.) Mill.), eastern white pine (*Pinus strobus* L.), red maple (*Acer rubrum* L.), and paper birch (*Betula papyrifera* Marsh.). The long-term study is comparing the effects of even-aged and uneven-aged silvicultural and exploitative practices on the stand growth and structure. Further details about this study can be found in Sendak et al. (2003), Brissette (1996) or Chapter 4.

The locations of 7,883 trees within five plots in each of 10 different stands were stem-mapped using a compass, and a Haglöf DME (Haglöf 2003) or metal tape. Stands included examples of commercial clearcutting (2 compartments), five-year, single-tree selection (2), fixed-diameter limit cutting (2), 3-stage shelterwood (1), 3-staged shelterwood with precommercial thinning (1), and an unharvested control (2), one of which had extensive spruce budworm (*Choristoneura fumiferana* (Clemens)) induced mortality in the early 1980s. The USFS study used a nested, circular plot design with all trees greater than 11.4 cm (4.5 in) measured on 0.081 ha (0.20 ac) plots and all trees greater than 1.3 cm (0.5 in) measured on 0.020 ha (0.05 ac) subplots. Sample sizes were 35.5 ± 18.1 (mean ± standard deviation; range = 4 – 77) for the "large tree" plots and 122.2 ± 104.8 (range = 0 – 475) for the "small tree" subplots. Five examples of these plots are shown in Figure 2.4; maps of all 50 plots are found in Appendix B.

Expansion of the small tree subplots has been problematic when trying to describe and simulate structure across the large tree plots. Often small-scale regularity or clustering is lost when predetermined patterns are used to expand the nested plots. Therefore, the morphing algorithm using the DIFF approach, i.e., morphing with plots from the same stand was used to scale these subplots. Unlike in the above simulation study, the underlying population parameters were not known. Therefore, scaling for each subplot was simulated with the morphing algorithm 100 times and bootstraped estimates of mean CE and weighted mean $\hat{L}(d)$ (from [2.15]) were calculated. These estimates were compared to the original CE and $\hat{L}(d)$ for the unscaled subplots. Subplots with

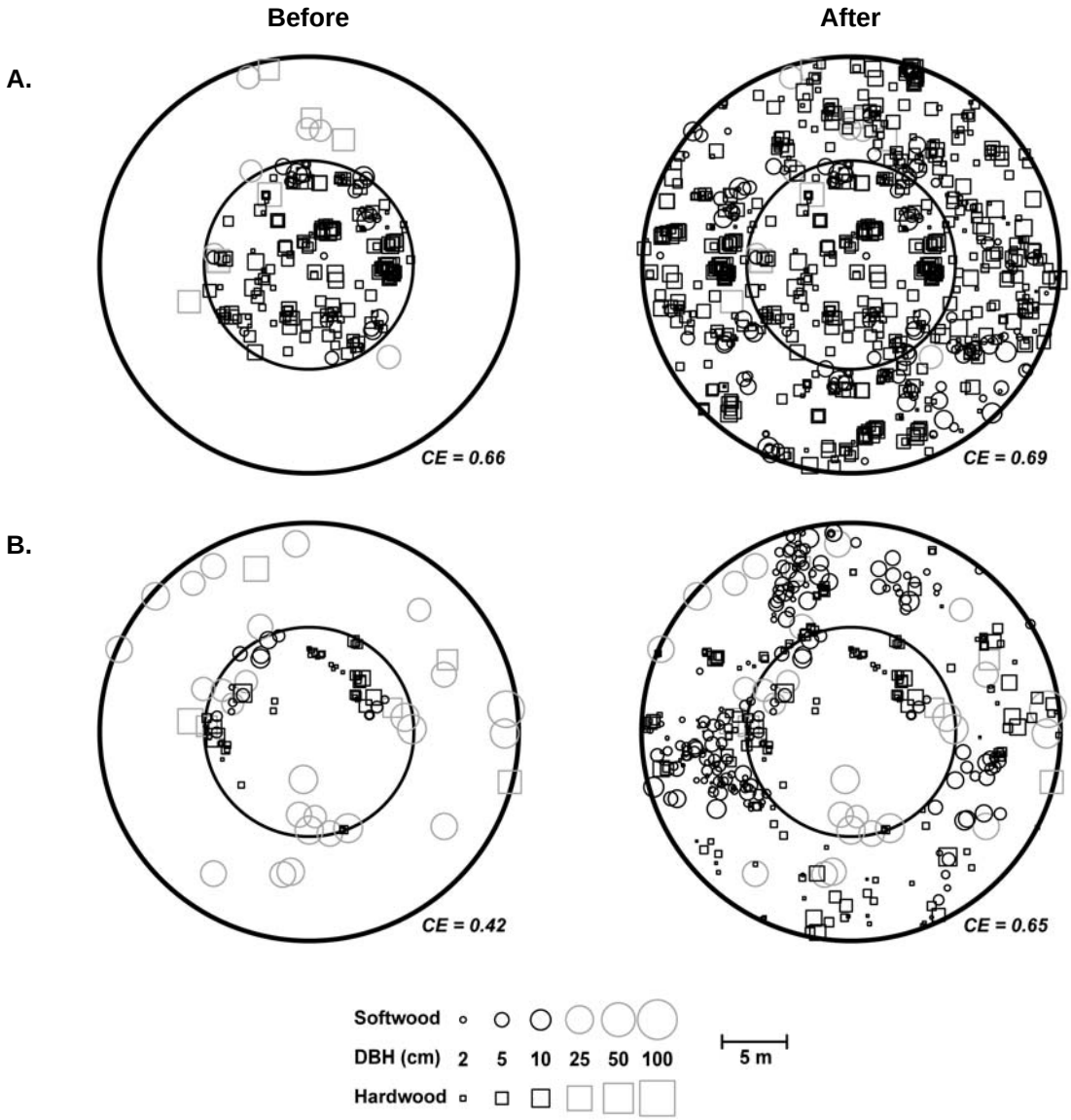

Figure 2.4. One example of a stem-mapped plot from the A) commercial clearcut, B) fixed diameter limit, C) 5-year selection, D) 3-stage shelterwood with spacing, and E) unharvested control. Maps on the left use only the measurements collected from the field; those on the right are one realization (out of 100 calculated per plot) of the morphing algorithm using different plots in the same sampling compartment to torodial wrap with. The area of point symbols is proportional to the natural log of the diameter at breast height (DBH) of the tree represented; softwood species are represented by circles and hardwood species by squares. Only trees <11.4 cm DBH were used to calculate the Clark-Evans (CE) statistic associated with each map. These trees are represented with black and the larger trees (> 11.4 cm DBH) represented in grey.

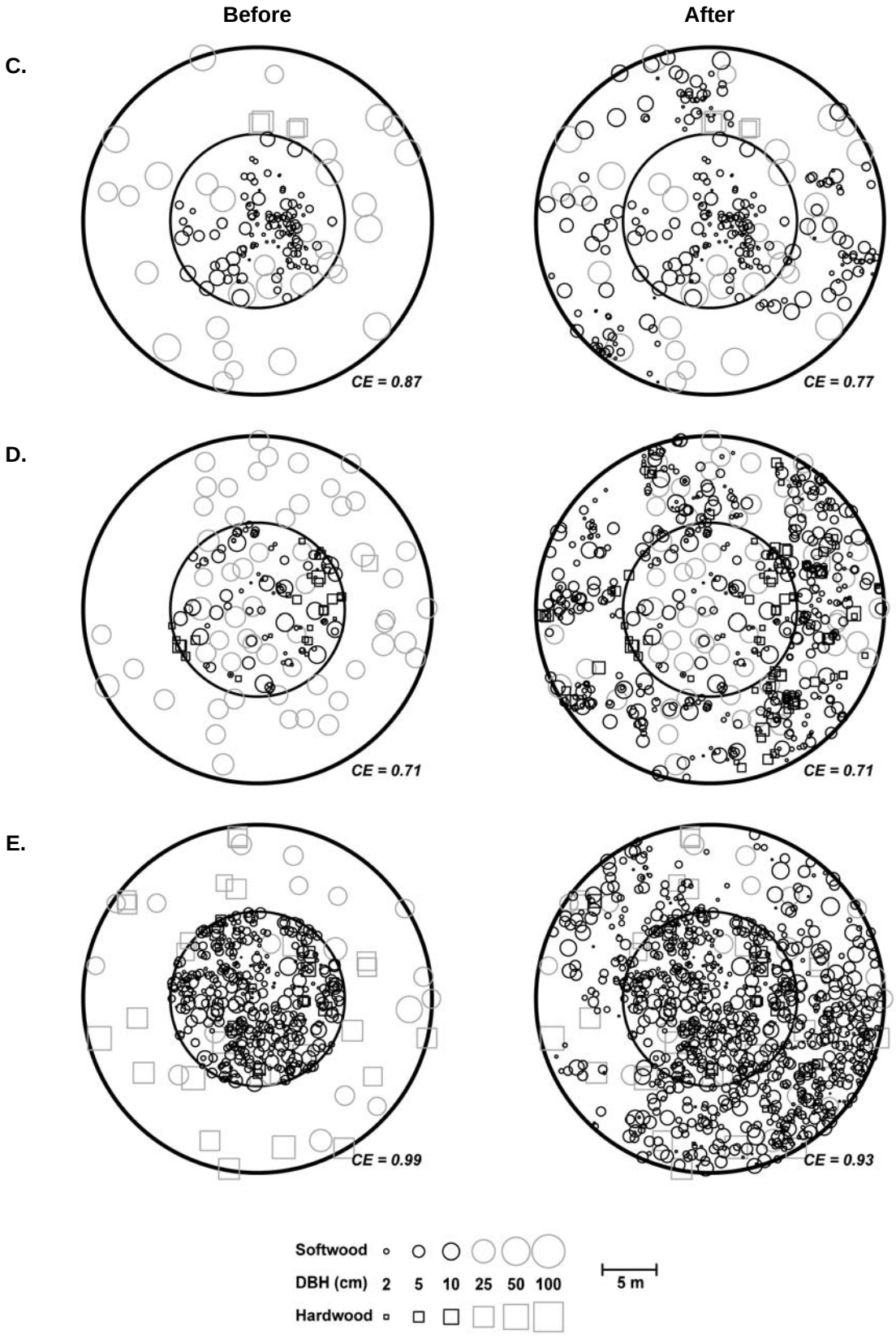

Figure 2.4. Continued.

less than 5 trees were excluded from the analysis, all of which were from one of the unharvested control stands.

Nearly all subplots showed evidence of clustering at the original scale. Specifically, the Clark-Evans statistics for the subplots (CE_{ori}) ranged from 0.438 to 1.115, with a mean of 0.766 (Figure 2.5). Many of the most extremely clustered subplots also had low numbers (< 20) of small trees, often confined to one localized area within the plot. Much of the clustering could be attributed to hardwood stump sprouts; these were especially prominent in clearcut and fixed diameter limit treatments (Figures 2.4a and 2.4b). Subplots approached a random distribution of stems only in stands with high densities of small trees (>15,000 stems/ha) that were well into the stem-exclusion phase of stand development (Oliver and Larson 1996, Figure 2.4e).

The use of morphing to scale these subplots had mixed results. For example, results from a paired t-test showed that CE_{ori} was not significantly different from the CE_{sca} calculated from the scaled subplot (t = 0.777, p = 0.442). However, a plot of CE_{ori} versus CE_{sca} (Figure 2.5) suggests that there is some bias in the procedure when comparing these estimates. This bias occurs because of the DIFF approach within the morphing algorithm; extreme CEs from subplots within a stratum are "muted" as the simulated plot approaches the average conditions as observed across the entire stand or stratum. An example is shown by Figure 2.4b, where the subplot had a low density and was highly clustered relative to other subplots within that stand. A linear regression of stand-average CE_{ori} on CE_{sca} confirmed this explanation and the relationship approached a 1:1 ratio ($CE_{sca} = 0.082 + 0.897\overline{CE}_{ori}$, $R^2_{adj} = 0.891$, F= 361).

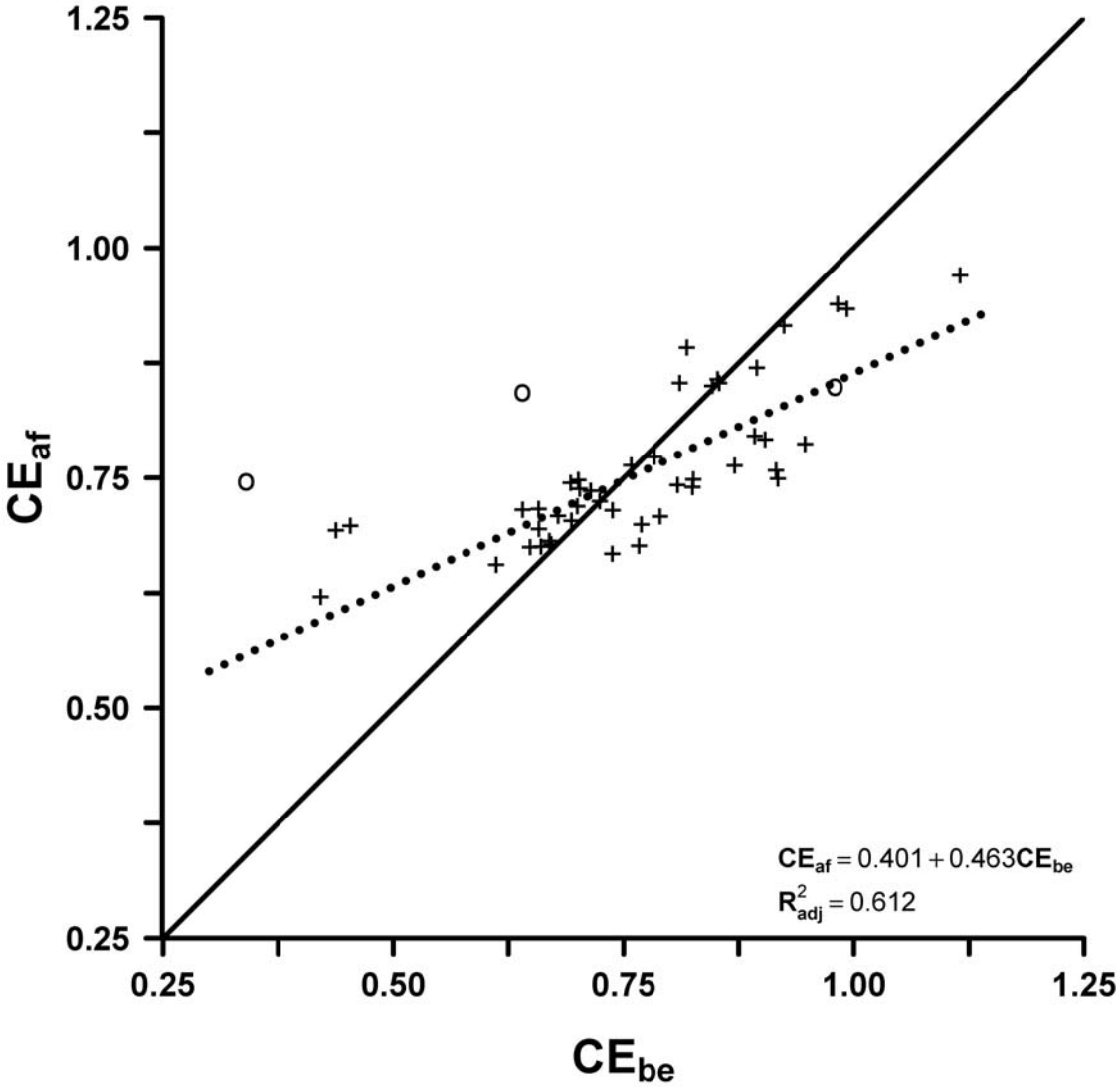

Figure 2.5. Relationship between the Clark-Evans statistic of the unscaled, 0.020 ha subplot (CE_{ori}), and the subplot as scaled to the 0.081 ha plot using the morphing algorithmn (CE_{sca}). The 1:1 line is shown by the solid black diagonal line. The regression (dotted line) excludes plots from one control stand since all 5 plots in that stand had fewer than 5 trees within each subplot and 2 of the 5 did not have defined CE_{ori}'s. Estimates from the three other plots are shown as circles.

The $\hat{L}_{sca}(d)$ after scaling consistently overestimated $\hat{L}_{ori}(d)$ calculated from the original unscaled plot (Figure 2.6). Most plots showed smoothed, less erratic changes in $\hat{L}_{sca}(d)$ as it varied by lag distance as compared to $\hat{L}_{ori}(d)$ and many $\hat{L}_{sca}(d)$ appeared to peak at distances of 3.0 – 5.0 m whereas there was no consistent "peaking" seen in $\hat{L}_{ori}(d)$. This pattern may again be a result of the muting of extreme plots by the DIFF approach and/or an artifical increase in sample size from the scaling itself. Differences between $\hat{L}_{sca}(d)$ and $\hat{L}_{ori}(d)$ were not different for lag distances below ~2.5 m suggesting that the morphing algorithm using the DIFF approach was unbiased over this range.

2.7. CONCLUSIONS

In the original work on the morphing algorithm, Williams et al. (2001) mathematically showed that the morphing algorithm was an unbiased technique for edge corrections only for stationary Poisson point patterns. While these patterns do occur in nature, I tested whether morphing could be extended to the clustered or regular distributions of trees commonly observed in unmanaged and managed stands. Results from this study suggest that morphing should not be preferred over weighting techniques based on torodial distances, like the Ripley correction for $\hat{K}(d)$, as an edge-correction technique for point-based spatial metrics unless the sample size is relatively large or the population is known not to be highly clustered (Table 2.2, Figure 2.2). However, as Williams et al. (2001, 2003) show, the morphing algorithm is adequate to approximate structural metrics where unmeasured trees outside a plot contribute to the overall value of the statistic for that plot.

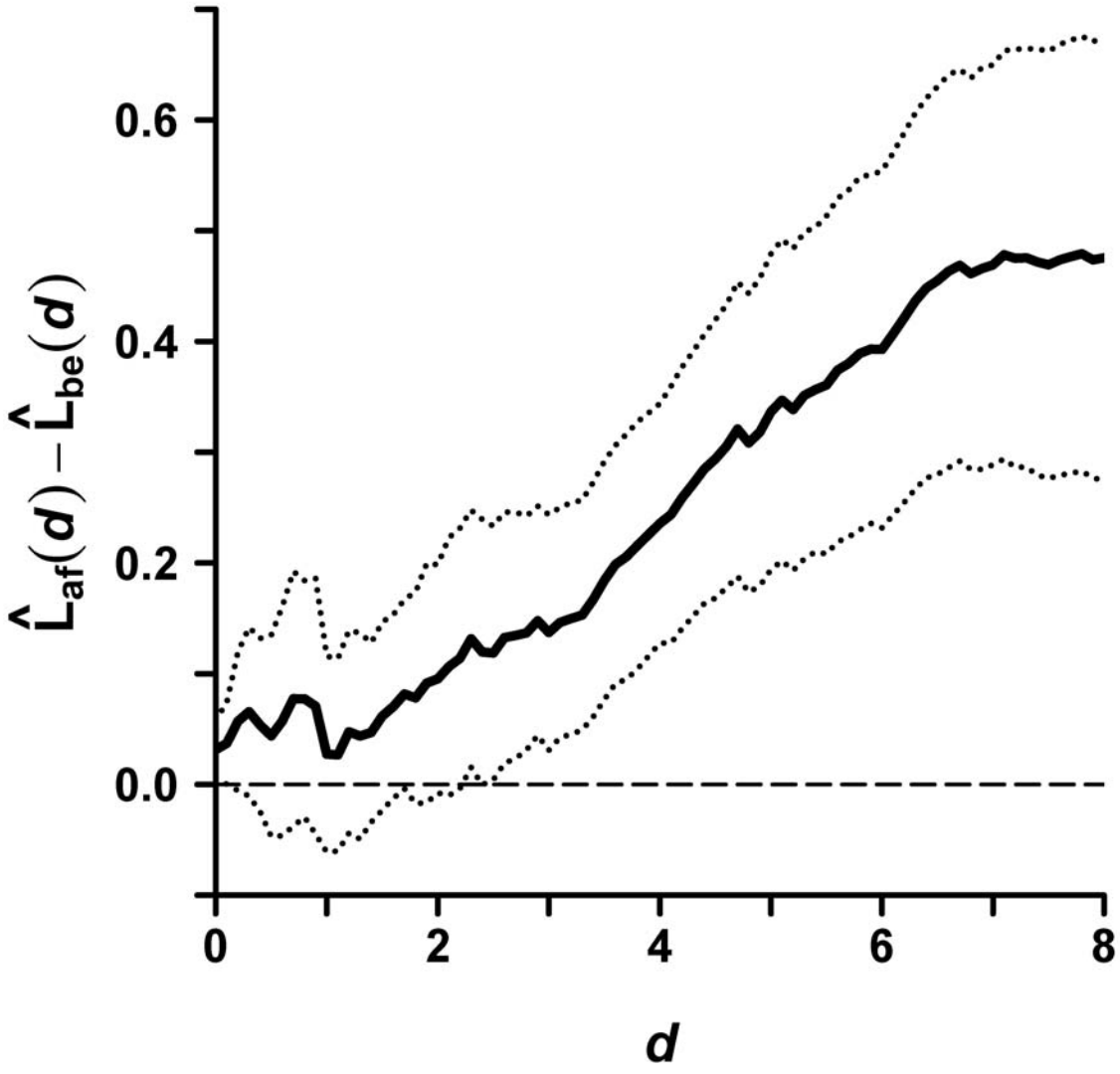

Figure 2.6. Mean difference between $\hat{L}_{sca}(d)$ and $\hat{L}_{ori}(d)$ versus lag distance (d) in m. $\hat{L}_{sca}(d)$ was calculated after morphing from the 0.020 ha subplot to the same scale as the 0.081 ha plot; $\hat{L}_{ori}(d)$ was calculated before morphing to the subplot. Dotted lines indicate ±2 standard errors.

As a scaling tool, morphing performed better, particularly if coupled with the use of different plots or subplots within the same stratum or stand for torodial wrapping within the algorithm (i.e., the DIFF approach). This approach performed significantly better than random allocation of tree stems during scaling, and approached larger, unscaled control plots in detection of clustering or regularity with either CE or $\hat{L}(d)$. However, as was shown during the application the DIFF approach to actual stands, information from individual, extreme plots may be lost during scaling, as the scaled plots will approach the average conditions observed across the entire stand or stratum.

Nevertheless, morphing can be a valuable tool that extends spatial analyses to smaller, circular plots that are common in forest inventory systems. Morphing can be used in several ways depending on the goals of study. If the scope of interest in a study is the plot, nested subplots should probably be scaled through morphing with themselves (i.e., the SAME approach) in order to preserve information on extreme plots and maintain the variability across plots. However, this approach can introduce regularity into the observed patterns (Tables 2.3 and 2.4, Figure 2.3) and interpretations would need to be adjusted accordingly. If the scope of interest is at the stand level, as is common in most forest inventory designs, nested subplots should be scaled with the DIFF approach and means and variances for all spatial metrics of interest should be approximated using bootstrapping or Monte Carlo methods (Diggle 2003). Ideally, the number of subplots should be large enough to assure that multiple realizations of the same pattern are not observed during the morphing procedure. If this is not the case, and the spatial data are isotropic (i.e., no directional trends), the circular subplots could be randomly rotated

when used for torodial wrapping. This approach will reduce the possibility that the same "side" of a subplot is used during the DIFF approach.

Lastly, morphing is not appropriate if the spatial arrangement among trees measured at different scales must be critically maintained during scaling of subplots. In this case, the only option available is the spatial analysis of tree locations shared among the plots and all nested subplots. Results from these analyses can then be used to simulate the subplot data across the entire plot, adjusting subplot positions to maintain proper spatial arrangement among tree types. This approach would be quite daunting, both because it is uncommon in these inventories to have large enough sample sizes of each tree type of interest to accurately determine spatial relationships among all types, and because it is computationally demanding as the number of types and plots increase.

Chapter 3

SPATIAL RECONSTRUCTION AND STRUCTURAL DYNAMICS OF ACADIAN MIXEDWOOD STANDS TREATED WITH VARIOUS SILVICULTURAL AND CUTTING METHODS

3.1. ABSTRACT

Using current and past inventory data from 10,225 stem-mapped trees, allometric relationships and a morphing algorithm, spatial reconstruction models were developed to analyze structural changes from 1974-2002 within 50 nested inventory plots across ten compartments of a long-term silvicultural experiment at the Penobscot Experimental Forest in east-central Maine. Differences in spatial pattern, species mingling, height differentiation, and relative stand complexity index (*rSCI*) were compared among five treatments: commercial clearcutting, fixed diameter-limit harvesting, 5-year selection system, 3-stage shelterwood (both with and without precommercial thinning), and an unharvested natural area. Regardless of treatment, regeneration events, whether induced through natural stand breakup or by harvesting, increased aggregation in spatial pattern and reduced species mingling. This pattern was heightened in the commercial clearcut and fixed diameter-limit harvest where hardwood densities were much higher. Regular spatial patterns were rare, occurring only in trees >11.4 cm diameter and within the two most recent inventories of a precommercially thinned shelterwood. Both differences among height differentiation values for individual trees and compartment-level average *rSCI* were generally highest in the natural areas and 5-year selection compartments, intermediate in commercial clearcut and fixed diameter-limit compartments, and lowest in 3-stage shelterwood compartments. After a short adjustment period, precommercial

thinning in a shelterwood compartment generally increased mingling, height differtiation, and *rSCI*. Results suggest that the natural areas represent two divergent, yet common, pathways of structural development in northeastern forests, and that uneven-aged management more closely resembles these dynamics than either shelterwood, commercial clearcut or fixed diameter-limit harvests.

3.2. INTRODUCTION

Forest management, through silvicultural intervention, has profound effects on stand structure and ecosystem function (Smith et al. 1997, Pommerening 2002, Kint et al. 2003). Obviously, silvicultural treatment can increase or decrease species diversity, change spatial pattern among stems or species, and/or change the size distribution of trees within the stand (Buongiorno et al. 1994, Solomon and Gove 1999, Sendak et al. 2003, Montes et al. 2005). For example, some traditional approaches to even-aged regeneration methods (i.e., silvicultural clearcut, uniform shelterwood, and seed-tree harvests) that do not retain legacy structures homogenize stand structure and, when applied broadly in some ecosystems, reduce landscape-level biodiversity over time (Seymour and Hunter 1999, O'Hara 2001, Lindenmayer and Franklin 2002). Intermediate treatments used within these same even-aged silvicultural systems may increase, but more likely reduce structural diversity by removing undesirable species and redistributing growing space more equally among residual stems (Seymour and Hunter 1999, Homyack et al. 2004). Uneven-aged systems are thought to retain high amounts of structural diversity, but in fact, may lead to structures as artificial as those created with even-aged methods (O'Hara 1996, Seymour and Kenefic 1998, Schütz 1999), particularly if the natural disturbance regime of the ecosystem is driven by stand-replacing events and/or if the selection system

does not explicitly maintain snag and downed woody material components. As a result, reducing uniformity in the application of silvicultural systems, either even- or uneven-aged, through retention of key stand structural elements is a significant paradigm shift in federal land management throughout much of the United States (Zenner 2004, Seymour et al., in press), and is one of the key tenets of the emerging subdiscipline of ecological or disturbance-based silviculture (Seymour and Hunter 1999). Maintainence and creation of structural complexity to protect ecosystem function and biodiversity increasingly dominates much of our silvicultural thinking (Schülz 1999, O'Hara 2001, Franklin et al. 2002, Palik et al. 2002, Zenner 2004, Frelich et al. 2005).

Traditionally, effects of silviculture on stand structure have been quantified by changes in species composition, basal area, stand density, and/or tree diameter distributions. It is now recognized that these variables, while important, do not adequately describe structural complexity, which explicitly depends upon the spatial pattern or position of tree stems, the mingling or intermixing of tree species, and the size differentiation among neighbors (Pommerening 2002, Kint et al. 2003, Zenner 2004). For example, Gadow and Hui (1999) give examples of theoretical stands that have identical basal areas, densities, and diameter distribution, but differ by spatial arrangement. These stands have vastly different structures, which both affect the inference on how each stand formed and what silvicultural options may exist for future management of each stand.

The spatial pattern of tree positions has been widely studied, most often in late-successional and old-growth stands. Spatial pattern influences both light regimes and regeneration patterns (Ward et al. 1996, Grassi et al. 2003) and is directly tied to plant

community dynamics and succession (Watt 1947). Early in stand development, regeneration processes commonly lead to aggregation of individuals in the stand at relatively short spatial scales either through the regenerative mechanism itself (e.g., vegetative reproduction), the disturbance agent, and/or environmental heterogenity (Phillips and MacMahon 1981, Skarpe 1991, Taylor and Halpern 1991, Mast and Veblen 1999). As stands age and individual tree sizes increase, the spatial distribution at fine spatial scales tends towards random and slightly regular distributions through density-dependent mortality due to competition between conspecifics (Greig-Smith and Chadwick 1965, Kenkel 1988, Mast and Veblen 1999). As stands enter understory reinitiation and progress into old growth development stages (Oliver and Larson 1996), overall spatial pattern across broader scales may again become clustered as regeneration processes in canopy gaps increase (Armesto et al. 1986, North et al. 2004), but spatial pattern among the original cohort at short spatial scales will usually remain random or slightly regular as density-independent mortality increases (Szwagrzyk and Czerwczak 1993), unless disturbance agents act in a spatially aggregated way (Fúle and Covington 1998). Interestingly, strongly regular patterns have been rarely observed in naturally regenerated stands except when density-dependent competition is extremely high and/or canopy disturbances are absent for an extended period of time (Phillips and MacMahon 1981, Kenkel 1988, Ward et al. 1996), and they usually are detected only at shorter scales that are indicative of the crown radius of the larger individuals (Pielou 1962, North et al. 2004, Koukoulas and Blackburn 2005, Motta and Edouard 2005).

Spatially explicit analysis of mingling during forest development is much less common, generally confined to identifying scales at which species pairs are attracted or

repulsed/segregated by one another (e.g.., bivariate $K_{12}(d)$ functions and the segregation index S [Pielou 1977]). Nevertheless, these bivariate relationships can be an important clue to processes that are driving spatial pattern. For example, Peterson and Squiers (1995) reported slightly significant repulsion between overstory aspen and understory eastern white pine, suggesting that clonal tendencies of aspen could competitively inhibit understory establishment of white pine. Although powerful, bivariate tests become much less useful in species-rich stands where the number of species pairs become exceedingly large and the stem densities decline. Indices that integrate mingling across the entire pattern—like *DM* (von Gadow and Hui 1999)—are better suited to quantifying structural development in these cases (Kint et al. 2003). One would expect changes in species mingling in unmanaged, even-aged communities to be largely controlled by the heterogeneity of site conditions. Competition among individuals on homogeneous sites would generally lead to relatively few species dominating the stand throughout stem-exclusion; therefore, mingling levels would decrease as species richness decreased. Conversely, competition among individuals on heterogeneous sites would generally maintain higher species diversity and higher mingling through stem-exclusion, although this would depend on reproduction patterns and the grain of the heterogeneity. During understory-reinitiation and old growth development stages, species mingling should increase as more species become established (Oliver and Larson 1996), although the pattern and grain of canopy disturbances may blur this trend.

Stand development theory (Oliver and Larson 1996, Franklin et al. 2002) suggest that size differentiation should be realitively low from stand initiation through the end of competitive exclusion of the overstory, and generally increase after this point. In a

spatially explicit context, however, differentiation indices like *TH* (von Gadow and Hui 1999) might not show a continuous increase as a stand progressed into old growth development stages; essentially they would be maximum when the size distribution of the stand was roughly bimodal, or when an understory stratum was well developed. However, the point at which a differentiation index peaks during development would depend on several factors including: 1) the size variable used—height growth peaks sooner than diameter growth, therefore differentiation should peak sooner if calculated with height; 2) the grain of density-independent mortality events—death of very large individuals would allow large patches of similar-sized trees to regenerate; and 3) differences in growth characteristics between the older and younger cohorts—for example, mountain ash forests of Australia often lack tolerant species that can develop into any significant canopy to replace the ash and, therefore maintain a bimodal distribution late into development (Franklin et al. 2004).

While there have been numerous studies describing spatial pattern in forests, relatively few have tracked changes in pattern over time or accessed the effect of different silvicultural and harvesting methods on spatial indices. Some studies have relied on temporary sample plots that cover a chronosequence or several stages of stand development (Franklin et al. 2002, Grassi et al. 2003, Zenner 2004), but these approaches often ignore individual stand histories (Montes et al. 2005). Many studies have reconstructed spatial pattern by stem-mapping of both live and dead stems and using dendrochronological techniques to date mortality events (Harrod et al. 1999, Mast and Veblen 1999, Motta and Edouard 2005). Inference in these studies, however, is often limited to the largest size classes, since smaller size classes have decayed and are not

represented in stem reconstructions. Repeat measurements on permanent plots are ideal, particularly if measurements are often enough to document silvicultural entries or natural disturbance events. These datasets are exceedingly rare, particularly at the larger scales ($\geq$ 0.5 ha) used in most spatial analyses (e.g., Peterson and Squiers 1995, Ward et al. 1996).

This study focuses on the structural development of mixed conifer stands in the Acadian ecoregion of North America. Through stem-mapping and modeling with a morphing algorithm (Chapter 3), spatial-explicit structure for approximately 30 years was reconstructed on 50 inventory plots within a long-term silviculture experiment in the Penobscot Experimental Forest in Bradley, Maine. The primary objective was to describe differences in structural development over time in management compartments previously treated by commercial clearcutting and fixed-diameter-limit harvest, 3-stage shelterwood and 5-year selection regeneration methods, and an untreated natural area. A secondary objective was to test the adequacy of the stand complexity index (SCI; Zenner and Hibbs 2000) which integrates spatial pattern and size differentiaion. I hypothesized that:

1) Spatial pattern after any harvest treatment would generally be more aggregated for both small and large individuals than in the unmanaged compartments. However, without further disturbance, pattern in any compartment should become more regular over time.

2) Species mingling, as measured by *DM*, should be higher in unmanaged stands and stands with uneven-aged structures (selection) than even-aged management (shelterwood) or exploitative harvesting (commercial clearcut, diameter-limit).

3) Size differentiation, as measured by *TH*, should be higher in unmanaged and uneven-aged stands than in either even-aged stands or stands with exploitative harvesting.

4) Structural complexity, as measured with SCI, will be highest in unmanaged and uneven-aged stands, lowest under even-aged management, and intermediate with exploitative harvesting.

3.3. METHODS

3.3.1. Study Area

This study took place on the Penobscot Experimental Forest (PEF) located near the town of Bradley, Maine (44° 49' 30" N, 68° 38' 00" W), and managed conjointly by the University of Maine and the USDA Forest Service—Northeastern Forest Experiment Station. The PEF lies in the Acadian Forest, an ecotone between the boreal forest of Canada and northern hardwood forests of southern New England (Brissette 1996). Climate is cool and humid with average temperatures ranging from –7.7 ºC in January to 20.0 ºC in July, and precipitation averaging 106 cm, approximately half of which falls as snow (Brissette 1996, Sendak et al. 2003). Soil types are derived from glacial till and ranging from well-drained loams and sandy loams on glacial till ridges to poorly and very poorly drained loams and silt loams in flat areas between the ridges. Soils are typically quite fine-grained and extremely variable within a site, as till ridges, flats and streams fall often fall within close proximity of one another (Brissette 1996).

Forest types within the PEF are mixedwoods, but usually dominated by Acadian Region softwoods (Sendak et al 2003). These include red (*Picea rubens* Sarg.), white (*P. glauca* (Moench) Voss) and black spruce (*P. mariana* (Mill.) B.S.P.), balsam fir (*Abies balsamea* (L.) Mill.), eastern white pine (*Pinus strobus* L.), eastern hemlock (*Tsuga canadensis* (L.) Carr.), and northern white cedar (*Thuja occidentalis* L.). Red pine (*Pinus resinosa* Ait.) and tamarack (*Larix laricina* (Du Roi) K. Koch) occur less frequently,

usually in stands that experienced a fire or very severe canopy disturbance. Several hardwoods are close associates in these cover types, often increasing in abundance after exploitative harvesting (Kenefic et al. 2005a). These include red maple (*Acer rubrum* L.), paper (*Betula papyrifera* Marsh.) and gray birch (*B. populifolia* Marsh.), and quaking (*Populus tremuloides* Michx.) and bigtooth aspen (*P. grandidentata* Michx.). Sugar maple (*Acer saccharum* Marsh.), yellow birch (*Betula alleghaniensis* Britt.), American beech (*Fagus grandifolia* Ehrh.), northern red oak (*Quercus rubra* L.), white ash (*Fraxinus americana* L.), black cherry (*Prunus serotina* Ehrh.), and basswood (*Tilia americana* L.) are infrequent to rare associates, particularly on higher quality sites, within the PEF.

Typically, natural stand structures in this region are irregularly uneven-aged resulting from partial canopy disturbances such as senescence, wind, ice storms, pathogens and insect herbivory. Disturbance frequencies average 0.7-1.3% per year (Runkle 1982, Seymour et al. 2002). Large-scale, stand-replacing disturbances, such as fire or major wind events, have return intervals of 250-800 years or more (Lorimer 1977, Seymour et al. 2002).

3.3.2. Long-Term Study

From 1952-1957, the USDA Forest Service (USFS) installed a replicated study to investigate the influences of silviculture and exploitive harvesting practices on the composition, growth, yield, and structure of mixed northern conifer stands (Sendak et al. 2003). Eight treatments were randomly assigned to one of sixteen 6.6 - 17.5 ha management compartments: 5-, 10-, and 20-year single-tree selection systems, 2- and 3-stage uniform shelterwood systems, fixed and flexible diameter-limit harvests, and

unregulated commercial clearcutting. In the early 1980s, both 3-stage shelterwood compartments were split to investigate the influence of precommercial thinning (PCT) on stand development. In addition, an unmanaged natural area was later set aside as a "pseudo-control" for the experiment; this compartment was split in 1993 when it had developed into two distinct stands. Marking prescriptions and harvesting techniques and timings for each treatment are described extensively in Sendak et al. (2003).

The history of the PEF before 1950 is not well documented, but the forest was thought to be irregularly uneven-aged as a result of natural stand development confounded with periodic partial harvesting (Sendak et al. 2003). A sawmill operated within the boundaries of the forest throughout much of the 1800s; pine and spruce were likely preferentially harvested from much of the forest during this period. The spruce budworm epidemic of the 1913-1919 also had a significant influence on pre-treatment species composition (Seymour 1992). Regardless, initial conditions throughout much of the northern half of the PEF were relatively constant, differing only slightly by the domination of spruce-fir or hemlock in the initial stocking inventories (Figure 3.1; Sendak et al. 2003). Therefore, since this area was regarded as an individual stand, nearly all changes in species composition and structure can be attributed to treatment effects (J. Brissette, pers. comm.).

This USFS study is one of the oldest continuously monitored silvicultural experiments in the United States (Seymour et al., in press). Tree inventories have been conducted within compartments before and after every cutting treatment and approximately every five years thereafter since the study's inception. A systematic grid (with a random start) of 8 – 21 permanent sample points is located within each

Figure 3.1. Two views of the initial stand conditions during the establishment (1952-1957) of USDA Forest Service's long-term silvicultural experiment in the Penobscot Experimental Forest, Bradley, ME.

compartment. Diameter and condition of all trees >11.4 cm diameter at breast height (dbh = 1.35 m) were measured within 0.081 ha (0.2 ac) circular plots; saplings between 1.2 and 11.4 cm dbh were measured in a concentric 0.020 ha (0.05 ac) circular subplot (Sendak et. al 2003). Beginning in 1974, individual trees and saplings within each plot were labeled using a systematic numbering scheme creating a longitudinal record of tree growth and mortality.

3.3.3. Field Measurements

This study focused on structural development within 10 compartments assigned to one of five treatments. Management treatments included two exploitative harvests, unregulated commercial clearcutting and fixed diameter limit harvests, and two silvicultural systems, 5-year selection and 3-stage shelterwood, both with and without spacing treatments. An unmanaged natural area was used as control. Prior USFS inventories and cutting entries for these compartments are shown in Figure 3.2.

From June 2001 through August 2002, 10,225 living and dead tree and sapling positions were located and mapped for five of the nested overstory/sapling plots in each compartment (50 plots total). These mapped plots were randomly chosen from all USFS inventory plots within a compartment with the restriction that chosen plots must be at least 20 m away from any permanent access road whenever possible. Dead tree or sapling positions were recorded by comparing stump locations and diameters to past USFS numbered tree lists for that plot; this reliably located between 15 – 85% of all dead stems, depending on compartment (Table 3.1). Azimuths were taken with hand compass and distances from plot center were taken with a Haglöf DME (Haglöf 2003). Positional errors increased with distance from plot center, but were generally no more than 0.25 m. Diameter at breast height was measured to the nearest 0.1 mm with calipers or metal tape, and condition (i.e., cull, declining, leaning stem, etc.) was recorded. Crown measurements were taken for each crown quadrat as defined by the four cardinal directions. Total tree or sapling height and the lowest live branch (continuous to the upper crown) were measured to the nearest 0.1 m either directly, using 10 and 15 m telescoping height poles, or as an average of 2-4 readings from a Haglöf hypsometer (Haglöf 2002). Crown radius in each quadrat were measured to the nearest 0.1 m using a metal tape.

3.3.4. Spatial Reconstruction Model

Three steps were used to reconstruct the structural development of the stands in each compartment. First, the height development of all past and current trees and saplings on each plot had to be reconstructed from the field measurements as the USFS

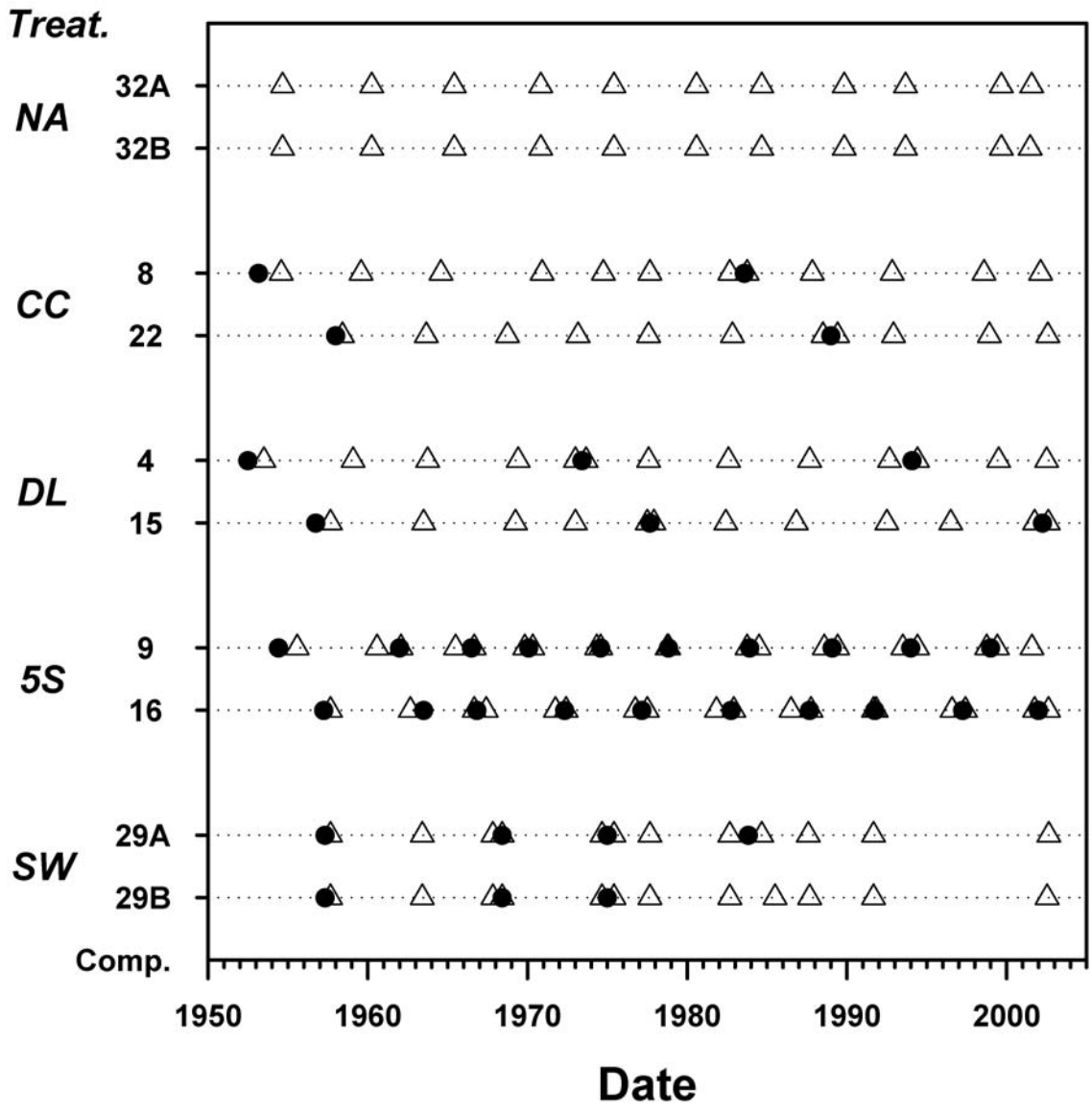

Figure 3.2. Inventory dates (open triangles) and harvest entries (filled circles) for the 10 USFS management compartments used in this study. Treatments include an unmanaged natural area (NA), commercial clearcutting (CC), fixed diameter-limit harvesting (DL), five-year selection system (5S) and three-stage shelterwood (SW). Compartments 29A and 29B are a split compartment that differ only by the precommercial thinning that took place in 1983.

Table 3.1. Number of locations and relocation rates for management compartments of the natural area (NA), commercial clearcut (CC), fixed-diameter limit (DL), the 5-year selection (5S) and the 3-stage shelterwood (SW). Low relocation rates in Compartment 29A is primarily from a precommercial spacing treatment in 1981.

Treat-ment	Compart-ment	Locations			Relocation Rates (% of)		
		Living	Dead	Unknown	Total	Dead	Dead > 11.4 cm dbh
NA	32A	1268	194	64	95.8%	75.2%	81.7%
	32B	309	79	20	95.1%	79.8%	88.0%
CC	8	888	326	800	60.3%	29.0%	41.6%
	22	962	307	646	66.3%	32.2%	47.8%
DL	4	814	314	362	75.7%	46.4%	79.0%
	15	410	255	241	73.4%	51.4%	73.3%
5S	9	394	205	175	77.4%	53.9%	75.8%
	16	422	154	128	81.8%	54.6%	75.5%
SW	29A	891	72	401	70.6%	15.2%	42.9%
	29B	1625	336	59	97.1%	85.1%	80.0%

had not collected height information during most of their inventories. The Chapman-Richards growth function was used in these modeling efforts:

$$HT = 1.35 + a\left[1 - \mathrm{e}^{(b \cdot DBH)}\right]^{c} + \varepsilon \qquad [3.1]$$

where HT is tree height in m, DBH is tree diameter at breast height in cm, *a*, *b*, and *c* are estimated parameters, and $\varepsilon \sim N(0, \phi)$. There were several modeling approaches taken. For nine tree species that had n >100 and that occurred across a majority of stands and plots, multi-level, mixed-effects models were developed to estimate plot-specific and compartment-specific *a* and *c* parameters; this increased model precision dramatically (see Chapter 2). For most remaining species, generalized nonlinear least squares (GNLS) regression was used to fit [3.1]; based on preliminary fits and scatterplots, some species were further grouped for analysis to allow better convergence of the final models. Lastly, early inventories in the USFS data used broad species groups that were dropped or

refined in later inventories (e.g., "soft hardwoods" were later separated into black ash, trembing aspen, basswood, gray birch, black cherry, pin cherry, and elm spp.); GNLS models were developed using those same species groupings with the field data collected in this study. Parameter estimates and fit statistics for the mixed-effects and GNLS models are presented in Tables 1.2 [Model II] and 3.2, respectively.

Height reconstructions of living trees and saplings use a modified proportional adjustment (MPA) that allows individual trees to grow proportionally more or less than the average tree or sapling as defined by the studywide, compartment-level, or plot-level models. This approach had the advantage of smoothing deviations from the average height development pattern. Therefore:

$$HT_i^* = MPA\left(HT_i - 1.35\right) + 1.35 \qquad [3.2]$$

where HT_i^* is the adjusted height prediction of the tree or sapling in inventory *i*, HT_i is the predicted height in inventory *i* from the plot-, compartment- and/or species-specific height equations, and:

$$MPA = \left(HT_{obs} - 1.35\right) / \left(HT_{pred} - 1.35\right) \qquad [3.3]$$

where HT_{obs} is the observed tree or sapling height and HT_{pred} is the predicted tree or sapling height using the dbh measured in this study. Dead and unlocated trees and saplings were assumed to follow the average height development patterns and, therefore, did not use MPA. Trees and saplings with broken tops were also assumed to follow average height development patterns until they reached HT_{obs}.

The next step in model development was simulating the location of all trees and saplings from the USFS inventories that could not be relocated during field measurements for this study. Tree numbering protocols within USFS inventories were

Table 3.2. Chapman-Richards height-diameter models (Equation 3.1) for less common species measured in this inventory and for archived USFS species categories. All models fit with general nonlinear least squares (Pinherio et al. 2005) and weighted by $1/\sigma^2$, if necessary, to reduce heteroscedasticity.

Species Group	n	a	b	c	MSE	R^2
Fagus grandifolia	26	8.45	0.116	0.94	0.0589	0.863
Picea glauca[1]						
Treatments NA & 5S	18	33.24	0.052	1.75	0.7312	0.925
Treatments CC, DL, & SW	26	17.02	0.047	1.12	0.1517	0.972
Thuja occidentalis	98	32.62	0.017	0.97	0.6266	0.796
Acer saccharum *Betula alleghaniensis* *Fraxinus americana* *Populus grandidentata* *Quercus rubra*	23	53.92	0.006	0.65	0.0755	0.928
Fraxinus nigra *Ostrya virginiana* *Prunus pensylvanica*	18	8.23	0.261	1.20	0.1903	0.815
Larix laricina[2] *Pinus resinosa* *Pinus* spp.	189	40.19	0.026	1.30	2.7890	0.914
"Soft" hardwoods[3]	382	19.57	0.078	0.99	0.2590	0.887
"Hard" hardwoods[4]	47	52.62	0.005	0.65	0.1423	0.804

[1] There was substantial difference in growth between older and younger age structures for this species.

[2] Sample sizes were inadequate and scatterplot suggested that the growth patterns were similar to *Pinus strobus*. Results are the pooled GNLS model.

[3] Old USFS category. Results are a pooled GNLS model for *Populus tremuloides*, *Populus grandidentata*, *Fraxinus nigra*, and *Betula populifera*.

[4] Old USFS category. Results are a pooled GNLS model for *Fraxinus americana*, *Fagus grandifolia*, *Betula alleghaniensis*, *Ostrya virginiana*, *Acer saccharum*, and *Quercus rubra*.

systematic based on azimuth, distance from plot center and tree size. Trees and saplings had three numbers. The first number (0 – 9) refers to the 36° pie section of the plot the tree or sapling is located within; the second and third numbers refer to the distance in feet (distance class) from the plot center to the center of the tree or sapling. If more than one tree and/or sapling occurred at the same distance in a pie, adjacent numbers or numbers above 54 (the radius of the large tree plot in feet) were assigned (R. Dionne, pers. comm.).

Exploratory analysis of the USFS numbering scheme using known tree positions showed the 36° pie sections to have the appropriate width (deviating the most in the CC treatment), but usually rotated from true north (range across plots: -39.6° to +44.5°). Since isotropy was assumed for all spatial analyses, the plots were "rotated" to remove bias and more closely approximate the USFS protocols. Random azimuths were then chosen from a uniform distribution in each pie class for all unknown locations. There was a relationship between the distance class and the distance to plot center, but the variation was quite high. Instead, pooled 10' distance classes were more robust and they differed for saplings and trees (Table 3.3). A "reflected" normal distribution (i.e., simulated distances < 0 or greater than a plot or subplot radius were reflected back into the plot or subplot) closely approximated the distribution of distances observed. Positions of trees and saplings that were known to deviate from distance protocols (a second digit above 5 and 2, respectively) were simulated using a uniform distribution from 0 to the plot or subplot radius.

The last step in model development was to scale the sapling subplot (0.020 ha) up to that of the tree plot (0.081 ha). I used a modified version of the morphing algorithmn (Williams et al. 2003, Chapter 3) to remap the locations of the sapling plot from the

Table 3.3. Distributional statistics for location types and distance classes within the stem-mapped trees of this study. These statistics were used to simulate unknown locations within the spatial analyses.

Location Type	Distance Class	Mean (m)	S.D. (m)
Sapling (dbh ≤ 11.4 cm)	0' – 10'	2.51	1.36
	10' – 20'	4.66	1.10
	20' – 26.3'	6.65	1.08
Tree (dbh > 11.4 cm)	0' – 10'	2.13	0.72
	10' – 20'	4.63	0.93
	20' – 30'	7.48	1.08
	30' – 40'	10.61	1.17
	40' – 50'	13.46	1.27
	50' – 52.7'	15.16	1.24

Euclidean space C with origin (0,0) and radius of r (= 8.05 m) to a square space D of equal area and a side length of $r\pi^{0.5}$. The normal morphing algorithm then proceeds by torodial wrapping D with copies of itself to create a 3 x 3 array. This array is then "demorphed" back to Euclidean space to a circle of radius $3r$ and can be trimmed to any scale between r and $3r$. I deviated from the normal algorithm in two ways. First, I randomly selected with replacement all subplots (C_i) within the same management compartment as the focal subplot for torodial wrapping within the algorithm; in other words, D could now be wrapped with copies of itself or with any other D_i from that compartment. Saunders (Chapter 3) reported that this technique was superior to the normal morphing algorithm for multiple plot analysis, generally reducing the regularity brought into the simulated pattern as normally happens with torodial wrapping. Second, all C_i's were rotated before morphing by adding a random azimuth to locations. This

reduced the chance that the same "side" of a subplot would be used again during the wrapping procedure, thereby further reducing induced regularity in the simulated pattern. However, the rotation required an assumption of isotrophy in the pattern and analysis.

3.3.5. Statistical Analysis of Structural Dynamics

Forest structure has three major characteristics—species diversity and mingling, spatial distribution of tree positions, and variation in tree dimensions like diameter or height (Pommerening 2002, Aguirre et al. 2003, Kint et al. 2003)—that can be measured using a variety of spatially independent and/or spatially dependent variables. Spatially independent variables summarized in this study include temporal changes in basal area, stand density, species composition, and diameter distribution, among the compartments and treatments. Spatial-dependent variables that were summarized included the Clark-Evans nearest neighborhood index (*CE*; Clark and Evans 1954), the *K(d)* function (Ripley 1976, 1977), the mingling index (*DM*; von Gadow and Hui 1999), and the size (height) differentiation index (*TH*; von Gadow and Hui 1999). In addition, the stand complexity index (*SCI*; Zenner and Hibbs 2000) was used to characterize three-dimensional physiognomic (i.e., positional) structure.

3.3.5.1. Clark-Evans Nearest Neighbor Index

The Clark-Evans nearest neighbor index (*CE*) is a ratio of the mean nearest neighbor distances in any spatial pattern (r_A) to that mean distance (r_E) expected under complete spatial randomness (*csr*). As defined by (Clark and Evans 1954), *CE* is biased from edge effects as points near the perimeter of the plot having longer nearest neighbor

distances than would be expected under *csr*. Therefore, a correction to r_E must be incorporated to account for edge effects (Donnelly 1978). *CE* is then calculated as:

$$CE = \frac{r_A}{r_E} = \frac{\frac{1}{\mathrm{N}}\sum_{i=1}^{N} r_i}{0.5\left(\frac{A}{N}\right)^{1/2} + 0.0514\frac{P}{N} + 0.041\frac{P}{N^{3/2}}} \qquad [3.4]$$

where r_i is the distance between tree *i* and its nearest neighbor, *N* is the total number of points in the pattern, *A* is the area, and P is the perimeter. *CE* ranges from 0 for completely aggregated points to 1 for *csr* to 2.1491 for perfectly regular hexagonally distributed points (Clark and Evans 1954, Kint et al. 2003). Significances of departure of *CE* from *csr* are tested with a standard, normal variate defined as:

$$c = \frac{r_A - r_E}{\sigma_{r_E}} \text{ where } \sigma_{r_E} = \frac{0.26136}{\sqrt{N \cdot \lambda}} \qquad [3.5]$$

where λ is the density of the point pattern (Clark and Evans 1954).

3.3.5.2. *K(d)* Function

A commonly used statistic in spatial point-pattern analysis, the *K(d)* function describes the spatial pattern as it relates to distance within the extent, or region of interest (Ripley 1976, 1977). *K(d)* is defined as the expected number of points within distance *d* of an event, relative to the overall density (λ) of the point process. *K(d)* is estimated from the distances (d_{ij}) between all points in the extent (Moeur 1993, Diggle 2003):

$$\hat{K}(d) = \frac{A}{N(N-1)}\sum_{i=1}^{N}\sum_{\substack{j=1 \\ i \neq j}}^{N} w_{ij}^{-1} \cdot I(d_{ij}) \qquad [3.6]$$

where

$$I(d_{ij}) = \begin{cases} 1 \text{ if } d_{ij} \le d \\ 0 \text{ if } d_{ij} > d \end{cases}$$

for $d > 0$, and w_{ij} is an edge-correction defined as the proportion of the circumference of a circle centered on point *i* and passing through point *j* that is inside *A* (Ripley 1976, as modified by Diggle 2003). $\hat{K}(d)$ is typically calculated for evenly spaced *d* between 0 to one-half of the length shortest boundary or of the radius of *A*, at steps that are greater than the measurement error of the points (Freeman and Ford 2002). $\hat{K}(d)$ is often reported as (Besag 1977):

$$\hat{L}(d) = \sqrt{\frac{\hat{K}(d)}{\pi}} - d \qquad [3.7]$$

$\hat{L}(d)$ eases interpretation by linearizing $\hat{K}(d)$ and stabilizing its variance, and has an expected value of approximately zero at all *d* under *csr*. Positive values of $\hat{L}(d)$ indicate clustering in the point pattern and negative values indicate regularity (Moeur 1993, Freeman and Ford 2002).

Significance of departure of $\hat{L}(d)$ from *csr* or any other point process of interest is usually estimated via Monte Carlo procedures (Diggle 2003). Confidence envelopes are generated by simulating several realizations (η) of the point process that conforms to the null hypothesis, e.g., a homogenous Poisson process to test for *csr*, and calculating $\hat{K}(d)$ for each realization. Simulations usually are conducted with the same λ, *d*, and extent as the observed point pattern. For a given α, local confidence envelopes are built from $\eta_{[\alpha/2]}$ and $\eta_{[1-\alpha/2]}$, sorted at each *d* (Goreaud and Pélissier 2000). Although many studies have set $\eta = 1 - \alpha^{-1}$ (Kenkel 1988, Harrod et al. 1999, Antos and Parish 2002),

Martens et al. (1997) suggest that these Monte Carlo confidence envelopes have low validity when $\eta \cdot \alpha < 5$. This study used $\eta = 1000$, although some studies suggest 10,000 realizations (Goreaud and Pélissier 2000).

3.3.5.3. Mingling Index

The mingling index (*DM*) measures the interspersion of marks within a point pattern (von Gadow and Hui 1999). It is a point-level variable, giving the proportion of *j* nearest neighbors that have the same mark as the reference point *i*. In this study, *DM* is defined using a 4-neighbor structural group as (Kint et al. 2001, Pommerening 2002):

$$DM_i = \frac{1}{3}\sum_{j=1}^{3} V_{ij} \qquad [3.8]$$

where:

$$V_{ij} = \begin{cases} 0 \rightarrow \text{tree } i \text{ and neighbor } j \text{ are the same species} \\ 1 \rightarrow \text{tree } i \text{ and neighbor } j \text{ are different species} \end{cases}$$

As defined, DM_i has only four possible values ($0, \frac{1}{3}, \frac{2}{3}$, and 1) and can be summarized as a frequency distribution, but the DM_i's are usually averaged at the species-level and/or across the entire point pattern. Low values of mean *DM* suggest a lack of species diversity within the pattern, and/or that individual species form highly segregated and clumped distribution within the pattern. Conversely, high values of mean *DM* suggest more species diversity and/or that individual species are regularly distributed forming a more complete mixture in the point pattern (Kint et al. 2001). The distributional properties of *DM* are not known, but a permutation approach can be used to test for significant differences between the observed *DM* and that of a random mixture of the same species proportions and point locations as the observed pattern (Kint et al. 2001).

3.3.5.4. Size Differentiation Index

The size differentiation index (*TH*) describes the variation in a continuous point attribute (i.e., tree height) among the *j* nearest neighbors and the reference point *I* (von Gadow and Hui 1999). Like *DM*, it is calculated as a point-level variable. In this study, *TH* is defined using tree heights within 4-neighbor structural group as (Kint et al. 2001):

$$TH_i = \frac{1}{3}\sum_{j=1}^{3}\left[1 - \frac{\min\left(HT_i, HT_j\right)}{\max\left(HT_i, HT_j\right)}\right] \quad [3.9]$$

TH_i varies from 0 to 1, but is usually summaried by species or for the entire point pattern either as a single mean index or as a frequency distribution of TH_i. Species with a mean *TH* near 0 would be subordinate to most of their neighbors, indicating that the tree most likely occurs in the lower crown classes or strata within the point pattern. Point patterns with a mean *TH* near 0 would have little height differentiation suggesting a uniformed, potentially even-aged structure (Kint et al. 2001, Aguirre et al. 2003). Significance of *TH* can be tested with the same permutation approach as *DM* (Kint et al. 2001).

3.3.5.5. Stand Complexity Index

The stand complexity index (*SCI*) integrates tree positioning and size variation as a measure structural variability. *SCI* is calculated by first creating a Delaunay triangulation of the spatial positions of the trees within a plot (Turner 2002), with the restriction that triangles along the edge of the 2-dimensional triangulation are omitted if they may have a closest neighbor outside the plot (Zenner and Hibbs 2000). Size attributes associated with each tree can then be attached to the 2-dimensional triangulation to form a ragged triangulation surface in 3 (or more) dimensions. The *SCI*

is then defined as the ratio of surface area of 3-dimensional triangulation to that of the 2-dimensional triangulation or:

$$SCI = \sum_{i=1}^{n} \frac{|a_i \times b_i|}{2} \Big/ A_T \qquad [3.10]$$

where A_T is the sum of the projected areas of all triangles (i.e., the 2-dimension triangulation), and $|a_i \times b_i|$ is the absolute value of the vector product of the vector AB with coordinates $a_i = (x_{ib} - x_{ia}, y_{ib} - y_{ia}, z_{ib} - z_{ia})$ and the vector AC with coordinates $b_i = (x_{ic} - x_{ia}, y_{ic} - y_{ia}, z_{ic} - z_{ia})$ (Zenner and Hibbs 2000).

The distributional statistics for *SCI* under various spatial and tree size distributions are not known. *SCI* has a lower limit of 1 when all trees are the same size (Zenner and Hibbs 2000). *SCI* does not appear to have an upper limit, as trial simulations have shown *SCI* to increase dramatically with increasing tree density and the range in size among the trees (Saunders et al. 2002, McElhinny et al. 2005).

3.3.5.6. Summarizing and Testing of Spatial Indices

The randomness of the simulation procedure in the reconstruction models—in particular, the simulation of missing tree and sapling locations and the scaling of sapling subplots—required a permutation-based approach for summarizing and testing with any of the aforementioned statistics. Therefore, 100 realizations of the complete spatial pattern, i.e. a "master" list of all known and unknown locations, were simulated for each plot. For any given realization, spatial pattern was then held constant across inventories by simply trimming out all trees not measured during an inventory from the master list of locations. Realizations that had $n < 5$ were discarded from further analysis since several of the spatial indices were unstable at such small sample sizes.

The various spatial indices were summarized by compartment and inventory. The estimator for the mean value of any given index ($\bar{I}$) was calculated as a weighted average of all realizations within a compartment or (Diggle 2003):

$$\bar{I} = \sum_{i=1}^{p}\sum_{j=1}^{r_p} n_{ij} I_{ij} \Big/ \sum_{i=1}^{p}\sum_{j=1}^{r_p} n_{ij} \qquad [3.11]$$

where p is the number of plots in a compartment, r_p is the realizations for each plot p, and n is the number of trees in realization r of plot p. For *K(d)*, $\bar{I}$ was calculated at each lag distance *d*. The sampling variance of $\bar{I}$ was estimated from 1000 bootstrapped samples of $\bar{I}^*$ defined as:

$$\bar{I}^* = \sum_{k=1}^{p} n_k I_k \Big/ \sum_{k=1}^{p} n_k \qquad [3.12]$$

where the I_k are sampled at random with replacement from all $i \times j = k$ realizations in the compartment (Diggle 2003). Bootstrapped 95% confidence intervals were calculated using ±1.96 standard errors of $\bar{I}^*$. For *CE* and *K(d)*, these bootstrapped 95% confidence intervals were tested against *csr* of a simulated plot of average density for each compartment in a particular inventory. Permutation-based tests of *DM* and *TH* against a random mixture hypothesis were not conducted since it would require separate testing for each realization of any given plot (this would exceed 3.8 x 10^7 resamples in this study!).

Lastly, the overall structural development of the compartments was summarized using a nonmetric multidimensional scaling (NMS) of the plot averages of basal area, density, hardwood importance (% hardwood density x % hardwood basal area), size class distribution, *CE*, *DM*, *TH*, number of stems with $TH_i \geq 0.6$ and $TH_i < 0.6$, and SCI_r. Each variable was standardized by the norm (Greig-Smith 1983) and Sørenson distances

were used. A random starting configuration was used with a step-down dimensionality algorthimn on 40 runs of the data. A Monte-Carlo test using 50 runs of permutated, randomized data was used to access the probability of obtaining a more stable solution by chance. All NMS analyses were conducted with PC-ORD© 4.07 (McCune and Mefford 1999) with the Kruskal-Mather algortithm (Kruskal 1964, Mather 1976, McCune and Grace 2002).

3.4. RESULTS

3.4.1. Stand Characteristics and Size Structure

Traditional metrics capture some of the structural development patterns for the different treatments. Trends in both basal area and density show the typical decline and subsequent regrowth after precommercial and commercial harvest entries for all four management treatments (Figure 3.3). Generally, replicates responded similarly to harvest, just staggered in time slightly due to the different timing of harvests. A notable exception is the two natural area (NA) compartments where there is a clear divergence in structure. Beginning about 1980, the proportion of balsam fir basal area and density increased dramatically within Compartment 32A, and continued to decline in Compartment 32B (Figures 3.4 and 3.5). The high proportion of small saplings suggests that Compartment 32A experienced a widespread regeneration event (Figure 3.6), likely from the loss of an older cohort of balsam fir from the canopy stratum of the stand due to the spruce budworm epidemic of the late 1970s. Compartment 32B, on the other hand, has had relatively constant species composition, with hemlock gradually replacing balsam fir over time (Figures 3.4 and 3.5). Structurally, the stand resembles an understory reinitiation stage within an even-aged development pathway (Figure 3.6;

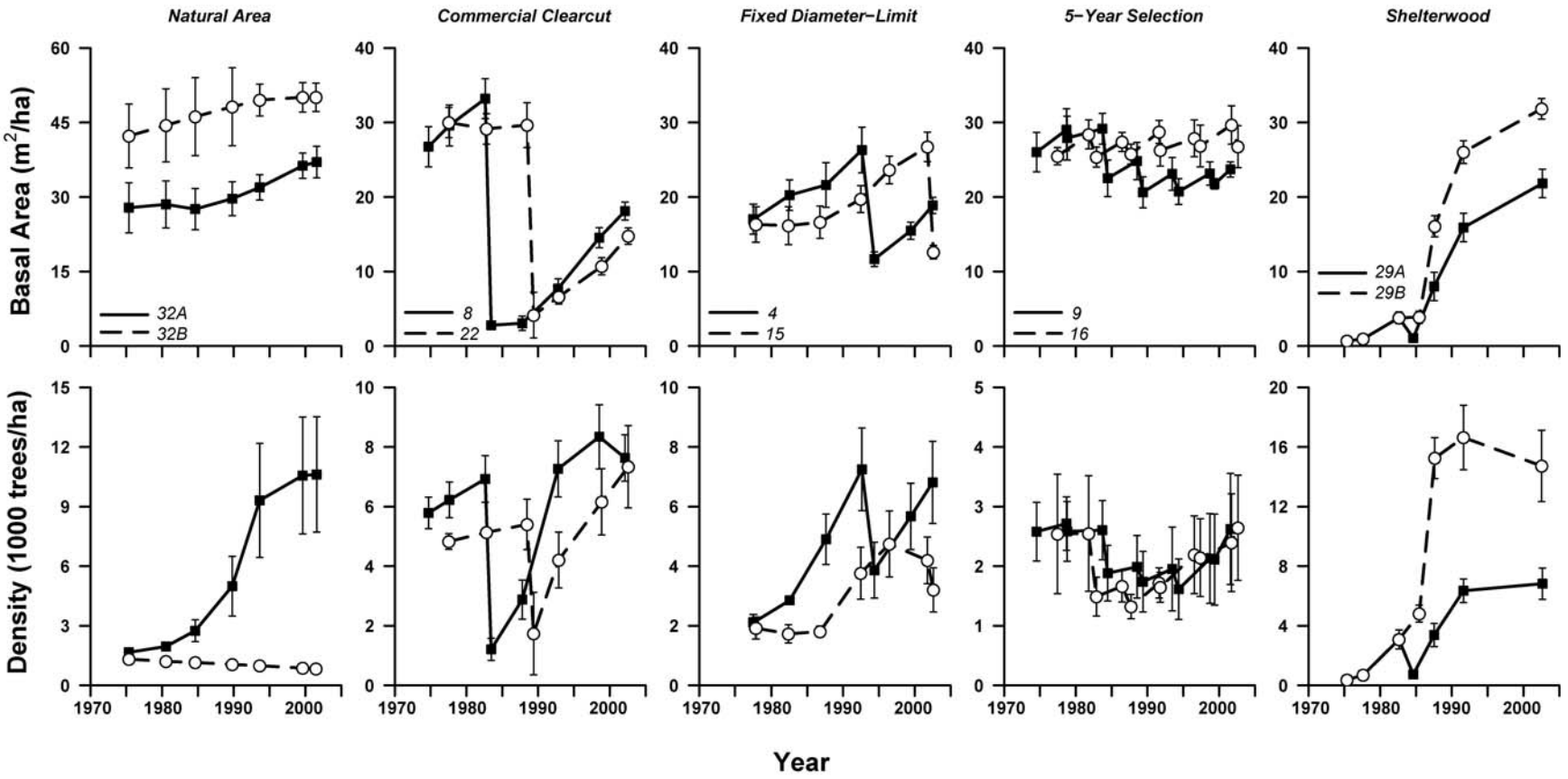

Figure 3.3. Basal area and stem density for all stems >1.2 cm dbh by compartment for the unmanaged natural area and four management treatments from 1974 – 2002. Corresponding drops in both basal area and density indicate a harvesting event within any given compartment. Error bars indicate ±1 standard error.

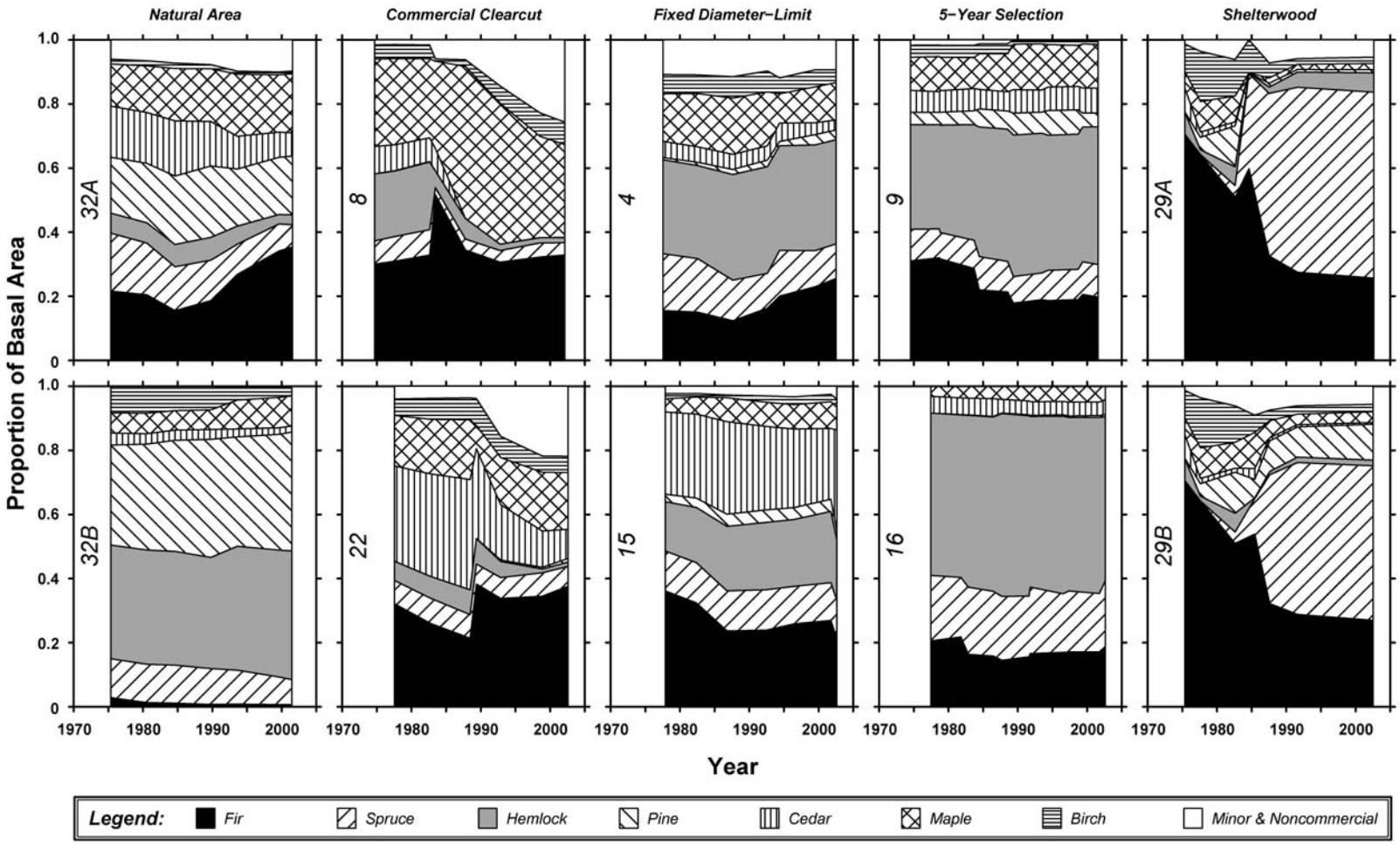

Figure 3.4. Proportion of basal area by species or species group for the unmanaged natural area and four management treatments on compartments from 1974 – 2002.

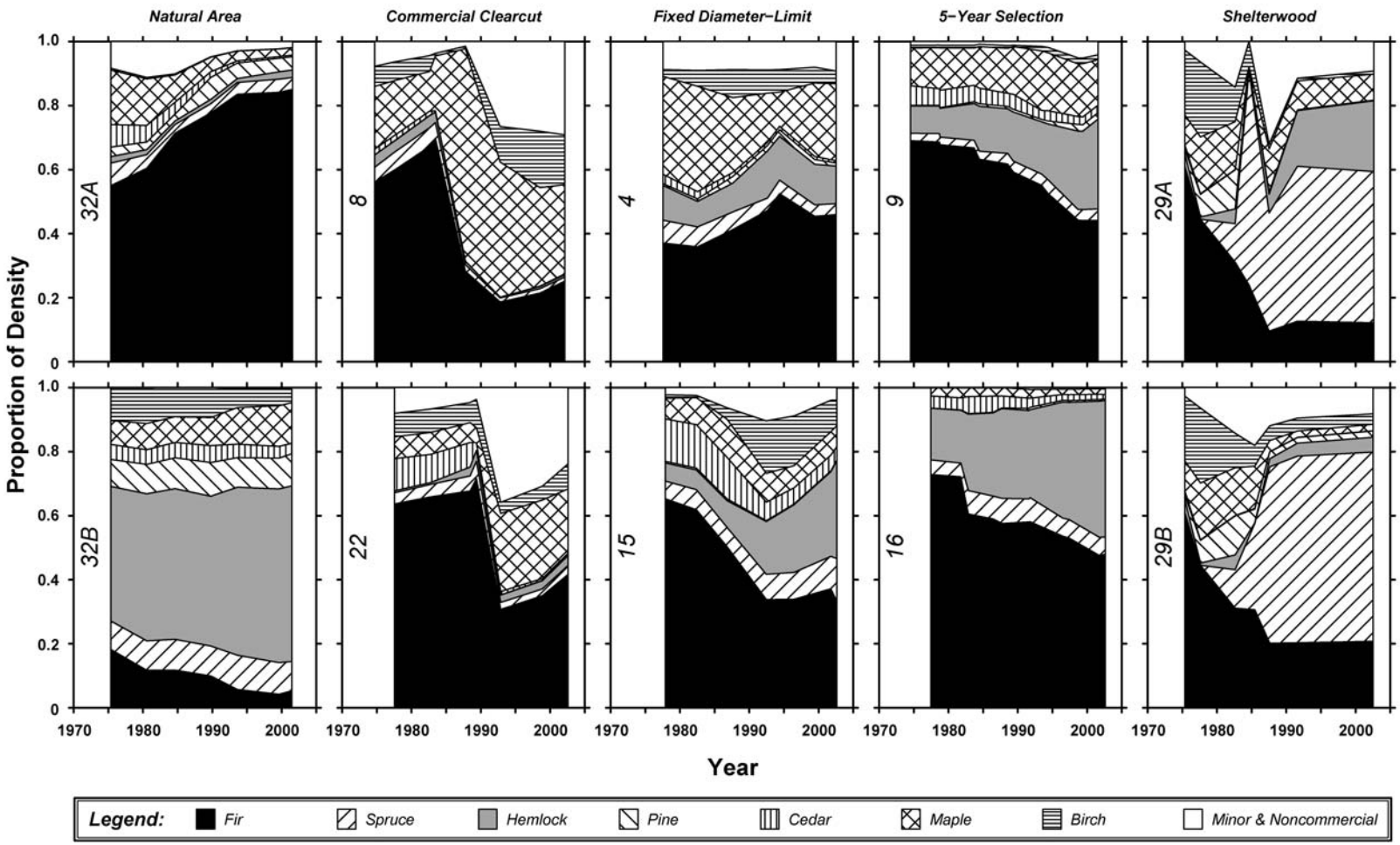

Figure 3.5 Proportion of density by species or species group for the unmanaged natural area and four management treatments on compartments from 1974 – 2002.

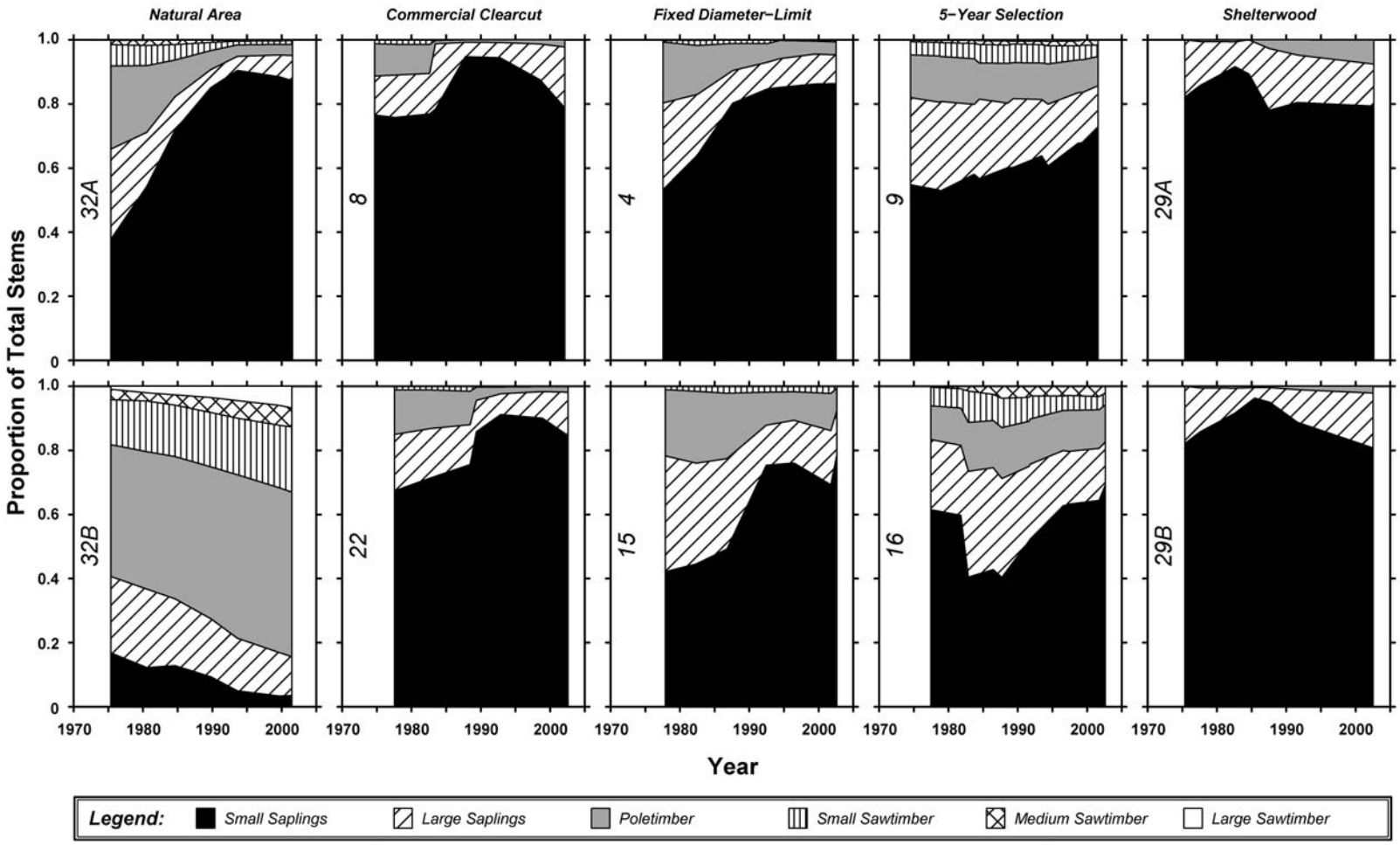

Figure 3.6 Shifts in diameter distributions for the unmanaged natural area and four management treatments on compartments from 1974 – 2002. Size groupings are defined by diameter as: small saplings = 1.2 – 6.3 cm; large saplings = 6.4 – 12.7 cm; poletimber = 12.8 – 25.4 cm; small sawtimber = 25.5 – 38.1 cm; medium sawtimber = 38.2 – 50.8 cm; and large sawtimber = 50.9+ cm.

Oliver and Larson 1996), even though the stand is likely uneven-aged after repeated partial harvesting prior to 1900 (Kenefic et al. 2005b).

Exploitative treatments that lead to irregular structures—the commercial clearcut and fixed-diameter limit harvest—shifted species composition away from the domination by spruce, fir and hemlock at the beginning of the experiment in the 1950s and towards hardwood species (Figure 3.5). This trend was evident by 1975 and only accelerated following the second entries into these treatments in the 1980s. Further, as indicated by a disproportionally large basal area relative to density, is a buildup of larger diameter cedar in three of the four compartments in these treatments (Figures 3.4 and 3.5). This trend is likely to be related to a buildup of cull material that occurred with these two treatments (Kenefic et al. 2005a). As expected, these stands had few trees in sawtimber size classes (Figure 3.6).

The 5-year selection treatement had generally maintained a relatively stable species composition over 30 years, although there had been a gradual replacement of balsam fir with hemlock in both density and basal area (Figures 3.4 and 3.5). This treatment maintained a wide diameter-distribution relative to the other treatments (Figure 3.6), although the proportion of poletimber is much lower than would be expected in a balanced uneven-aged distribution (L. Kenefic, pers. comm.). The wide error bars for density and basal area estimates (Figure 3.3), suggests that horizontal variability in the selection treatment may be high, likely due to skid trail network used in previous harvests.

Both 3-stage shelterwood (SW) compartments received final removal cuts in 1974 (Figure 3.2), prior to the inventories analyzed in this study. Since all residual stems ≥6.4 cm dbh were removed in this harvest, these compartments experienced a stand-wide

regeneration event and have since developed typical even-aged developmental pathways, with both density and basal area increasing as regeneration grew into the inventory (Figure 3.2). In contrast to the other treatments, composition was dominated by spruce and fir, with the precommercial thinning (PCT) during 1983 within Compartment 29A further strengthening the dominance by these species (Figures 3.4 and 3.5). By reducing competition and increasing individual tree growth, PCT also increased the proportion of stems in poletimber size classes relative to Compartment 29B that did not receive PCT (Figure 3.6).

3.4.2. Spatial Patterning

Treatments differed dramatically in spatial patterning, either as measured with CE or $\hat{K}(d)$. When both saplings and trees were considered together, CE statistics indicated a significantly aggregated pattern ($p < 0.05$) for all compartments except for Compartment 32B and for Compartment 16 from 1981 -1991 (Figure 3.7a). Regeneration events, either triggered naturally (Compartment 32A) or by harvesting, tended to reduce CE statistics for all treatments almost immediately. Differences in the amount of decline in CE among compartments may be attributed to harvest methods and/or the density of hardwoods in the pre-harvest stand as it affects the proportion of stump sprouts to seed-origin seedlings recorded in subsequent inventories (Figure 3.5).

$\hat{K}(d)$ was almost always significantly clustered, and often for all distances up to 8 m (Table 3.4; Appendix C). Changes in the scale of aggregation (i.e., the peak of significance from *csr*) could not always be explained, probably because the higher proportion of simulated stem positions in some treatments muted some trends (Table 3.1).

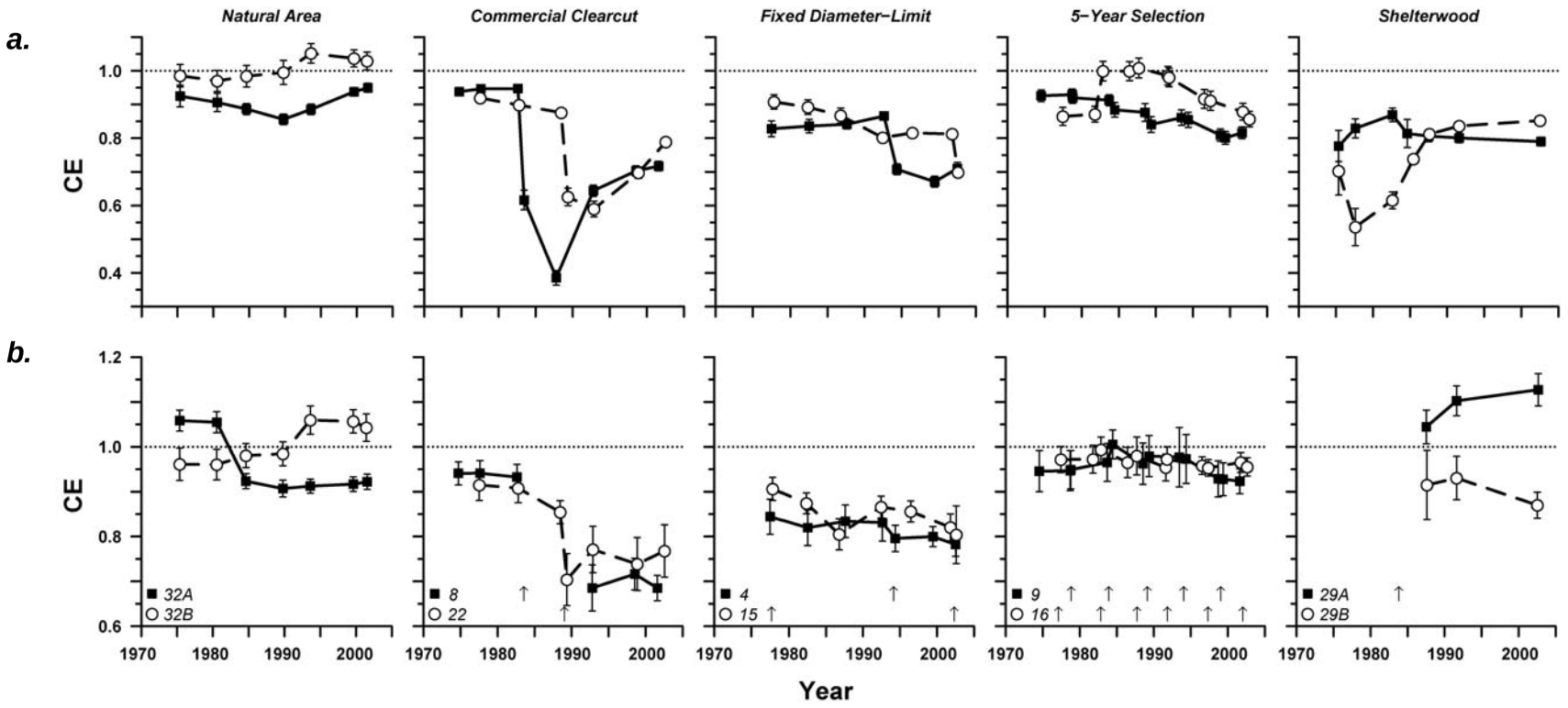

Figure 3.7. Mean Clark-Evans (*CE*) nearest neighbor index for both saplings and trees (a) and only trees >11.4 cm dbh (b) for the unmanaged natural area and four management treatments on compartments from 1974 – 2002. Error bars represent ±2 bootstrapped standard errors. As reference, arrows denote harvest entries for each compartment. *CE* values <1 suggest aggregation among tree stems, *CE* >1 suggests regularity.

Table 3.4. Significantly clustered (C) or uniform (U), or nonsignificant (-) spatial patterns of compartments for inventories from 1974-2002, based on a 95% bootstrapped confidence envelope of mean *K(d)* at 0.5 m steps and a 95% confidence interval calculated on 1,000 simulations of complete spatial randomness (*csr*) of the same average density. Bolded symbols indicate the maximum deviation of significance from *csr*. Data for table comes from figures in Appendix C.

Treatment[1]	Compartment	Inventory Date	All Saplings &Trees								Trees >11.4 cm dbh							
			Distance (m)								Distance (m)							
			1	2	3	4	5	6	7	8	1	2	3	4	5	6	7	8
NA	32A	1975	-	C	C	C	-	C	**C**	-	-	-	-	-	-	-	-	-
		1980	C	C	C	C	C	**C**	C	C	C	C	C	C	C	-	-	-
		1984	C	C	C	C	C	C	**C**	C	C	C	C	C	C	C	C	C
		1989	C	C	C	C	C	C	C	C	C	C	**C**	C	C	C	C	C
		1993	C	C	C	C	C	C	C	C	C	C	C	**C**	C	C	C	C
		1999	C	C	C	C	C	C	C	C	C	C	C	**C**	C	C	C	C
		2001	C	C	C	C	C	C	C	C	C	C	C	**C**	C	C	C	C
	32B	1975	-	-	-	-	-	-	-	-	-	-	-	-	-	-	-	-
		1980	-	-	-	-	-	-	-	-	-	-	-	-	-	-	-	-
		1984	-	-	-	-	-	-	-	-	-	-	-	-	-	-	-	-
		1989	-	-	-	-	-	-	-	-	-	-	-	-	-	-	-	-
		1993	-	-	-	-	-	-	-	-	-	-	-	-	-	-	-	-
		1999	-	-	-	-	-	-	-	-	-	-	-	-	-	-	-	-
		2001	-	-	-	-	-	-	-	-	-	-	-	-	-	-	-	-
CC	8	1974	C	C	C	C	C	C	C	**C**	C	C	C	C	C	C	C	-
		1977	C	C	C	C	C	C	C	**C**	C	C	C	C	C	C	-	-
		1982	C	C	C	C	C	C	C	**C**	C	C	C	C	C	C	C	-
		1983	C	C	C	C	**C**	C	C	C	C	C	C	C	C	C	C	C
		1987	C	**C**	C	C	C	C	C	C	C	C	C	C	C	C	C	C
		1992	C	**C**	C	C	C	C	C	C	C	C	C	C	C	C	C	C
		1998	C	**C**	C	C	C	C	C	C	C	C	C	C	C	C	C	C
		2001	C	**C**	C	C	C	C	C	C	C	C	C	C	C	C	-	-

insufficient sample size

insufficient sample size

[1] Treatment codes are: NA = unmanaged natural area, CC = commercial clearcut, DL=fixed-diameter limit harvest, 5S-five-year selection system, and SW=3-stage shelterwood.

Table 3.4. Continued.

Treatment[1]	Compartment	Inventory Date	All Saplings &Trees								Trees >11.4 cm dbh							
			Distance (m)															
			1	2	3	4	5	6	7	8	1	2	3	4	5	6	7	8
CC	22	1977	C	C	C	C	C	C	C	C	-	-	-	-	-	-	-	-
		1982	C	C	C	C	C	C	C	C	-	-	-	-	-	-	-	-
		1988	C	C	C	C	C	C	C	C	-	-	-	-	-	-	-	-
		1989	C	C	C	C	C	C	C	C	-	-	-	-	-	-	-	-
		1992	C	C	C	C	C	C	C	C	-	-	-	-	-	-	-	-
		1998	C	C	C	C	C	C	C	C	-	-	-	-	-	-	-	-
		2002	C	C	C	C	C	C	C	C	-	-	-	-	-	-	-	-
DL	4	1977	C	C	C	C	C	C	C	-	-	-	-	-	-	-	-	-
		1982	C	C	C	C	C	C	C	-	-	C	-	-	-	-	-	-
		1987	C	C	C	C	C	C	C	C	-	C	-	-	-	-	-	-
		1992	C	C	C	C	C	C	C	C	C	C	C	-	-	-	-	-
		1994	C	C	C	C	C	C	C	C	-	-	-	-	-	-	-	-
		1999	C	C	C	C	C	C	C	C	-	-	-	-	-	-	-	-
		2002	C	C	C	C	C	C	C	C	-	-	-	-	-	-	-	-
	15	1977	C	C	C	C	C	C	C	-	-	-	-	-	-	-	-	-
		1982	C	C	C	C	C	C	C	-	-	-	-	-	-	-	-	-
		1986	C	C	C	C	C	C	C	-	-	-	-	-	-	-	-	-
		1992	C	C	C	C	C	C	C	C	-	-	-	-	-	-	-	-
		1996	C	C	C	C	C	C	C	C	-	-	-	-	-	-	-	-
		2001	C	C	C	C	C	C	C	C	-	-	-	-	-	-	-	-
		2002	C	C	C	C	C	C	C	C	-	-	-	-	-	-	-	-
5S	9	1974	-	C	C	C	C	C	C	-	-	-	-	-	-	-	-	-
		1978	-	C	C	C	C	C	C	-	-	-	-	-	-	-	-	-
		1978	-	C	C	C	C	C	C	-	-	-	-	-	-	-	-	-
		1983	C	C	C	C	C	C	C	-	-	-	-	-	-	-	-	-
		1984	C	C	C	C	C	C	C	C	-	-	-	-	-	-	-	-
		1988	C	C	C	C	C	C	C	C	-	-	-	-	-	-	-	-
		1989	C	C	C	C	C	C	C	C	-	-	-	-	-	-	-	-
		1993	C	C	C	C	C	C	C	C	-	-	-	-	-	-	-	-

[1] Treatment codes are: NA = unmanaged natural area, CC = commercial clearcut, DL=fixed-diameter limit harvest, 5S-five-year selection system, and SW=3-stage shelterwood.

Table 3.4. Concluded.

Treatment[1]	Compartment	Inventory Date	All Saplings &Trees								Trees >11.4 cm dbh							
			Distance (m)															
			1	2	3	4	5	6	7	8	1	2	3	4	5	6	7	8
5S	9	1994	C	C	C	C	C	C	C	C	-	-	-	-	-	-	-	-
		1998	C	C	C	C	C	C	C	C	-	-	-	-	-	-	-	-
		1999	C	C	C	C	C	C	C	C	-	-	-	-	-	-	-	-
		2001	C	C	C	C	C	C	C	C	-	-	-	-	-	-	-	-
	16	1977	C	C	C	C	C	C	C	C	-	-	-	-	-	-	-	-
		1981	C	C	C	C	C	C	C	C	-	-	-	-	-	-	-	-
		1982	-	-	-	-	-	-	C	C	-	-	-	-	-	-	-	-
		1986	-	-	-	-	-	-	-	-	-	-	-	-	-	-	-	-
		1987	-	-	-	-	-	-	-	-	-	-	-	-	-	-	-	-
		1991	-	-	C	C	C	C	C	C	-	-	-	-	-	-	-	-
		1991	C	C	C	C	C	C	C	C	-	-	-	-	-	-	-	-
		1996	C	C	C	C	C	C	C	C	-	-	-	-	-	-	-	-
		1997	C	C	C	C	C	C	C	C	-	-	-	-	-	-	-	-
		2001	C	C	C	C	C	C	C	C	-	-	-	-	-	-	-	-
		2002	C	C	C	C	C	C	C	C	-	-	-	-	-	-	-	-
SW	29A	1975	-	-	C	C	C	C	C	C	*insufficient sample size*							
		1977	-	-	C	C	C	C	C	C	*insufficient sample size*							
		1982	C	C	C	C	C	C	C	C	*insufficient sample size*							
		1984	-	-	-	-	C	C	C	C	*insufficient sample size*							
		1987	C	C	C	C	C	C	C	C	-	-	-	-	-	-	-	-
		1991	C	C	C	C	C	C	C	C	-	-	U	-	-	-	-	-
		2002	C	C	C	C	C	C	C	C	-	-	U	-	-	-	-	-
	29B	1975	-	-	-	-	C	C	C	C	*insufficient sample size*							
		1977	C	C	C	C	C	C	C	C	*insufficient sample size*							
		1982	C	C	C	C	C	C	C	C	*insufficient sample size*							
		1985	C	C	C	C	C	C	C	C	*insufficient sample size*							
		1987	C	C	C	C	C	C	C	C	-	-	-	-	-	-	-	-
		1991	C	C	C	C	C	C	C	C	-	-	-	-	-	-	-	-
		2002	C	C	C	C	C	C	C	C	-	-	-	-	-	-	-	-

[1] Treatment codes are: NA = unmanaged natural area, CC = commercial clearcut, DL=fixed-diameter limit harvest, 5S-five-year selection system, and SW=3-stage shelterwood.

For example, the scale of pattern in Compartment 32A, an unmanaged natural area where over 95% of locations are known, generally increased with time, suggesting density-dependent competition in local neighborhoods that reduced small-scale aggregation of regeneration (Table 3.4). Harvesting in the two exploitative treatments often, but not consistently, reduced the scale of aggregation to <2 m in later inventories, suggesting a strong influence of hardwood stump sprouting. The scale of clustering in 5-year selection compartments was relatively constant or slightly increased. PCT in Compartment 29A had a relatively short-term influence on broadening the scale of aggregation, but resprouting hardwoods and ingrowth quickly returned the scale to pre-PCT levels. Scale of aggregation in Compartment 29B, managed as a 3-stage shelterwood without PCT, declined for several years and then increased; this may have resulted from a higher proportion of ingrowth from hardwood sprouts and their subsequent density-dependent mortality (Figure 3.5).

When only trees (dbh >11.4 cm) were considered, spatial pattern was rarely significantly ($p < 0.05$) nonrandom. CE detected aggregation in pattern for trees within three of the four compartments experiencing exploitative harvesting: Compartment 4, Compartment 15 during the 1986 and 2000 inventories, and Compartment 8 for all inventories after 1990 (Figure 3.7b). Although not always significant, $\hat{K}(d)$ values suggested that the scale of this aggregration was around 2 m (Table 3.4, Appendix C), particularly for the fixed-diameter limit harvest. Significant uniformity in pattern was detected with $\hat{K}(d)$ only for the two most recent inventories in the Compartment 29A (Table 3.4).

3.4.3. Species Mingling

Mingling among species within spatial pattern appeared to be driven by the relative proportion of hardwood and softwood species within the pattern. Overall mean *DM* for most treatments were intermediate to low, largely clustered in the range of 0.4 - 0.6 (Figure 3.8a). Exploitative harvesting and PCT immediately reduced mingling in most cases, likely because these treatments would be applied with strong selection for certain species (i.e., exploitative harvests would leave cedar and noncommercial species, and PCT would remove balsam fir and most hardwoods). Regeneration events appeared to further reduce mingling, suggesting that regeneration by any given species could be clumped in space (e.g., hardwood sprouting) or time (e.g., conifer masting). Only Compartment 32B had relatively high *DM* values. This stand had experienced the longest period without significant regeneration; one may assume that density-dependent competition probably had reduced many clusters to one or two individuals.

As a group, hardwood species had higher *DM* values than softwood species in most treatments (Figures 3.8b and 3.8c). Hardwood species were less common in most stands and much more dispersed, particularly in the older age structures. Harvesting had much more dramatic impacts on hardwood *DM* values, presumably because of the stump and root sprouting of these species. Softwood species had *DM* values that mirrored mean *DM* values in most stands because they made up a majority of stems (Figures 3.8a and 3.8c). Species-species *DM* values (not shown) generally exceeded 0.8 in most treatments and inventories, with the exceptions of balsam fir and red maple which mirrored the softwood and hardwood *DM* values, respectively. The shelterwood treatment had the most pronounced difference between the species-specific *DM* and mean softwood *DM*

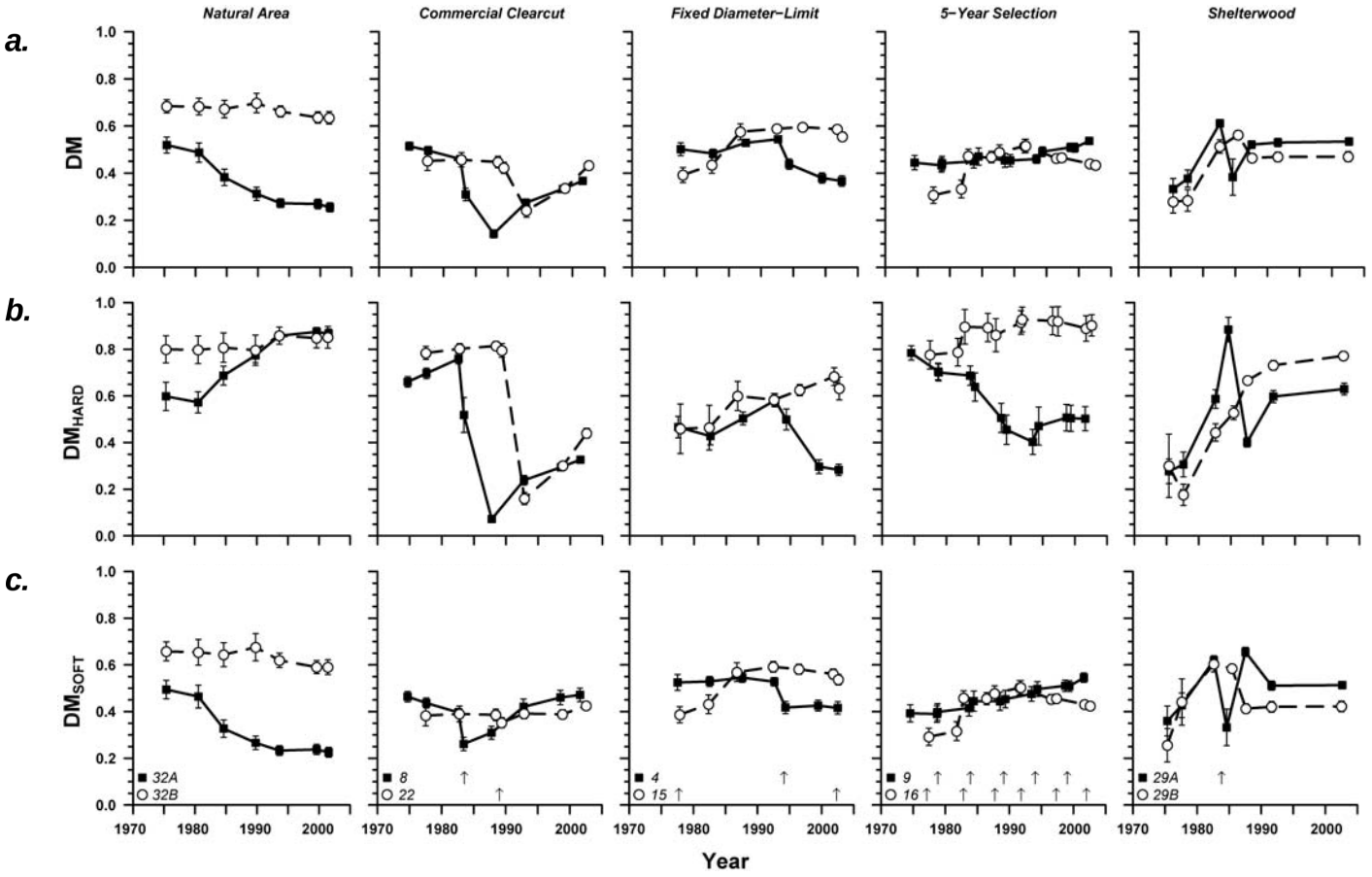

Figure 3.8. Mean species mingling index (*DM*) for all stems (a), hardwood stems only (b) and softwood stems only (c) for the unmanaged natural area and four management treatments on compartments from 1974 – 2002. Error bars represent ±2 bootstrapped standard errors. As reference, arrows denote harvest entries for each compartment. *DM* values can range from 0 (no intermixing of species) to 1 (perfect intermixing).

values. Here mingling of balsam fir increased over time, and spruce and hemlock decreased over time, presumably because densities were high enough for spruce and hemlock to outcompete the balsam fir. PCT increased the mingling of fir and of spruce; hemlock *DM* values were lowered because it became a much larger component of the stand (Figure 3.5).

3.4.4. Height Differentiation

Average height differentiation (*TH*) was not dramatically different among the treatments (Figure 3.9). Treatments with uneven-aged structures, the unmanaged natural area and 5-year selection, had equal to slightly greater *TH* values than exploitative treatments, which in turn were almost always significantly greater than the 3-stage shelterwood. The effect of harvesting on *TH* was not dramatic, except in the commercial clearcut.

Although the mean *TH* values did not separate treatments well, the frequency distribution of TH_i at each inventory did (Figure 3.10). Both the unmanaged natural area and 5-year selection treatments showed wide distributions of TH_i over time, with a large component of the trees having a $TH_i > 0.6$. Commercial clearcut, fixed-diameter limit harvesting, and especially 3-stage shelterwood treatments have few trees in these TH_i ranges. This observation suggests that there is far more variability in height differentiation in localized tree neighborhoods in uneven-aged structures than in the irregular- or even-aged structures.

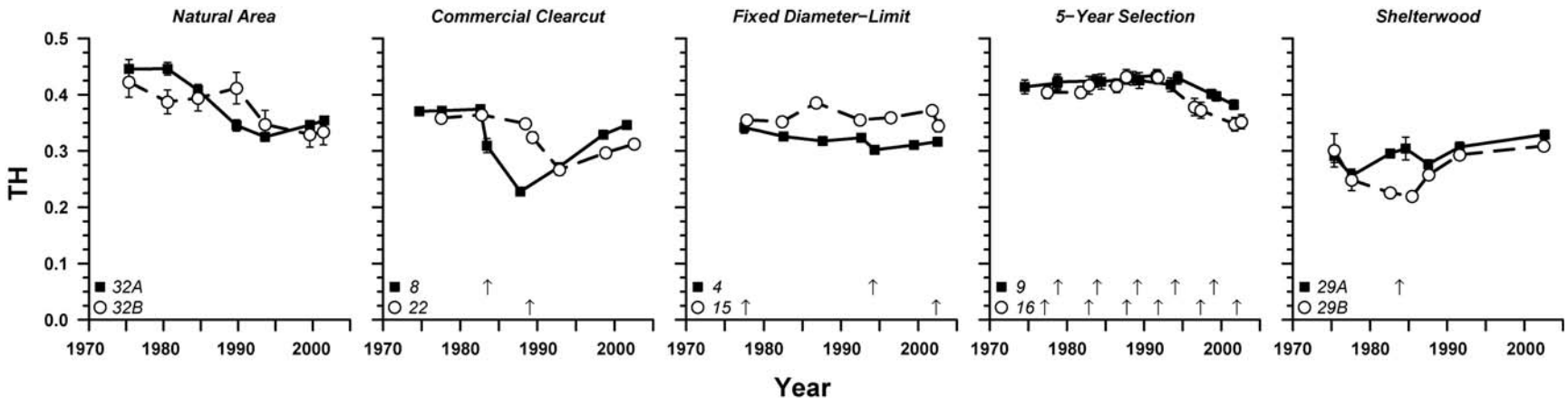

Figure 3.9. Mean height differentiation index (*TH*) for the unmanaged natural area and four management treatments on compartments from 1974 – 2002. Error bars represent ±2 bootstrapped standard errors. As reference, arrows denote harvest entries for each compartment. A *TH* of 0 indicates that all trees in the stand are the same height.

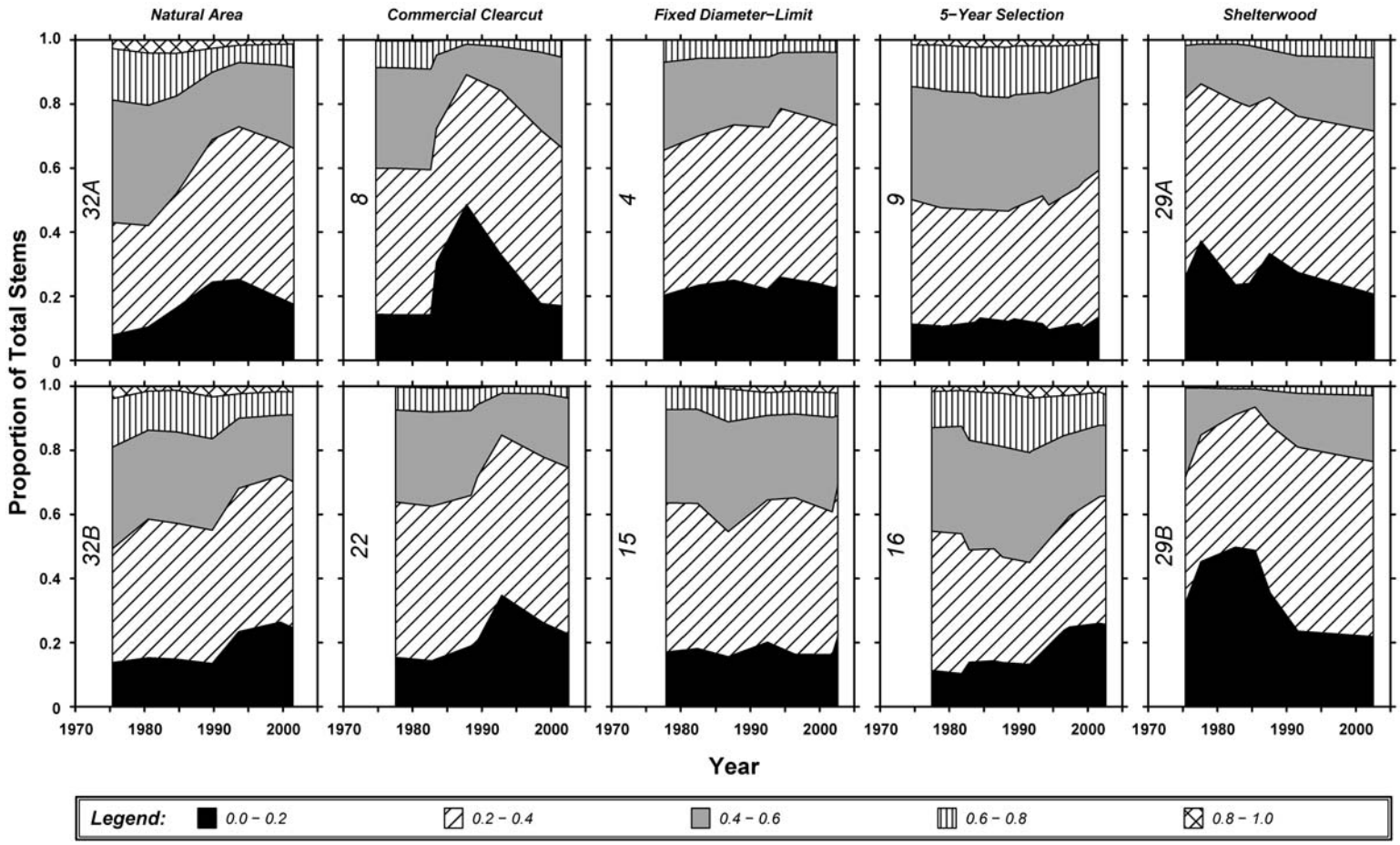

Figure 3.10. Frequency distribution of the height differentiation index value for individual tree stems (TH_i) or the unmanaged natural area and four management treatments on compartments from 1974 – 2002. Higher values indicate more vertically diverse structural neighborhoods.

3.4.5. Structural Complexity

The stand complexity index (*SCI*), when calculated as defined by Zenner and Hibbs (2000), gave rather unexpected results and did not separate treatments well across inventories (Figure 3.11a). Although *SCI* for the unmanaged natural area and 5-year selection treatments was consistently high, values of *SCI* for both the commerciaclearcut and 3-stage shelterwood treatments were equally high at certain stages in their developments. The disparity among the unmanaged natural area compartments also suggested a major problem with *SCI*. Compartment 32A was increasing in *SCI* even though the stand was becoming much denser with only 1-2 canopy layers, while Compartment 32B was declining in *SCI* even though the stand was becoming less dense with multiple canopy layers.

On closer inspection, I determined that there was a direct correlation between *SCI* and tree density, and that this correlation limited interpretations for the index. Simulations done by Saunders et al. (2002) suggested that *SCI* should be weighted by density$^{-\gamma}$ where γ ranged from 0.3 to 0.5 depending on spatial pattern and size range of the trees. Since trends among the treatments using γ equal to 0.3, 0.4, and 0.5 were not appreciably different, *SCI* was weighted by density$^{-0.5}$ (*rSCI*). The result was that *rSCI* for the uneven-aged compartments (the unmanaged natural area and 5-year selection system) were consistently higher than for either commercial clearcutting, fixed-diameter limit harvesting or 3-stage shelterwood compartments (Figure 3.11b). However, *rSCI* could distort trends when tree densities are very low ($n<20$), as in the earliest inventories of the shelterwood compartments.

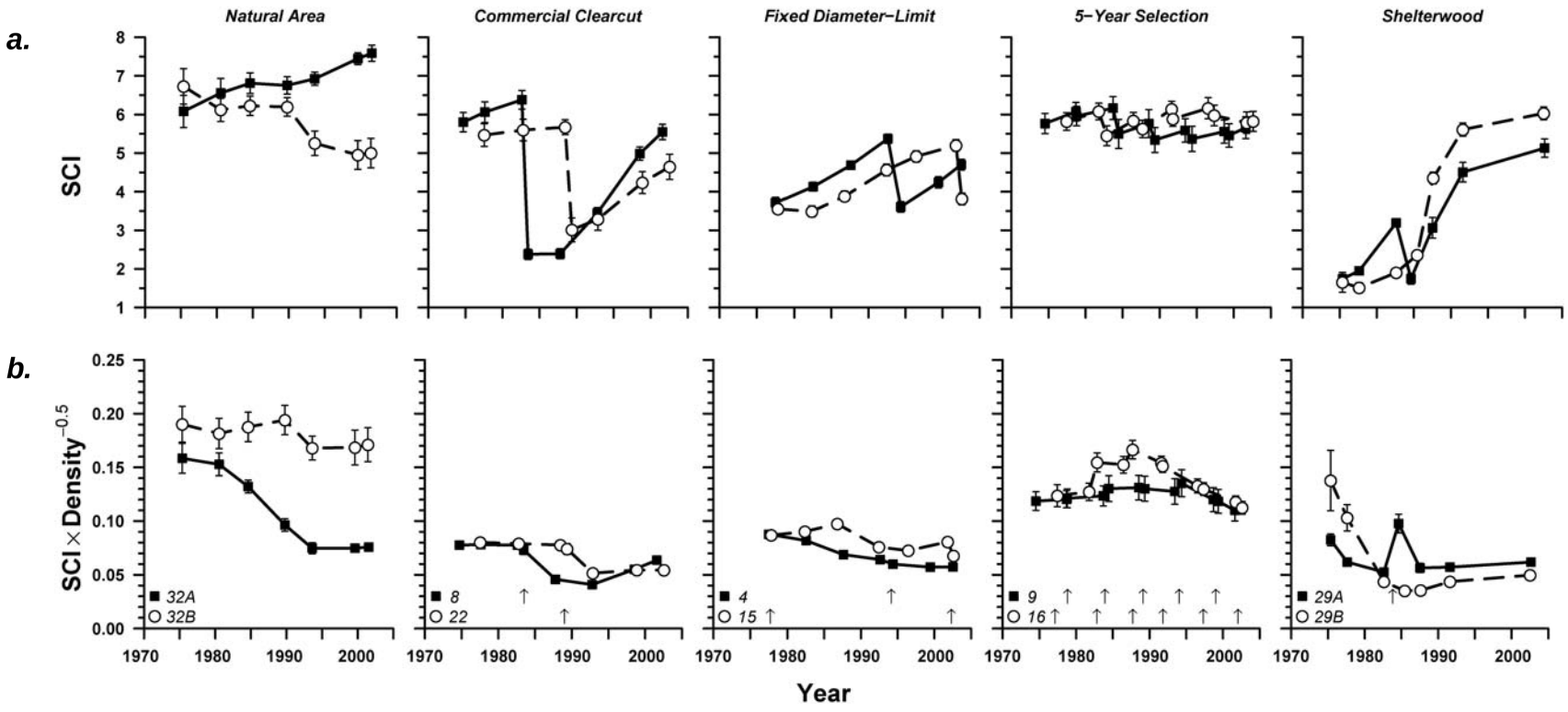

Figure 3.11. Mean absolute (a) and relative (b) stand complexity index (*SCI*) or the unmanaged natural area and four management treatments on compartments from 1974 – 2002. Error bars represent ±2 bootstrapped standard errors. As reference, arrows denote harvest entries for each compartment. *SCI* ranges upwards from 0, which occurs only when all tree stems are the same height.

3.4.6. Summary of Structural Development

The final nonmetric multidimensional scaling (NMS) ordination of structural variables was significant ($p = 0.0196$), converging on a 2-dimensional solution after 78 interations and accounting for 97.4% of the variation (Figure 3.12). Final stress was 6.59 and final instability was 2.45×10^{-6}. Axis I of the ordination was positively related to stem density, number of saplings, and the number of stems with $TH_i < 0.6$; these were generally collinear. Axis II of the ordination was most strongly related to hardwood importance (positively) and the number of sawlog-sized stems (negatively). Surprisingly, mean *CE*, *TH*, and *DM* had relatively minor effects on ordination scores along any axis (Figure 3.12).

The NMS ordination showed a clear separation among uneven-aged, irregular-aged, and even-aged compartments, primarly along Axis II (Figure 3.12). Natural area compartments showed a clear divergence within the NMS and were progressing into two different structural spaces. The two 5-year selection compartments are remarkably static in ordination space, generally located between the two natural area compartments, and harvests in these compartments had only minor effects on the ordination scores. On the other hand, harvests in the fixed-diameter limit and commercial clearcut, and the precommercial thin in the 3-stage shelterwood, dramatically affected ordination scores, generally moving the stands upwards and to the left in ordination space which would reflect increasing hardwood importance and decreasing density. Further, since the harvests created younger stands, the fixed-diameter, commercial clearcut and 3-stage shelterwood compartments are changing the most rapidly in ordination space over time.

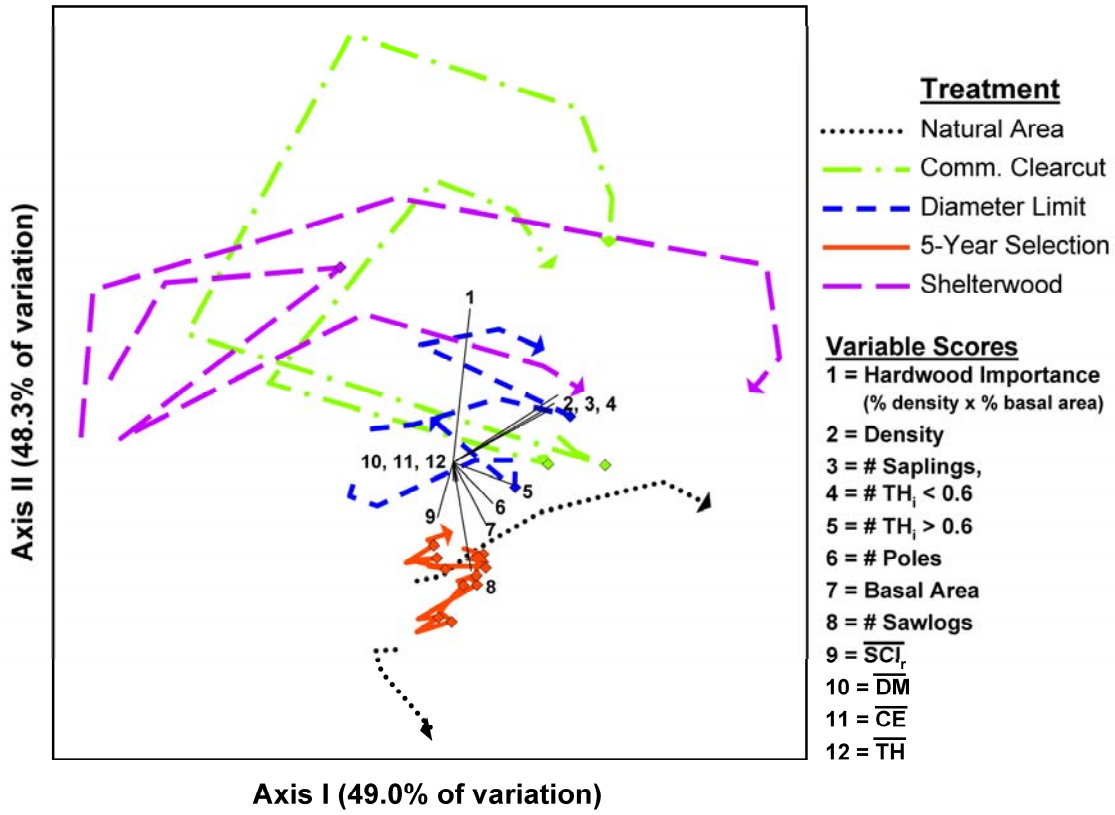

Figure 3.12. Nonmetric multidimensional scaling (NMS) ordination of spatial and nonspatial structural variables for the management compartments over the period of approximately 1974-2002, as separated by treatment. Harvest entries are indicated by the diamonds. Variable scores are plotted from the centroid of the data and represent both the strength and direction of "pull" of that variable on the ordination.

3.5. DISCUSSION

3.5.1. Silvicultural Effects on Structural Development

Harvesting strongly affects the structural development of any forest stand, yet few studies have quantified the spatially explicit changes in point patterns, species mingling, or size differentiation resulting from its application. Sendak et al. (2003), Kenefic et al. (2005a), and several earlier studies of this particular experiment focused on conventional changes in basal area distributions, species composition, and diameter-distributions to investigate ecological and financial viability of the various systems. Results from these studies suggested that there were differences among the treatments in some structural parameters, but the low replication often limited the power of formal ANOVA-style statistical testing. Instead, this study took a Monte Carlo-based approach that incorporated the variability at the plot level, thereby detecting strongly significant differences among treatments in most of the spatial-explicit structural metrics.

Harvesting consistently increased the aggregation and reduced species mingling within spatial pattern through inducing a regeneration event (Figures 3.7 and 3.8). This generally agrees with Phillips and MacMahon (1981), Skarpe (1991), Harrod et al. (1999), and Montes et al. (2005), whom all report increases in aggregation due to plant regeneration. Within the Acadian ecoregion, natural regeneration of trees is prolific, ranging from 25,000-80,000 trees ha^{-1}, across a wide array of intensities and frequencies of partial overstory harvests (Brissette 1996). Balsam fir, in particular, seeds frequently, disperses widely, and can dominate the seed rain contribution from other less frequent and masting species like spruce and eastern white pine (Westveld 1931, Seymour 1992, Greenwood et al. 2003). Balsam fir's early dominance in these stands tended to reduce

mingling levels over time and during any regeneration event. Further, several northern hardwood species employed either a root or stump sprouting regeneration strategy. Harvesting of these species would cause strong aggregation at short scales (<2 m) and a large decrease in mingling, as the single-stemmed canopy tree would be replaced by multiple sprouts. These trends were clearly seen in this study within the exploitative harvests that shifted species composition towards hardwood dominance (Table 3.4, Figure 3.8, and Appendix C).

Second, the harvesting operations themselves inherently changed the spatial pattern. Most skid trail and road networks that became established in the compartments are not regularly spaced. Regeneration and regrowth of existing regeneration on the skid trails was stunted or even absent, likely because of increased soil compaction. Soil disturbance along the trail edges appeared to promote regeneration. Therefore, regeneration in many of the compartments appears clustered, although at scales beyond those measured in this study (Saunders, pers. obs.). Nevertheless, this clumpiness would still be detected in the CE index and $\hat{K}(d)$ function, particularly when a trail bisected a sampling plot, but largely confounded with the direct effects of regeneration. The reduction in CE statistics for larger trees (Figure 3.6) suggests these harvest effects may be quite pronounced in both exploitative treatments (i.e., commercial clearcutting and fixed-diameter limit harvesting), where skid trails are not designated but harvesting equipment moved across a large proportion of the site. It is also likely that the 5-year selection treatment increased this effect since the skid trail network was particularly dense, continually reused, and rarely regenerated in these compartments.

Both height differentiation and stand complexity (as measured by *rSCI*) were highest in multiple-strata, uneven-aged unmanaged natural area and 5-year selection system, intermediate in the irregularly aged exploitative harvests, and lowest in the even-aged, 3-stage shelterwood compartment. This result was largely a function of tree size distribution within each compartment, and not necessarily a valid comparison as each treatment is at different point in stand development. However, the distribution of TH_i values (Figure 3.10) suggested that it will likely take several decades before the commercial clearcutting and 3-stage shelterwood approach the differentiation levels in 5-year selection or unmanaged natural area.

Although unreplicated in this study, the effect of precommercial thinning (PCT) had mixed effects on structural development. PCT increased height differentiation and structural complexity (Figures 3.10 and 3.11), agreeing with the findings of Homyack et al. (2004) who reported that PCT increased canopy stratification and vertical height diversity by 11 years after thinning. However in constrast to Homyack et al. (2004), this study found that PCT unexpectedly increased mingling primarily through increasing the species diversity of the stand (Figures 3.5 and 3.8a). Vacant growing space created by PCT allowed a larger component of hardwood sprouts to survive rather than be outcompeted by neighboring softwoods (Lingren and Sullivan 2001, Daggett 2003). Aggregation in the spatial pattern after PCT also increased as a function of the higher hardwood component. Only recently has regularity imposed by the thinning treatment itself been detected (Table 3.4); this is probably because enough hardwood sprouts have died from self-thinning to "unmask" the treatment.

As suggested by Kenefic et al. (2005b), the unmanaged natural area was not an "ideal" control for comparison with the silvicultural and exploitative treatments because it was added as an afterthought to the experiment and not included within the randomization used to assign compartments to treatments. Further, one could argue that by splitting the original compartment in the early 1990s, the natural areas were pseudoreplicated and their value further diminished. However, the structural divergence between the two compartments may represent two distinct developmental pathways for these forest types (Figure 3.12). Poor soil drainage in Compartment 32A (Kenefic et al. 2005b) likely favored balsam fir over hemlock, and removal of overstory balsam fir by spruce budworm in the early 1970s caused that stand to prolifically regenerate to balsam fir, thus becoming much more aggregated (Figure 3.7), unmingled (Figure 3.8), and less differentiated (Figures 3.9 and 3.10) over time. The structure of the stand is now more characteristic of an irregular, two-aged stand. Compartment 32B, on the other hand, had a much higher proportion of hemlock in the overstory and subsequently did not experience a regeneration event. Structurally, the stand has been relatively stable in spatial pattern and mingling (Figures 3.7 and 3.8), but is becoming slightly less differentiated (Figure 3.10) as lower strata individuals slowly fall out of the stand. This late-successional stand will likely follow this trajectory until either some density-independent mortality event creates openings in the canopy and/or hemlock eventually (over several decades) outcompetes the other less shade-tolerant species. These two structural pathways would not be atypical on an undisturbed landscape as the proportion of balsam fir and hemlock often drive dynamics in softwood-dominated stands within the Acadian ecoregion (Seymour 1992).

In this respect, the structural developments within the two natural area compartments are important benchmarks to compare with management of softwood and, to a lesser extent, mixedwood sites across central Maine. Results from this study suggest that only 5-year selection would fall within the natural range of variability in spatial structure captured by the two natural area compartments (Figure 3.12). Exploitative treatments, like commercial clearcutting and diameter-limit harvesting, can create a more aggregated and less complex structure than natural development on softwood sites after multiple entries, primarly because they strongly shift composition towards early successional, sprouting hardwood species. A uniform shelterwood, as was applied in this study, created an undifferentiated and less complex structure that is atypical in natural stands. As a result the exploitative treatments and the even-aged shelterwood were quite distinct in overall structural attributes from even Compartment 32B which had experienced a stand re-initiation event from spruce budworm mortality (Figure 3.12, upper right natural area trajectory). Structural retention of some larger-diameter, mature overwood during the last shelterwood removal cut or within the commercial clearcut or diameter-limit harvests, would likely reduce these differences.

3.5.2. Adequacy of the Stand Complexity Index

The stand complexity index (SCI) in its original form appears to be biased when comparing stands of vastly different structures and densities. For the few applications of *SCI* that are found in the literature (Zenner and Hibbs 2000, Zenner 2000, Zenner 2004), the compared stands had tree densities that varied by only a factor of 2-3, were all of the same general forest type and composition, and represented a chronosequence along the same development pathway. In this study, tree densities varied by 45-fold across

compartments and inventories, were of vastly different forest types and compositions, and were not on the same development pathways. Although one could argue that the inherent bias in *SCI* has been inflated in this study since it was calculated on all measured tree stems (e.g., Zenner and Hibbs [2000] used a 5 cm dbh lower threshold), small diameter stems make up a significant component of the structure in many early-successional stands and several of these stands would have no *SCI* value until far into stem-exclusion. Use of *rSCI* is preferred as it removes the influence of density on *SCI*, making the index far more responsive to size differentiation and spatial pattern.

Regardless of its form, *SCI* also can be criticized in that it does not explicitly recognize that canopy gaps increase structural complexity (McElhinny et al. 2005). With large scale plots, this weakness can be overcome using a "moving-window" approach and quantifying the distribution of local *SCI* values within a stand (Zenner 2005). Canopy gaps would then occur in locations where *SCI* was extremely low compared to neighboring windows. In reality, this approach would roughly mimic the distribution of TH_i, where the number of neighbors included in each TH_i estimate increases with window size. TH_i does not necessarily require a complete enumeration of all tree locations and sizes in a stand (von Gadow and Hui 1999), and therefore might be more practical than *SCI* for many applications. Further, the distribution of TH_i values within a stand may have higher discrimatory power than *rSCI* alone (Figure 3.12).

3.5.3. Discriminatory Power of the Spatial Indices

Generally, the spatial indices investigated in this study had relatively low discriminatory power compared to other, more traditional structural variables (Figure 3.12). Plot-level means of *CE*, *DM*, and *TH* were not very useful, but the distribution of

values for those indexes (e.g., DM_i or TH_i) across subpopulations were. $\hat{K}(d)$ was useful in detecting the scale of clustering among the treatments, which further clarified the potential pathways of development, but the information gain was marginal given the high computional cost of $\hat{K}(d)$ within a Monte Carlo modeling framework. Reasons for this low discriminatory power of the spatial indices may include: 1) similarly in spatial relationships among seedlings and saplings as all stands were regenerated naturally; and 2) compartment-level spatial relationships are averaged across realizations of plots possibly muting differences.

3.5.4. Effectiveness of the Spatial Model

Overall, results from the structural model developed in this study generally agreed with other observations from the PEF by Brissette (1996), Sendak et al. (2003), Kenefic et al. (2005), and others. However, the model had some weaknesses that were not immediately apparent. For compartments with low tree relocation rates (Table 3.1), the random placement of unknown stem locations within the model likely caused an underprediction of aggregation, an overprediction of mingling, and some bias within size differentiation patterns, which in sum further weakened the discriminatory power of the spatial indices (Figure 3.12). These biases were generally greatest in the earlier inventories (before 1990) since far fewer of the dead stems where relocated. Further, Saunders (Chapter 3) noted that the morphing algorithm would introduce some bias into plot estimates of spatial pattern, particularly for plots that were extremes within any particular compartment. However, the morphing algorithm itself should not appreciably change the mingling or size differentiation patterns, as most local, spatial relationships

would not change except where the various subplots abut one another. Obviously, overlay of the scaled sapling subplot onto the tree plot would change some spatial characteristics, but since saplings dominate the spatial pattern in most compartments, this bias should be minimal.

This structural model was designed to take advantage of spatially explicit, longitudinal measurements on small-scale (<0.1 ha), forest inventory plots. Generally, spatial analyses of these types of inventory plots have generally been avoided due to a lack of spatial inference from the small plot size, and difficulties in scaling patterns of subpopulations from nested plot designs. Instead, most researchers have relied on a very few (≤5) large plots that map spatial relationships among only the largest size classes. This approach has power in that larger-scaled patterns can be detected and edge influences on pattern are minimized. However, there are few studies of repeatedly measured, large-scale plots. One rare example is that of Ward et al. (1996) where spatial dynamics in an old-growth deciduous forest were characterized across three inventories spanning a total of 60 years. For most studies, therefore, there is an obvious tradeoff between spatial and temporal scale. I choose to take advantage of the temporal scale with the model presented here.

Spatial analysis of forest inventory plots offers additional benefits over the traditional analysis of larger plots. Forest inventories can be designed to more efficiently and economically capture the average and range of neighborhood conditions within a stand than one large plot of the same total sampled area (Husch et al. 1982). Therefore, plots can be randomly located within stands or strata, rather than biasedly placed to capture the range of spatial relationships found in the stand. Multiple plots also allow

spatial inference to be drawn from the experimental design rather than comparisons with stochastic models (i.e., *csr*) that must be assumed for individual plots (Diggle 2003). Lastly, at adequate sample intensities, broader scaled spatial analyses beyond the scale of an individual plot can still be conducted using the sample plot averages for any spatial indices of interest (Fúle and Covington 1998).

EPILOGUE

This study developed, tested, and applied a new approach for spatial analysis of typical growth-and-yield type inventory designs where plots were circular and small (<0.2 ha), with different subpopulations of trees nested at different scales. While this approach had some limitations, it has potential use for validation of spatially explicit growth models, for scaling subplots in realistic structural simulations of forest stands, and for exploratory spatial analysis of large, longitudinal datasets.

In Chapter 1, I compared two modeling approaches for estimation of height-diameter relationships for nine common northeastern tree species. Nonlinear, mixed-effect models that included random parameters to account for the sampling design (i.e., compartment and plot levels) consistently outperformed models fit by generalized nonlinear least squares with only fixed parameters. Inclusion of plot density or basal area only slightly improved model fits and rarely supplanted the plot-level random parameter. However, anecdotal evidence suggested that stand structure might influence the height-diameter relationship; a better-structured dataset would be needed to statistically test for this effect.

The extension of the morphing algorithm, originally used by Williams et al. (2001, 2003) to edge-correct canopy cover estimates, to spatial point pattern analysis was explored in Chapter 2. Simulation experiments suggested that the unaltered morphing algorithm introduced bias into the point pattern, mostly as regularity at a scale near the plot radius. However, when combined with Monte Carlo and other resampling techniques across replicated point patterns, the morphing algorithm showed promise as a scaling tool for nested plot/subplot designs, introducing minimal bias into the

aggregation/regularity found in spatial patterns characteristic of naturally-regenerated forest stands.

In Chapter 3, I reconstructed spatial relationships within ten compartments of a long-term silvicultural experiment at the Penobscot Experimental Forest (PEF) by using current and past inventory data from 10,225 stem-mapped trees, the allometric relationships from Chapter 1, and the morphing algorithm from Chapter 2. Regeneration events, whether induced by natural stand dynamics or through harvesting, determined spatial pattern, generally increasing the aggregation in the spatial pattern, and reducing both species mingling (i.e., intermixing) and height differentiation. Further, only structural dynamics within uneven-aged managed compartments were representative of the natural stand dynamics within the PEF. Lastly, the reconstruction model clearly suggested that the Stand Complexity Index (*SCI*), developed by Zenner and Hibbs (2000) to characterize both spatial pattern and size differentiation, was highly correlated with tree density and was not adequate for comparing widely different stand structures.

STRENGTHS AND LIMITATIONS

The modeling approach developed for this study took advantage of temporal scale from long-term inventory plots at the expense of a smaller spatial scale. This approach has been rarely used in previous studies. Instead, many authors have conducted spatial analyses on a few, large (≥0.5 ha) plots and inferred spatial dynamics directly or across a chronosequence, mostly only using the pattern of the largest tree size classes (e.g., Mast and Veblen 1999, Zenner 2004, von Oheimb et al. 2005). A more insightful and analytically stronger approach would be to pair spatial pattern analysis with dendrochonological reconstruction of a stand. Motta and Edouard (2005), for example,

used this retrospective approach and found that land-use changes and not natural disturbances were responsible for most of the changes in structure across a mixedwood, multiaged forest. The study reported here is similar and has many of the same strengths as a retrospective study, except that this study is prospective (Gratzer et al. 2002) by using repeat measurements on sample plots rather than dendrochonological reconstructions to add a temporal component to the analysis. Further, this study takes advantage of efficient sampling methodology (i.e., nested plots) to estimate pattern for most established size classes, rather than truncating analyses to only largest size classes.

In terms of detecting true change in forest structure as affected by silviculture, the relatively long temporal scale (30+ years) was a major strength of this study. For example, since the area within the PEF where the long-term silviculture experiment was installed was largely one contiguous stand (Sendak et al. 2003, J. Brissette, pers. comm.), I am relatively confident that the differences in spatial structure detected in this study were true treatment effects. However, without this history or the repeated plot measurements within the compartments, the limited spatial scale of the analysis would strongly support this conclusion.

The morphing algorithm is the key component in my reconstruction model, so any biases introduced by that algorithm (i.e., increased regularity at the scale of the subplot) will strongly affect any conclusions from Chapter 3. Overall, I feel that the morphing algorithm is an appropriate avenue to conducting an exploratory analysis of spatial structure using nested growth and yield inventory systems, only if 1) multiple subplots are available from the stand or stratum for torodial wrapping within the algorithm; 2) isotropy (i.e., no directional trends) in the pattern can be assumed; and 3) the spatial

attributes at the stand or stratum level are the primary objects of interest, not the plot-level attributes. If any of these conditions are not met, data should be trimmed to the smallest shared spatial scale of the subpopulations of interest, or trimmed of the subpopulations from the smaller scale plots. Spatial interactions between subpopulations measured on different scales should be cautiously interpreted after morphing, as the algorithm makes no attempt to adjust positions of smaller-scaled patterns based on locations of individuals within larger-scaled patterns.

Although the morphing algorithm and reconstruction model described in this study can be computationally demanding (primarily from calculation of spatial statistics on multiple realizations of the same plot), there are few alternatives for spatial analysis in nested or clustered plot designs. Woodall and Graham (2004) proposed trimming Forest Inventory and Analysis clustered 0.0168 ha circular subplots and then combining them into a 0.0427 ha square for spatial analysis, but this approach disregarded 36% of the spatial information. Point process models may be fit to observed point patterns in simple-structured stands, thereby inferring information about underlying ecological mechanisms (Stamatellos and Panourgias 2005). In more complicated stands with multiple species and many size classes, it is unlikely this approach would work with current process models as the knowledge of the underlying interactions among species and size classes, the complexity of the model, and the computational demands increase factorially with the combined number of species and size classes. Unlike these methods, morphing is relatively simple, quite efficient, generally robust, and maintains approximately the same spatial structure (pattern, mingling, and differentiation). Morphing should be valuable for scaling measured plots within stands to larger extents

needed in spatially explicit, individual-based growth models and for visualization systems like the Stand Visualization System (McGaughey 2004).

Height models were another major component of the reconstruction model. As outlined in Chapter 1, the mixed-effect approach had a major advantage over generalized nonlinear least squares in that it explicitly incorporated the hierarchical sampling design. This approach helped account for site effects that could have biased a more general model and made the plot-level estimates much more accurate. In the reconstruction model, I made a further assumption that height of individual trees within a plot should develop allomorphically; this assumption prevented trees from "jumping up" or "falling down" suddenly at the end of the simulation cycle to their observed heights from plot average height. However, trees rarely have smooth height growth patterns with growth developing somewhat erratically as conditions favor sudden pulses of growth (e.g., sudden death of competitor).

Lastly, the reconstruction model made several simplifications to be consistent with the U.S. Forest Service's sampling protocols, particularly with the tree numbering system. These simplifications introduced some bias into the spatial metrics, primarily increasing randomness and reducing mingling, since stems were randomly located within the "distance-pie" locations. For example, I made no explicit attempt to model stump sprouting for missing hardwood stems.

RECOMMENDATIONS

Results and observations form this study indicate several recommendations for improving the long-term U.S. Forest Service study at the PEF. First, the study needs to be made more spatially explicit by mapping the locations of, at the very least, the large

trees in the plot and resisting convolution of the plot design. The morphing algorithm developed here may be inappropriate to use for ecological analysis with multiple nesting levels, although it still would be appropriate to use for visualization purposes.

Second, heights should be measured on a subset of sample trees, chosen from a representatively across plots, compartments and size classes in order to realize a dense enough sample to calibrate regional height-diameter equations. These height readings should be complimented with similar measurements in other experimental forests in the Northeast. There is a real need to develop these relationships for NE-TWIGS, as current height-diameter models are directly from work in the Lake States.

Third, and most importantly, the analysis of the silviculture study would greatly benefit from a mixed-modeling framework. Past publications have analyzed the study as an ANOVA-type design, based on the most current compartment-wide averages in order to avoid psuedoreplication. While appropriate, this approach has likely failed to detect differences between compartments in some circumstances due to a lack of replication at the compartment level. Further, these past statistical approaches are statistically inefficient because they overlook both the individual sample plots and the repeat measures nature of the data. A mixed-modeling framework can incorporate both, by assigning both plot (specifically time) and compartment random coefficients to a model of volume growth (or any other plot-level variable) over time, and partition the variability in the model to treatment-, compartment- or even plot-level sources. In this respect, one can look at the trends in the changes in variables, not the absolute values of the variables themselves at some predetermined time.

FUTURE DIRECTIONS

Based on the findings of this research, there are potentially several directions for future, productive investigation. First, more robust crown-width and crown-length relationships for the PEF study are needed, perhaps including spatial relationships among competitors. This effort would permit the comparison of crown development over time within the U.S. Forest Service compartments. Second, a more thorough analysis of the species-specific interactions in pattern is needed, perhaps across a larger dataset than available from the PEF. This effort would help illuminate the competitive interactions among species as affected by stand-level structure and tree size.

This information, along with many of the results from this dissertation, could then be used to help calibrate spatially explicit, individual-based physiological growth models like SORTIE (Pacala et al. 1993, 1996) or ZELIG (Urban et al. 1991). I believe that these types of models are essential for future silvicultural research in the Northeast, particularly as existing forest types become more and more stressed from climate change and other related stressors (e.g., invasive insects). Fine-scale, heterogeneous patterns of canopy disturbance, typical of northeastern stands, are difficult to model with traditional patch-based models of forest dynamics. Spatially explicit, individual-based models can be parameterized with spatial models of environmental factors and distributions of trees as measured in descriptive field studies (Gratzer et al. 2004), thus allowing a much tighter linkage between modeling pattern and process at the stand scale. Further, as Kenefic et al. (2005b) suggested, control and reference stands are lacking in the region; simulations with spatially explicit individual-based models could serve as a surrogate to assess risk with various silvicultural and management options.

There is a great need to develop methodology for collecting and analyzing forest structural patterns across larger extents in order to relate patterns and processes operating on fine scales (e.g., competition) to those operating on broader scales (e.g., natural disturbance) (Levin 1992, Gratzer et al. 2004). Spatially-explicit sampling can be very time-consuming and costly, and does not always yield a large increase in knowledge of the sampled ecosystem over more traditional, non-spatial analyzes (e.g., Figure 3.12). These drawbacks often are primarly because a broad enough range of scales cannot be studied since sampling costs rise exponentially as plots increase in size. As discussed in Chapters 2 and 3, use of small plots within a well-designed inventory system could increase the scale, by using the plot averages of any spatial parameter; however, this approach would still require a large amount of fieldwork and may not be appropriate for spatial analysis of canopy patterns. Further, although spatially explicit individual-tree models may be calibrated with this fine-scale spatial data, they are not feasible for modeling pattern and process at broader scales because of computational expense due the vast size of the datasets that would be involved and the model's stochasticity (Gratzer et al. 2004). For example, a run of a 100 ha area with an average of 10,000 trees/ha simulated over 100 years would likely require » 5 x 10^{12} calculations. Remote sensing approaches for quantifying spatial structure over large areas will be required. One of the most promising, light detection and ranging systems (LiDAR), has been used to estimate height and crown properties (Næsset and Økland 2002), leaf area index (Roberts et al. 2005), and spatial positions (Yu et al. 2004), of individual trees, and stand-level vertical structure, volume and biomass (Zimble et al. 2003, Popescu et al. 2004, Hyde at al. 2006). Koukoulas and Blackburn (2005) provides one example of the use of LiDAR for

spatial pattern analysis. Using a combination of LiDAR, airborne thematic mapper, and ground measurements, they developed a spatially-explicit canopy model for a oak-beech forest and then conducted $K(d)$ analysis to investigated spatial relationships among tree sizes, tree species and gap locations. Repeated successively over several years, spatially-explicit datasets developed from or supplemented by LiDAR and other similar remotes systems, might illuminate the dynamics of forest canopy structure over broad scales at a fraction of the cost and effort from solely ground-based approaches.

BIBLIOGRAPHY

Aguirre, O., Gangying, H., von Gadow, K., and Jiménez, J. 2003. An analysis of spatial forest structure using neighbourhood-based variables. For. Ecol. Manage. **183**(1-3): 137-145.

Antos, J.A., and Parish, R. 2002. Structure and dynamics of a nearly steady-state subalpine forest in south-central British Columbia, Canada. Oecologia **130**(1): 126-135.

Armesto, J.J., Mitchell, J.D., and Villagran, C. 1986. A comparison of spatial patterns of trees in some tropical and temperate forests. Biotropica **18**(1): 1-11.

Assmann, E. 1970. The principles of forest yield study. Pergamon Press, Oxford. 520 p.

Baddeley, A., Turner, van Lieshout, M-C, et al. 2004. spatstat: Spatial point pattern analysis, model-fitting and simulation. Version 1.5-4. Available online at http://www.maths.uwa.edu.au/~adrian/spatstat.html.

Bailey, T.C., and Gatrell, A.C. 1995. Interactive spatial data analysis. John Wiley & Sons, New York, NY. 413 p.

Barnes, B.V., Zak, D.R., Denton, S.R., and Spurr, S.H. 1998. Forest ecology. 4th Edition. John Wiley & Sons, Inc., New York, NY. 774 p.Besag, J. 1977. Contribution to the discussion of Dr. Ripley's paper. J. Royal Stat. Soc., Series B **39**(2): 193-195.

Bragg, D.C. 2001. A local basal area adjustment for crown width prediction. North. J. Appl. For. **18**(1): 22-28.

Briggs, R.S. 1994. Site classification field guide. CFRU Tech. Note 6, MAFES Misc. Publ. 724. Maine Agri. For. Exp. Station, Orono, ME. 15 p.

Briggs, R.S., and Lemin, R.C., Jr. 1994. Soil drainage class effects on early response of balsam fir to precommercial thinning. Soil Sci. Soc. Am. J. **58**(4): 1231-1239.

Brissette, J.C. 1996. Effects of intensity and frequency of harvesting on abundance, stocking and composition of natural regeneration in the Acadian Forest of eastern North America. Silva Fennica **30**(2-3): 301-314.

Brissette, J.C., and Kenefic, L.S. 2000. Eastern hemlock response to even- and uneven-age management in the Acadian Forest: Results from the Penobscot Experimental Forest long-term silviculture study. Pages 23-28 in McManus, KA, Shields, KS, and Souto, DR, eds. Proceedings: Symposium on sustainable management of hemlock ecosystems in eastern North America (June 22-24, 1999). Gen. Tech. Rep. 267. USDA Forest Service, Northeast Research Station, Durham, NH. 237 p.

Brissette, J.C., Frank, R.M., Jr., Stone, T.L., and Skratt, T.A. 1999. Precommercial thinning in a northern conifer stand: 18-year results. For. Chron. **75**(6): 967-972.

Brokaw, N.L., and Lent, R.A. 1999. Vertical structure. Pages 373-399 in Hunter, ML, Jr., ed. Maintaining biodiversity in forest ecosystems. Cambridge University Press, New York, NY. 698 p.

Buongiorno, J., Dahir, S., Lu, H., Lin. C. 1994. Tree size diversity and economic returns in uneven-aged forest stands. For. Sci. **40**(1): 83-103.

Bush, R.R. 1995. Northeastern TWIGS variant of the Forest Vegetation Simulator. USDA Forest Service, Forest Management Service Center. Available online at http://www.fs.fed.us/fmsc/fvs/variants/ne.php.

Calama, R. and Montero, G. 2004. Interregional nonlinear height-diameter model with random coefficients for stone pine in Spain. Can. J. For. Res. **34**(1): 150-163.

Clark, P.J., and Evans, F.C. 1954. Distance to nearest neighbor as a measure of spatial relationships in populations. Ecology **35**(3): 445-453.

Coates, K.D., Canham, C.D., Beaudet, M., Sachs, D.L., and Messier, C. 2003. Use of a spatially explicit individual-tree model (SORTIE/BC) to explore the implications of patchiness in structurally complex forests. For. Ecol. Manage. **186**(1-3): 297-310.

Cressie, N.A.C. 1993. Statistics for spatial analysis. Revised edition. John Wiley & Sons, New York, NY. 900 p.

Curtis, R.O. 1967. Height-diameter and height-diameter-age equations for second-growth Douglas-fir. For. Sci. **13**(4): 365-375.

Daggett, H. 2003. Long-term effects of herbicide and precommercial thinning treatments on species composition stand structure, and net present value in spruce-fir stands in Maine: The Austin Pond study. M.S. Thesis. Dept. Forest Ecosystem Science, University of Maine, Orono, ME. 136 p.

Demidenko, E. 2004. Mixed models: Theory and applications. John Wiley & Sons, Inc., Hoboken, NJ. 704 p.

Diggle, P.J. 2003. Statistical analysis of spatial point patterns. 2nd Edition. Arnold Publishing, London. 159 p.

Donnelly, K. 1978. Simulations to determine the variance and edge-effect of total nearest neighbour distance. Pages 91-95 in Hodder, I., ed. Simulation methods in archaeology. Cambridge University Press, London. 139 p.

Ek, A.R., Birdsall, E.T., and Spears, R.J. 1981. Total and merchantable tree height equations for Lake States tree species. Staff Paper Series 27. College of Forestry, University of Minnesota, St. Paul, MN. 43 p.

Ek, A.R., Birdsall, E.T., and Spears, R.J. 1984. A simple model for estimating total and merchantable tree heights. Res. Note NC-309. USDA Forest Service, North Central Forest Experiment Station, St. Paul, MN. 5 p.

Fang, Z., and Bailey, R.L. 1998. Height-diameter models for tropical forests on Hainan Island in southern China. For. Ecol. Manage. **110**(1-3): 315-327.

Fang, Z., Bailey, R.L., and Shiver, B.D. 2001. A multivariate simultaneous prediction system for stand growth and yield with fixed and random effects. For. Sci. **47**(4): 550-562.

Ferrari, J.B. 1999. Fine-scale patterns of leaf litterfall and nitrogen cycling in an old-growth forest. Can. J. For. Res. **29**(3): 291-302.

Franklin, J.F., and Van Pelt, R. 2004. Spatial aspects of structural complexity in old growth forests. J. For. **102**(3): 22-28.

Franklin, J.F., Spies, T.A., Van Pelt, R., Carey, A.B., Thornburgh, D.A., Berg, D.R., Lindenmayer, D.B., Harmon, M.E., Keeton, W.S., Shaw, D.C., Bible, K., and Chen, J. 2002. Disturbances and structural development of natural forest ecosystems with silvicultural implications, using Douglas-fir forests as an example. For. Ecol. Manage. **155**(1-3): 399-423.

Fraver, S., and White, A.S. 2005. Disturbance dynamics of old-growth *Picea rubens* forests of northern Maine. J. Veg. Sci. **16**(6): 597-610.

Freeman, E.A., and Ford, E.D. 2002. Effects of data quality on analysis of ecological pattern using the $\hat{K}(d)$ statistical function. Ecology **83**(1): 35-46.

Frelich, L.E., Cornett, M.W., and White, M.A. 2005. Controls and reference conditions in forestry: the role of old-growth and retrospective studies. J. For. **103**(7): 339-344.

Fúle, P.Z., and Covington, W.W. 1998. Spatial patterns of Mexican pine-oak forests under different recent fire regimes. Plant Ecol. **134**(2): 197-209.

Goreaud, F., and Pélissier, R. 2000. Spatial structure analysis of heterogenous point patterns: examples of application to forest stands. ADS in ADE-4. 49 p. Available online at http://iubio.bio.indiana.edu/soft/iubionew/molbio/dna/analysis/ADE4/DocThemPDFUS/Thema81.pdf.

Goreaud, F., and Pélissier, R. 2003. Avoiding misinterpretation of biotic interactions with the intertype K_{12}-function: population independence vs. random labelling hypotheses. J. Veg. Sci. **14**(5): 681-692.

Grassi, G., Minotta, G., Giannini, R., and Bagnaresi, U. 2003. The structural dynamics of managed uneven-aged conifer stands in the Italian eastern Alps. For. Ecol. Manage. **185**(3): 225-237.

Gratzer, G., Canham, C., Dieckmann, U., Fischer, A., Iwasa, Y., Law, R., Lexer, M.J., Sandmann, H., Spies, T.A., Splechtna, B.E., and Szwagrzyk, J. 2002. Spatio-temporal development of forests – current trends in field methods and models. Oikos **107**(1): 3-15.

Greenwood, M., O'Brien, C., and McConville, D. 2003. Factors affecting regeneration of red spruce and balsam fir. Pages 32-34 in McConville, D., ed. Cooperative Forestry Research Unit 2003 Annual Report. MAFES Misc. Publ. 2684. Cooperative Forestry Research Unit, Orono, ME. 73 p.

Greig-Smith, P. 1983. Quantitative plant ecology. 3rd edition. Blackwell Scientific, Oxford, England. 359 p.Greig-Smith, P., and Chadwick, M.J. 1965. Data on pattern in plant communities: III. *Acadia-Capparis* semi-desert scrub in the Sudan. J. Ecol. **53**(2): 465-474.

Haglöf, AB. 2002. Users guide Vertex III and Transponder T3. Haglöf Sweden, AB, Långsele, Sweden. 11 p.

Haglöf, AB. 2003. DME users manual. Version 1.3. Haglöf Sweden, AB, Långsele, Sweden. 4 p.

Harrod, R.J., McRae, B.H., and Hartl, W.E. 1999. Historical stand reconstruction in ponderosa pine forests to guide silvicultural prescriptions. For. Ecol. Manage. **114**(2-3): 433-446.

Hawley, R.C., and Hawes, A.F. 1925. Manual of forestry for the Northeastern United States. Vol. 1, 2nd Edition. John Wiley & Sons, New York, NY. 281 p.

Homyack, J.A., Harrison, D.J., and Krohn, W.B. 2004. Structural differences between precommercially thinned and unthinned conifer stands. For. Ecol. Manage **194**(1-3): 131-143.

Huang, S., Titus, S.J., and Wiens, D.P. 1992. Comparison of nonlinear height-diameter functions for major Alberta tree species. Can. J. For. Res. **22**(9): 1297-1304.

Hyde, P., Dubayah, R., Walker, W., Blair, J.B., Hofton, M., and Hunsaker, C. 2006. Mapping forest structure for wildlife habitat analysis using multi-sensor (LiDAR, SAR/InSAR, ETM+, Quickbird) synergy. Remote Sens. Environ. In press.

Husch, B., Miller, C.I., and Beers, T.W. 1982. Forest mensuration. 3rd Edition. John Wiley & Sons, Inc., New York. 402 p.

Isham, V. 1984. Multitype Markov point processes: some approximations. Proc. Royal Soc. London, Ser. A **391**: 39-53.

Keeton, W.S. 2005. Managing for old-growth in northern hardwood. Pages 107-117 in Peterson, C.E., and Maguire, D.A., eds. Balancing ecosystem values: innovative experiments for sustainable forestry. Gen. Tech. Rep. PNW-GTR-635. USDA Forest Service, Pacific Northwest Research Station, Portland, OR. 389 p.

Kenefic, L.S., Sendak, P.E., and Brissette, J.C. 2005a. Comparison of fixed diameter-limit and selection cutting in northern conifers. North. J. Appl. For. **22**(2): 77-84.

Kenefic, L.S., White, A.S., Cutko, A.R., and Fraver, S. 2005b. Reference stands for silvicultural research: a Maine perspective. J. For. **103**(7): 363:367.

Kenkel, N.C. 1988. Pattern of self-thinning in jack pine: testing the random mortality hypothesis. Ecology **69**(4): 1017-1024.

Kimmins, J.P. 1997. Biodiversity and its relationship to ecosystem health and integrity. For. Chron. **73**(2): 229-232.

Kint, V., Van Meirvenne, M., Nachtergale, L., Geudens, G., and Lust N. 2001. Spatial methods for quantifying forest stand structure development: a comparison between nearest-neighbor indices and variogram analysis. For. Sci. **49**(1): 36-49.

Koukoulas, S., and Blackburn, G.A. 2005. Spatial relationships between tree species and gap characteristics in broad-leaved deciduous woodland. J. Veg. Sci. **16**(5): 587-596.

Kruskal, J.B. 1964. Nonmetric multidimensional scaling: a numerical method. Psychometrika **29**(2): 115-129.

Kuha, J. 2004. AIC and BIC: Comparisons of assumptions and performance. Soc. Methods & Res. **33**(2): 188-229.

Laessle, A. 1965. Spacing and competition in natural stands of sand pine. Ecology **46**(1-2): 65-72.

Lähde, E., Laiho, O., Norokorpi, Y., and Saksa, T. 1999. Stand structure as the basis of diversity index. For. Ecol. Manage. **115**(2): 213-220.

Lappi, J. 1991. Calibration of height and volume equations with random parameters. For. Sci. **37**(3): 781-801.

Lappi, J., and Bailey, R.I. 1988. Height prediction model with random stand and tree parameters: An alternative to traditional site index methods. For. Sci. **34**(4): 907-927.

Lappi, J., and Malinen, J. 1994. Random-parameter height/age models when stand parameters and stand age are correlated. For. Sci. **40**(4): 715-731.

Larsen, D.R., and Bliss, L.C. 1998. An analysis of structure of tree seedling populations on a Lahar. Landscape Ecol. **13**(5): 307-322.

Le Guerrier, C., Marceau, D.J., Bouchard, A., and Brisson, J. 2003. A modeling approach to assess the long-term impact of beech bark disease in northern hardwood forest. Can. J. For. Res. **33**(12): 2416-2425.

Levin, S.A. 1992. The problem of pattern and scale in ecology. Ecology **73**(6): 1943-1967.

Lindenmayer, D.B., and Franklin, J.F. 2002. Conserving forest biodiversity. Island Press, Washington, D.C. 351 p.

Lindgren, P.M.F., and Sullivan, T.P. 2001. Influence of alternative vegetation management treatments on conifer plantation attributes: Abundance, species diversity, and structural diversity. For. Ecol. Manage. **142**(1-3): 163–182.

Loehle, C. 2000. Forest ecotone response to climate change: sensitivity to temperature response functional forms. Can. J. For. Res. **30**(10): 1632-1645.

Lorimer, C.G. 1977. The presettlement forest and natural disturbance cycle of northeastern Maine. Ecology **58**(1): 139-148.

Lotwick, H.W., and Silverman, B.W. 1982. Methods for analysing spatial processes of several types of points. J. Royal Stat. Soc., Series B **44**(3): 406-413.

Lynch, T.B., Holley, A.G., and Stevenson, D.J. 2005. A random-parameter height-dbh model for cherrybark oak. South. J. Appl. For. **29**(3): 22-26.

MacArthur, R.H., and MacArthur, J.W. 1961. On bird species diversity. Ecology **42**(3): 594-598.Marascuilo, L.A., and McSweeney, M. 1967. Nonparametric post hoc comparisons for trend. Psychol. Bull. **67**: 401-412.

Martens, S.N., Breshears, D.D., Meyer, C.W., and Barnes, F.J. 1997. Scales of above-ground and below-ground competition in a semi-arid woodland detected from spatial patterns. J. Veg. Sci. **8**(5): 655-664.

Mast, J.N., and Veblen, T.T. 1999. Tree spatial patterns and stand development along the pine-grassland ecotone in the Colorado Front Range. Can. J. For. Res. **29**(5): 575-584.

Mather, P.M. 1976. Computational methods of multivariate analysis in physical geography. J. Wiley & Sons, London, England. 532 p.

McComb, W., and Lindenmayer, D. 1999. Dying, dead, and down trees. Pages 335-372 in Hunter, M.L., Jr., eds. Maintaining biodiversity in forest ecosystems. Cambridge University Press, Cambridge, Great Britain. 698 p.

McCune, B., and Grace, J.B. 2002. Analysis of ecological communities. MjM Software Design, Gleneden Beach, OR. 300 p.

McCune, B., and Mefford, M.J. 1999. Multivariate analysis of ecological data. Version 4.07. MjM Software Design, Gleneden Beach, OR.

McElhinny, C., Gibbons, P., Brack, C., Bauhas, J. 2005. Forest and woodland stand structural complexity: its definition and measurement. For. Ecol. Manage. **218**(1-3): 1-24

McGaughey, R.J. 2004. Stand Visualization System. Version 3.30. USDA Forest Service, Pacific Northwest Experiment Station. 141 p. Available online at http://www.fs.fed.us/fmsc/fvs/documents/gtrs_winsvsguide.php.

Mehtäto, L. 2004. A longitudinal height-diameter model for Norway spruce in Finland. Can. J. For. Res. **34**(1): 131-140.

Ménard, A., Dubé, P., Bouchard, A., Canham, C.D., and Marceau, D.J. 2002. Evaluating the potential of the SORTIE forest succession model for spatio-temporal analysis of small-scale disturbances. Ecol. Model. **153**(1): 81-96.

Meyer, H.A. 1940. A mathematical expression for height curves. J. For. **38**(5): 415-420.

Moeur, M. 1993. Characterizing spatial patterns of trees using stem-mapped data. For. Sci. **39**(4): 756-775.

Montes, F., Sánchez, M., del Río, M. and Cañellas, I. 2005. Using historic management records to characterize the effects of management on the structural diversity of forests. For. Ecol. Manage. **207**(3): 279-293.

Motta, R. and Edouard, J.L. 2005. Stand structure and dynamics in a mixed and multilayered forest in the Upper Susa Valley, Piedmont, Italy. Can. J. For. Res. **35**(1): 21-36.

Næsset, E., and Økland, T. 2002. Estimating tree height and tree crown properties using airborne scanning laser in a boreal nature preserve. Remote Sens. Environ. **79**(1): 105-115.

Nanos, N., Calama, R., Montero, G., and Gil, L. 2004. Geostatistical prediction of height/diameter models. For. Ecol. Manage. **195**(1-2): 221-235.

North, M., Chen, J., Oakley, B., Song, B., Rudnicki, M., Gray, A., and Innes, J. 2004. Forest stand structure and pattern of old-growth western hemlock/Douglas-fir and mixed-conifer forests. For. Sci. **50**(3): 299-311.

O'Hara, K.L. 1996. Dynamics and stocking-level relationships of multi-aged ponderosa pine stands. For. Sci. **42**, Monograph 33. 34 p.

O'Hara, K.L. 2001. The silviculture of transformation – a commentary. For. Ecol. Manage. **151**(1-3): 81-86.

O'Hara, K.L., and Gersonde, R.F. 2004. Stocking control concepts in uneven-aged silviculture. Forestry **77**(2): 131-143.

Oliver, C.D., and Larson, B.C. 1996. Forest stand dynamics. Update edition. John Wiley & Sons, Inc., New York, NY. 520 p.

Pacala, S.W., Canham, C.D., and Silander, J.A.J. 1993. Forest models defined by field measurements. I. The design of a northeastern forest simulator. Can. J. For. Res. **23**(10): 1980–1988.

Pacala, S.W., Canham, C.D., Saponara, J., Silander, J.A., Jr., Kobe, R.K., and Ribbens, E. 1996. Forest models defined by field measurements: estimation, error analysis and dynamics. Ecol. Monogr. **66**(1): 1-43.

Palik, B.J., Mitchell, R.J., and Hiers, J.K. 2002. Modeling silviculture after natural disturbance to sustain biodiversity in the longleaf pine (*Pinus palustris*) ecosystem: Balancing complexity and implementation. For. Ecol. Manage. **155**(1-3): 347-356.

Papaik, M.J., Canham, C.D., Latty, E.F., and Woods, K.D. 2005. Effects of an introduced pathogen on resistance to natural disturbance: beech bark disease and windthrow. Can. J. For. Res. **35**(8): 1832-1843.

Peng, C., Zhang, L., and Liu, J. 2001. Developing and validating nonlinear height-diameter models for major tree species of Ontario's boreal forests. North. J. Appl. For. **18**(3): 87-94.

Peterson, C.J., and Squiers, E.R. 1995. An unexpected change in spatial pattern across 10 years in an aspen-white pine forest. J. Ecol. **83**(5): 847-855.

Phillips, D.L., and MacMahon, J.A. 1981. Competition and spacing patterns in desert shrubs. J. Ecol. **69**(1): 97-115.

Picket, S.T.A., and White, P.S., eds. 1985. The ecology of natural disturbance and patch dynamics. Academic Press, New York, NY. 472 p.

Pielou, E.C. 1962. The use of plant-to-neighbor distances for the detection of competition. J. Ecol. **50**(2): 357-367.

Pielou, E.C. 1977. Mathematical ecology. Wiley, Oxford, United Kingdom. 385 p.

Pinheiro, J.C., and Bates, D.M. 2000. Mixed-effects models in S and S-PLUS. Springer, New York, NY. 528 p.

Pinheiro, J.C., Bates, D.M., DebRoy, S., and Sarkar, D. 2005. nlme: Linear and nonlinear mixed effects models. R package version 3.1-65. Available online at http://www.R-project.org.

Pommerening, A. 2002. Approaches to quantifying forest structures. Forestry **75**(3): 305-324.

Popescu, S.C., Wynne, R.H., and Scrivani, J.A. 2004. Fusion of small-footprint LiDAR and multispectral data to estimate plot-level volume and biomass in deciduous and pine forest in Virginia, USA. For. Sci. **50**(4): 551-565.

Pretzsch, H. 1997. Analysis and modeling of spatial stand structures. Methodological considerations based on mixed beech-larch stands in Lower Saxony. For. Ecol. Manage. **97**(3): 237-253.

R Development Core Team. 2005. R: A language and environment for statistical computing. Version 2.2. R Foundation for Statistical Computing, Vienna, Austria. ISBN 3-900051-07-0. Available online at http://www.R-project.org.

Ratkowsky, D.A. 1983. Nonlinear regression modeling: a unified practical approach. Marcel Dekker, Inc., New York, NY. 276 p.

Ratkowsky, D.A., and Reedy, T.J. 1986. Choosing near-linear parameters in the four-parameter logistic model for radioligand and related assays. Biometrics **42**(3): 575-582.

Richards, F.J. 1959. A flexible growth function for empirical use. J. Exp. Bot. **10**(29): 290-300.

Ripley, B.D. 1976. The second-order analysis of stationary point processes. J. Appl. Probab. **13** (2): 255-266.

Ripley, B.D. 1977. Modelling spatial patterns. J. Royal Stat. Soc., Series B **39**(2): 172-212.

Roberts, S.D., Dean, T.J., Evans, D.L., McCombs, J.W., Harrington, R.L., and Glass, P.A. 2005. Estimating individual tree leaf area in loblolly pine plantations using LiDAR-derived measurements of height and crown dimensions. For. Ecol. Manage. **213**(1-3): 54-70.

Rowlingson, B., Diggle, P., Bivand, R., Petris G., and Eglen, S. 2005. splancs: Spatial and space-time point pattern analysis. Version 2.01-16. Available online at http://www.maths.lancs.ac.uk/~rowlings/Splancs/.

Runkle, J.R. 1982. Patterns of disturbance in some old-growth mesic forests of eastern North America. Ecology **63**(5): 1533-1546.

Saunders, M.R., Wagner, R.G., and Brissette, J. 2002. Developing metrics for 3-dimensional forest stand structure: A test of the stand complexity index hypothesis. Page 63 in Wagner, R.G., comp. Proceedings of the Eastern CANUSA Forest Science Conference, October 19-20, Orono, ME. 122 p.

Saunders, M.R., and Wagner, R.G. 2005. Ten-year results of the Forest Ecosystem Reseach Program—successes and challenges. Pages 147-153 in Peterson, C.E., and Maguire, D.A., eds. Balancing ecosystem values: innovative experiments for sustainable forestry. Gen. Tech. Rep. PNW-GTR-635. USDA Forest Service, Pacific Northwest Research Station, Portland, OR. 389 p.

Schütz, J.-P. 1999. Close-to-nature silviculture: is this concept compatible with species diversity? Forestry **72**(4): 359-366.

Sendak, P.E., Brissette, J.C., and Frank, R.M. 2003. Silviculture affects composition, growth, and yield in mixed northern conifers: 40-year results from the Penobscot Experimental Forest. Can. J. For. Res. **33**(11): 2116-2128.

Seymour, R.S. 1992. The red spruce-balsam fir forest of Maine: evolution of silvicultural practice in response to stand development patterns and disturbances. Pages 217-244 in Kelty, M.J., Larson, B.C., and Oliver, C.D., eds. The ecology and silviculture of mixed-species forests. A festschrift for David M. Smith. Kluwer Publishers, Norwell, MA. 372 p.

Seymour, R.S., and Hunter, M.L., Jr. 1999. Principles of ecological forestry. Pages 22-61 in Hunter, M.L., Jr., eds. Maintaining biodiversity in forest ecosystems. Cambridge University Press, Cambridge, Great Britain. 698 p.

Seymour, R.S., and Kenefic, L.S. 1998. Balance and sustainability in multiaged stands: a northern conifer case study. J. For. **96**(7): 12-17.

Seymour, R.S., Guilden, J., Marshall, D., and Palik, B. In press. Large-scale, long-term silvicultural experiments in the United States. Allgemeine Forst-und Jagdzeitung.

Seymour, R.S., White, A.S., and deMaynadier, P.G. 2002. Natural disturbance regimes in northeastern North America—evaluating silvicultural systems using natural scales and frequencies. For. Ecol. Manage. **155**(1-3): 357-367.

Skarpe, C. 1991. Spatial patterns and dynamics of woody vegetation in an arid savanna. J. Veg. Sci. **2**(4): 565-572.

Smith, D.M. 1962. The practice of silviculture. 7th Edition. John Wiley & Sons, Inc., New York, NY. 578 p.

Solomon, D.S., and Gove, J.H. 1999. Effects of uneven-aged management intensity on structural diversity in two major forest types in New England. For. Ecol. Manage. **114**(2): 265-274.

Stamatellos, G., and Panourgias, G. 2005. Simulating spatial distributions of forest trees by using data from fixed area plots. Forestry **78**(3): 305-312.

Szwagrzyk, J., and Czerwczak, M. 1993. Spatial patterns of trees in natural forests of east-central Europe. J. Veg. Sci. **4**(4): 469-476.

Taylor, A.H., and Halpern, C.B. 1991. The structure and dynamics of *Abies magnifica* forests in the southern Cascade Range, USA. J. Veg. Sci. **2**(2): 189-200.

Thomson, J.D., Weiblen, G., Thomson, B.A., Alfaro, S., and Legendre, P. 1996. Untangling multiple factors in spatial distributions: lilies, gophers, and rocks. Ecology **77**(6): 1698-1715.

Tillman, K.M., compiler. 2004. Forest Inventory and Analysis: National core field guide. Volume I: Field data collection procedures for phase 2 plots. Version 2.0. USDA Forest Service, Northeastern Research Station, Newtown Square, PA. 252 p.

Toumey, J.W. 1928. The foundations of silviculture upon an ecological basis. Volume 1. John Wiley & Sons, Inc., London, England. 438 p.

Tremblay, M., Messier, C., and Marceau, D.J. 2005. Analysis of deciduous tree species dynamics after a severe ice storm using SORTIE model simulations. Ecol. Model. **187**(2-3): 297-313.

Trorey, L.G. 1932. A mathematical method for the construction of diameter height curves based on site. For. Chron. **8**(2): 121-132.

Turner, R. 2002. deldir: Delaunay triangulation and Dirichlet (Voronoi) tesselation. R package version 0.0-4. Available online at http://www.math.unb.ca/~rolf/.

Upton, G.J.G. and Fingleton, B. 1985. Spatial data analysis by example. Volume 1: Point pattern and quantitative data. John Wiley & Sons, Inc., New York, NY. 410 p.

Urban, D.L., Bonan, G.B., Smith, T.H., and Shugart, H.H. 1991. Spatial application of gap models. For. Ecol. Manage. **42**(1): 95-110.

von Gadow, K., and Hui, G. 1999. Modelling forest development. Kluwer Academic Publishers, Dordrecht, The Netherlands. 213 p.

von Oheimb, G., Westphal, C., Tempel, H., and Härdtle, W. 2005. Structural pattern of a near-natural beech forest (*Fagus sylvatica*) (Serrahn, North-east Germany). For. Ecol. Manage. **212**(1-3): 253-263.

Ward, J.S., Parker, G.R., and Ferrandino, F.J. 1996. Long-term spatial dynamics in an old-growth deciduous forest. For. Ecol. Manage. **83**(3): 189-202.

Watt, A.S. 1947. Pattern and process in the plant community. J. Ecol. **35**(1-2): 1-22.

Weibull, W. 1951. A statistical distribution function of wide applicability. J. Appl. Mech. **18**: 293-296.

Westveld, M. 1931. Reproduction on pulpwood lands in the Northeast. Tech. Bul. 223. USDA Forest Service, Northeastern Forest Experiment Station, Amhert, MA. 52 p.

Wilkinson, R.C. 1983. Leader and growth characteristics of eastern white pine associated with white pine weevil attack susceptibility. Can. J. For. Res. 13(1): 78-84.

Williams, M.S., Patterson, P.L., and Mowrer, H.T. 2003. Comparison of ground sampling methods for estimating canopy cover. For. Sci. **49**(2): 235-246.

Williams, M.S., Williams, M.T., and Mowrer, H.T. 2001. A boundary reconstruction method for circular for fixed-area plots in environmental survey. J. Agric. Biol. & Environ. Stat. **6**(4): 479-494.

Willson, M.F. 1974. Avian community organization and habitat structure. Ecology **55**(5): 1017-1029.

Woodall, C.W., and Graham, J.M. 2004. A technique for conducting point pattern analysis of cluster plot stem-maps. For. Ecol. Manage. **198**(1-3): 31-37.

Yu, X., Hyyppä, J., Haartinen, H., and Maltamo, M. 2004. Automatic detection of harvested trees and determination of forest growth using airborne laser scanning. Remote Sens. Environ. **90**(4): 451-462.

Yuancai, L., and Parresol, B.R. 2001. Remarks on height-diameter modeling. Res. Note SRS-10. USDA Forest Service, Southern Research Station, Asheville, NC. 5 p.

Zar, J.H. 1999. Biostatistical analysis. 4th edition. Prentice Hall, Upper Saddle Hill, NJ. 929 p.

Zenner, E.K. 2000. Do residual trees increase structural complexity in Pacific Northwest coniferous forests? Ecol. Appl. **10**(3): 800-810.

Zenner, E.K. 2004. Does old-growth condition imply high live-tree structural complexity? For. Ecol. Manage. **195**(1-2): 243-258.

Zenner, E.K. 2005. Investigating scale-dependent stand heterogeneity with structure-area curves. For. Ecol. Manage. **209**(1-2): 87-100.

Zenner, E.K., and Hibbs, D.E. 2000. A new method for modeling the heterogeneity of forest structure. For. Ecol. Manage. **129**(1): 75-87.

Zhang, S., Burkhart, H.E., and Amateis, R.L. 1997. The influence of thinning on tree height and diameter relationships in loblolly pine plantations. South. J. Appl. For. **21**(4): 199-205.

Zimble, D.A., Evans, D.L., Carlson, G.C., Parker, R.C., Grado, S.C., and Gerard, P.D. 2003. Characterizing vertical forest structure using small-footprint airborne LiDAR. Remote Sens. Environ. **87**(2-3): 171-182.

APPENDICES

APPENDIX A

R CODE USED FOR MORPHING EXPERIMENTS

The following code was used within Chapter 2 to build simulated point patterns (A.1), calculate the population-levels parameters of these patterns (A.2), generate sample plots drawn from each pattern and calculate summary statistics from each plot (A.4). Custom functions used within the morphing algorithm are listed in A.3.

A.1. POINT PATTERN GENERATION

Clustered pattern:

```
# The following commands generate a point pattern using the Thomas
# cluster process, which is a special case of the Neyman-Scott process.
# This process generates a Poisson distribution of "parent" points,
# from which the clustering algorithm generates a set of "offspring"
# points.  The intensity of the points is given by BETA and the
# intensity of the cluster centers is given by BETA.clust.  The process
# is simulated over the extent defined by x.size and y.size.
#
# Outputs are BETA, BETA.clust, x.size, y.size, and sim.clu.

require(spatstat,quietly=TRUE)
require(splancs,quietly=TRUE)
BETA<-1
BETA.clust<-0.1
x.size<-125
y.size<-125


# These commands define the average number of offspring points per
# cluster (mu.clust) and the average spacing between clusters.  Because
# this is a random process and the full intensity of points is not
# assured (i.e., simulated beta could be greater or less than BETA),
# mu.clust is inflated by 10% and then random points are deleted to get
# simulated beta = BETA*x.size*y.size.  Sigma, or the standard
# deviation of displacement of the offspring points from a parent
# point, is a fraction of spacing.  This was set at spacing/3 to
# simulate moderate clustering.

mu.clust<-BETA/BETA.clust
spacing<-(BETA.clust^(-0.5))
sim.clu<-rThomas(BETA.clust,spacing/3,mu.clust*1.1,
   win=owin(c(0,x.size),c(0,y.size)))
sim.clu<-as.points(sim.clu)
```

```
sim.clu<-thin(sim.clu,BETA*x.size*y.size)
sim.clu<-ppp(sim.clu[,1],sim.clu[,2],window=owin(c(0,x.size),
   c(0,y.size)))


# This command cleans the workspace of unnecessary variables.

rm(mu.clust,spacing)
```

Random pattern:

```
# These commands produce sim.ran, a random Poisson point pattern with
# intensity of BETA and spatial extent of x.size by y.size.
#
# Output is BETA, x.size, y.size, and sim.ran.

require(spatstat,quietly=TRUE)
BETA<-1
x.size<-125
y.size<-125
sim.ran<-rpoint(BETA*x.size*y.size,win=c(0,x.size,0,y.size),
   giveup=1000)
```

Regular pattern:

```
# These commands produce a hardcore Strauss point pattern using the
# Metropolis- Hastings algorithm.  BETA is the intensity on a per unit
# area basis (i.e., 0.5 = 5000 tpha).  GAMMA is the "strength" of the
# inhibition between points over the radius IR; when GAMMA = 0, it is
# effectively a hardcore  inhibition, and when GAMMA = 1 there is no
# inhibition between points. HR is the hardcore radii, meaning that no
# points occur closer than this distance apart.  I used GAMMA, IR and
# HR of 0.75, 0.75 and 0.50, respectively, to simulate a strongly
# regular pattern with no points closer than 0.5, or 1/2 the expected
# point spacing, and a reduced chance that points could occur within
# 0.50-0.75 of one another.
#
# Normally, the Metropolis-Hastings algorithm allows three processes of
# point pattern generation: births, deaths, and shifts.  This can lead
# to simulated intensities less than the desired intensities.  I fixed
# this by turning off the births and deaths routines and conditioning
# the model with the proper number of points, drawn from a random
# uniform distribution. Points are only shifted in location according
# to the GAMMA, IR, and HR in this manner.  The window size is defined
# by x.size and y.size.  Output includes BETA, GAMMA, IR, HR, x.size,
# y.size and sim.reg.

require(spatstat,quietly=TRUE)
BETA<-1
GAMMA<-0.75
IR<-0.75
HR<-0.50
x.size<-125
y.size<-125
n.start<-BETA*x.size*y.size
```

```
mod1<-list(cif="straush",par=list(beta=BETA,gamma=GAMMA,r=IR,hc=HR),
   w=c(0,x.size,0,y.size))
sim.reg<-rmh.default(model=mod1,start=list(n.start=n.start),control =
   list(p=1,periodic=TRUE,ptypes=BETA,nrep=1e5,nverb=1e4))


# This command cleans the workspace of unnecessary variables.

rm(n.start,mod1)
```

A.2. POPULATION-LEVEL STATISTICS AND FIGURES

```
# OVERALL SUMMARY:
# This file calculates the Clark-Evans statistic (CE.popl & CEp.popl)
# and the K-function (KHAT.popl) for the entire extent/simulated point
# population (mat).  It also calculates a Monte-Carlo estimate for
# KHAT.popl with nsim1 simulations of the K-function calculated from

# CSR populations.  The entire set of simulations is in the KSIM object
# with $L95 and $U95 defining 95% Monte-Carlo envelopes.
#
# Output includes CE.popl, CEp.popl, KHAT.popl, and KSIM.  This file
# also creates two summary plots for the population:
#     A) * pt map -> map of point pattern
#     B) * Lhat popl -> Lhat for pattern with 95% Monte-Carlo intervals
# Both are saved as *.pdf files.
#
# NOTE: Most computations are done with the splancs, not the spatstat,
# package of R.  This is done to speed computations of K (and
# associated) functions of the large simulated point patterns since
# they do not need to be calculated over the entire spatial extent.
# K (and other  similar) functions in spatstat cannot be calculated on
# limited extents.


# These commands load the splancs package and reformat the input matrix
# mat.

require(splancs,quietly=TRUE,warn.conflicts=FALSE)
mat.1<-as.points(mat)


# The following commands convert the window defined in the ppp.matrix
# to a polygon that can be used by splancs.

xmin<-mat$window$xrange[1]
xmax<-mat$window$xrange[2]
ymin<-mat$window$yrange[1]
ymax<-mat$window$yrange[2]
poly<-matrix(c(xmin,xmax,xmax,xmin,ymin,ymin,ymax,ymax),nrow=4,ncol=2)


# The following commands calculate the Clark-Evans Positioning Index
# (CE.popl) that describes overall spatial pattern of a point dataset.
# The CE calculation assumes a square polygon.  CEp.popl gives the
```

```
# p-value associated with CE.popl.

nn.dist<-nndist(mat.1,method="C")
CEnum<-mean(nn.dist)
CEden<-0.5*sqrt(BETA) + 0.0514*(2*(xmax+ymax))/(BETA*x.size*y.size) +
   0.041*(2*(xmax+ymax))/(BETA*x.size*y.size)^(1.5)
CE.popl<-CEnum/CEden
CEp.popl<-2*pnorm(abs(CEnum-CEden)/(0.26136/(BETA*sqrt(x.size*y.size)))
   ,lower.tail=FALSE)


# The following commands calculate the K-function on a range of (0,15).
# The envelopes are created from nsim1 (set to 1000 currently)
# simulations of a completely random spatial process (i.e., a Poisson
# process).  95% Monte Carlo confidence envelope for KHAT.popl are
# calculated from the sorted output (KSIMS)at each interval in Krange
# and are listed as KSIMS$L95 and KSIMS$U95.

Krange<-seq(0,15,0.1)
KHAT.popl<-khat(mat.1,poly,Krange,newstyle=FALSE)
KHAT.popl<-data.frame(dis=Krange,khat=KHAT.popl)
nsim1<-1000
KSIMS1<-matrix(rep(0,length(KHAT.popl$dis)*1000),
   nrow=length(KHAT.popl$dis),ncol=nsim1)
for (i in 1:nsim1) {
   KSIMS1[,i]<-khat(csr(poly,dim(mat.1)[1]),poly,Krange,newstyle=FALSE)
   cat("Simulation # ",i,"\n")
}
KSIMS2<-KSIMS1
for (i1 in 1:length(Krange)) {
   KSIMS2[i1,]<-sort(KSIMS1[i1,],method="quick")
}
L95<-KSIMS2[,ceiling(nsim1*0.025)]
U95<-KSIMS2[,ceiling(nsim1*0.975)]
KSIMS<-data.frame(dis=Krange,nsim=KSIMS1,L95,U95)


# The following commands produce a point map for the point process.

par(mar=c(0.5,0.5,0.5,0.5))
plot(mat,pch=20,cex=0.4,main=NULL)
rect(0,0,x.size,y.size,lwd=4)
savePlot(filename=paste("## ENTER FILE NAME HERE ##",base.name," pt
   map",sep=""),type="pdf")


# The following commands produce a plot of the L-function (a
# transformed form of the K-function equal to dist - sqrt(K-value/pi),
# for all distances) along with the 95% Monte Carlo simulation
# envelopes.

par(mar=c(6.5,6.5,1,1))
par(mgp=c(4,1,0))
par(xaxs="i")
par(yaxs="i")
x.ticks<-seq(0,15,3)
x.labels<-c("0","3","6","9","12","15")
```

```
maxabsy<-max(abs(sqrt(KHAT.popl$khat/pi)-KHAT.popl$dis),
   abs(sqrt(KSIMS$L95/pi)-KHAT.popl$dis),abs(sqrt(KSIMS$U95/pi)-
   KHAT.popl$dis))
y.ticks<-seq(min(-0.2,-round(maxabsy*1.1,1)),max(0.2,
   round(maxabsy*1.1,1)),0.1)
y.labels<-as.character(y.ticks)
plot(KHAT.popl$dis,sqrt(KHAT.popl$khat/pi)-KHAT.popl$dis,type="l",
   xlab=expression(bolditalic(d)),ylab=expression(bold(hat(L))[popl]
   (bolditalic(d))),ylim=range(y.ticks),lwd=5,bty="l",cex.lab=1.75,axes
   =F)
lines(KSIMS$dis,sqrt(KSIMS$L95/pi)-KSIMS$dis,type="l",lwd=4,lty="11")
lines(KSIMS$dis,sqrt(KSIMS$U95/pi)-KSIMS$dis,type="l",lwd=4,lty="11")
axis(side=1,at=x.ticks,labels=x.labels,font=2,lwd=3,cex.axis=1.5)
axis(side=2,at=y.ticks,labels=y.labels,font=2,lwd=3,cex.axis=1.5,las=1)
savePlot(filename=paste("##ENTER FILE NAME HERE##",base.name," Lhat
   popl",sep=""),type="pdf")


# The last commands remove the excess variables.

rm(mat.1,xmin,xmax,ymin,ymax,poly,nn.dist,CEnum,CEden,i,i1,L95,U95,x.ti
   cks,x.labels,y.ticks,y.labels,maxabsy,nsim1,Krange,KSIMS1,KSIMS2)
```

A.3. FUNCTION DEFINITIONS USED FOR SAMPLE PLOT CALCULATIONS

```
# The following function morphs the coordinates in the circular plot
# defined by mat into a square plot to be used for torodial edge
# correction.  It uses the algorithn developed by Williams, M. S.,
# M. T. Williams, and H. T. Mowrer. 2001. A boundary reconstruction
# method for circular fixed-area plots in environmental survey.  J.
# Agric. Biol. and Environ. Stat. 6(4).  The first two columns of mat
# should consist of x and y coordinates of points relative to plot
# center.  All columns beyond column 2 are assumed to be marks for the
# points, and carried through calculations unaltered.

morph<-function(mat) {

   # Checks for proper format of the matrix or data frame.

   if(!(is.matrix(mat) | is.data.frame(mat))) {
      stop("Input must be a matrix or data frame and have at least 2
         columns.")
   }
   if(!is.vector(c(mat[,1:2]),mode="numeric")) {
      if(!is.data.frame(mat)) {
         stop("The first two columns must contain numeric X & Y
            coordinates and not any marks.")
      }
   }


   # Converts Cartesian coordinates to polar coordinates.

   r<-sqrt(mat[,1]^2+mat[,2]^2)
   theta<-atan2(mat[,2],mat[,1])
```

```
   # Rescales polar coordinates for "morphing" transformation.

   s<-sqrt(pi)*r
   theta<-ifelse(theta <= 0, theta+2*pi, theta)


   # Calculation of numerous dummy variable that identify which
   # part of the circle that the point is in.

   DUMMY<-matrix(c(rep(0,10*length(s))),ncol=10)
   DUMMY[,1]<-ifelse(theta > 0.00*pi & theta <= 0.75*pi,1,0)
   DUMMY[,2]<-ifelse(theta > 1.75*pi & theta <= 2.00*pi,1,0)
   DUMMY[,3]<-ifelse(theta > 0.75*pi & theta <= 1.75*pi,1,0)
   DUMMY[,4]<-ifelse(theta > 0.25*pi & theta <= 0.75*pi,1,0)
   DUMMY[,5]<-ifelse(theta > 1.25*pi & theta <= 1.75*pi,1,0)
   DUMMY[,6]<-ifelse(theta > 0.25*pi & theta <= 1.25*pi,1,0)
   DUMMY[,7]<-ifelse(theta > 1.25*pi & theta <= 2.00*pi,1,0)
   DUMMY[,8]<-ifelse(theta > 0.00*pi & theta <= 0.25*pi,1,0)
   DUMMY[,9]<-ifelse(theta > 0.75*pi & theta <= 1.25*pi,1,0)
   DUMMY[,10]<-ifelse(theta > 1.75*pi & theta <= 2.00*pi,1,0)


   # Equations for the morphing transformation.

   morph.x<-((DUMMY[,1]+DUMMY[,2]-DUMMY[,3])*s/2) - (DUMMY[,4]*
      (2*s*(theta-0.25*pi))/pi) + (DUMMY[,5]*(2*s*(theta-1.25*pi))/pi)
   morph.y<-((DUMMY[,6]-DUMMY[,7])*s/2)+(DUMMY[,8]*2*s*theta/pi)-
      (DUMMY[,9]*(2*s*(theta-0.75*pi))/pi) + (DUMMY[,10]*(2*s*(theta-
      1.75*pi))/pi)


   # Output is the morphed coordinates along with associated marks
   # (columns 3+ in mat).

   if (dim(mat)[2]>2) {
      morph<-cbind(morph.x,morph.y,mat[,-(1:2)])
   } else morph<-cbind(morph.x,morph.y)
}


# The following function demorphs coordinates back to the original
# Cartesian space.

demorph<-function(mat) {

   # Checks for proper format of the matrix or data frame.

   if(!(is.matrix(mat) | is.data.frame(mat))) {
      stop("Input must be a matrix or data frame and have at least 2
         columns.")
   }
   if(!is.vector(c(mat[,1:2]),mode="numeric")) {
      if(!is.data.frame(mat)) {
         stop("The first two columns must contain numeric X & Y
            coordinates and not any marks.")
      }
   }
```

```
   # Calculation of dummy variables to define which part of the morphed
   # set space a particular point is within.

   r2<-sqrt(mat[,1]^2+mat[,2]^2)
   theta2<-atan2(mat[,2],mat[,1])
   theta2<-ifelse(theta2 <= 0, theta2+2*pi, theta2)
   DUMMY2<-matrix(c(rep(0,5*dim(mat)[1])),ncol=5)
   DUMMY2[,1]<-ifelse(theta2 > 0.00*pi & theta2 <= 0.25*pi,1,0)
   DUMMY2[,2]<-ifelse(theta2 > 0.75*pi & theta2 <= 1.25*pi,1,0)
   DUMMY2[,3]<-ifelse(theta2 > 1.75*pi & theta2 <= 2.00*pi,1,0)
   DUMMY2[,4]<-ifelse(theta2 > 0.25*pi & theta2 <= 0.75*pi,1,0)
   DUMMY2[,5]<-ifelse(theta2 > 1.25*pi & theta2 <= 1.75*pi,1,0)


   # Equations for the demorphing transformation.

   new.r<-abs((2*mat[,1]*pi^(-0.5))*(DUMMY2[,1]+DUMMY2[,2]+DUMMY2[,3])
      + (2*mat[,2]*pi^(-0.5))*(DUMMY2[,4]+DUMMY2[,5]))
   new.theta<-(0.25*pi*mat[,2]/mat[,1])*(DUMMY2[,1]+DUMMY2[,3]) +
      (1.00*pi+0.25*pi*mat[,2]/mat[,1])*(DUMMY2[,2])+(0.50*pi-
      0.25*pi*mat[,1]/mat[,2])*(DUMMY2[,4])+(1.50*pi-
      0.25*pi*mat[,1]/mat[,2])*(DUMMY2[,5])
   new.theta<-ifelse(mat[,1]==0 & mat[,2]==0,0,new.theta)
   new.theta<-ifelse(mat[,1]==0 & (mat[,2]>0 | mat[,2]<0),(0.50*pi-
      (0.25*pi*mat[,1]/mat[,2]))*DUMMY2[,4]+(1.50*pi-
      (0.25*pi*mat[,1]/mat[,2]))*DUMMY2[,5],new.theta)
   new.theta<-ifelse(mat[,2]==0 & (mat[,1]>0 | mat[,1]<0),(0.25*pi*
      mat[,2]/mat[,1])*DUMMY2[,3]+(1.00*pi+(0.25*pi*mat[,2]/mat[,1]))*
      DUMMY2[,2],new.theta)


   # Converts points to Cartesian coordinates and attaches marks.

   x<-c(new.r*cos(new.theta))
   y<-c(new.r*sin(new.theta))
   if (dim(mat)[2]>2) {
      demorph<-cbind(x,y,mat[,-(1:2)])
   } else demorph<-cbind(x,y)
}



# The following function torodial wraps square or rectangular point
# patterns.  There are three components. First, mat defines a point
# pattern with any associated marks.  It must have at least two columns
# that define x and y coordinates.  Second, dim defines the dimensions
# of the point pattern in the form (xmin,xmax,ymin,ymax).  It defaults
# to the minimums and maximums of the x and y coordinates in mat.
# Third, rep defines the number of replicated point patterns to do in
# the x and y directions.  It defaults to a 3 x 3 array.  Components of
# rep must be odd and integers.

torus.wrap<-function(mat,dim,repl = c(3,3)) {

   # Checks the inputs to the function for proper format.

   if(!(is.matrix(mat) | is.data.frame(mat))) {
```

```
      stop("Input must be a matrix or data frame and have at least 2
         columns.")
   }
   if(!is.vector(c(mat[,1:2]),mode="numeric")) {
      if(!is.data.frame(mat)) {
         stop("The first two columns must contain numeric X & Y
            coordinates and not any marks.")
      }
   }
   if(missing(dim)) {
      dim<-c(min(mat[,1]),max(mat[,1]),min(mat[,2]),max(mat[,2]))
   }
   if(!is.vector(dim,mode="numeric") | length(dim)!=4) {
      stop("Supplied dim must be a vector in form (xmin,xmax,ymin,ymax)
         defining the bounding box for the point pattern. The default
         is the min and max of the X & Y coordinates in mat.")
   }
   if(!is.vector(repl,mode="numeric") | length(repl)!=2) {
      stop("Supplied repl must be a vector in form (x,y) where x is the
         number of replicated point patterns in the horizontal
         direction and y is replicated point patterns in the vertical
         direction.  The default is (3,3).")
   }
   x.exp<-(repl[1]-1)/2
   y.exp<-(repl[2]-1)/2
   if(x.exp-floor((repl[1]-1)/2)!=0 | y.exp-floor((repl[2]-1)/2)!=0) {
      stop("Repl must contain only odd integers.")
   }


   # Commands to create the torodial wrap.

   x.size<-dim[2]-dim[1]
   y.size<-dim[4]-dim[3]
   mat.exp<-integer()
   for(i in 1:x.exp) {
      mat.neg<-mat
      mat.neg[,1]<-mat[,1]-i*x.size
      mat.pos<-mat
      mat.pos[,1]<-mat[,1]+i*x.size
      mat.exp<-rbind(mat.exp,mat.neg,mat.pos)
   }
   mat<-rbind(mat,mat.exp)
   mat.exp2<-integer()
   for(j in 1:y.exp) {
      mat.neg2<-mat
      mat.neg2[,2]<-mat[,2]-j*y.size
      mat.pos2<-mat
      mat.pos2[,2]<-mat[,2]+j*y.size
      mat.exp2<-rbind(mat.exp2,mat.neg2,mat.pos2)
   }
   mat<-rbind(mat,mat.exp2)
}

# The following function torodial wraps square or rectangular point
# patterns derived from multiple plots.  This differs only from
# torus.wrap in that mat must contain a minimum of 3 columns, with the
```

```
# first column indicating what plot the X and Y coordinates (columns 2
# and 3, respectively) are from.  Columns 4+ are assumed to be marks.
# Plot numbers do not need to be consecutive or sorted.  The item
# base defines which plot is the base plot to wrap around; the
# function then randomly picks with replacement among all plots
# (including the base plot) to wrap with.  Output is an expanded matrix
# with all border plot and base plot points and marks; the base plot
# info is not sorted to the top of the matrix.
#
# Refer to torus.wrap for definitions and limitations for dim and repl.

torus.wrap2<-function(mat,base,dim,repl = c(3,3)) {

   # Checks the inputs to the function for proper format.

   if(!(is.matrix(mat) | is.data.frame(mat))) {
      stop("Input must be a matrix or data frame and have at least 3
         columns.")
   }
   if(!is.vector(c(mat[,1:3]),mode="numeric")) {
      if(!is.data.frame(mat)) {
         stop("The first three columns must contain plot numbers,
            numeric X & Y coordinates, and not any marks.")
      }
   }
   if(missing(base)) {
      stop("Must provide plot number for center plot (base).")
   }
   if(missing(dim)) {
      dim<-c(min(mat[,2]),max(mat[,2]),min(mat[,3]),max(mat[,3]))
   }
   if(!is.vector(dim,mode="numeric") | length(dim)!=4) {
      stop("Supplied dim must be a vector in form (xmin,xmax,ymin,ymax)
         defining the plot size for the point pattern. The default is
         the min and max of the X & Y coordinates across all plots
         listed in mat.")
   }
   if(!is.vector(repl,mode="numeric") | length(repl)!=2) {
      stop("Supplied repl must be a vector in form (x,y) where x is the
         number of replicated point patterns in the horizontal
         direction and y is replicated point patterns in the vertical
         direction.  The default is (3,3).")
   }
   x.exp<-(repl[1]-1)/2
   y.exp<-(repl[2]-1)/2
   if(x.exp-floor((repl[1]-1)/2)!=0 | y.exp-floor((repl[2]-1)/2)!=0) {
      stop("Repl must contain only odd integers.")
   }


   # Commands to create the torodial wrap.

   x.size<-dim[2]-dim[1]
   y.size<-dim[4]-dim[3]
   p.nums<-mat[duplicated(mat[,1])==FALSE,1]
   p.sams<-sample(p.nums,repl[1]*repl[2],replace=TRUE)
```

```
   coor.adj<-matrix(c(x.size*sort(c(rep(-x.exp:x.exp,repl[2]))),
      y.size*c(rep(-y.exp:y.exp,repl[1]))),ncol=2)
   p.sams[coor.adj[,1]==0 & coor.adj[,2]==0]<-base
   mat.exp<-integer()
   for(i in 1:length(p.sams)) {
      mat2<-mat[mat[,1]==p.sams[i],]
      if(!(is.data.frame(mat2) | is.matrix(mat2))) {
         mat2<-t(as.matrix(mat2))
      } else mat2<-mat2
      mat2[,2]<-mat2[,2]+coor.adj[i,1]
      mat2[,3]<-mat2[,3]+coor.adj[i,2]
      mat.exp<-rbind(mat.exp,mat2)
   }
   return(mat.exp)
}



# The following function trims points from a sample plot that are
# outside a specified distance (rad) from plot center.  Although
# designed specifically for circular plots, it could be used with
# any plot shape. X and Y coordinates should be in the first two
# columns. Output is a matrix for the smaller, trimmed circular
# plot that includes all marks.

cplot.trim<-function(mat,rad) {
   if(!(is.matrix(mat) | is.data.frame(mat))) {
      stop("Input must be a matrix or data frame and have at least 2
         columns.")
   }
   if(!is.vector(c(mat[,1:2]),mode="numeric")) {
      if(!is.data.frame(mat)) {
         stop("The first two columns must contain numeric X & Y
            coordinates and not any marks.")
      }
   }
   if(missing(rad)) {
      stop("Must supply max distance from plot center for trimming
         (rad).")
   }
   return(mat[sqrt(mat[,1]^2+mat[,2]^2)<=rad,])
}



# The following function selects nsim circular plots of radius rad
# from a rectangular point pattern defined by mat.  It works if mat
# is a point pattern, a point object, a data frame, or a matrix.
# Dimensions of the point pattern are given by dim; it defaults to
# the maximum and minimum X & Y coordinates. If the point pattern is
# buffered (buf), plot centers will not be selected closer to the edge
# than this distance.  It defaults to rad. Nonuniform buffers are given
# as a vector starting with the buffer on the top of the pattern and
# working clockwise. Nsim defaults to 1 plot. If existing plot centers
# are to be used, cen is used; cen should be formated as a data
# frame or matrix with X & Y coordinates in columns 1 and 2, with
# existing plot names or numbers given in column 3.  Minn sets the
```

```
# minimum plot sample size desired; i.e., the plot will be resampled if
# n < minn. Results are returned in a list, with $plot.centers giving
# the plot centers and plot sample size, $raw.points giving the X & Y
# coordinates and any associated marks by plot, and $centered.points
# giving X & Y coordinates relative to plot center and any associated
# marks by plot. These three components are data frames within the
# list.

cplot.sel<-function(mat,rad,dim,nsim=1,buf=rad,cen=NULL,minn=NULL) {

   # The commands load the required R packages “spatstat” and
   # “splancs”.

   require(spatstat,quietly=TRUE)
   require(splancs,quietly=TRUE)


   # The following commands check the format of the inputs, and set
   # defaults if they are missing.

   if(missing(rad)) {
      stop("Sample plot size not specified (rad).")
   }
   if(is.ppm(mat) | is.ppp(mat)) {
      dim<-c(min(corners(mat)$x),max(corners(mat)$x),
         min(corners(mat)$y),max(corners(mat)$y))
      if(is.marked(mat)) {
         marks<-c(mat$marks)
         mat<-as.points(mat)
         mat<-data.frame(x=mat$x,y=mat$y,marks=marks)
      }
      mat<-data.frame(x=mat$x,y=mat$y)
   } else if(missing(dim)) {
      dim<-c(min(mat[,1]),max(mat[,1]),min(mat[,2]),max(mat[,2]))
   } else if(!is.vector(dim,mode="numeric") | length(dim)!=4) {
      stop("Supplied dim must be a vector in form (xmin,xmax,ymin,ymax)
         defining the size for the point pattern.  The default is the
         min and max of the X & Y coordinates across all points listed
         in mat.")
   }
   if(!is.vector(c(mat[,1:2]),mode="numeric")) {
      if(!is.data.frame(mat)) {
         stop("The first two columns must contain numeric X & Y
            coordinates and not any marks.")
      }
   }
   if(!is.vector(buf,mode="numeric") | !length(buf)==4) {
      ifelse(length(buf)==1,buf<-c(buf,buf,buf,buf),stop("Buffer format
         not correct."))
   }


   # The following statments either use the points listed in cen or
   # chooses a set of random points within dim.

   if(!is.null(cen)) {
      if(!mode(as.matrix(cen[,1:2]))=="numeric") {
```

```
         stop("Existing plot centers (cen) not formatted correctly.")
      }
      plot.cen<-data.frame(x=cen[,1],y=cen[,2],plot=cen[,3])
      nsim<-dim(cen)[1]
   } else plot.cen<-data.frame(x=runif(nsim,dim[1]+buf[4],dim[2]-
      buf[2]),y=runif(nsim,dim[1]+buf[4],dim[2]-buf[2]))


   # These commands create the plots and return the original
   # coordinates and coordinates centered on the plot coordinates.

   plot.pts<-data.frame()
   plot.pts2<-data.frame()
   n<-integer()
   for(i in 1:nsim) {
      pts<-mat[c((mat[,1]-plot.cen[i,1])^2 + (mat[,2]-plot.cen[i,2])^2
         <= rad^2),]
      pts2<-pts
      pts2[,1]<-pts2[,1]-plot.cen[i,1]
      pts2[,2]<-pts2[,2]-plot.cen[i,2]
      n<-c(n,dim(pts)[1])
      if(!is.null(minn)) {
         while(n[i]<minn) {
            plot.cen$x[i]<-runif(1,dim[1]+buf[4],dim[2]-buf[2])
            plot.cen$y[i]<-runif(1,dim[1]+buf[4],dim[2]-buf[2])
            pts<-mat[c((mat[,1]-plot.cen[i,1])^2 + (mat[,2]-
               plot.cen[i,2])^2 <= rad^2),]
            pts2<-pts
            pts2[,1]<-pts2[,1]-plot.cen[i,1]
            pts2[,2]<-pts2[,2]-plot.cen[i,2]
            n[i]<-dim(pts)[1]
         }
      }
      if(!is.null(cen)) {
         plot.names<-rep(plot.cen[i,3],n[i])
      } else plot.names<-rep(i,n[i])
      pts<-cbind(data.frame(plot=plot.names),pts)
      pts2<-cbind(data.frame(plot=plot.names),pts2)
      plot.pts<-rbind(plot.pts,pts)
      plot.pts2<-rbind(plot.pts2,pts2)
   }
   plot.cen<-cbind(plot.cen,n=n)
   row.names(plot.pts)<-c(1:dim(plot.pts)[1])
   row.names(plot.pts2)<-c(1:dim(plot.pts2)[1])
   res<-list(sum.info=plot.cen,raw.pts=plot.pts,cent.pts=plot.pts2)
   return(res)
}
```

A.4. SAMPLE PLOT GENERATION AND SUMMARY STATISTICS CALCULATION

```
# OVERALL SUMMARY:
# The following commands randomly select plots from a sample space
# (mat). The plot size (plot.size) and number of simulations (nsim)
# must also be specified.  There are several outputs, corresponding to
# different border corrections:
```

```
#     a) plots.r --> list of plot centers of radius r and associated
#        points (uncentered and re-centered at zero)
#     b) plots.r2 --> list of plot centers of radius 2r and associated
#        points (uncentered and re-centered at zero)
#     c) plots.r2.same --> data frame of plots of radius r morphed to a
#        radius 2r, using the exact same plot to morph with (a true
#        torodial wrap)
#     d) plots.r2.diff --> data frame of plots of radius r morphed to a
#        radius 2r, using different plots to morph with
#     e) plots.r2.rand --> data frame of plots of radius r surrounded
#        by a ring with randomly located points to achieve simulated
#        plot of radius 2r
#
# Beyond these point patterns, the commands also summarize the point
# patterns using the Clark-Evans statistic and K functions:
#     f) CE --> Clark Evans statistics (plot level [$data] and summary
#        statistics [$sum.stat, $bon.p.counts]) as follows:
#        1) .ra --> plot radius r & Donnelly correction
#        2) .rb --> plot radius r with morphed ring for edge correction
#        3) .r2 --> plot radius 2r & Donnelly correction
#        4) .r2.same -> from c) above & Donnelly correction
#        5) .r2.diff -> from d) above & Donnelly correction
#        6) .r2.rand -> from e) above & Donnelly correction
#     g) KHAT --> K-functions (plot level and summary statistics as
#        listed data frame for each below)
#        1) .r.unc --> plot radius r & uncorrected for edge effects
#        2) .r.bor --> plot radius r with morphed ring for edge
#           correction
#        3) .r.rip --> plot radius r with Ripley's edge correction
#           technique
#        4) .r2 --> plot radius 2r and Ripley's edge correction
#           technique
#        5) .r2.same --> from c) above and Ripley's edge correction
#           technique
#        6) .r2.diff --> from d) above and Ripley's edge correction
#           technique
#        7) .r2.rand --> from e) above and Ripley's edge correction
#           technique


# These first commands load the spatstat and splancs packages and the
# custom functions used for the morphing procedures.

require(spatstat,quietly=TRUE)
require(splancs,quietly=TRUE,warn.conflicts=FALSE)
source("Morphed Functions.txt")


# The following commands determine the coordinates of the marked points
# using different assumptions.  These are:
#     A) plots.r$cent.pts --> sample plot of radius r.  Note that all
#        selected plots have a minimum of 10 points.  This was done to
#        assure enough points for K-analysis.
#     B) plots.r2$cent.pts --> sample plot of radius 2r.  This has the
#        same plot centers as (A).
#     C) plots.r2.same --> morphed plot of radius 2r using the plot
#        itself for morphing.
```

```
#     D) plots.r2.diff --> morphed plot of radius 2r using 8 different
#        plots for morphing the base plot.
#     E) plots.r2.rand --> sample plot of radius r surrounded by a 3n
#        ring of randomly located points at a distance between r and
#        2r.  This is similar to what SVS uses to spatially inflate a
#        plot.
# All 5 objects are formated similarly as a data frame with the plot
# ($plot) and the x- ($x) and y- ($y) coordinates.  (D) slightly
# differs in that $ori.plot is used to keep track of what plot was used
# to torodial wrap with.  (C), (D) and (E) also include a mark ($r) to
# indicate which points are at the original scale and unmorphed (i.e.,
# they are in the 1*rad inner plot).
#
# Note because of randomization, only (C) and (E) will have a sample
# size 4 times that of the original plot listed in (A)!

rad<-(plot.size/pi)^0.5
plots.r<-cplot.sel(mat,rad,buf=12.5,nsim=nsim,minn=10)
plots.r2<-cplot.sel(mat,rad*2,cen=data.frame(plots.r$sum.info[,-3]
   ,plot=c(1:dim(plots.r$sum.info)[1])))
plots.morph<-plots.r$cent.pts
for(i in 1:nsim) {
   mor<-morph(plots.morph[plots.morph[,1]==i,-1])
   plots.morph[plots.morph[,1]==i,-1]<-mor
}
plots.torus<-integer()
for(i2 in 1:nsim) {
   torus<-torus.wrap(plots.morph[plots.morph[,1]==i2,-1],c(rep(c(-0.5*
      rad*sqrt(pi),0.5*rad*sqrt(pi)),2)))
   torus<-cbind(plot=c(rep(i2,dim(torus)[1])),torus)
   plots.torus<-rbind(plots.torus,torus)
}
row.names(plots.torus)<-c(1:dim(plots.torus)[1])
plots.demorph<-plots.torus
for(i3 in 1:nsim) {
   demor<-demorph(plots.torus[plots.torus[,1]==i3,-1])
   plots.demorph[plots.demorph[,1]==i3,-1]<-demor
}
plots.r2.same<-plots.demorph[sqrt(plots.demorph[,2]^2 +
   plots.demorph[,3]^2) <=2*rad,]
row.names(plots.r2.same)<-c(1:dim(plots.r2.same)[1])
r.in1<-ifelse(sqrt(plots.r2.same[,2]^2 + plots.r2.same[,3]^2)<=rad,1,0)
plots.r2.same<-cbind(plots.r2.same,r=r.in1)
plots.torus2<-integer()
for(i4 in 1:nsim) {
   torus2<-torus.wrap2(plots.morph,i4,c(rep(c(-0.5*rad*sqrt(pi),0.5*
      rad*sqrt(pi)),2)))
   torus2<-cbind(tmp=rep(i4,dim(torus2)[1]),torus2)
   plots.torus2<-rbind(plots.torus2,torus2)
}
plots.demorph2<-plots.torus2
for(i5 in 1:nsim) {
   demor2<-demorph(plots.torus2[plots.torus2[,1]==i5,-(1:2)])
   plots.demorph2[plots.demorph2[,1]==i5,-(1:2)]<-demor2
}
plots.r2.diff<-plots.demorph2[sqrt(plots.demorph2[,3]^2 +
   plots.demorph2[,4]^2)<=2*rad,]
```

```
row.names(plots.r2.diff)<-c(1:dim(plots.r2.diff)[1])
plots.r2.diff<-data.frame(plot=plots.r2.diff$tmp,plots.r2.diff[,3:
   dim(plots.r2.diff)[2]],ori.plot=plots.r2.diff$plot)
r.in2<-ifelse(sqrt(plots.r2.diff[,2]^2 + plots.r2.diff[,3]^2)<=rad,1,0)
plots.r2.diff<-cbind(plots.r2.diff,r=r.in2)
plots.r2.rand<-plots.r$cent.pts
for(i6 in 1:nsim) {
   n6<-3*dim(plots.r2.rand[plots.r2.rand[,1]==i6,])[1]
   ring<-matrix(c(runif(n6,0,2*pi),runif(n6,rad,2*rad)),ncol=2)
   ring<-data.frame(plot=rep(i6,n6),x=ring[,2]*cos(ring[,1]),y=ring[,2]
      *sin(ring[,1]))
   plots.r2.rand<-rbind(plots.r2.rand,ring)
}
plots.r2.rand<-plots.r2.rand[order(plots.r2.rand$plot),]
row.names(plots.r2.rand)<-c(1:dim(plots.r2.rand)[1])
r.in3<-ifelse(sqrt(plots.r2.rand[,2]^2 + plots.r2.rand[,3]^2)<=rad,1,0)
plots.r2.rand<-cbind(plots.r2.rand,r=r.in3)


# The following commands calculate Clark-Evans (CE) statistics for the
# various point patterns.  The output is a list with three parts.  The
# first part is a data frame ($data) with plot level estimates of the
# following:
#     1) plot --> plot number
#     2) n.r --> n of (A)
#     3) CE.ra --> CE statistic for (A)
#     4) CEp.ra --> p-value associated with (3)
#     5) CE.rb --> CE statistic for (A) using (C) for edge correction
#     6) CEp.rb --> p-value associated with (5)
#     7) n.r2 --> n of (B)
#     8) CE.r2 --> CE statistic for (B)
#     9) CEp.r2 --> p-value associated with (6)
#     10) n.r2.same --> n of (C)
#     11) CE.r2.same --> CE statistic for (C)
#     12) CEp.r2.same --> p-value associated with (9)
#     13) n.r2.diff --> n of (D)
#     14) CE.r2.diff --> CE statistic for (D)
#     15) CEp.r2.diff --> p-value associated with (13)
#     16) n.r2.rand --> n of (E)
#     17) CE.r2.rand --> CE statistic for (E)
#     18) CEp.r2.rand --> p-value associated with (15)
# All CEs except #5 are edge-corrected with the Donnelly (1978)
# technique.  The second part is a data frame ($sum.stat) that contains
# the mean, standard deviation, maximum, and minimum of columns 2-13
# above.  The third part is a data frame ($bon.p.counts) that counts
# the number of times the p-value of a calculated CE (the individual
# plot values given in columns 4, 6, 9, 12, 15 and 18 above) falls
# within Bonferronized error regions, i.e. alpha/nsim.

CE<-data.frame(plot = integer(),n.r = integer(),CE.ra = integer(,CEp.ra
   = integer(),CE.rb = integer(),CEp.rb = integer() ,n.r2 = integer(),
   CE.r2 = integer(),CEp.r2 = integer(),n.r2.same = integer(),
   CE.r2.same = integer(),CEp.r2.same = integer(),n.r2.diff =
   integer(), CE.r2.diff = integer(),CEp.r2.diff = integer(),n.r2.rand
   = integer(),CE.r2.rand = integer(),CEp.r2.rand = integer())
for(i7 in 1:nsim) {
   CE[i7,1]=i7
```

```
CE$n.r[i7]<-plots.r$sum.info$n[i7]
CE$n.r2[i7]<-plots.r2$sum.info$n[i7]
CE$n.r2.same[i7]<-dim(plots.r2.same[plots.r2.same[,1]==i7,])[1]
CE$n.r2.diff[i7]<-dim(plots.r2.diff[plots.r2.diff[,1]==i7,])[1]
CE$n.r2.rand[i7]<-dim(plots.r2.rand[plots.r2.rand[,1]==i7,])[1]
num.ra<-mean(nndist(plots.r$cent.pts[plots.r$cent.pts[,1]==i7,2:3],
   method="C"))
den.ra<-(0.5*sqrt(pi*rad^2/CE$n.r[i7]))+(0.0514*2*pi*rad/CE$n.r[i7])
   +(0.041*2*pi*rad/(CE$n.r[i7]^1.5))
inners<-plots.r2.same[plots.r2.same[,1]==i7 & plots.r2.same[,4]==1,
   2:3]
outers<-plots.r2.same[plots.r2.same[,1]==i7 & plots.r2.same[,4]!=1,
   2:3]
inn.out<-data.frame(inn=nndist(inners,method="C"),out=n2dist(outers,
   inners)$dists)
num.rb<-mean(inn.out[matrix(c(1:dim(inn.out)[1],max.col(-inn.out)),
   ncol=2)])
den.rb<-1/(2*sqrt(CE$n.r[i7]/plot.size))
num.r2<-mean(nndist(plots.r2$cent.pts[plots.r2$cent.pts[,1]==i7,
   2:3],method="C"))
den.r2<-(0.5*sqrt(4*pi*rad^2/CE$n.r2[i7])) + (0.0514*4*pi*rad/
   CE$n.r2[i7]) + (0.041*4*pi*rad/(CE$n.r2[i7]^1.5))
num.r2.same<-mean(nndist(plots.r2.same[plots.r2.same[,1]==i7,2:3],
   method="C"))
den.r2.same<-(0.5*sqrt(4*pi*rad^2/CE$n.r2.same[i7])) + (0.0514*4*pi*
   rad/CE$n.r2.same[i7]) + (0.041*4*pi*rad/(CE$n.r2.same[i7]^1.5))
num.r2.diff<-mean(nndist(plots.r2.diff[plots.r2.diff[,1]==i7,2:3],
   method="C"))
den.r2.diff<-(0.5*sqrt(4*pi*rad^2/CE$n.r2.diff[i7])) + (0.0514*4*pi*
   rad/CE$n.r2.diff[i7]) + (0.041*4*pi*rad/(CE$n.r2.diff[i7]^1.5))
num.r2.rand<-mean(nndist(plots.r2.rand[plots.r2.rand[,1]==i7,2:3],
   method="C"))
den.r2.rand<-(0.5*sqrt(4*pi*rad^2/CE$n.r2.rand[i7])) + (0.0514*4*pi*
   rad/CE$n.r2.rand[i7]) + (0.041*4*pi*rad/(CE$n.r2.rand[i7]^1.5))
CE$CE.ra[i7]<-num.ra/den.ra
CE$CE.rb[i7]<-num.rb/den.rb
CE$CE.r2[i7]<-num.r2/den.r2
CE$CE.r2.same[i7]<-num.r2.same/den.r2.same
CE$CE.r2.diff[i7]<-num.r2.diff/den.r2.diff
CE$CE.r2.rand[i7]<-num.r2.rand/den.r2.rand
c.ra<-2.15866844*(num.ra-den.ra)*CE$n.r[i7]/rad
c.rb<-((num.rb-den.rb)*CE$n.r[i7]*plot.size^-0.5)/0.26136
c.r2<-1.07933422*(num.r2-den.r2)*CE$n.r2[i7]/rad
c.r2.same<-1.07933422*(num.r2.same-den.r2.same)*CE$n.r2.same[i7]/rad
c.r2.diff<-1.07933422*(num.r2.diff-den.r2.diff)*CE$n.r2.diff[i7]/rad
c.r2.rand<-1.07933422*(num.r2.rand-den.r2.rand)*CE$n.r2.rand[i7]/rad
CE$CEp.ra[i7]<-pnorm(-abs(c.ra),lower.tail=TRUE)+pnorm(abs(c.ra),
   lower.tail=FALSE)
CE$CEp.rb[i7]<-pnorm(-abs(c.rb),lower.tail=TRUE)+pnorm(abs(c.rb),
   lower.tail=FALSE)
CE$CEp.r2[i7]<-pnorm(-abs(c.r2),lower.tail=TRUE)+pnorm(abs(c.r2),
   lower.tail=FALSE)
CE$CEp.r2.same[i7]<-pnorm(-abs(c.r2.same),lower.tail=TRUE) +
   pnorm(abs(c.r2.same),lower.tail=FALSE)
CE$CEp.r2.diff[i7]<-pnorm(-abs(c.r2.diff),lower.tail=TRUE) +
   pnorm(abs(c.r2.diff),lower.tail=FALSE)
```

```
   CE$CEp.r2.rand[i7]<-pnorm(-abs(c.r2.rand),lower.tail=TRUE) +
      pnorm(abs(c.r2.rand),lower.tail=FALSE)
}
CE.sum<-rbind(colMeans(CE[,-1]),sd(CE[,-1]),cummin(CE[,-1])[nsim,],
   cummax(CE[,-1])[nsim,])
rownames(CE.sum)<-c("mean","sd","min","max")
p.counts<-as.data.frame(matrix(rep(0,24),ncol=6),row.names=c("0.00 -
   0.01","0.01 - 0.05","0.05 - 0.10","0.10 - 1.00"))
colnames(p.counts)<-c("ra","rb","r2","r2.same","r2.diff","r2.rand")
p.counts[,1]<-as.matrix(hist(CE$CEp.ra,breaks=c(0,0.01/nsim,0.05/nsim,
   0.1/nsim,1),plot=FALSE)$counts)
p.counts[,2]<-as.matrix(hist(CE$CEp.rb,breaks=c(0,0.01/nsim,0.05/nsim,
   0.1/nsim,1),plot=FALSE)$counts)
p.counts[,3]<-as.matrix(hist(CE$CEp.r2,breaks=c(0,0.01/nsim,0.05/nsim,
   0.1/nsim,1),plot=FALSE)$counts)
p.counts[,4]<-as.matrix(hist(CE$CEp.r2.same,breaks=c(0,0.01/nsim,
   0.05/nsim,0.1/nsim,1),plot=FALSE)$counts)
p.counts[,5]<-as.matrix(hist(CE$CEp.r2.diff,breaks=c(0,0.01/nsim,
   0.05/nsim,0.1/nsim,1),plot=FALSE)$counts)
p.counts[,6]<-as.matrix(hist(CE$CEp.r2.rand,breaks=c(0,0.01/nsim,
   0.05/nsim,0.1/nsim,1),plot=FALSE)$counts)
CE<-list(data=CE,sum.stat=CE.sum,bon.p.counts=p.counts)


# The following commands calculate the K values for the different
# morphing procedures.  Small plots ($r) are calculated over the common
# range of 0.5*rad; large plots ($r2) at 1.0*rad.  The output is a list
# (KHAT) with the data frames corresponding to each morphing option
# ($r2 for (B), $r2.same for (C), $r2.diff for (D), and $r2.rand for
# (E)).  All data frames have columns to the far right that give the
# weighted mean, weighted sd, min, and max of the K values for that
# option.

poly.r<-matrix(c(rad*cos(seq(-pi,pi,length=1000)),rad*sin(seq(-pi,pi,
   length=1000))),ncol=2)
poly.r2<-matrix(c(2*rad*cos(seq(-pi,pi,length=1000)),2*rad*sin(seq(-pi,
   pi,length=1000))),ncol=2)
range.r<-seq(0,round(0.5*rad,1),0.1)
range.r2<-seq(0,round(rad,1),0.1)
tmp1<-data.frame(dist=range.r,plot=matrix(rep(0,nsim*length(range.r)),
   ncol=nsim))
tmp2<-data.frame(dist=range.r2,plot=matrix(rep(0,nsim*
   length(range.r2)),ncol=nsim))
KHAT<-list(r.unc=tmp1,r.bor=tmp1,r.rip=tmp1,r2=tmp2,r2.same=tmp2,
   r2.diff=tmp2,r2.rand=tmp2)
for(i8 in 1:nsim) {
   tmp3<-pairdist(plots.r$cent.pts[plots.r$cent.pts$plot==i8,2:3],
      method="C")
   tmp3<-c(tmp3)
   tmp3<-tmp3[order(tmp3)]
   tmp3<-tmp3[tmp3!=0]
   KHAT$r.unc[,i8+1]<-plt(tmp3,range.r)*plot.size*
      (plots.r$sum.info$n[i8]/(plots.r$sum.info$n[i8]-1))
   tmp4<-pairdist(plots.r2.same[plots.r2.same$plot==i8,2:3],method="C")
   tmp4<-tmp4[,1:plots.r$sum.info$n[i8]]
   tmp4<-c(tmp4)
   tmp4<-tmp4[order(tmp4)]
```

```
   tmp4<-tmp4[tmp4!=0]
   KHAT$r.bor[,i8+1]<-plt(tmp4,range.r)*plot.size*4
   KHAT$r.rip[,i8+1]<-khat(plots.r$cent.pts[plots.r$cent.pts[,1]==i8,
      2:3],poly.r,range.r)
   KHAT$r2[,i8+1]<-khat(plots.r2$cent.pts[plots.r2$cent.pts[,1]==i8,
      2:3],poly.r2,range.r2)
   KHAT$r2.same[,i8+1]<-khat(plots.r2.same[plots.r2.same[,1]==i8,
      2:3],poly.r2,range.r2)
   KHAT$r2.diff[,i8+1]<-khat(plots.r2.diff[plots.r2.diff[,1]==i8,
      2:3],poly.r2,range.r2)
   KHAT$r2.rand[,i8+1]<-khat(plots.r2.rand[plots.r2.rand[,1]==i8,
      2:3],poly.r2,range.r2)
}
.mean<-(as.matrix(KHAT$r.unc[,-1]) %*% as.matrix(CE$data$n.r))/
   sum(CE$data$n.r)
.sd<-apply(KHAT$r.unc[,-1],2,function(x) (x-.mean)^2)
.sd<-(.sd %*% as.matrix(CE$data$n.r))/sum(CE$data$n.r)
KHAT$r.unc<-data.frame(KHAT$r.unc,mean=.mean,sd=.sd,
   min=apply(KHAT$r.unc[,-1],1,min),max=apply(KHAT$r.unc[,-1],1,max))
.mean<-(as.matrix(KHAT$r.bor[,-1]) %*% as.matrix(CE$data$n.r))/
   sum(CE$data$n.r)
.sd<-apply(KHAT$r.bor[,-1],2,function(x) (x-.mean)^2)
.sd<-(.sd %*% as.matrix(CE$data$n.r))/sum(CE$data$n.r)
KHAT$r.bor<-data.frame(KHAT$r.bor,mean=.mean,sd=.sd,
   min=apply(KHAT$r.bor[,-1],1,min),max=apply(KHAT$r.bor[,-1],1,max))
.mean<-(as.matrix(KHAT$r.rip[,-1]) %*% as.matrix(CE$data$n.r))/
   sum(CE$data$n.r)
.sd<-apply(KHAT$r.rip[,-1],2,function(x) (x-.mean)^2)
.sd<-(.sd %*% as.matrix(CE$data$n.r))/sum(CE$data$n.r)
KHAT$r.rip<-data.frame(KHAT$r.rip,mean=.mean,sd=.sd,
   min=apply(KHAT$r.rip[,-1],1,min),max=apply(KHAT$r.rip[,-1],1,max))
.mean<-(as.matrix(KHAT$r2[,-1]) %*% as.matrix(CE$data$n.r2))/
   sum(CE$data$n.r2)
.sd<-apply(KHAT$r2[,-1],2,function(x) (x-.mean)^2)
.sd<-(.sd %*% as.matrix(CE$data$n.r2))/sum(CE$data$n.r2)
KHAT$r2<-data.frame(KHAT$r2,mean=.mean,sd=.sd,min=apply(KHAT$r2[,-1],1,
   min),max=apply(KHAT$r2[,-1],1,max))
.mean<-(as.matrix(KHAT$r2.same[,-1]) %*% as.matrix(CE$data$n.r2.same))/
   sum(CE$data$n.r2.same)
.sd<-apply(KHAT$r2.same[,-1],2,function(x) (x-.mean)^2)
.sd<-(.sd %*% as.matrix(CE$data$n.r2.same))/sum(CE$data$n.r2.same)
KHAT$r2.same<-data.frame(KHAT$r2.same,mean=.mean,sd=.sd,min=
   apply(KHAT$r2.same[,-1],1,min),max=apply(KHAT$r2.same[,-1],1,max))
.mean<-(as.matrix(KHAT$r2.diff[,-1]) %*% as.matrix(CE$data$n.r2.diff))/
   sum(CE$data$n.r2.diff)
.sd<-apply(KHAT$r2.diff[,-1],2,function(x) (x-.mean)^2)
.sd<-(.sd %*% as.matrix(CE$data$n.r2.diff))/sum(CE$data$n.r2.diff)
KHAT$r2.diff<-data.frame(KHAT$r2.diff,mean=.mean,sd=.sd,min=
   apply(KHAT$r2.diff[,-1],1,min),max=apply(KHAT$r2.diff[,-1],1,max))
.mean<-(as.matrix(KHAT$r2.rand[,-1]) %*% as.matrix(CE$data$n.r2.rand))/
   sum(CE$data$n.r2.rand)
.sd<-apply(KHAT$r2.rand[,-1],2,function(x) (x-.mean)^2)
.sd<-(.sd %*% as.matrix(CE$data$n.r2.rand))/sum(CE$data$n.r2.rand)
KHAT$r2.rand<-data.frame(KHAT$r2.rand,mean=.mean,sd=.sd,min=
   apply(KHAT$r2.rand[,-1],1,min),max=apply(KHAT$r2.rand[,-1],1,max))
```

```
# This last command cleans the workspace of all temporary variables,
# thereby outputting only the 7 items listed in the SUMMARY above.

rm(.mean,.sd,c.r2,c.r2.diff,c.r2.rand,c.r2.same,c.ra,c.rb,CE.sum,demor,
   demor2,den.r2,den.r2.diff,den.r2.rand,den.r2.same,den.ra,den.rb,i,
   i2,i3,i4,i5,i6,i7,i8,inn.out,inners,mor,n6,num.r2,num.r2.diff,
   num.r2.rand,num.r2.same,num.ra,num.rb,outers,p.counts,plots.demorph,
   plots.demorph2,plots.morph,plots.torus,plots.torus2,poly.r,poly.r2,
   r.in1,r.in2,r.in3,rad,range.r,range.r2,ring,tmp1,tmp2,tmp3,tmp4,
   torus,torus2)
```

APPENDIX B

STEM MAPS OF FOREST SERVICE PLOTS

The following stem maps represent the 7883 tree positions measured on 50 plots of the U.S. Forest Service's long-term silvicultural study at the Penobscot Experimental forest in Bradley, ME. Maps are paired and listed by treatment, then sequentially by compartment and plot. The top map refers to the actual tree positions measured during Summer 2001-2002, while the bottom map is a representation of the plot after using the morphing algorithm to scale the 0.020 ha (0.05 ac) inner, small tree (1.2 – 11.4 cm diameter at breast height [DBH]) subplot to the 0.081 ha (0.20 ac) large tree (>11.4 cm DBH) plot. CE refers to the Clark-Evans statistic (Clark and Evans 1954) for the small trees only. See Section 2.6 for more details.

These maps exclude trees for which there were errors made collecting the positional data. There also are a small number of trees that had been measured by the Forest Service in their inventories that were determined to be outside of the plot or subplot boundaries during my survey. In total, there are about 69 trees excluded.

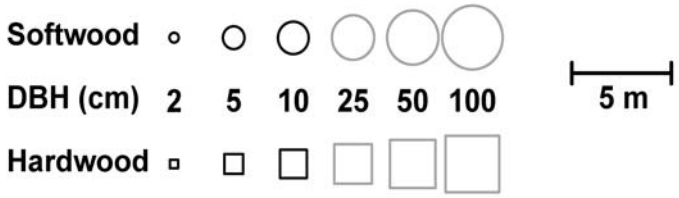

Figure B.1. Example realization of the morphing algorithm used to scale each of the 50 U.S. Forest Service plots at the Penobscot Experimental Forest in Bradley, ME, measured within this study. Each realization uses all subplots within a given compartment for wrapping within the morphing algorithmn. The Clark-Evans statistic (CE) is listed for both pre-scaled (top figure on each page) and post-scaled spatial patterns (bottom figure on each page). Symbol size is proportional to the natural log of diameter at breast height (DBH), softwood species are represented by circles and hardwood species by squares, and trees >11.4 cm DBH are colored grey, not black. The overall legend for this figure is shown above, with symbols and distances to scale.

Treatment: Natural Area Control
Compartment: 32A
Plot: 13

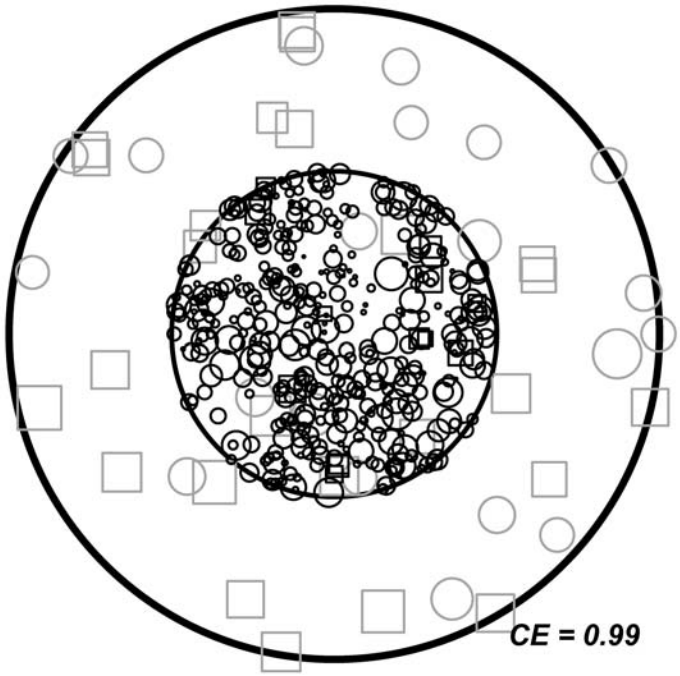

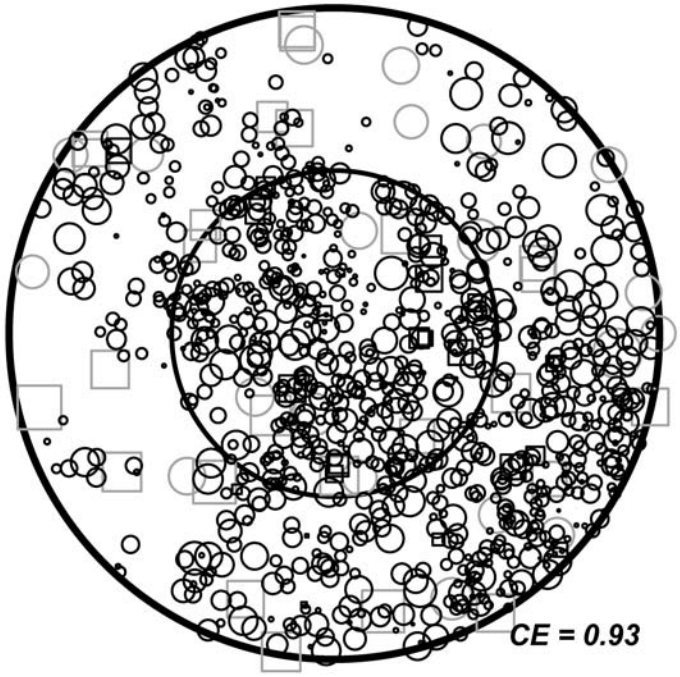

Treatment: Natural Area Control
Compartment: 32A
Plot: 24

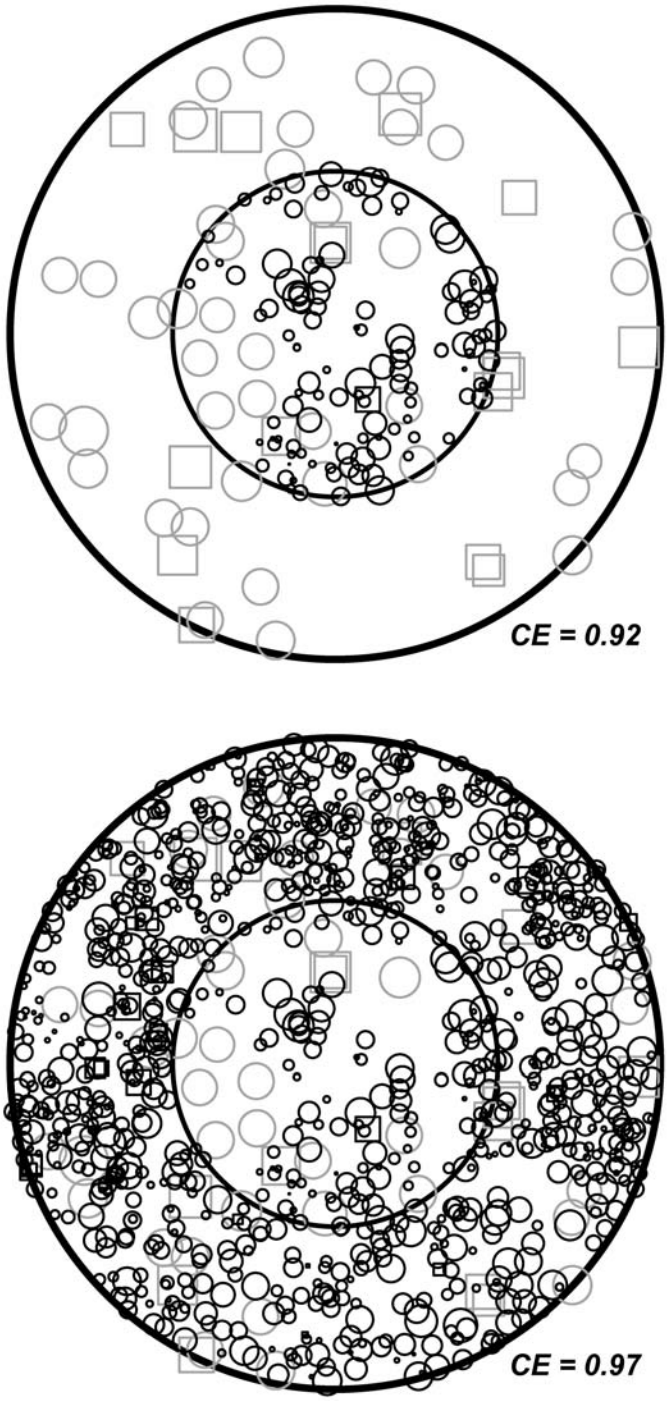

Figure B.1. Continued.

Treatment: Natural Area Control
Compartment: 32A
Plot: 42

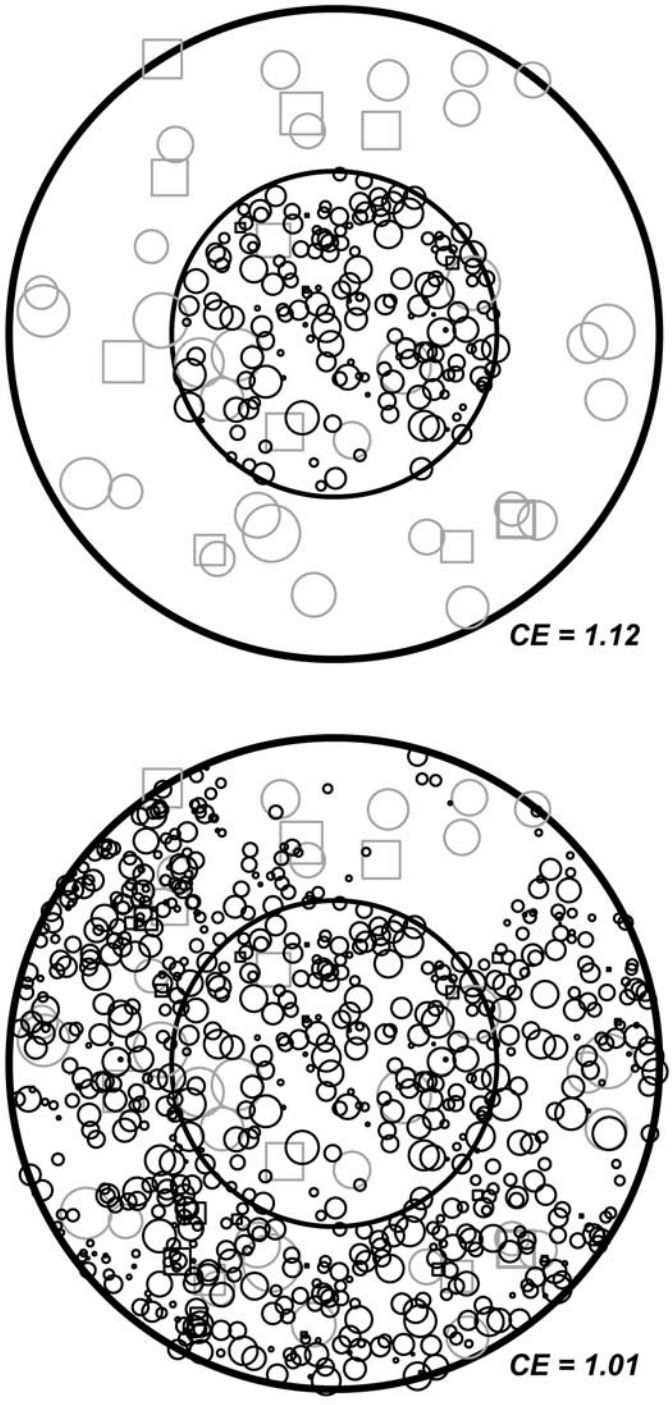

Figure B.1. Continued.

Treatment: Natural Area Control
Compartment: 32A
Plot: 43

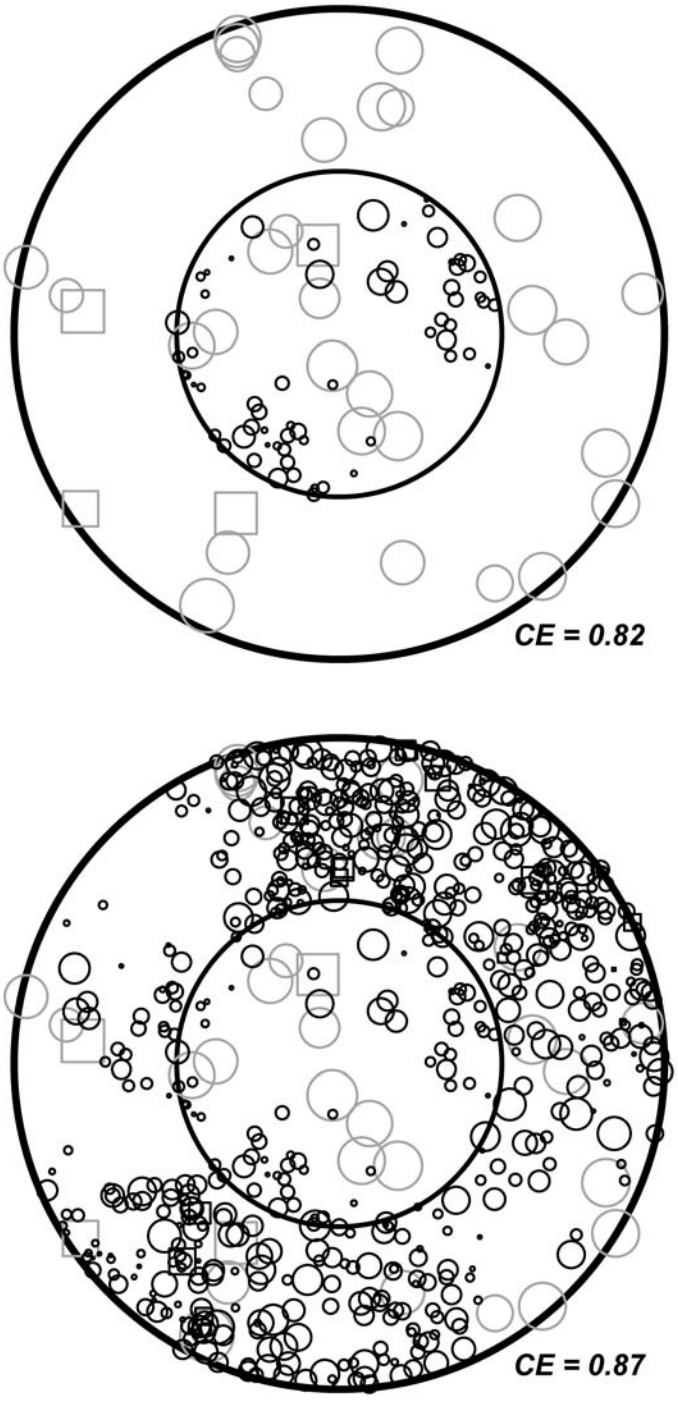

Figure B.1. Continued.

Treatment: Natural Area Control
Compartment: 32A
Plot: 54

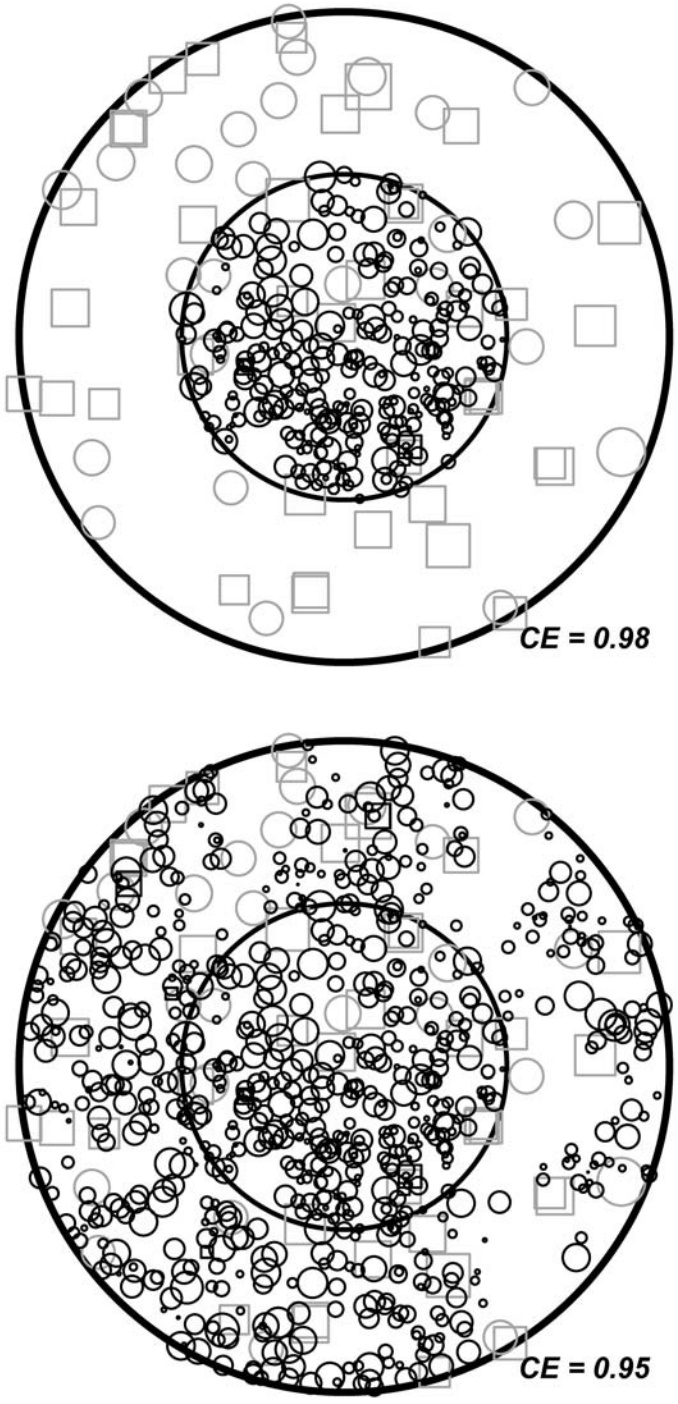

Figure B.1. Continued.

Treatment: Natural Area Control
Compartment: 32B
Plot: 23

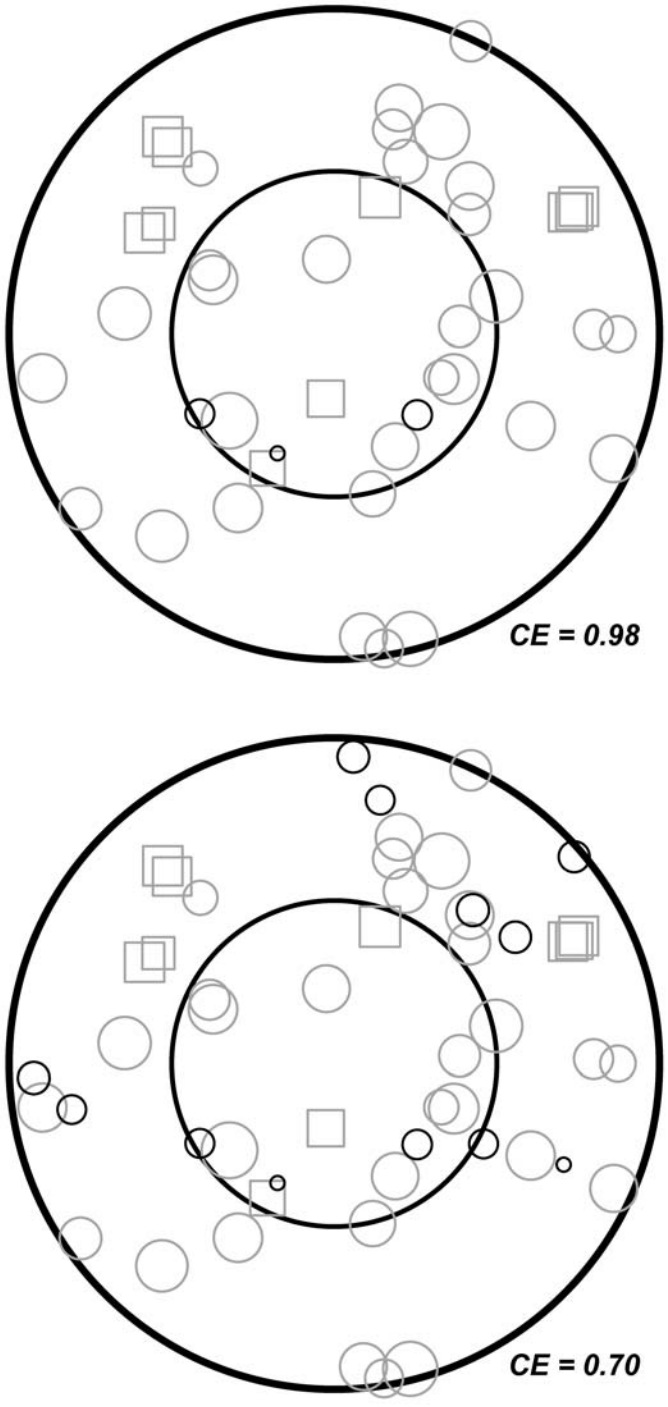

Figure B.1. Continued.

Treatment: Natural Area Control
Compartment: 32B
Plot: 32

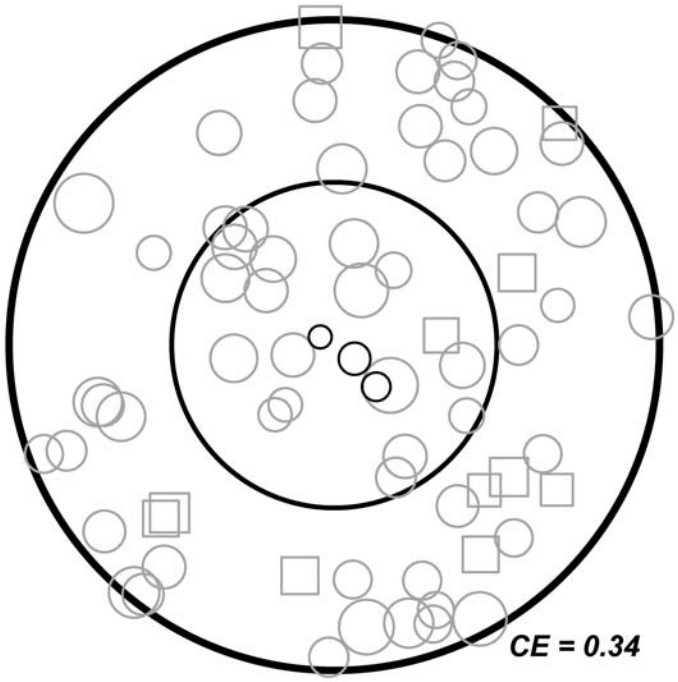

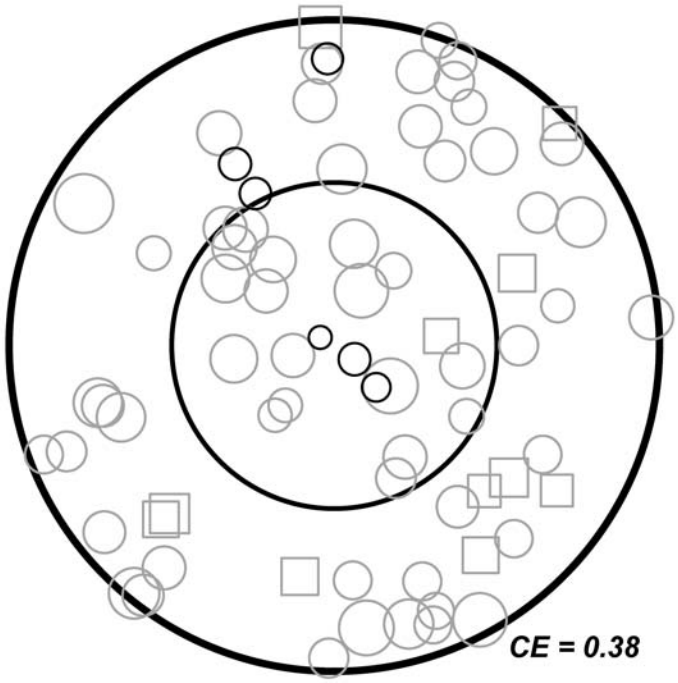

Figure B.1. Continued.

Treatment: Natural Area Control
Compartment: 32B
Plot: 73

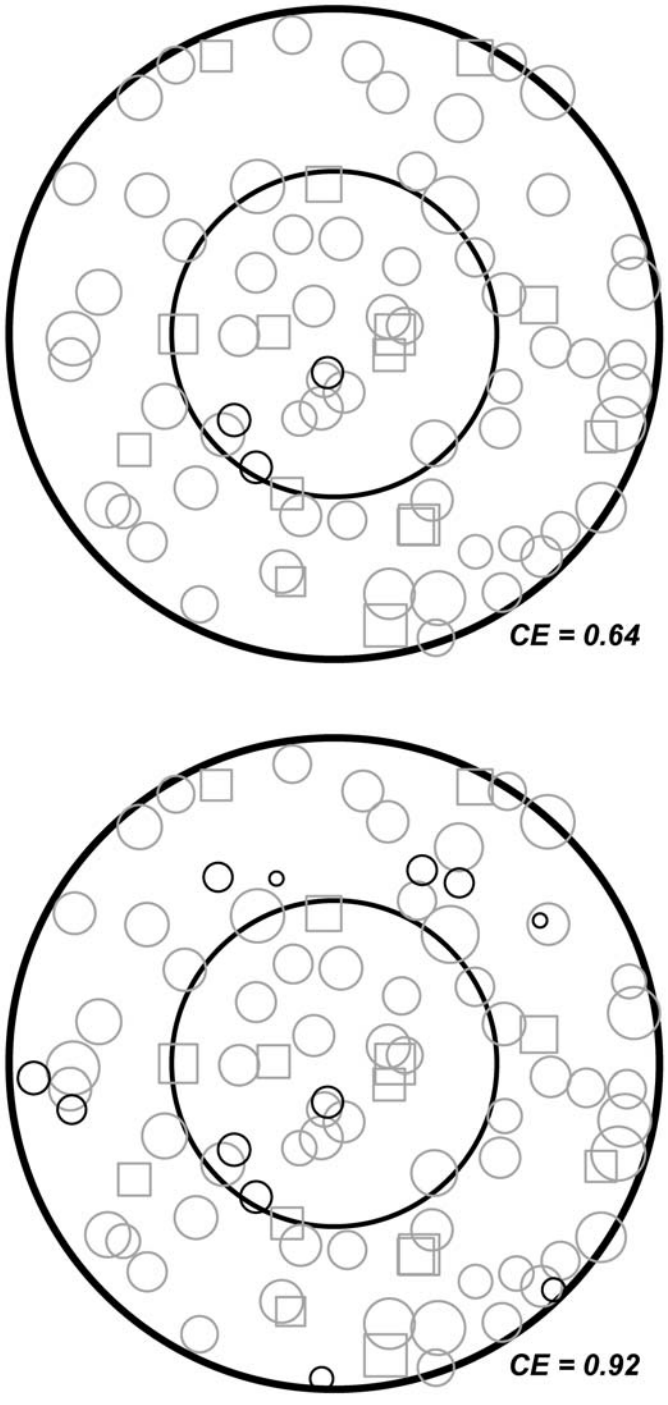

Figure B.1. Continued.

Treatment: Natural Area Control
Compartment: 32B
Plot: 74

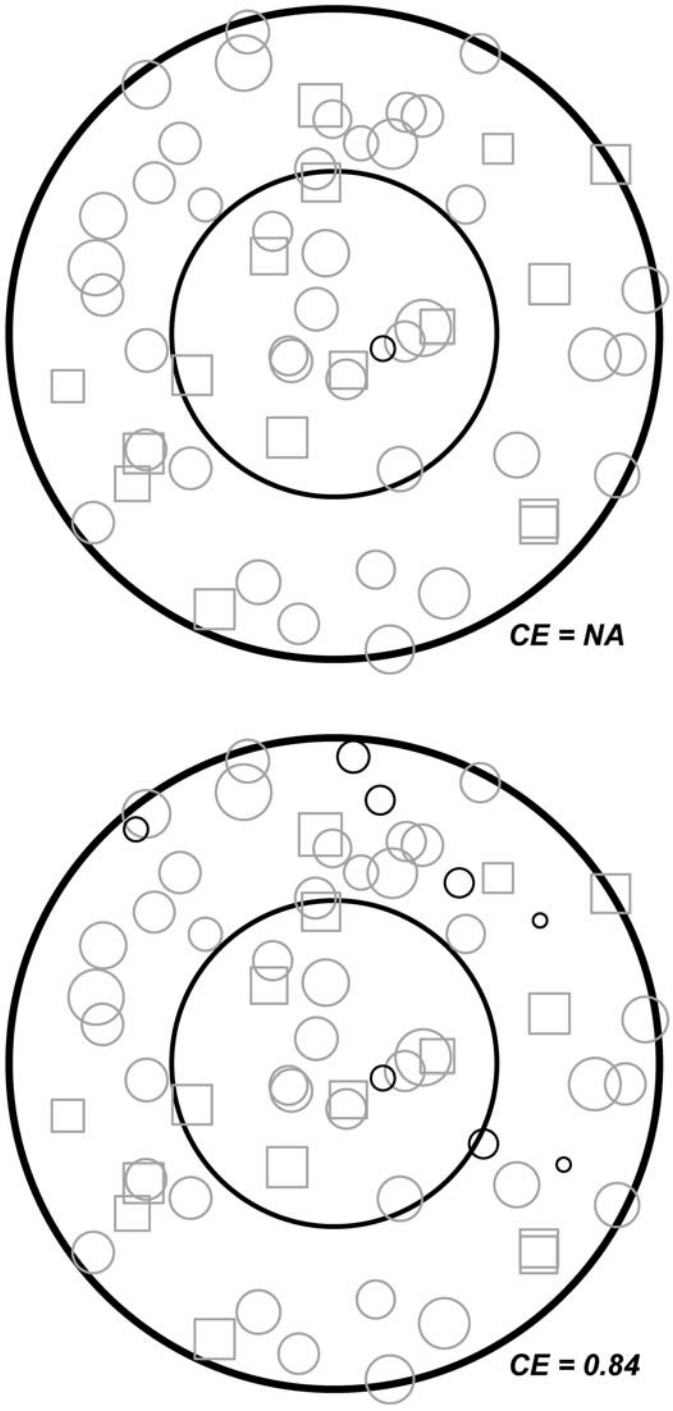

Figure B.1. Continued.

Treatment: Natural Area Control
Compartment: 32B
Plot: 83

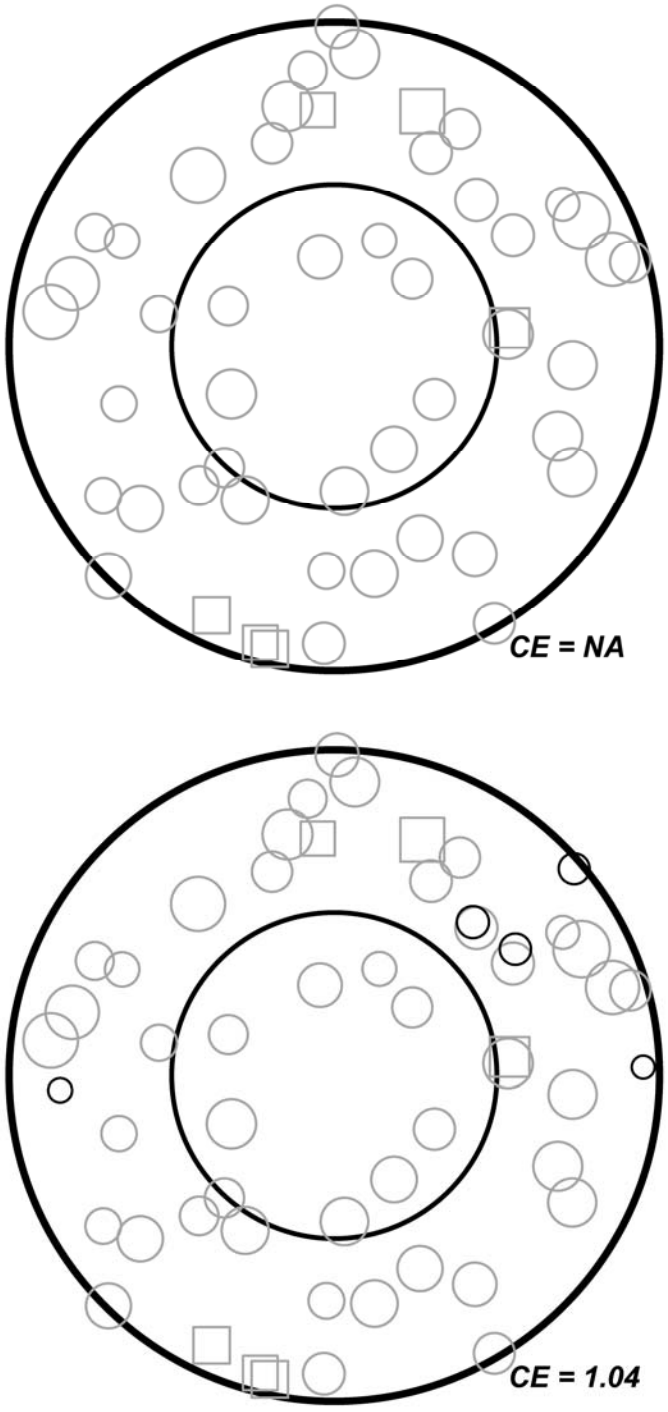

Figure B.1. Continued.

Treatment: Commercial Clearcut
Compartment: 8
Plot: 14

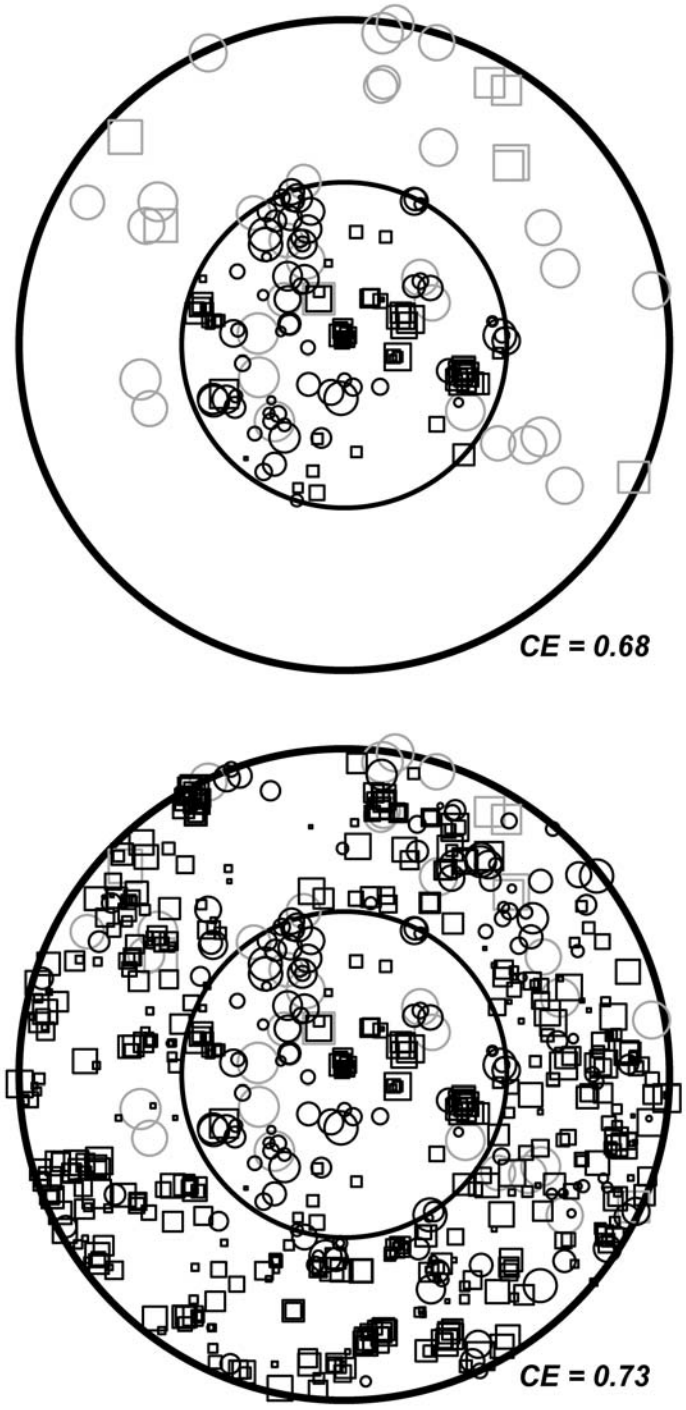

Figure B.1. Continued.

Treatment: Commercial Clearcut
Compartment: 8
Plot: 23

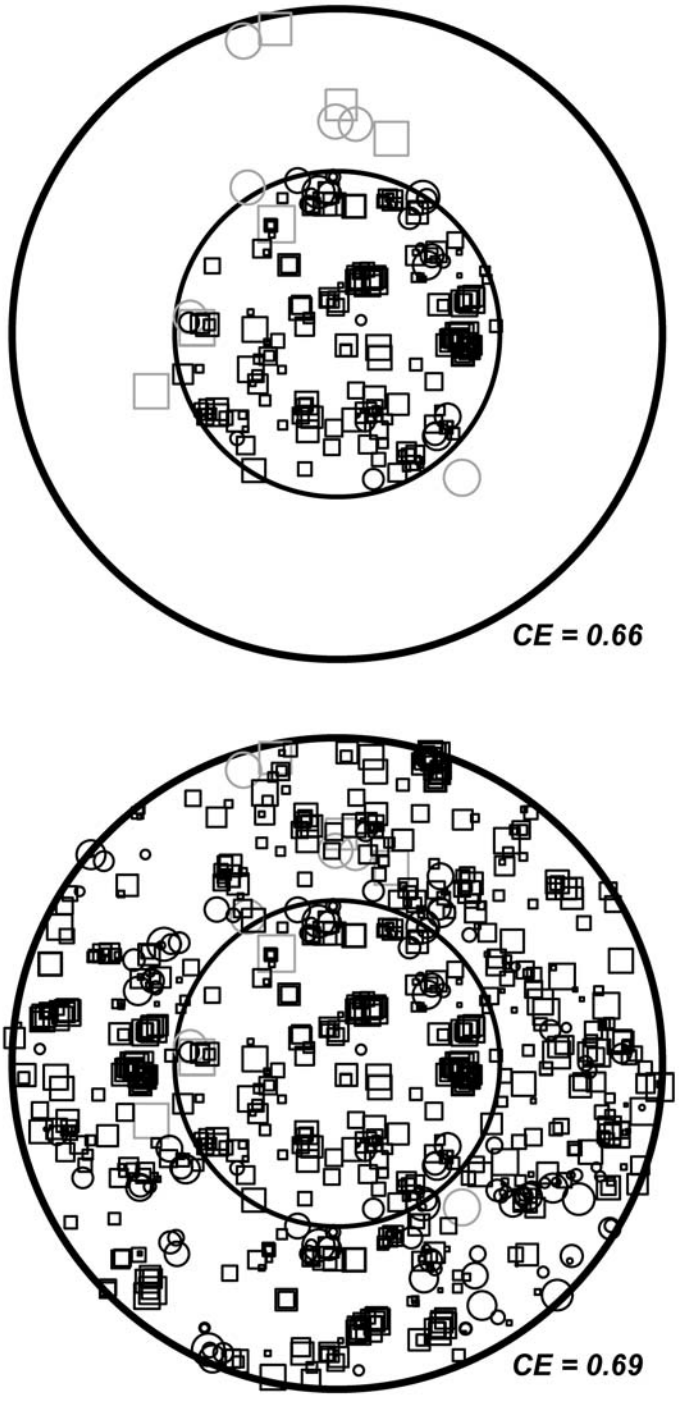

Figure B.1. Continued.

Treatment: Commercial Clearcut
Compartment: 8
Plot: 31

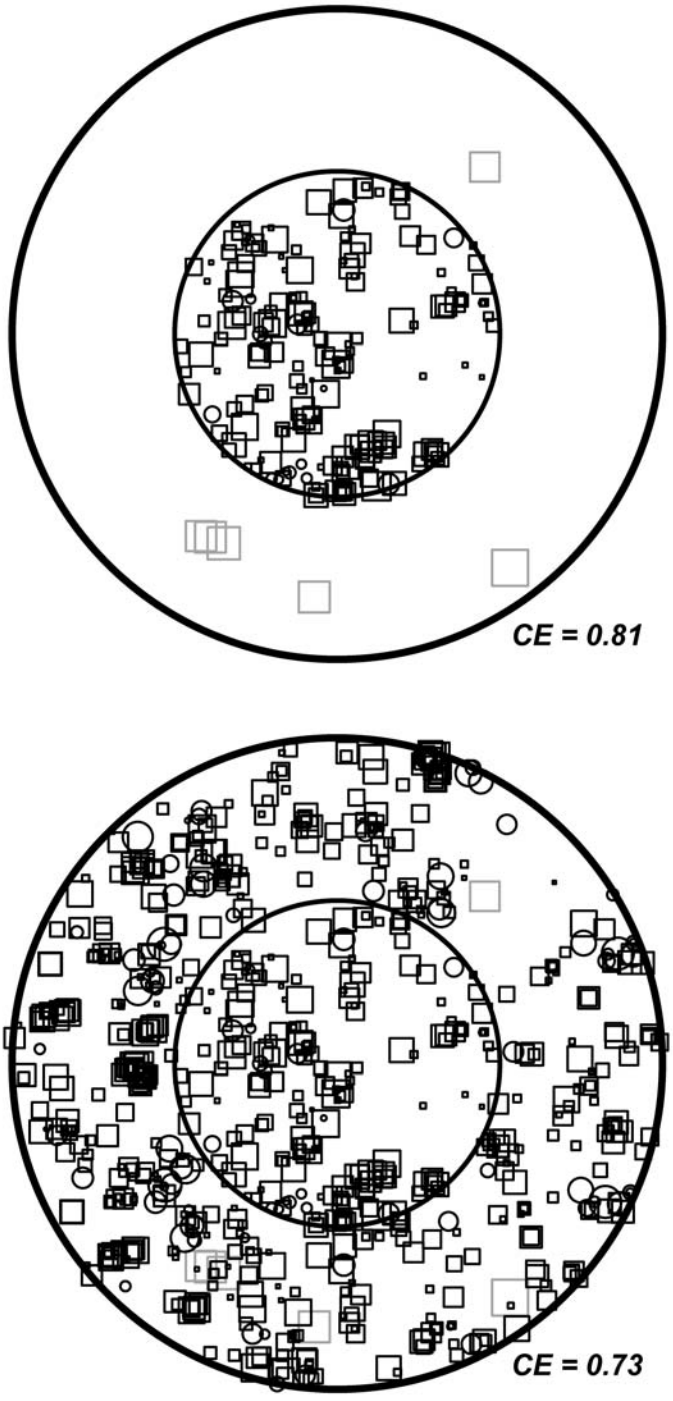

Figure B.1. Continued.

Treatment: Commercial Clearcut
Compartment: 8
Plot: 52

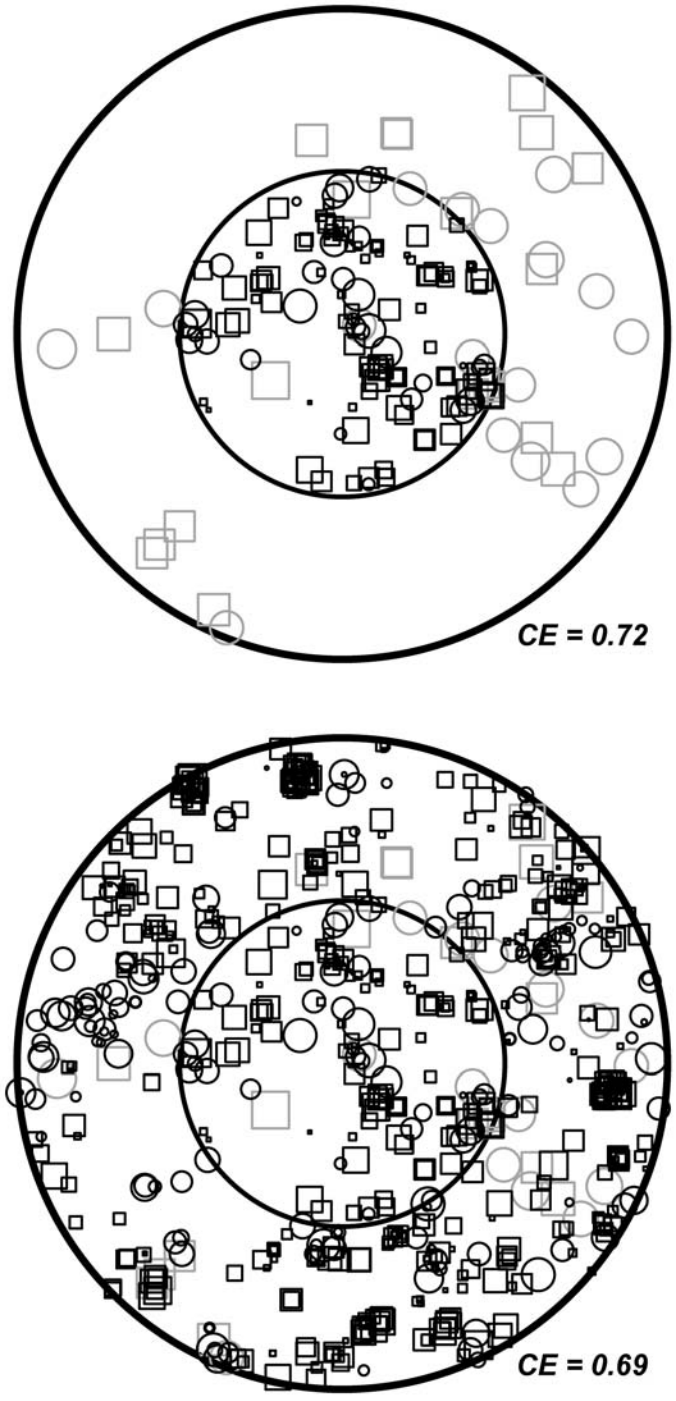

Figure B.1. Continued.

Treatment: Commercial Clearcut
Compartment: 8
Plot: 71

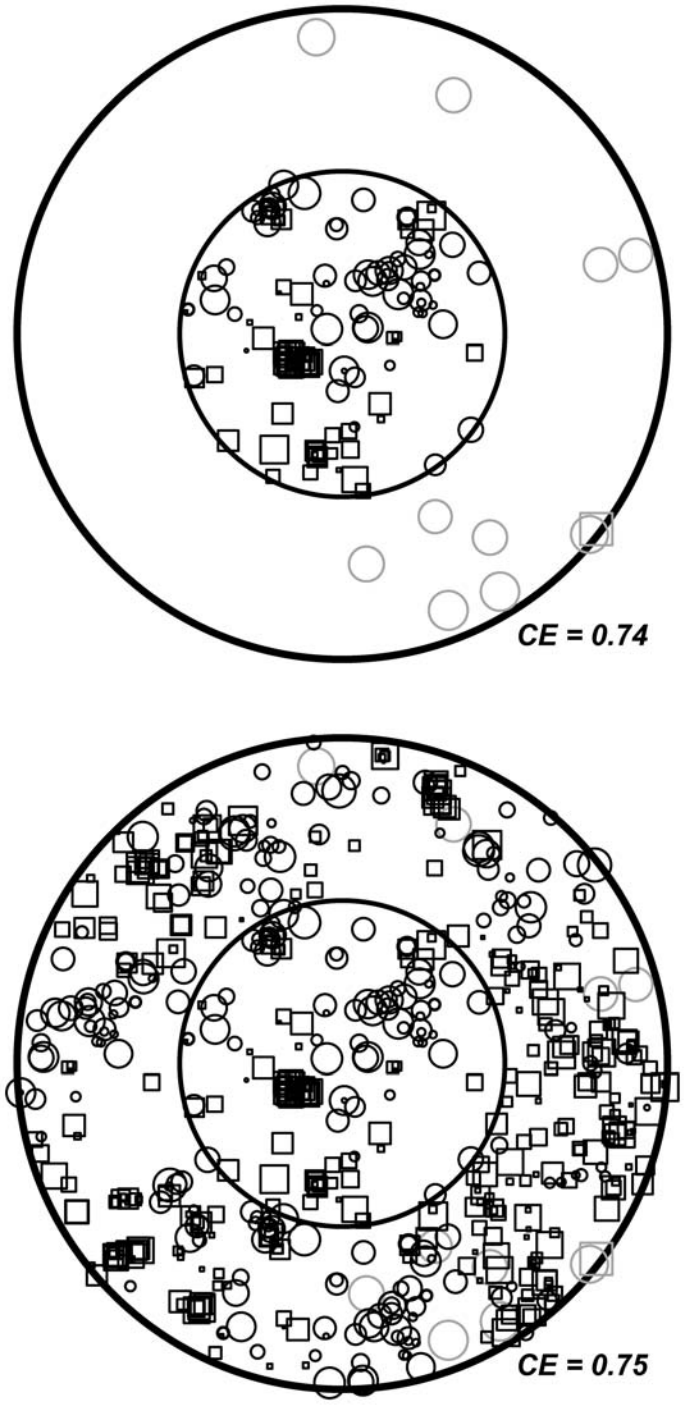

Figure B.1. Continued.

Treatment: Commercial Clearcut
Compartment: 22
Plot: 22

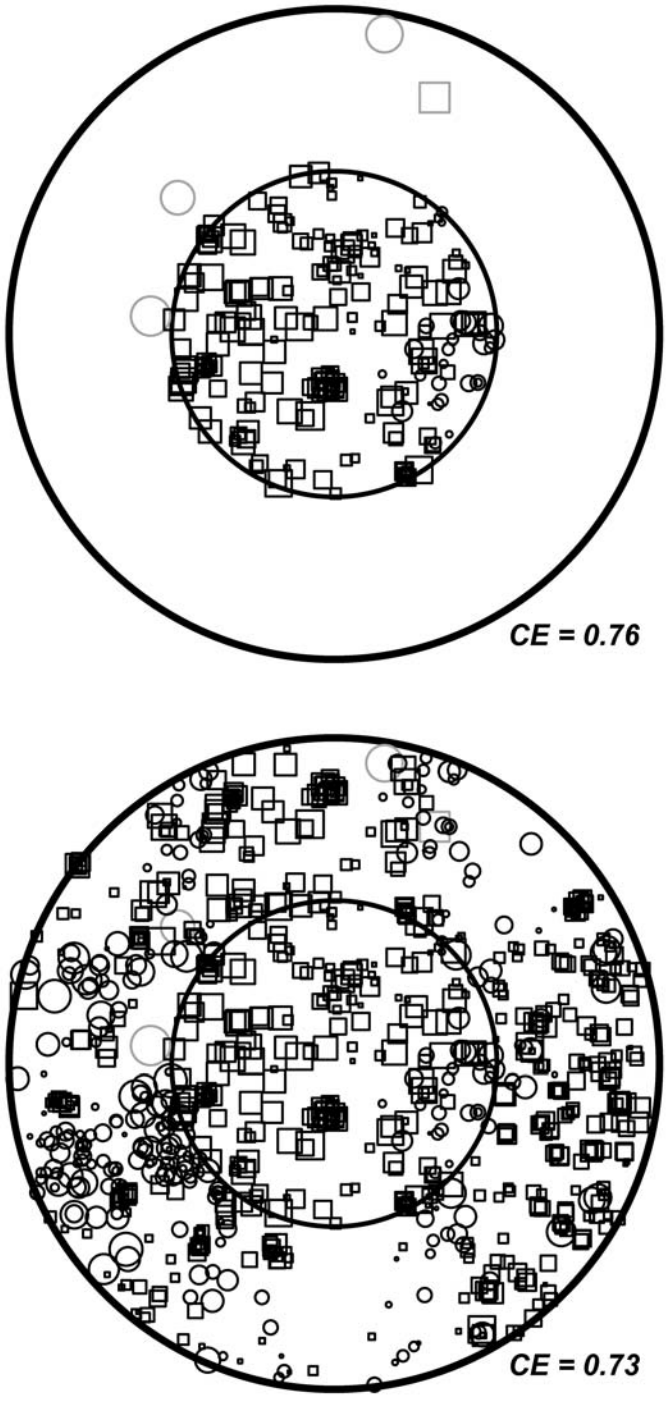

Figure B.1. Continued.

Treatment: Commercial Clearcut
Compartment: 22
Plot: 32

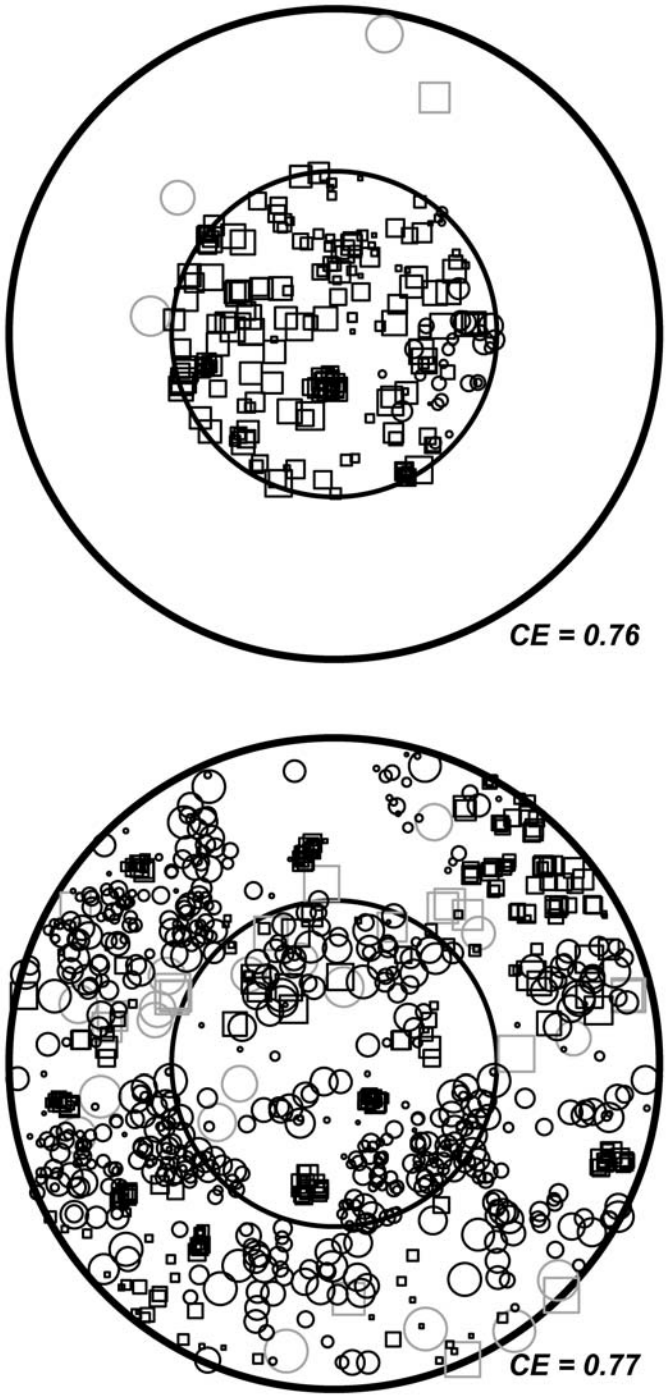

Figure B.1. Continued.

Treatment: Commercial Clearcut
Compartment: 22
Plot: 34

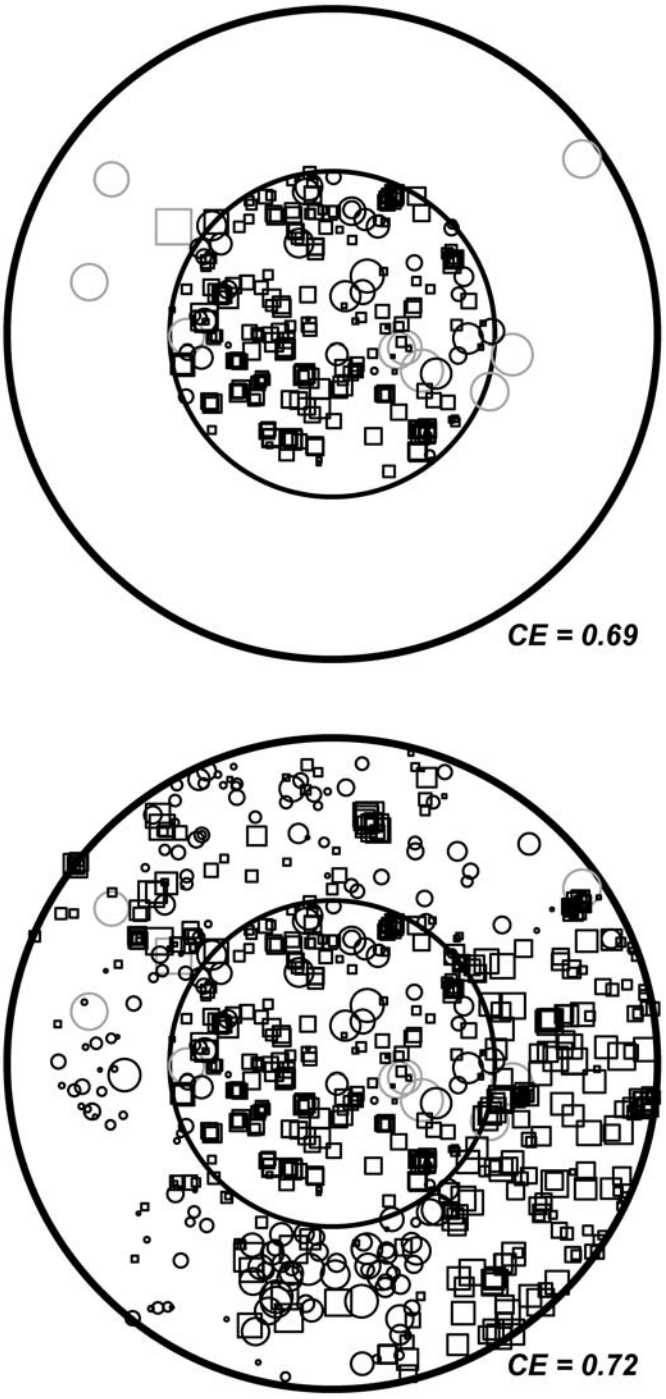

Figure B.1. Continued.

Treatment: Commercial Clearcut
Compartment: 22
Plot: 42

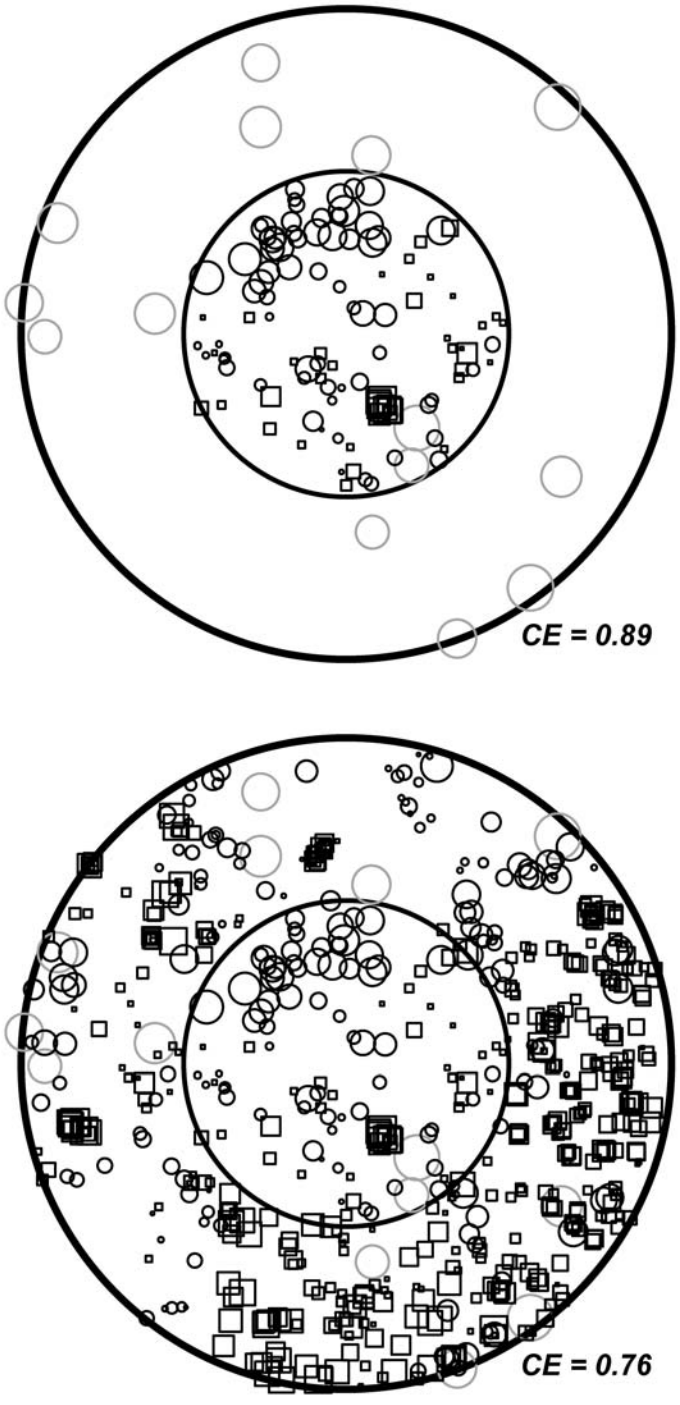

Figure B.1. Continued.

Treatment: Commercial Clearcut
Compartment: 22
Plot: 53

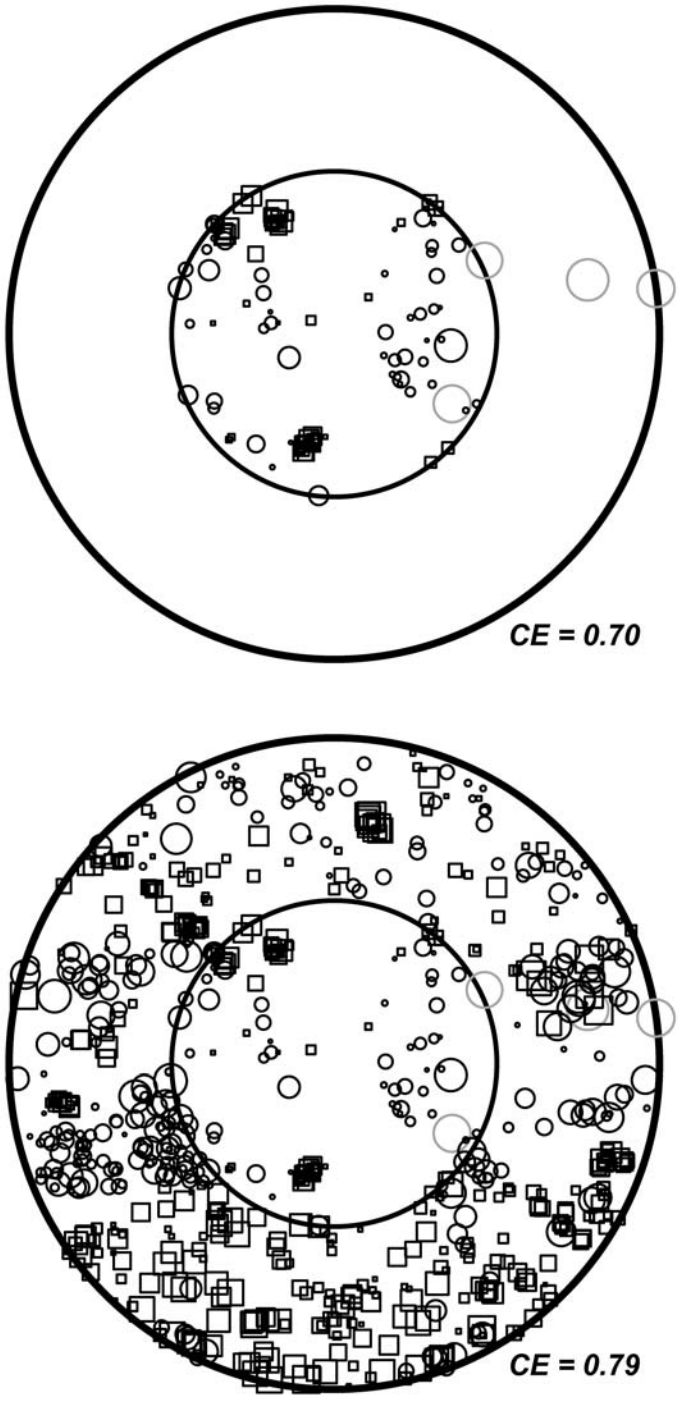

Figure B.1. Continued.

Treatment: Fixed Diameter Limit
Compartment: 4
Plot: 14

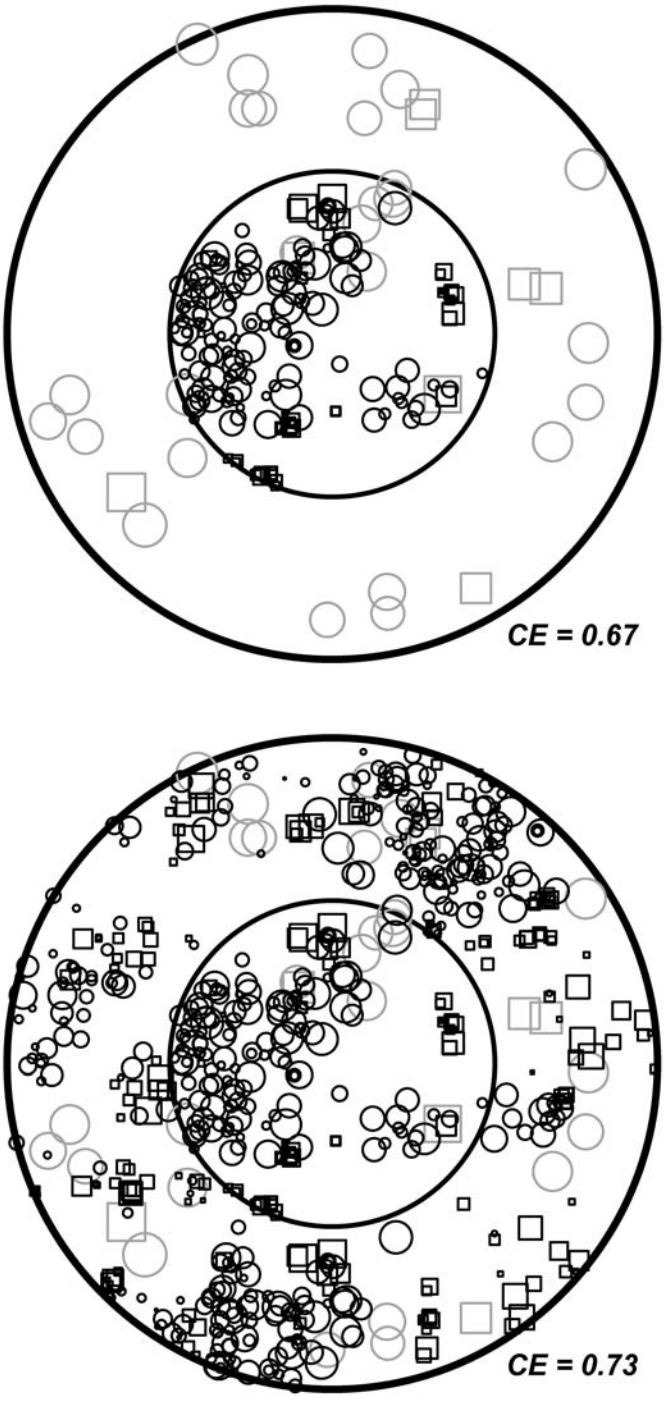

Figure B.1. Continued.

Treatment: Fixed Diameter Limit
Compartment: 4
Plot: 21

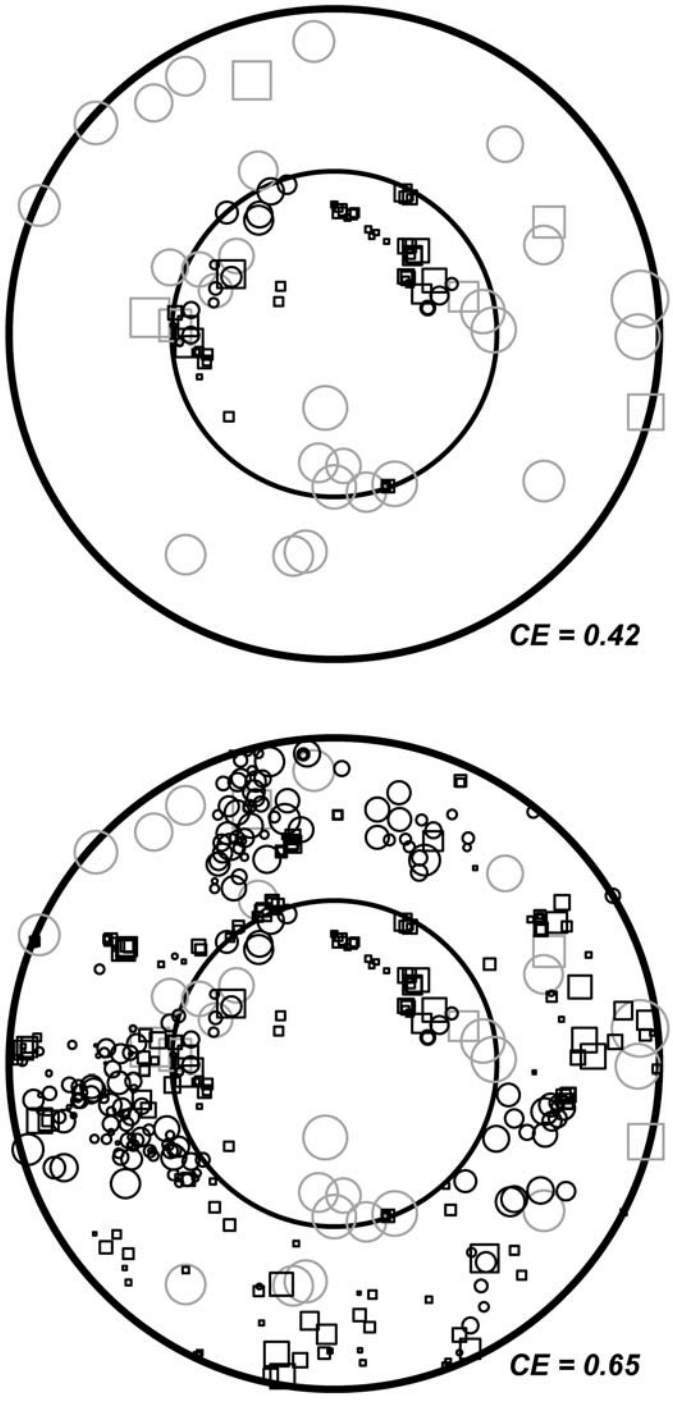

Figure B.1. Continued.

Treatment: Fixed Diameter Limit
Compartment: 4
Plot: 31

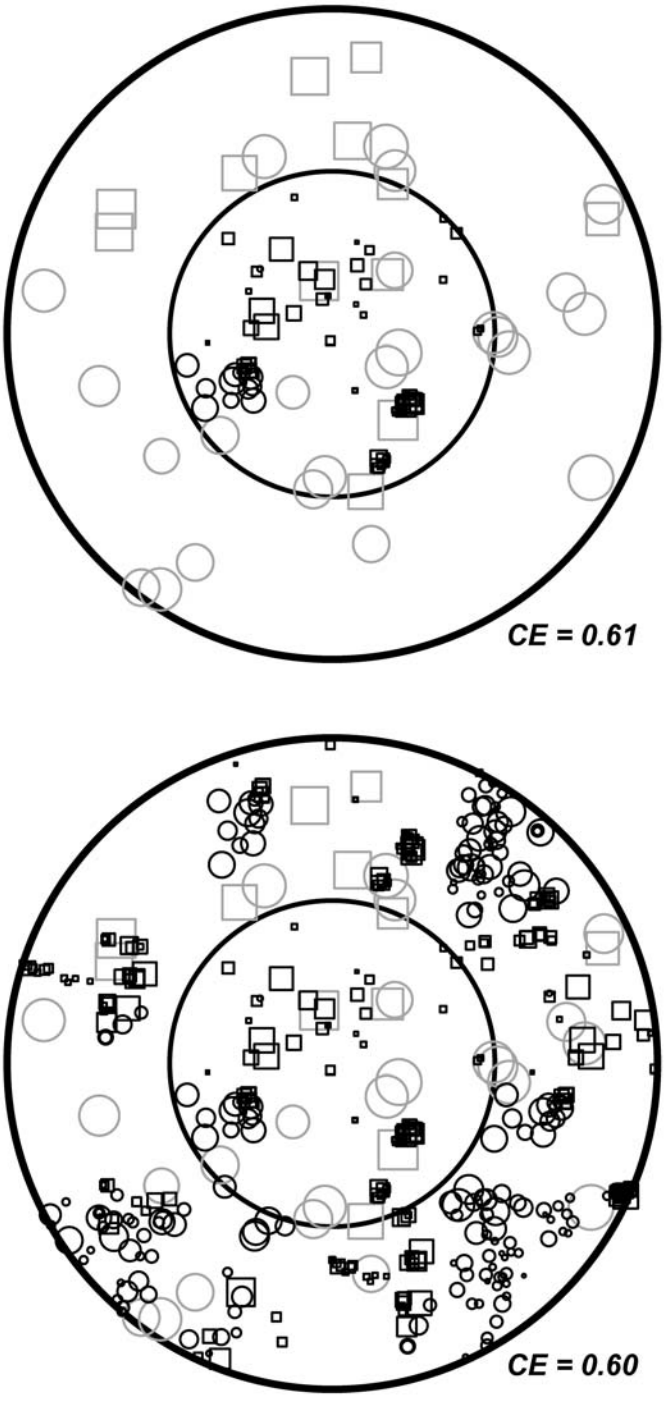

Figure B.1. Continued.

Treatment: Fixed Diameter Limit
Compartment: 4
Plot: 42

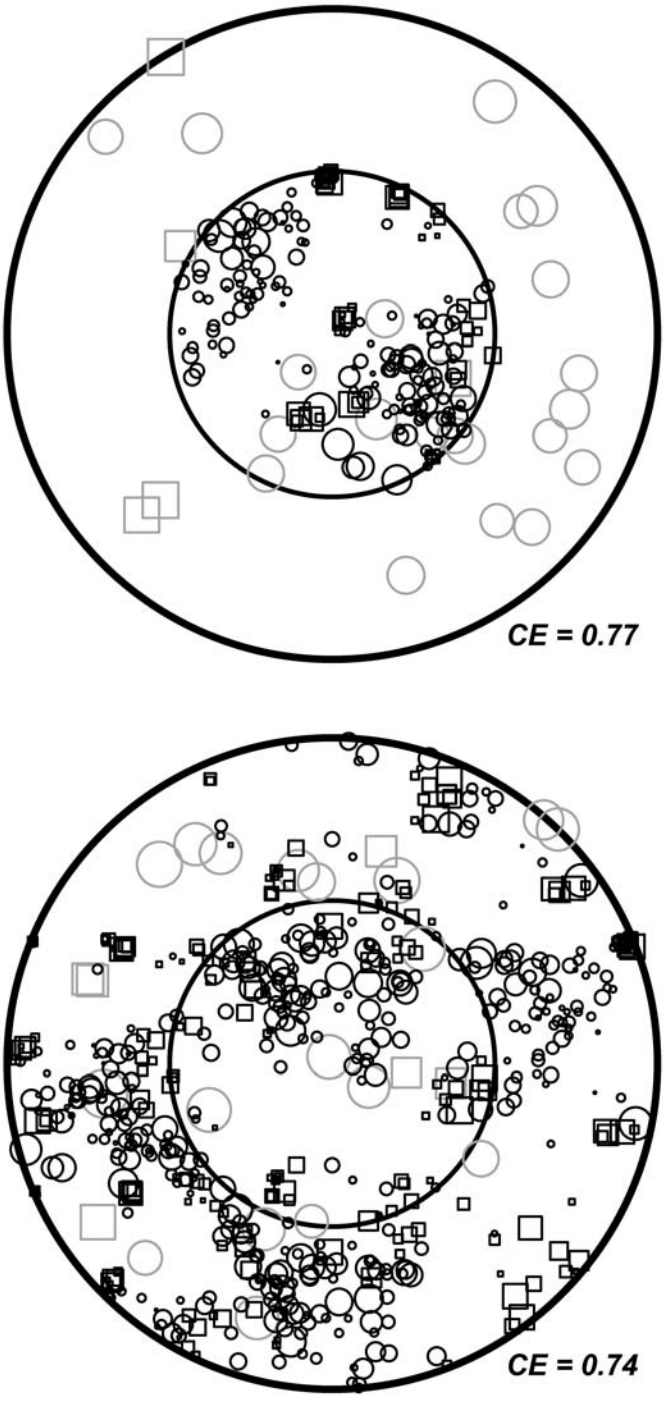

Figure B.1. Continued.

Treatment: Fixed Diameter Limit
Compartment: 4
Plot: 44

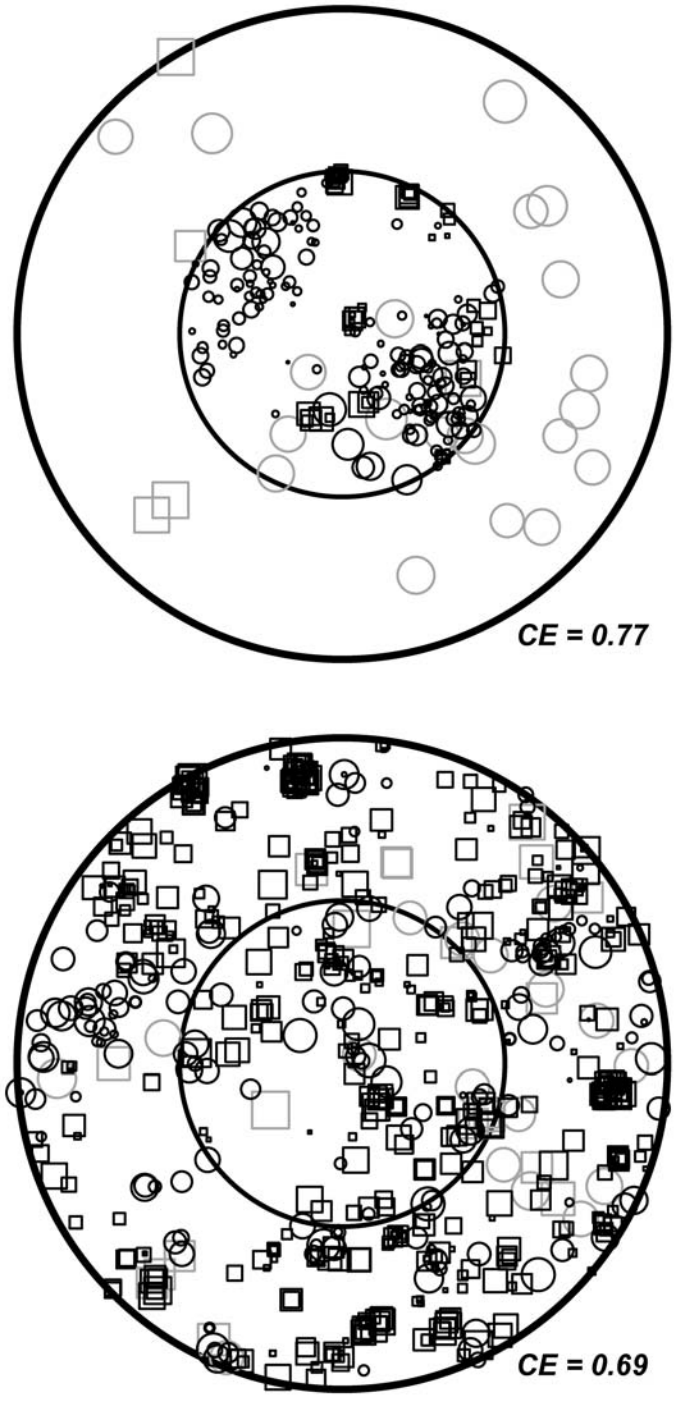

Figure B.1. Continued.

Treatment: Fixed Diameter Limit
Compartment: 15
Plot: 15

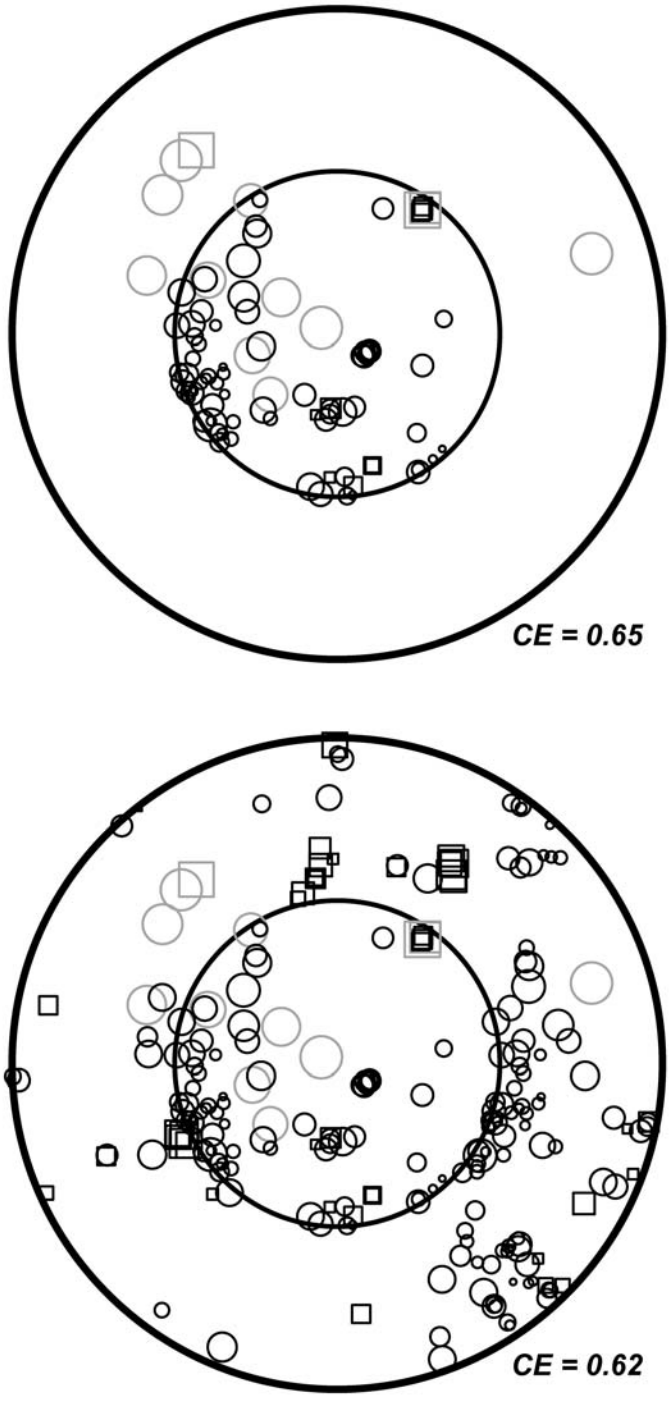

Figure B.1. Continued.

Treatment: Fixed Diameter Limit
Compartment: 15
Plot: 22

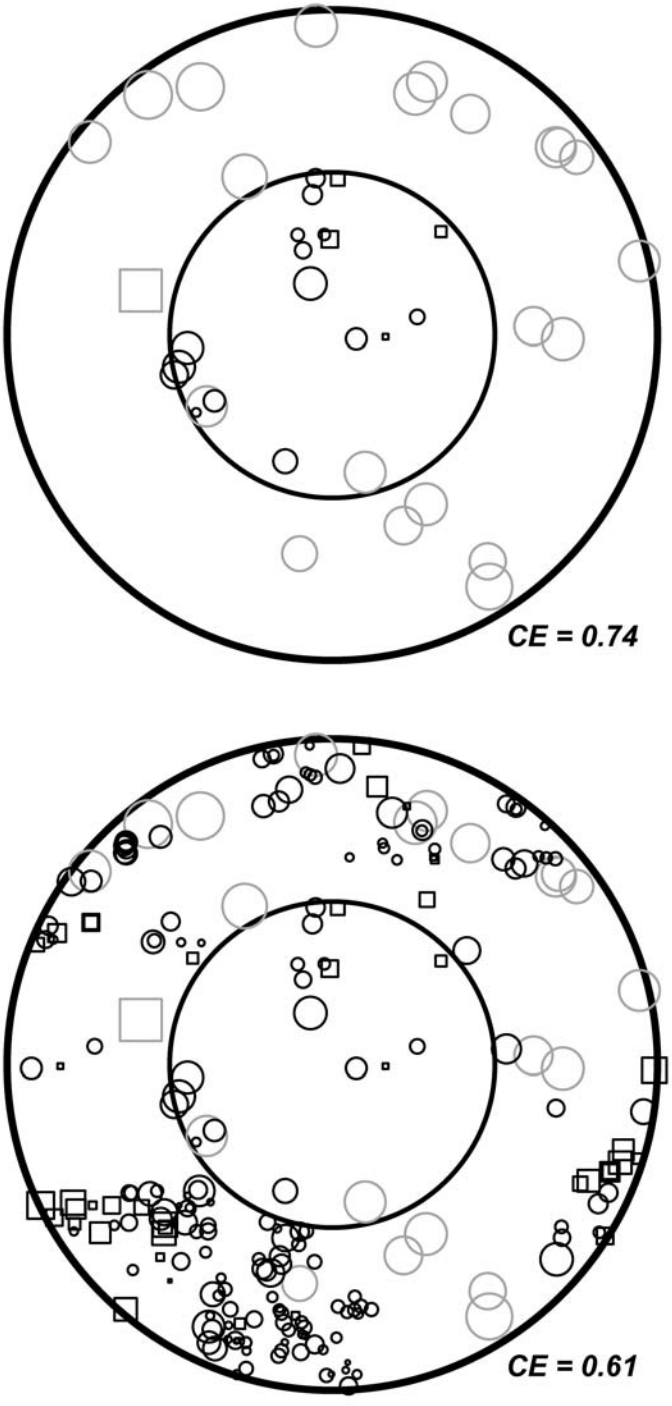

Figure B.1. Continued.

Treatment: Fixed Diameter Limit
Compartment: 15
Plot: 32

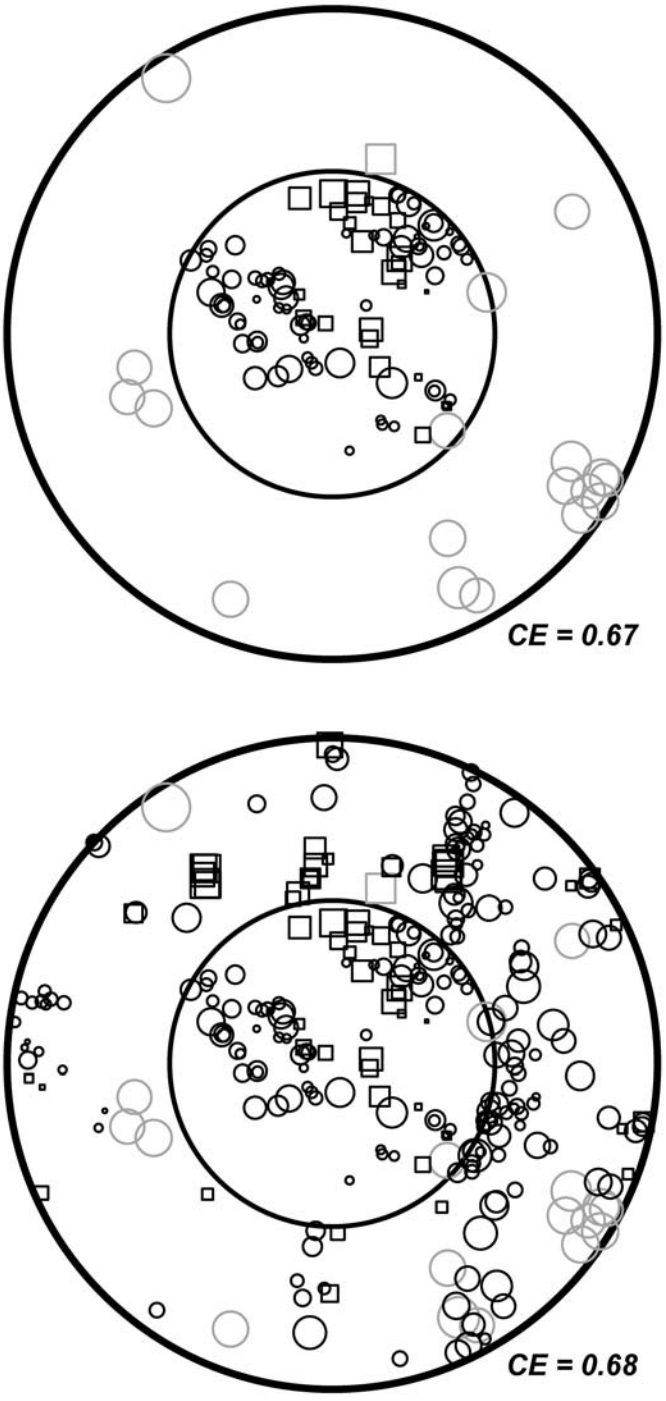

Figure B.1. Continued.

Treatment: Fixed Diameter Limit
Compartment: 15
Plot: 41

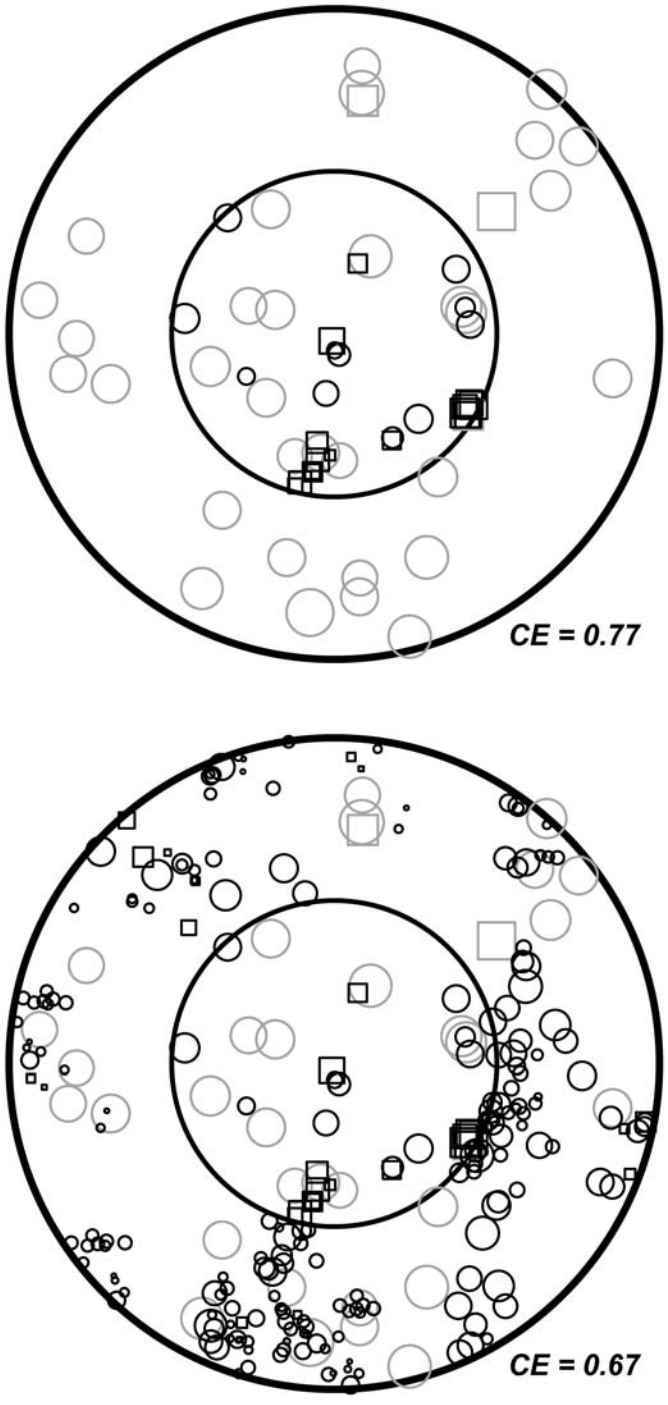

Figure B.1. Continued.

Treatment: Fixed Diameter Limit
Compartment: 15
Plot: 45

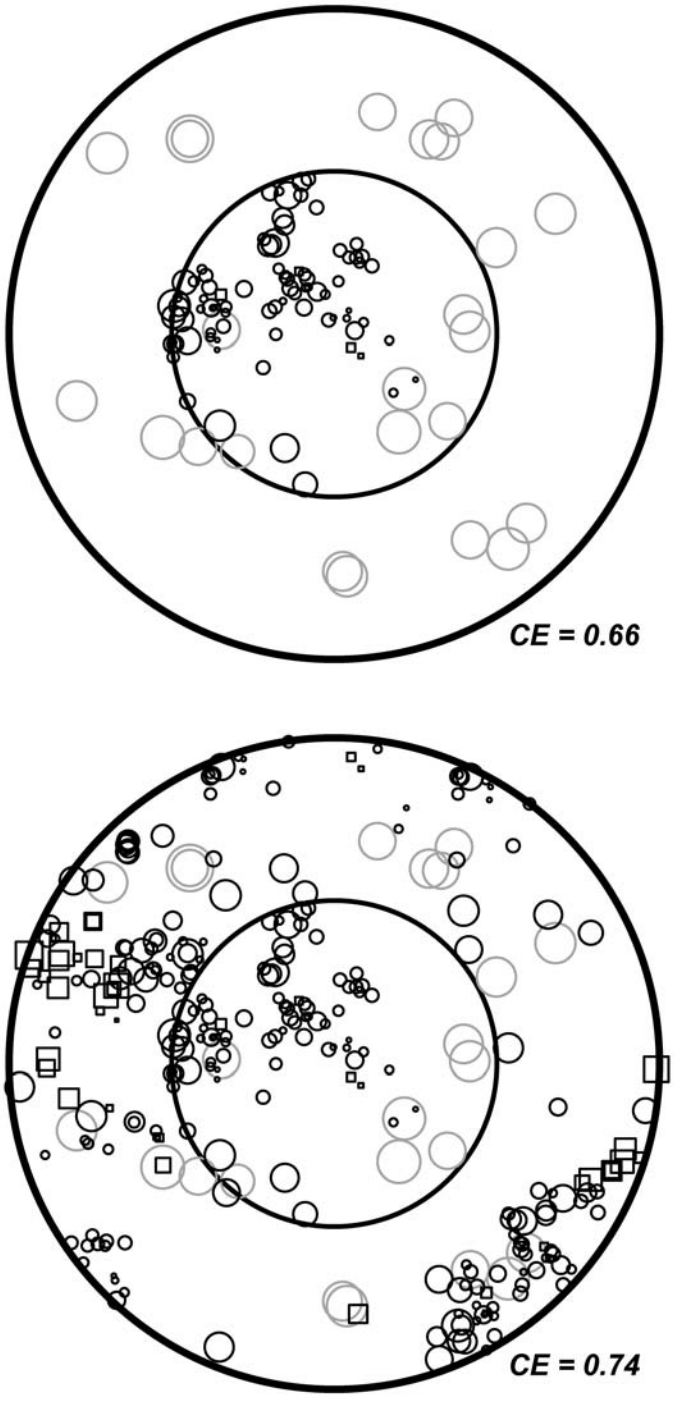

Figure B.1. Continued.

Treatment: Five-Year Selection
Compartment: 9
Plot: 14

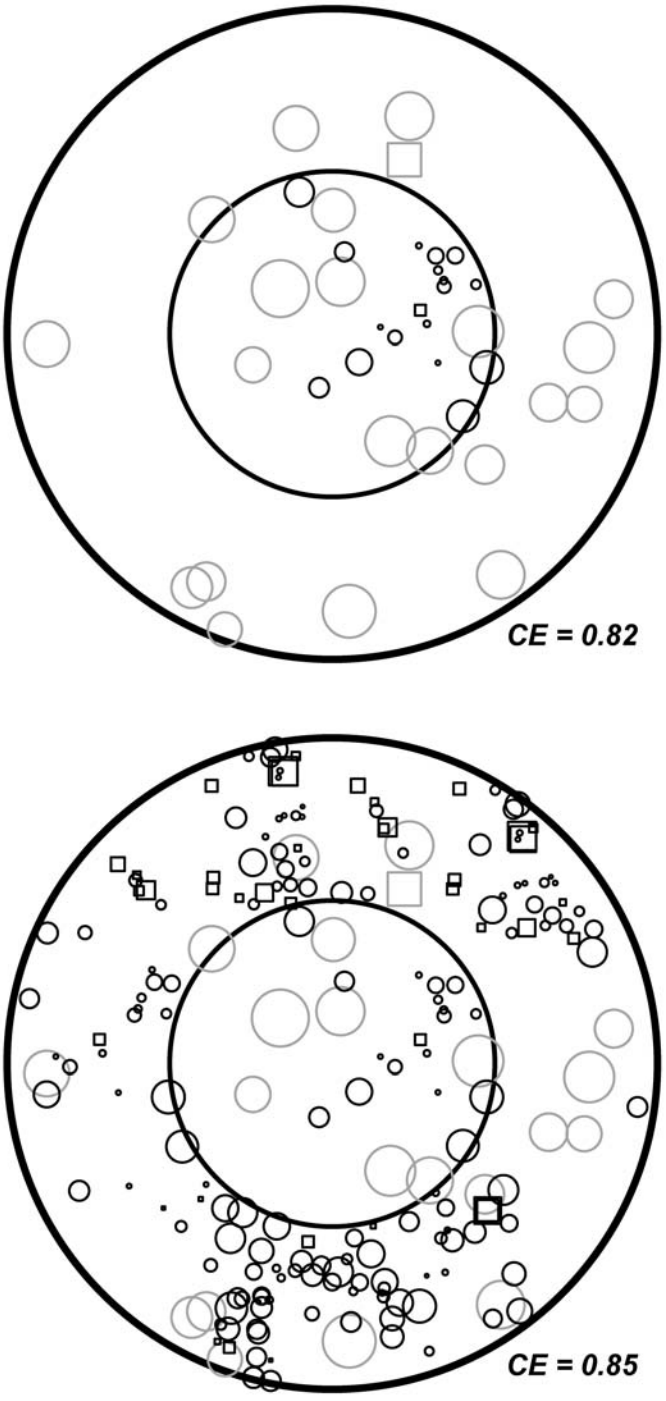

Figure B.1. Continued.

Treatment: Five-Year Selection
Compartment: 9
Plot: 23

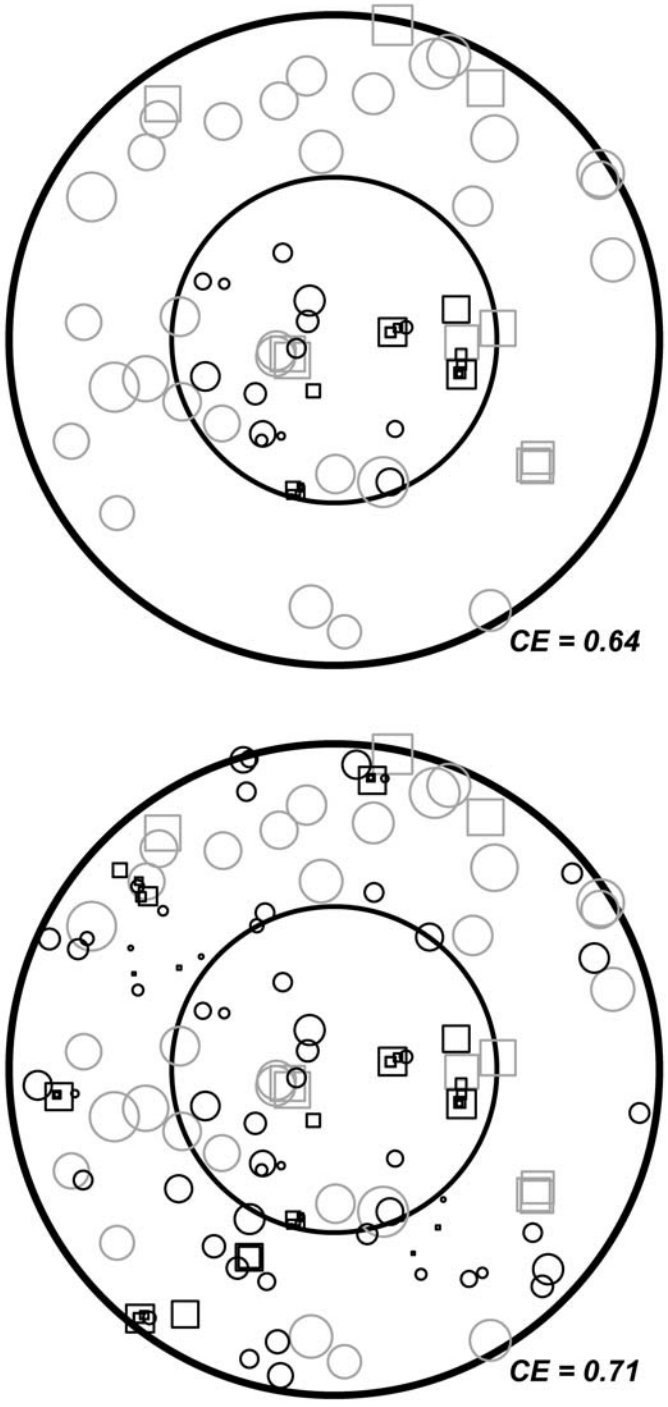

Figure B.1. Continued.

Treatment: Five-Year Selection
Compartment: 9
Plot: 34

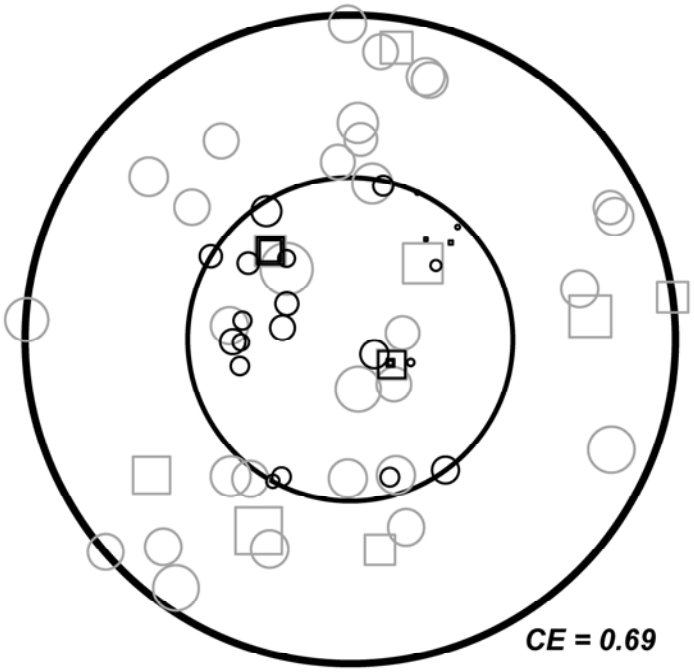

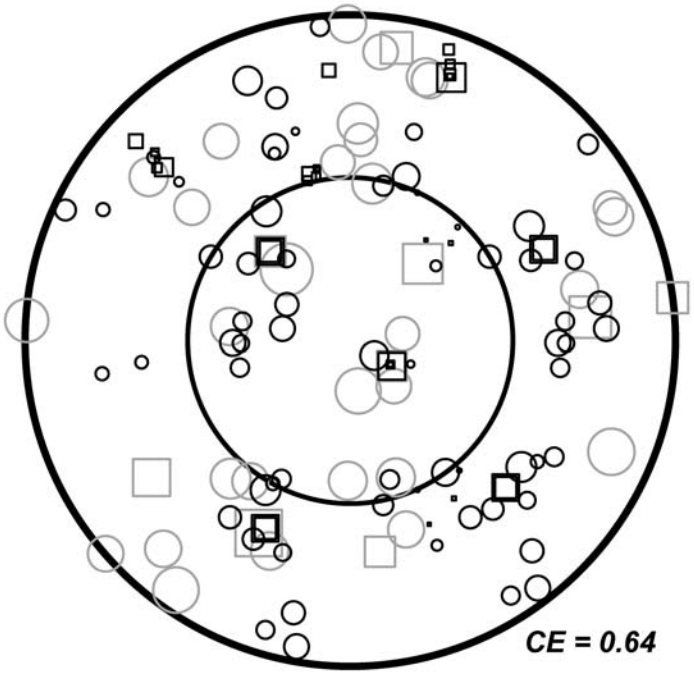

Figure B.1. Continued.

Treatment: Five-Year Selection
Compartment: 9
Plot: 43

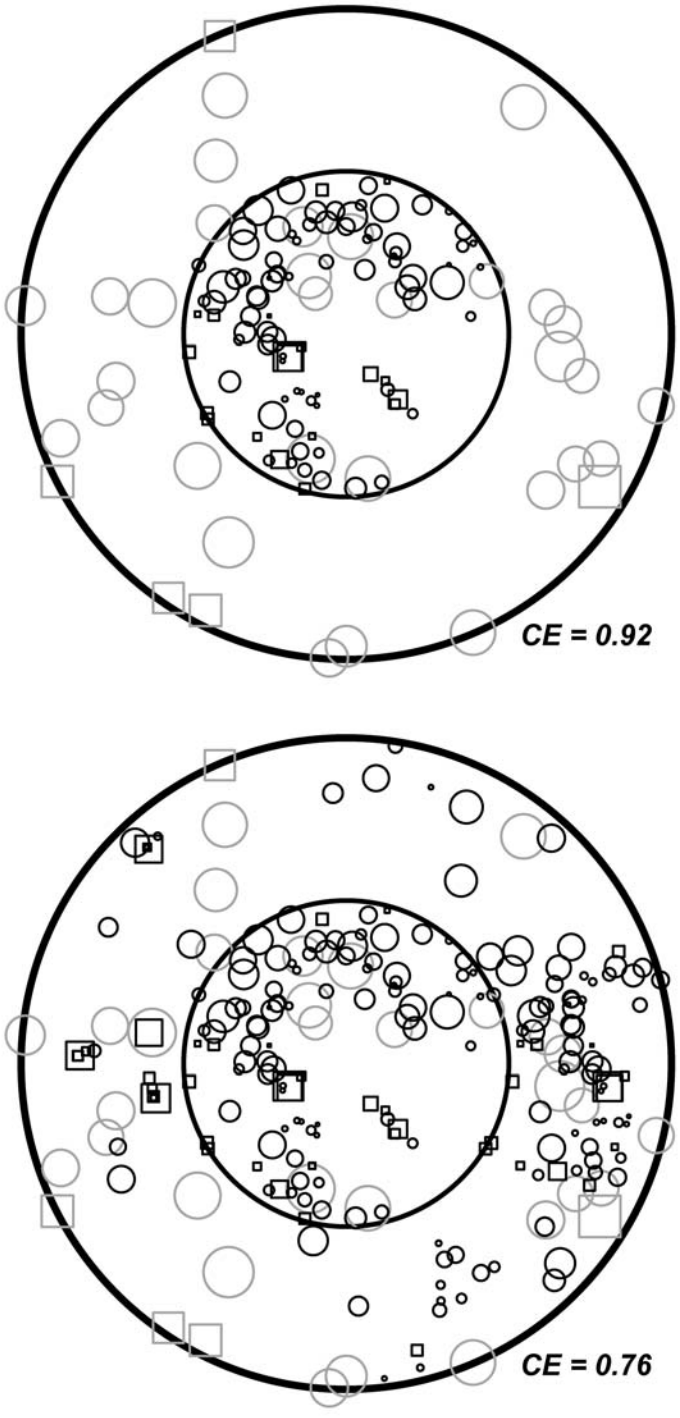

Figure B.1. Continued.

Treatment: Five-Year Selection
Compartment: 9
Plot: 44

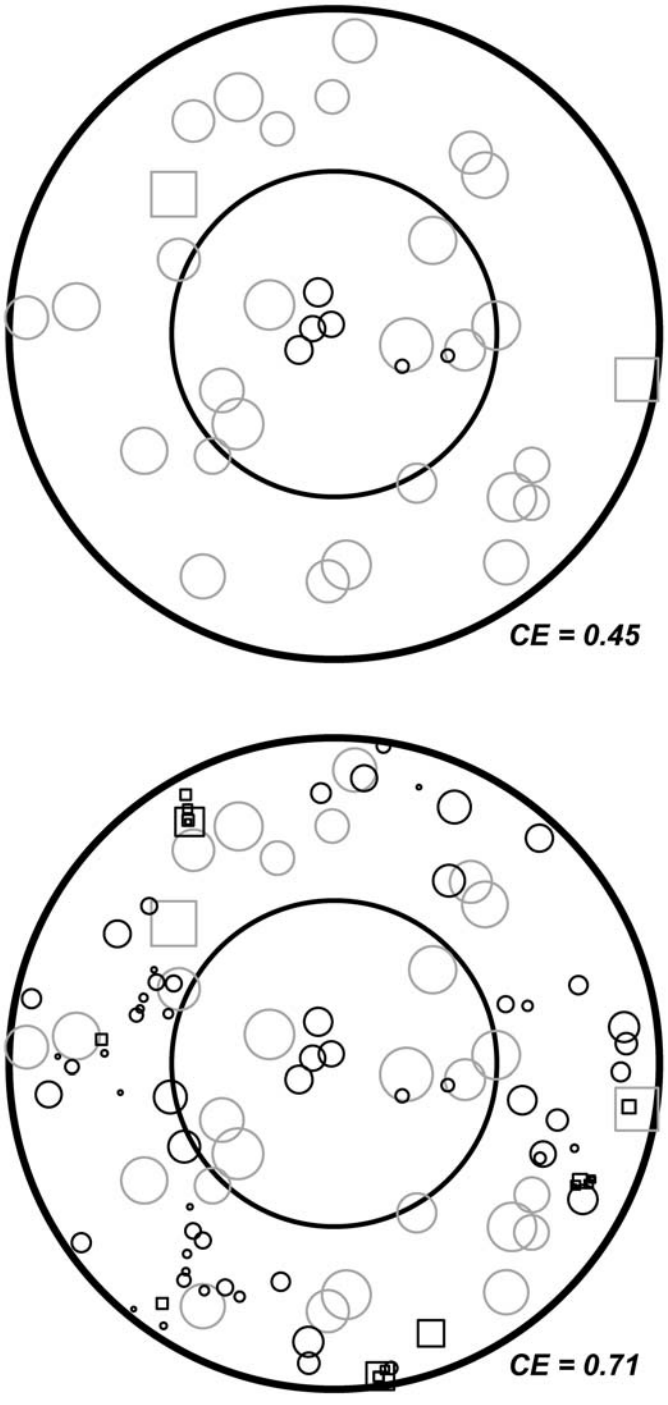

Figure B.1. Continued.

Treatment: Five-Year Selection
Compartment: 16
Plot: 12

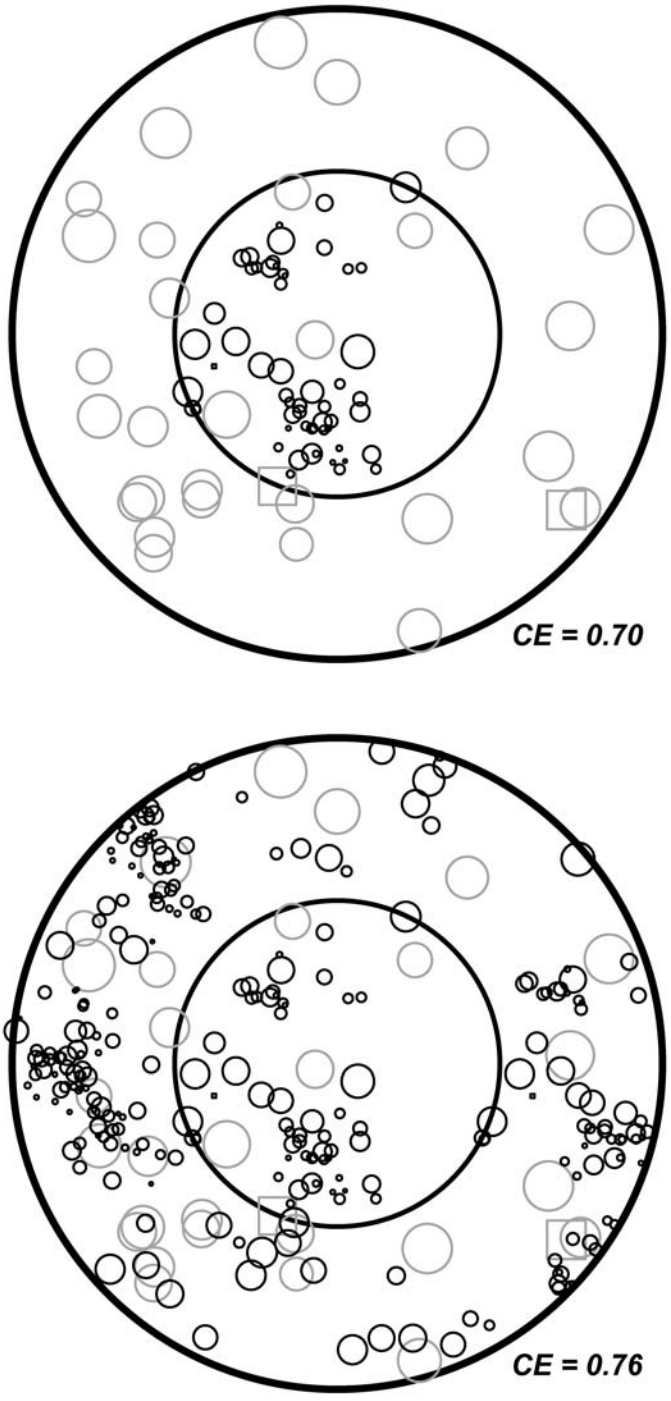

Figure B.1. Continued.

Treatment: Five-Year Selection
Compartment: 16
Plot: 22

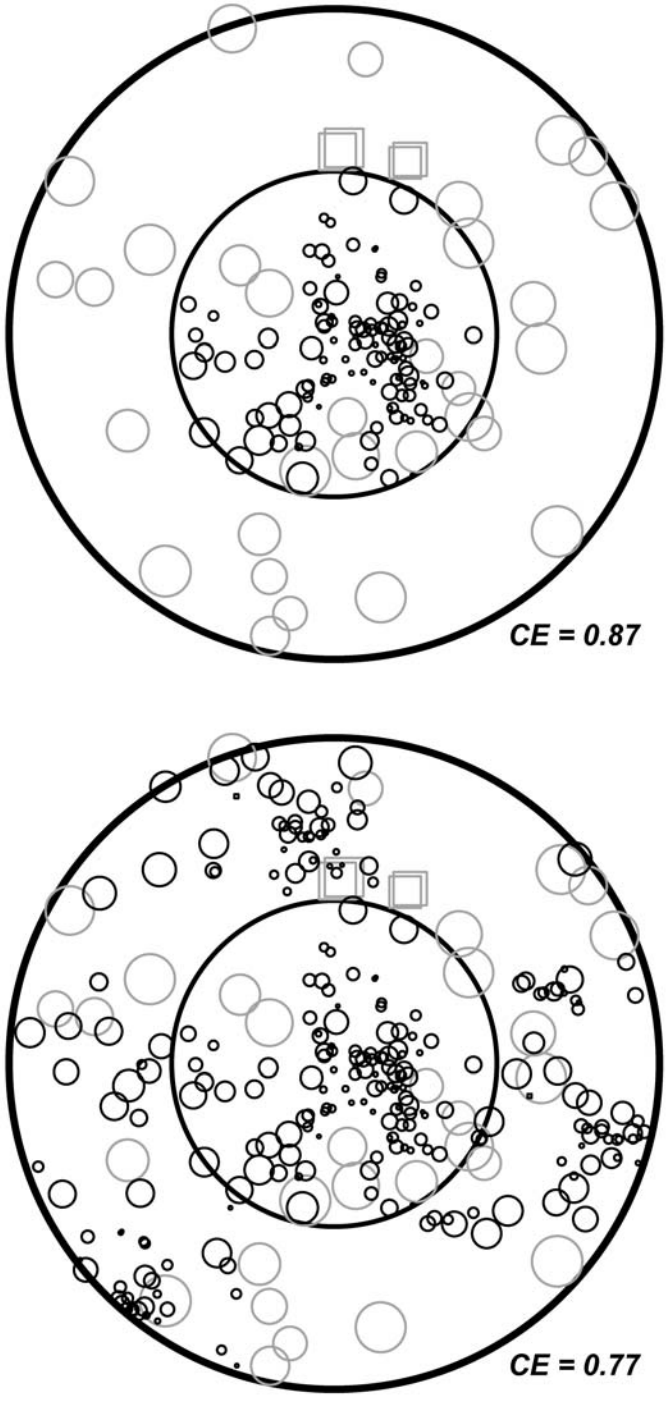

Figure B.1. Continued.

Treatment: Five-Year Selection
Compartment: 16
Plot: 31

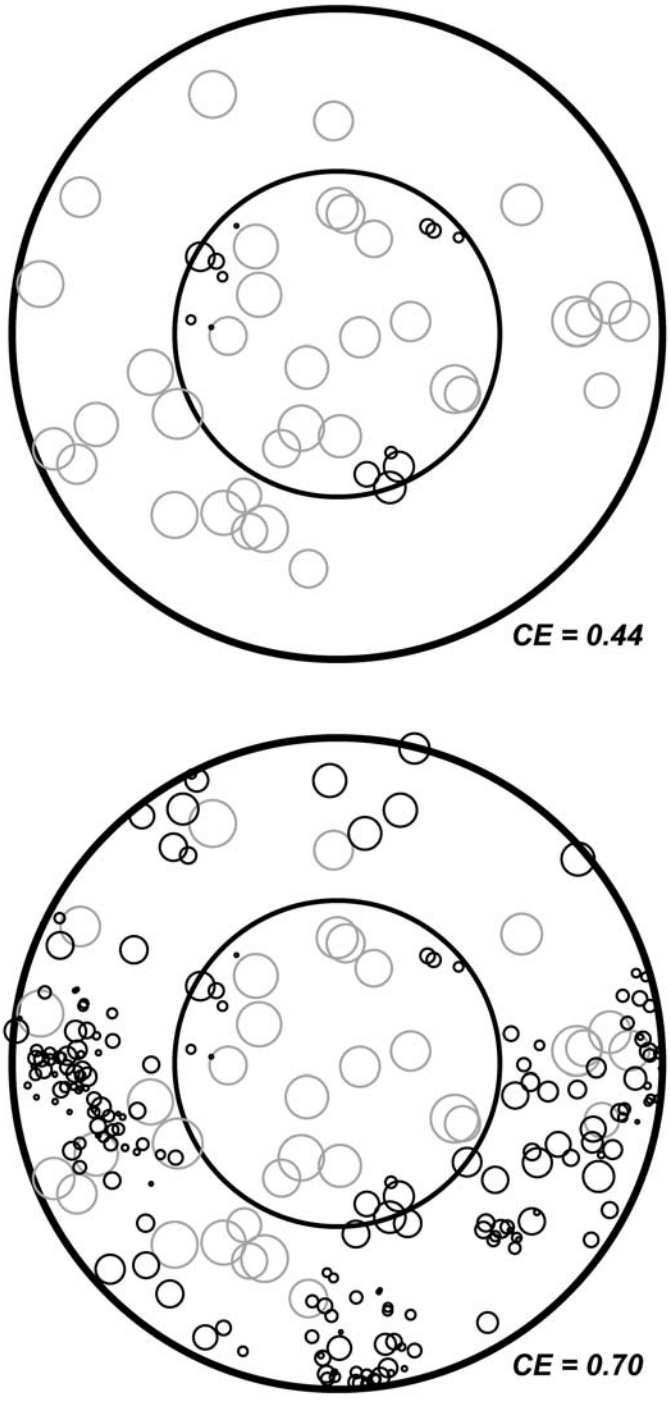

Figure B.1. Continued.

Treatment: Five-Year Selection
Compartment: 16
Plot: 44

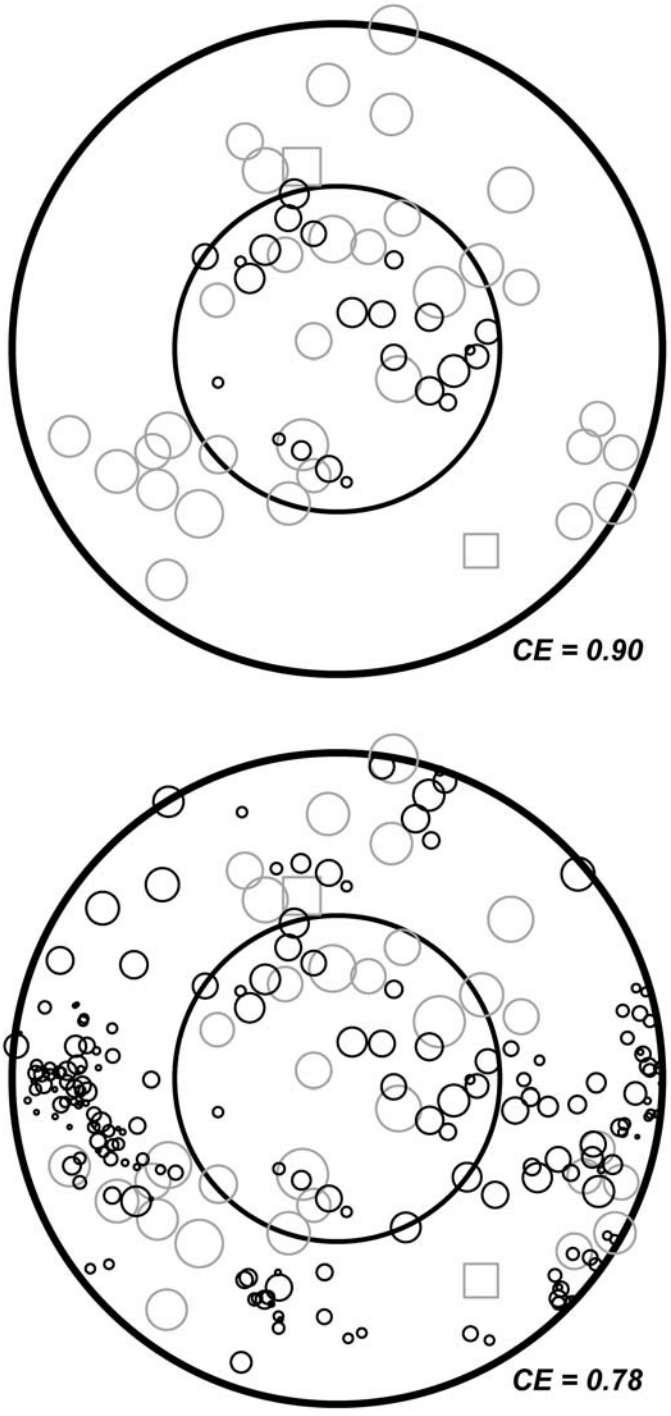

Figure B.1. Continued.

Treatment: Five-Year Selection
Compartment: 16
Plot: 56

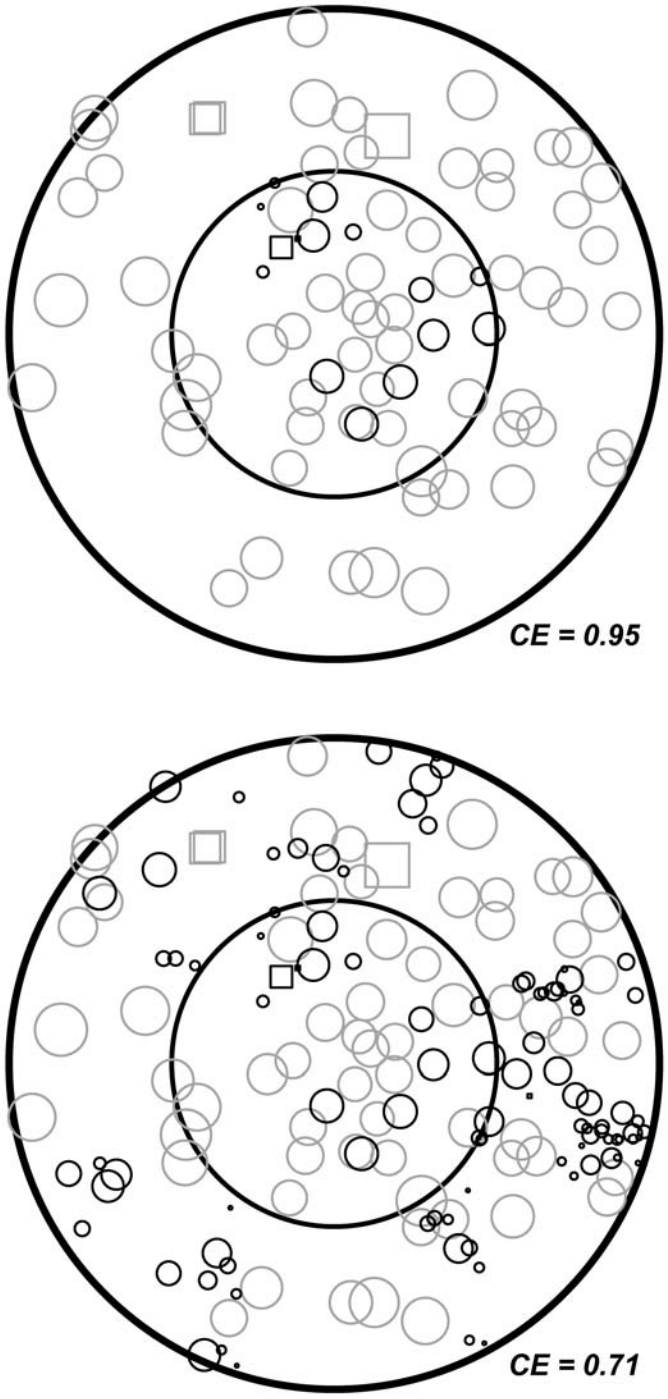

Figure B.1. Continued.

Treatment: Three-stage Shelterwood w/Spacing
Compartment: 29A
Plot: 31

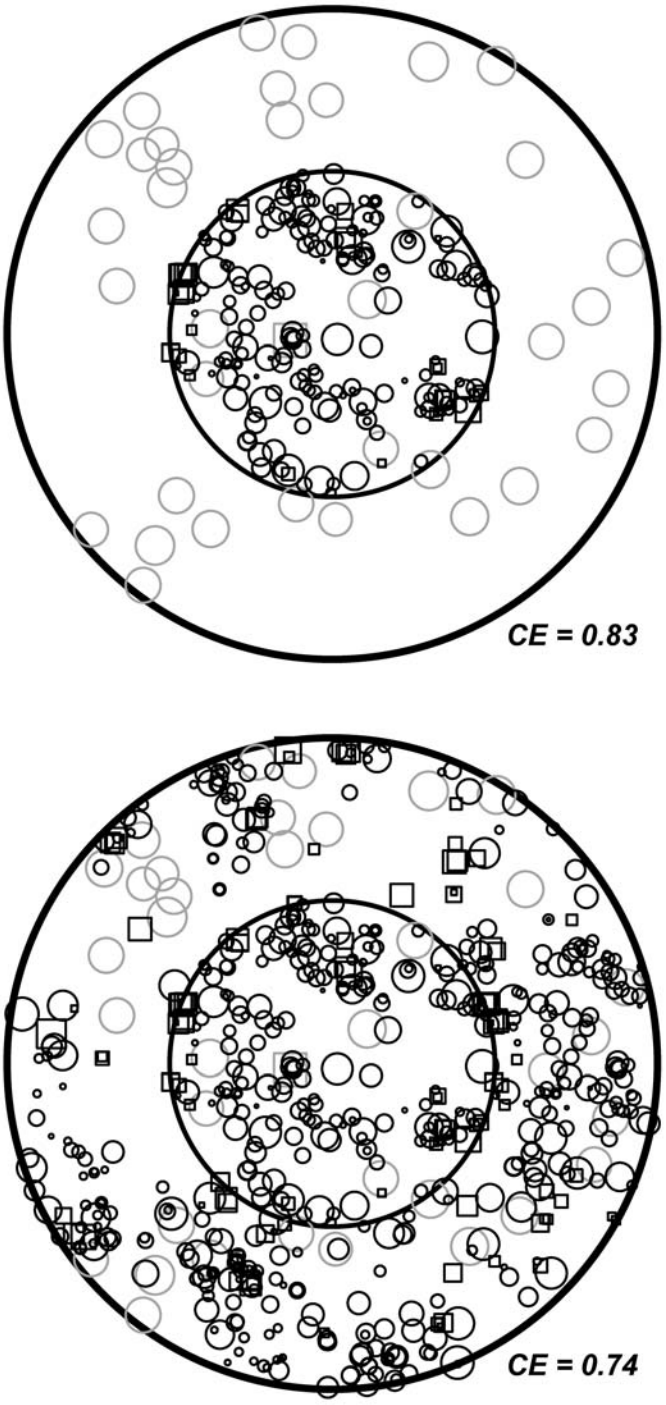

Figure B.1. Continued.

Treatment: Three-stage Shelterwood w/Spacing
Compartment: 29A
Plot: 32

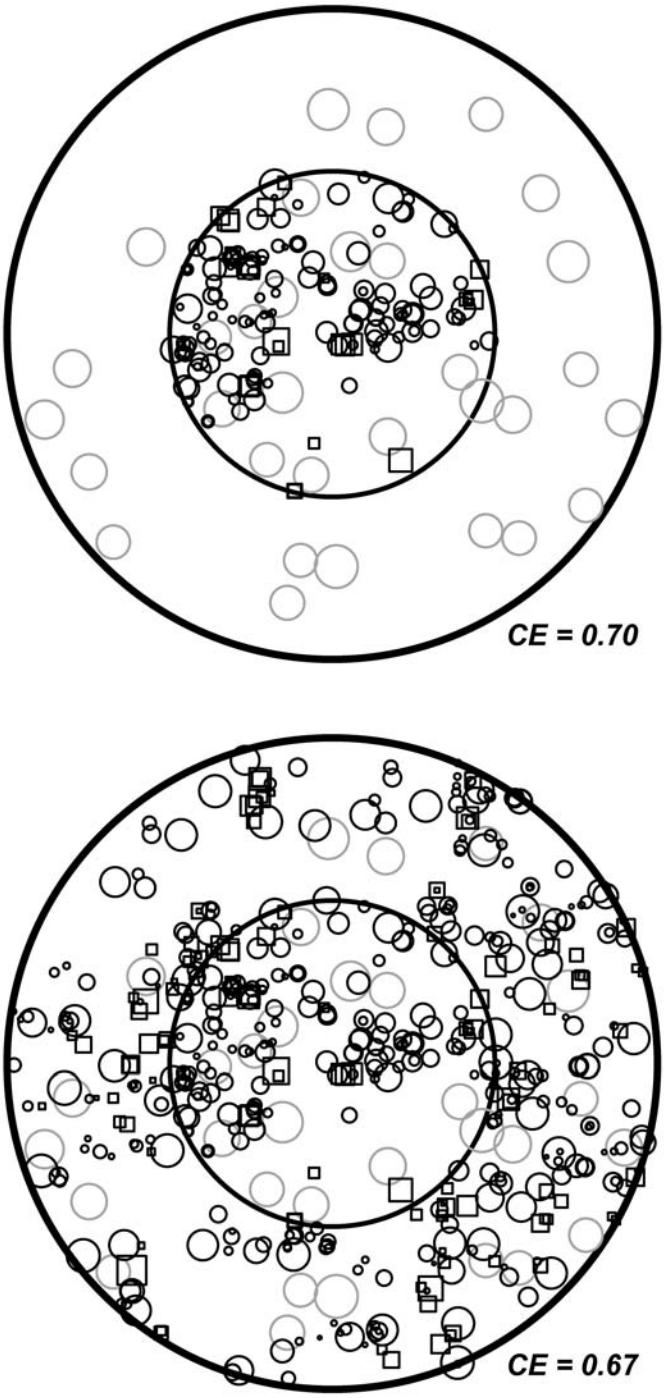

Figure B.1. Continued.

Treatment: Three-stage Shelterwood w/Spacing
Compartment: 29A
Plot: 41

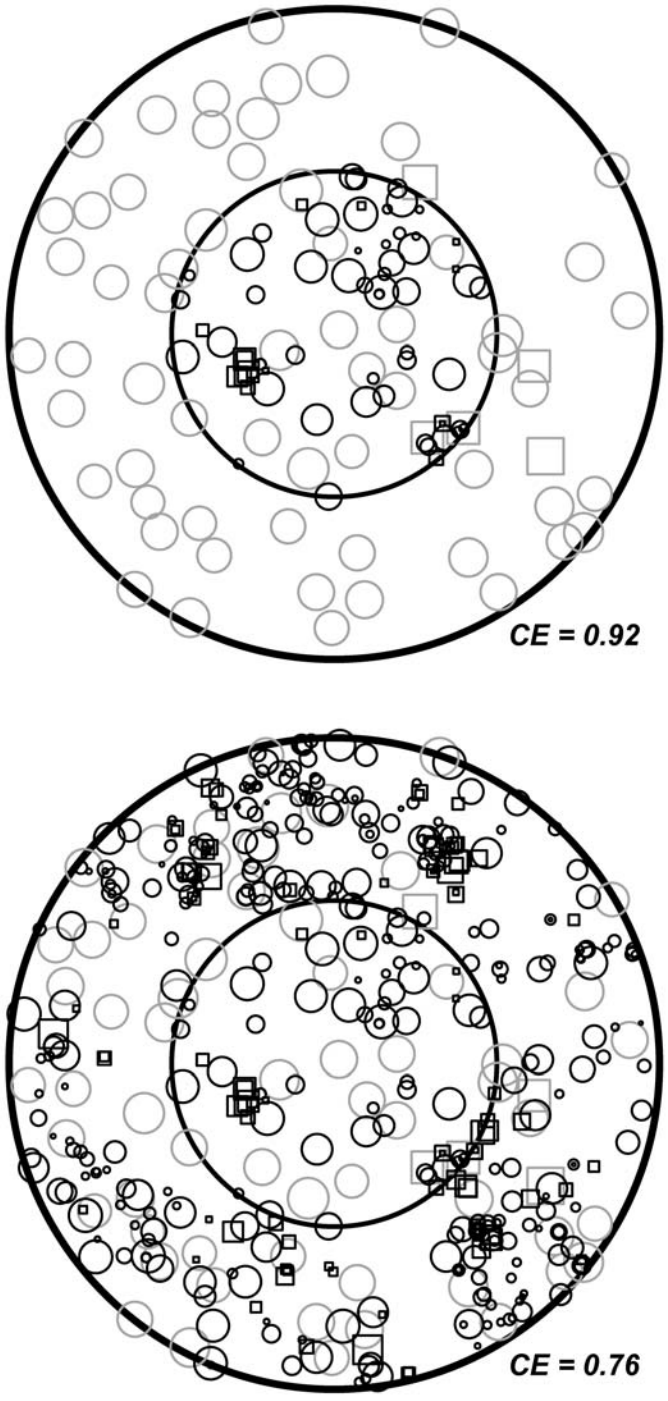

Figure B.1. Continued.

Treatment: Three-stage Shelterwood w/Spacing
Compartment: 29A
Plot: 52

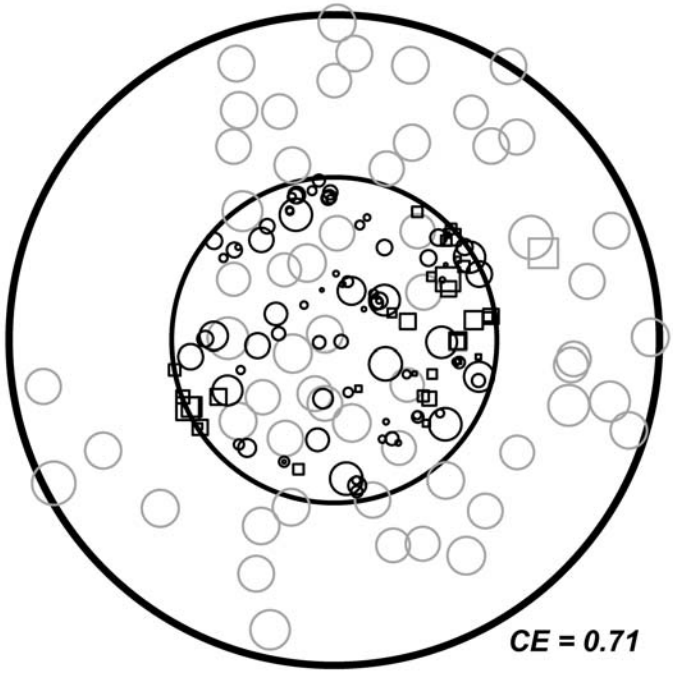

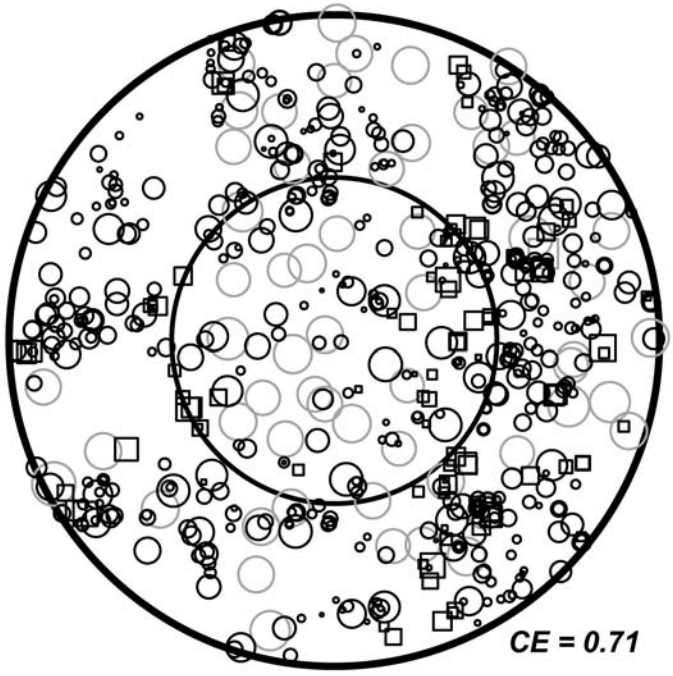

Figure B.1. Continued.

Treatment: Three-stage Shelterwood w/Spacing
Compartment: 29A
Plot: 61

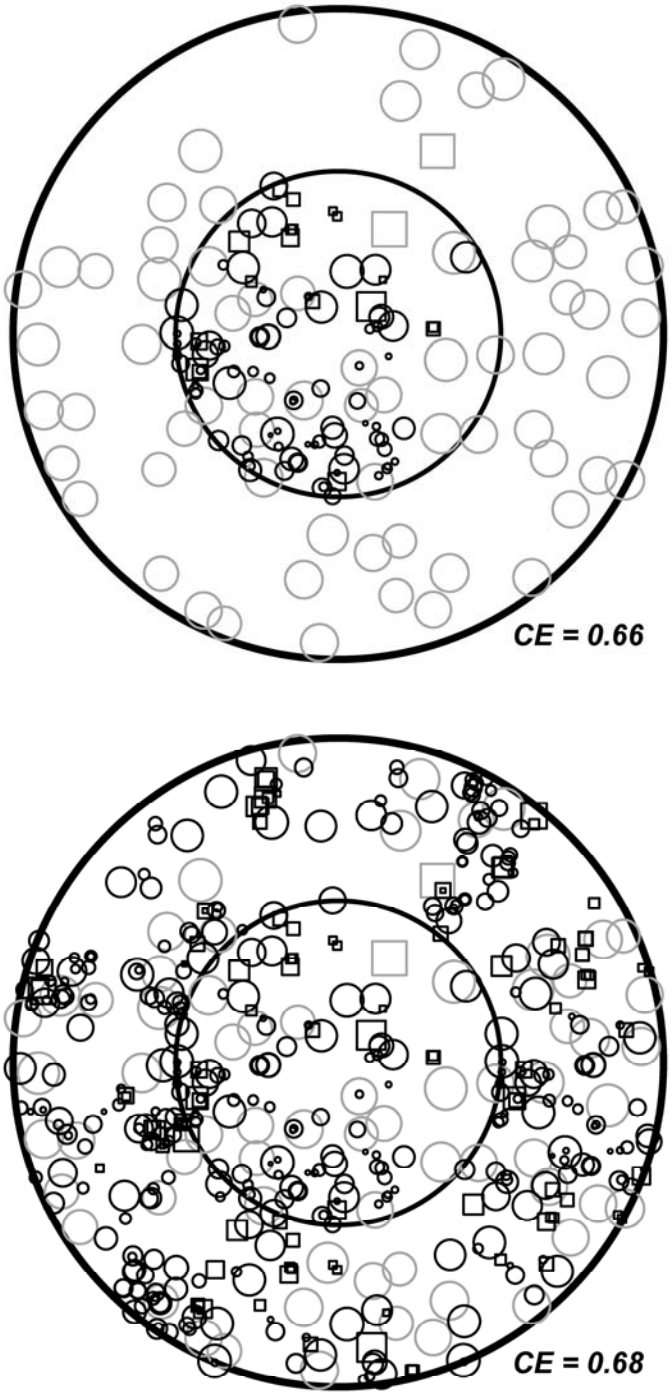

Figure B.1. Continued.

Treatment: Three-stage Shelterwood w/o Spacing
Compartment: 29B
Plot: 11

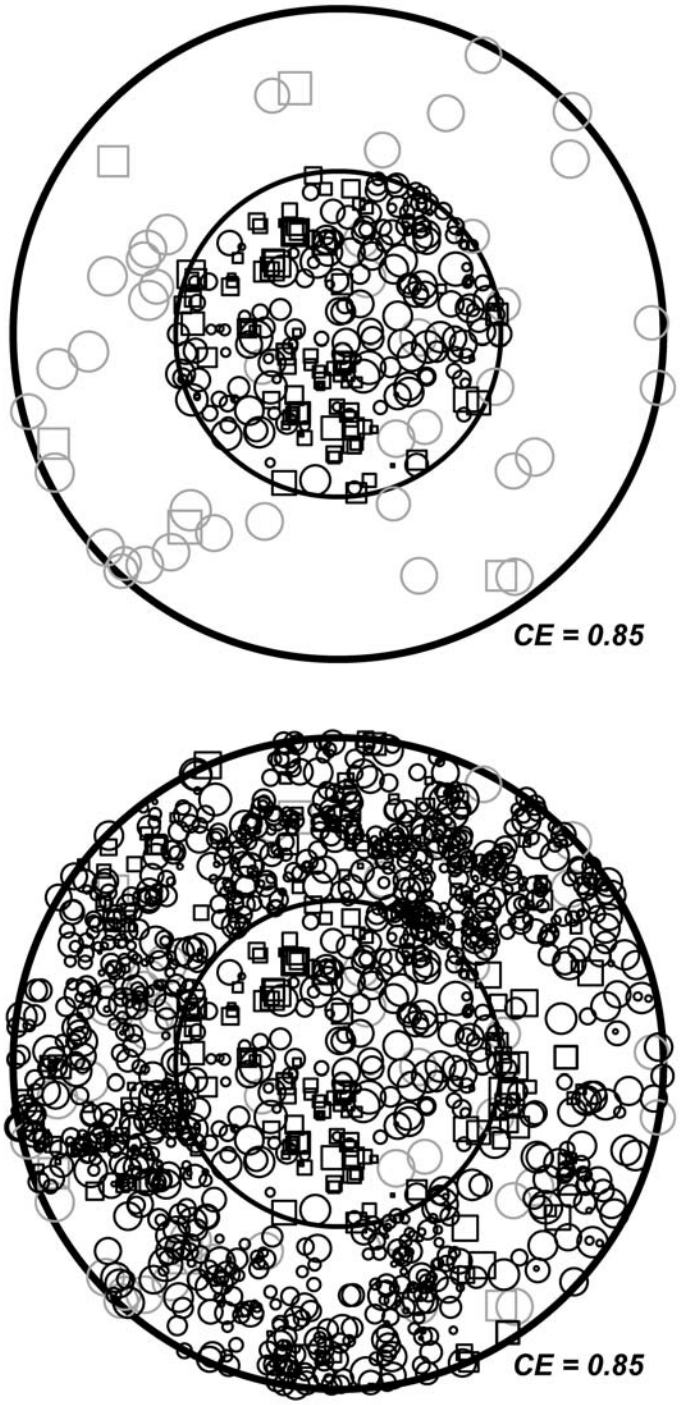

Figure B.1. Continued.

Treatment: Three-stage Shelterwood w/o Spacing
Compartment: 29B
Plot: 12

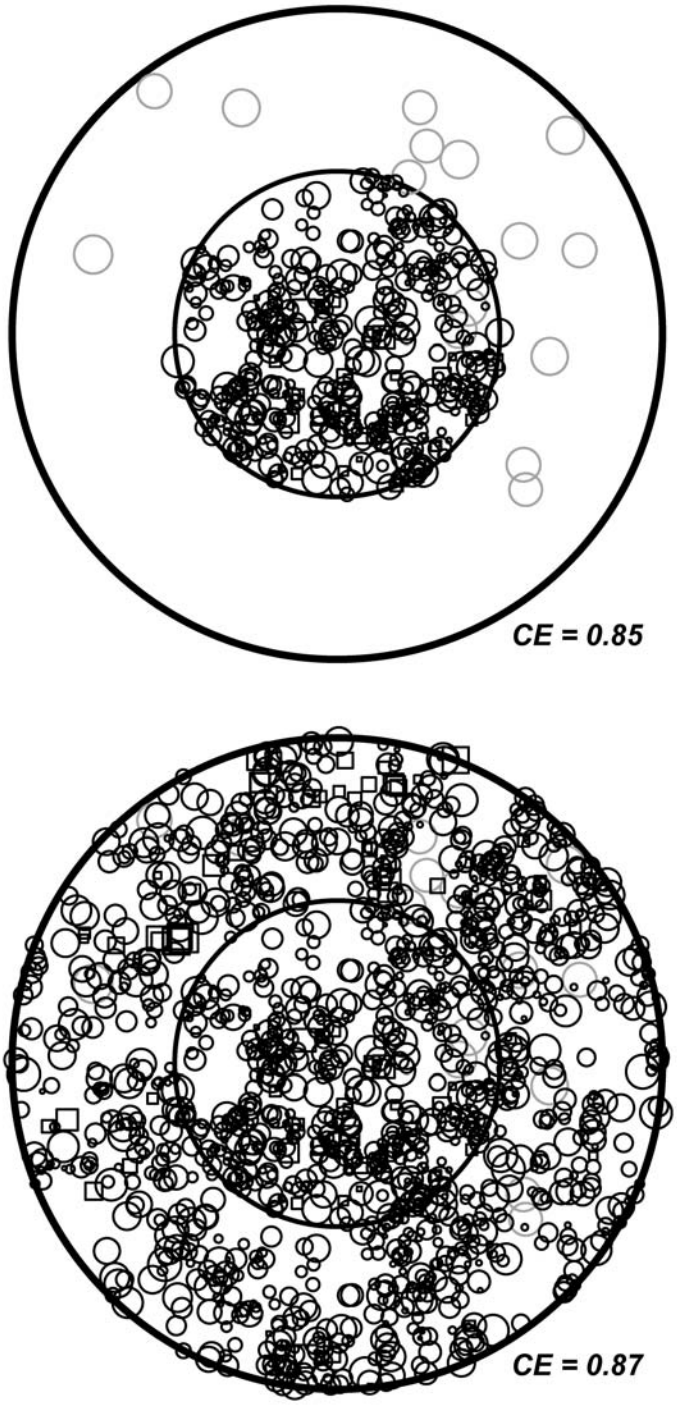

Figure B.1. Continued.

Treatment: Three-stage Shelterwood w/o Spacing
Compartment: 29B
Plot: 22

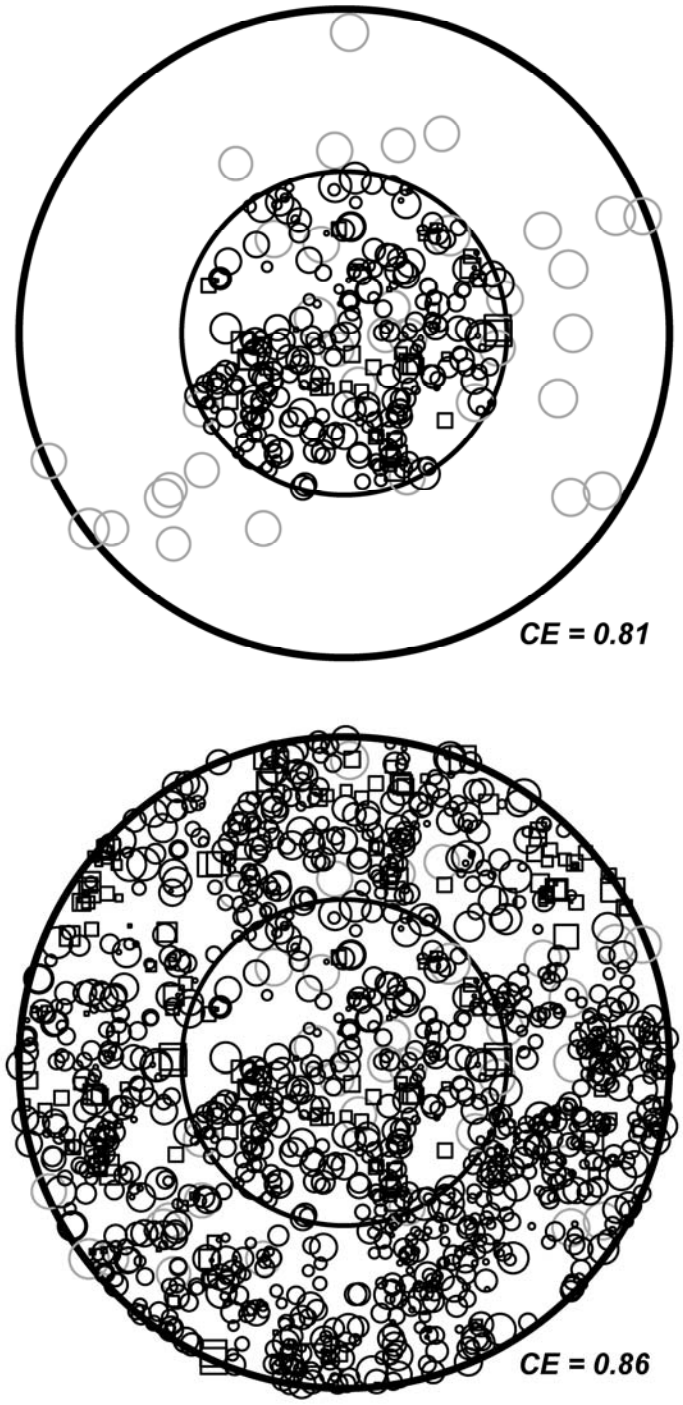

Figure B.1. Continued.

Treatment: Three-stage Shelterwood w/o Spacing
Compartment: 29B
Plot: 24

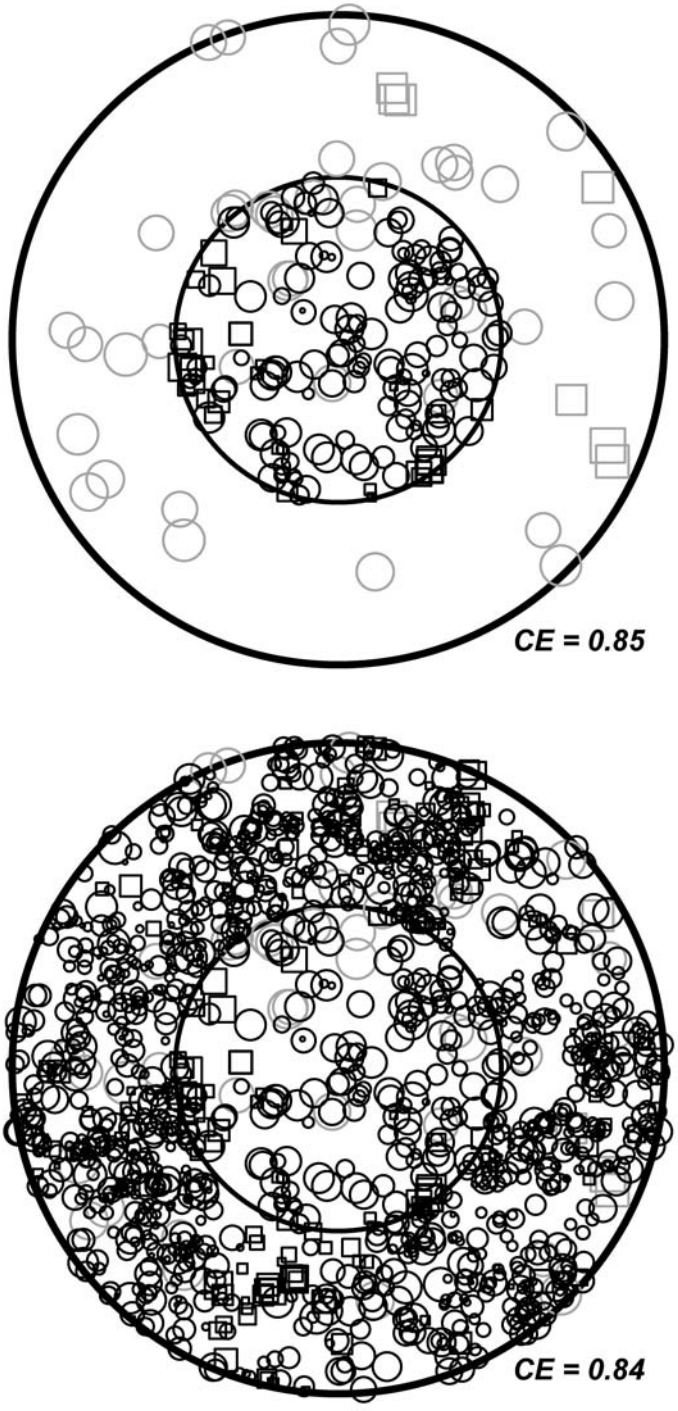

Figure B.1. Continued.

Treatment: Three-stage Shelterwood w/o Spacing
Compartment: 29B
Plot: 35

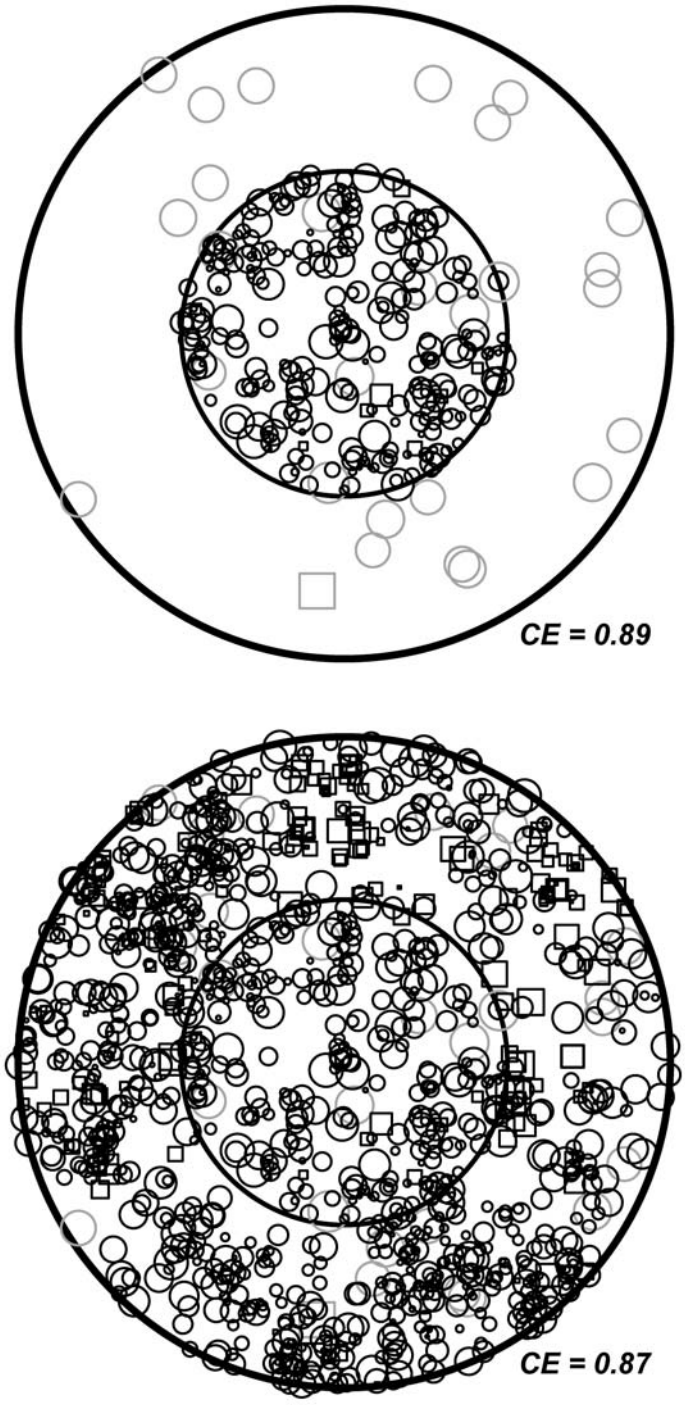

Figure B.1. Concluded.

APPENDIX C

BOOTSTRAPPED $\hat{L}(d)$ FUNCTIONS OF FOREST SERVICE COMPARTMENTS

The following figures are bootstrapped $\hat{L}(d)$ functions, a transformed version of the $\hat{K}(d)$ function (Besag 1977), for spatial pattern within 10 management compartments of the U.S. Forest Service's long-term silvicultural study at the Penobscot Experimental forest in Bradley, ME. Spatial pattern for each inventory period since 1974 was reconstructed using both ground measurements of all live and any relocated dead stems, and simulated positions of missing dead stems. Further, since the USFS uses a nested plot design, reconstructions extrapolate the pattern measured within the sapling plots (0.020 ha for stems between 1.2 and 11.4 cm diameter at breast height [dbh = 1.35 m]) to the large tree plots (0.081 ha for stems > 11.4 cm dbh). Details of the reconstruction algorithm are given in Section 3.3.4.

Each graph summarizes spatial pattern across 100 realizations of each of 5 plots in every management compartment by inventory combination. Therefore, each graph represents approximately 500 simulations of pattern, either of all saplings and large trees or of only large trees. Reconstructions with less than 5 stems were discarded from spatial analyses; this was common for large tree simulations and resulted in no estimation of $\hat{L}(d)$ for the shelterwood compartments (29A and 29B) during some inventory cycles.

A permutation-based approach was taken to summarize $\hat{K}(d)$ for each compartment. Following Diggle (2003), a weighted average of the individual estimates of $\hat{K}_{ij}(d)$ was calculated as:

$$\hat{K}(d) = \sum_{i=1}^{p}\sum_{j=1}^{r_p} n_{ij}\hat{K}(d)_{ij} \Big/ \sum_{i=1}^{p}\sum_{j=1}^{r_p} n_{ij} \qquad [C.1]$$

where p is the number of plots in a compartment, r_p is the realizations for each plot p, and n is the number of trees in realization r of plot p. The sampling variance of $\hat{K}(d)$ was calculated from 1000 bootstrapped samples of $\hat{K}^*(d)$ defined as:

$$\hat{K}^*(d) = \sum_{k=1}^{p} n_k \hat{K}_k(d) \Big/ \sum_{k=1}^{p} n_k \qquad [C.2]$$

where the $\hat{K}_k(d)$ are sampled at random with replacement from all $i \times j = k$ realizations in the compartment (Diggle 2003). Bootstrapped 95% confidence intervals of $\hat{K}(d)$ were calculated using ±1.96 standard errors.

To test the departure of $\hat{K}(d)$ from a random spatial pattern, 95% confidence envelopes of complete spatial randomness (*csr*) were developed from 1000 simulations of a Poisson pattern across a 0.081 ha circular plot and at a density equal to the average stem density for the management compartment in that inventory cycle. This density was calculated directly from the tree list for an inventory and was thus not affected by the variation in density observed within realizations from the reconstruction algorithm. Separation of the 95% confidence intervals for *csr* and $\hat{K}(d)$ were used as a threshold for significantly clustered or uniform spatial pattern. This information is summarized in Table 3.4.

Figure C.1. Bootstrapped $\hat{L}(d)$ functions for the U.S. Forest Service compartments at the Penobscot Experimental Forest in Bradley, ME. Values at each inventory are displayed and separately for all trees measured (≥ 1.3 cm diameter at breast height [dbh]; left column) and large trees (> 11.4 cm dbh; right column). Positive and negative values of $\hat{L}(d)$ represent clustered and uniformed spatial patterns, respectively. Mean and 95% confidence intervals of $\hat{L}(d)$ are represented by heavy black and dotted lines, respectively. The 95% confidence envelope of *csr* is indicated by a red, dotted and dashed line. $\hat{L}(d) = 0$ is indicated by the light red solid line.

NATURAL AREA CONTROL (NA)
Compartment 32A

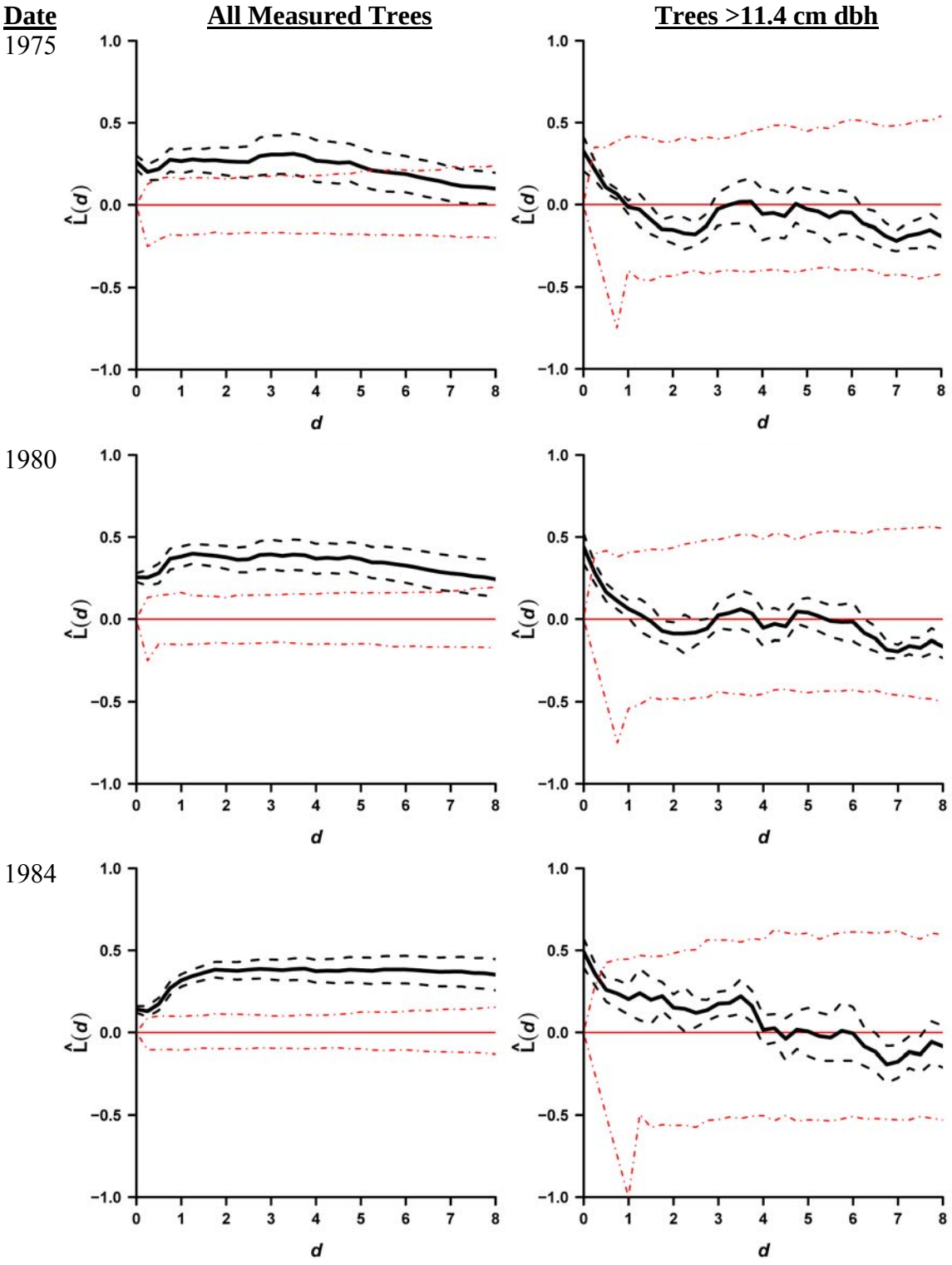

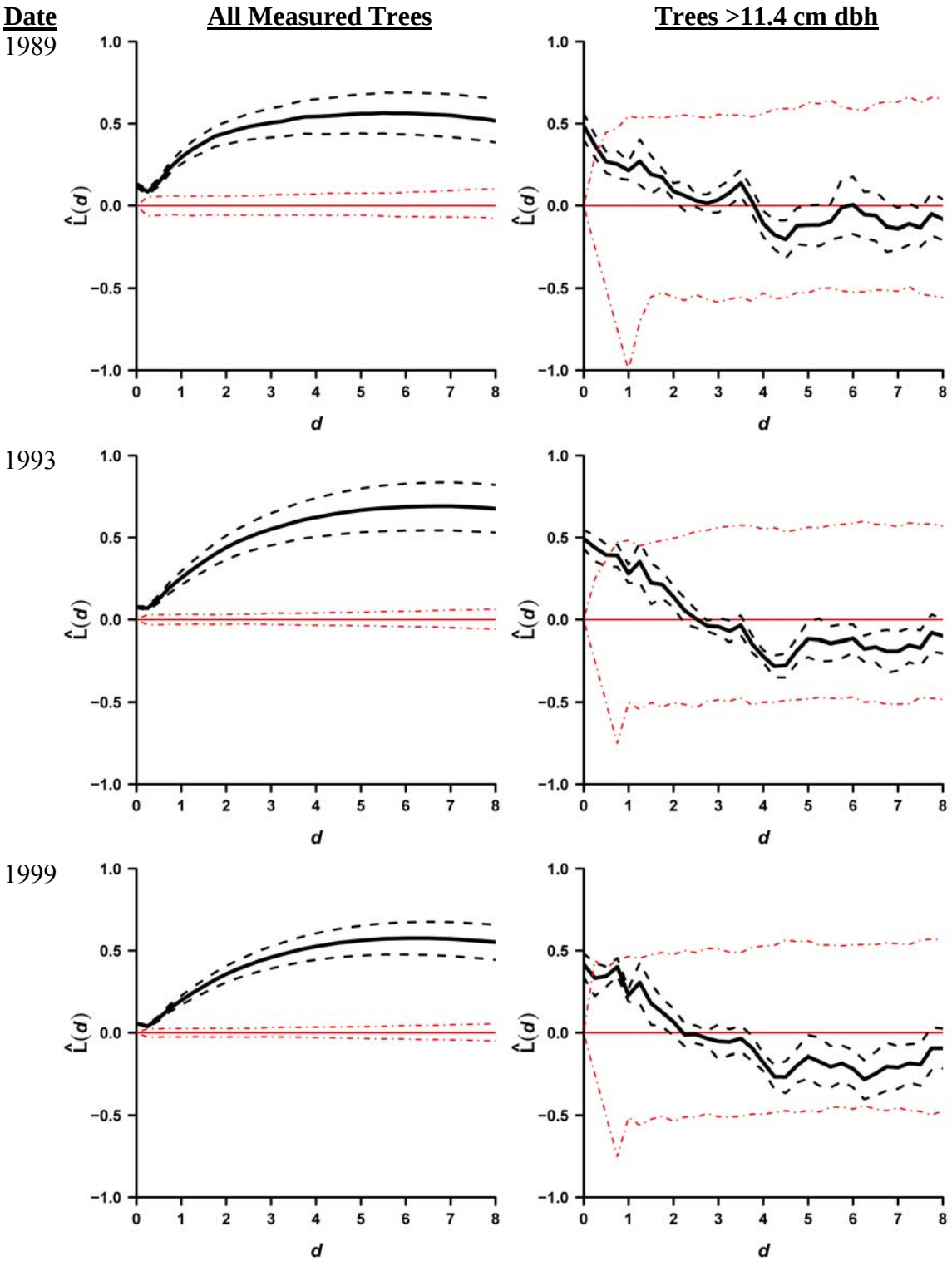

Figure C.1. Continued.

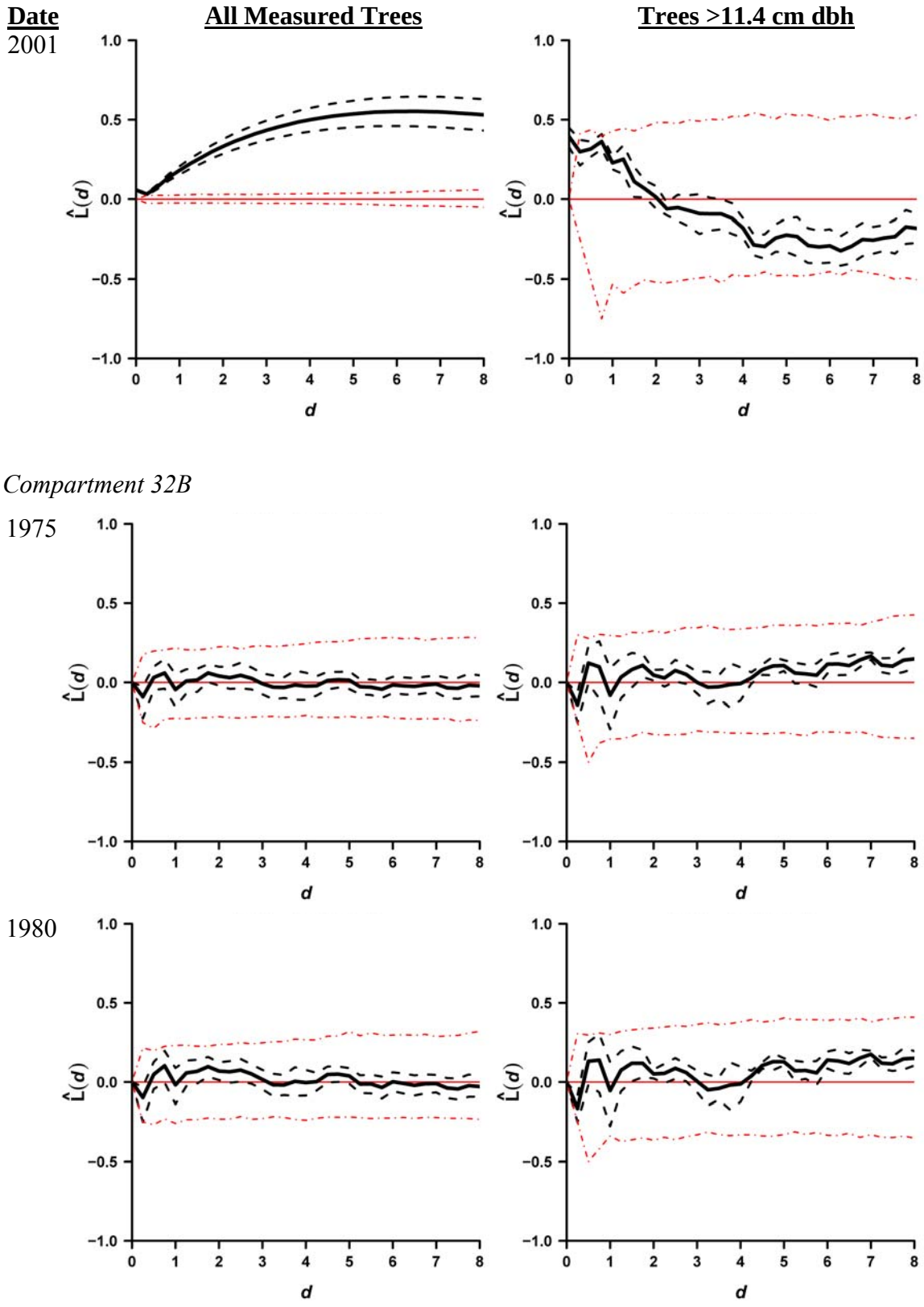

Figure C.1. Continued.

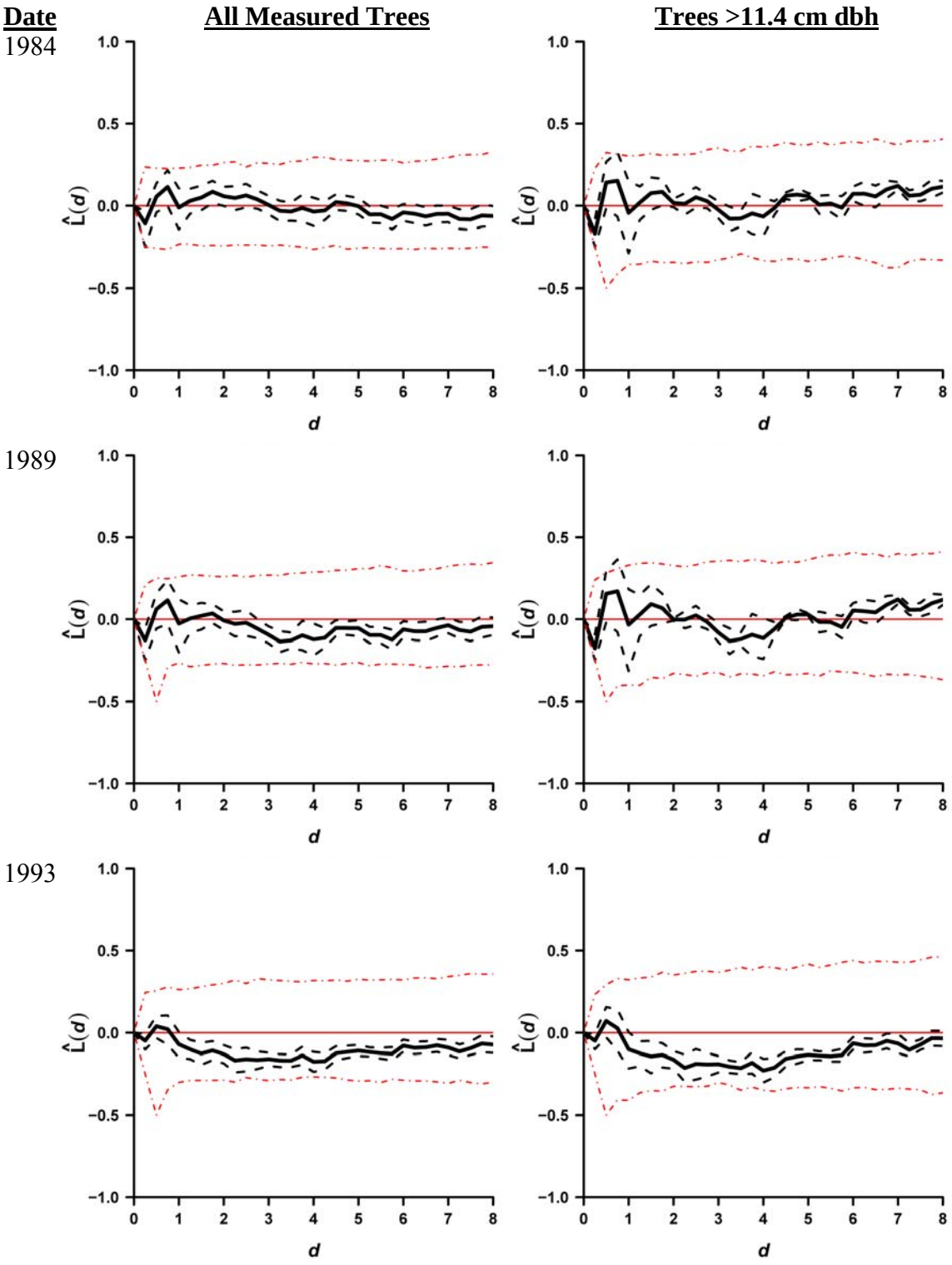

Figure C.1. Continued.

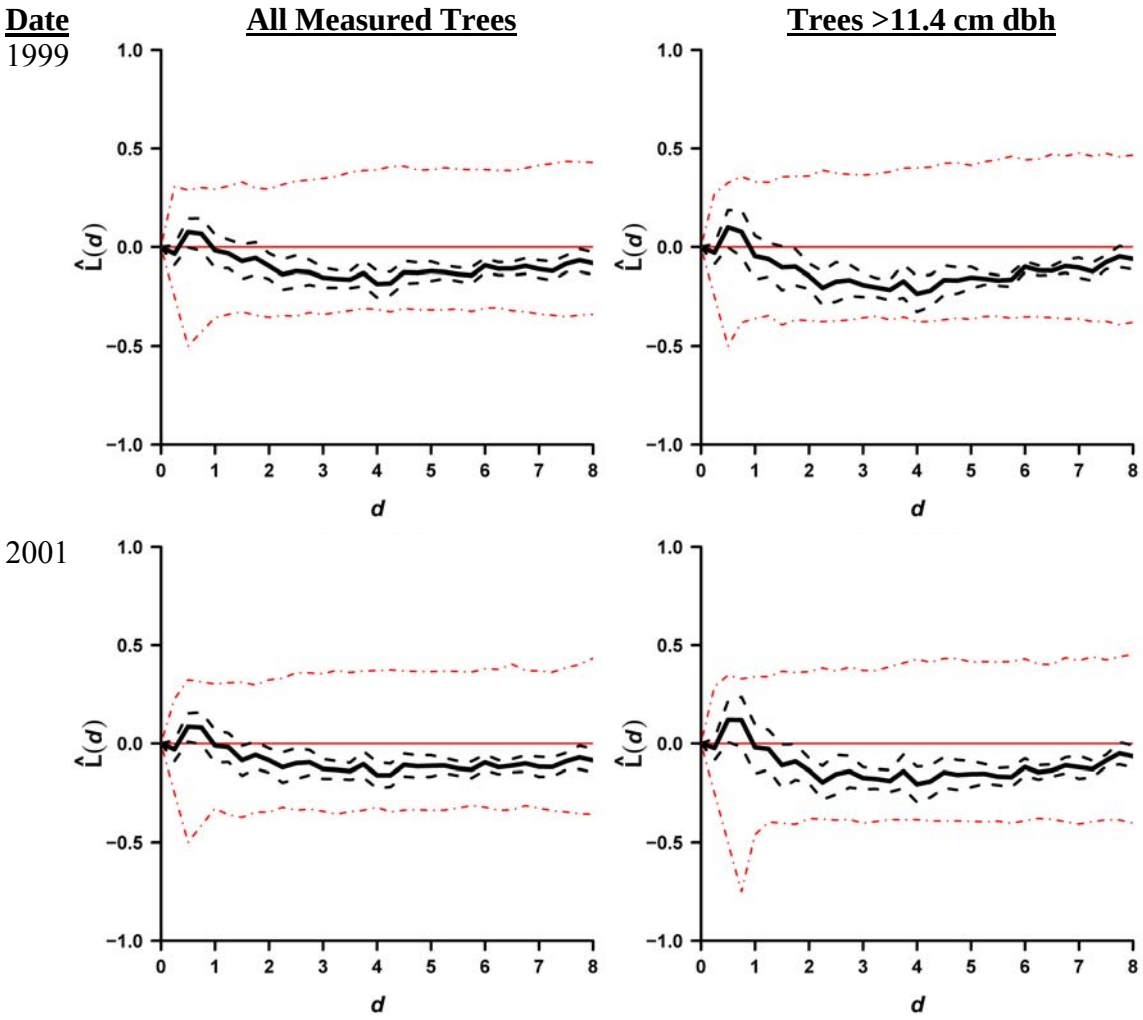

Figure C.1. Continued.

COMMERCIAL CLEARCUT (CC)
Compartment 8

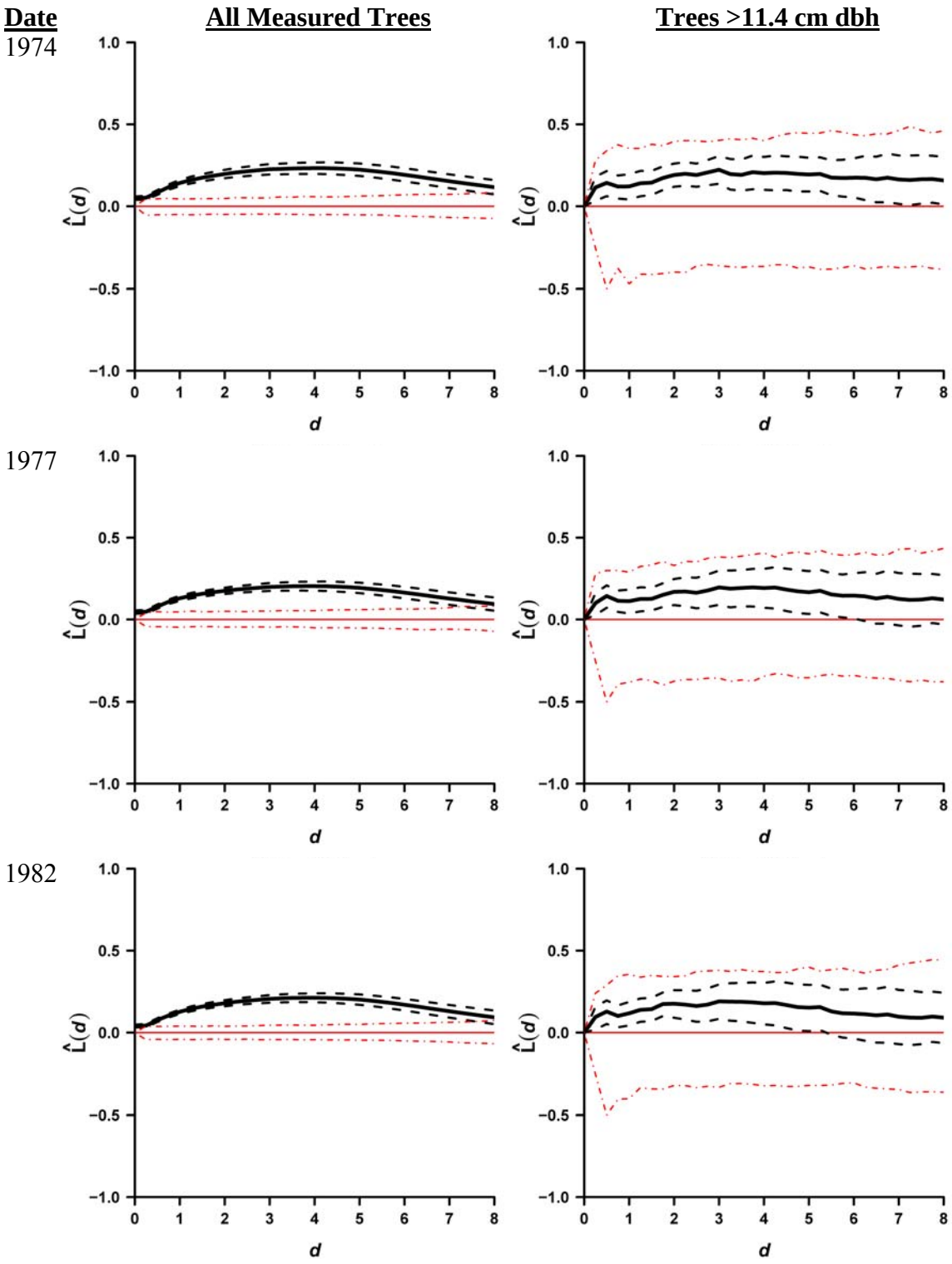

Figure C.1. Continued.

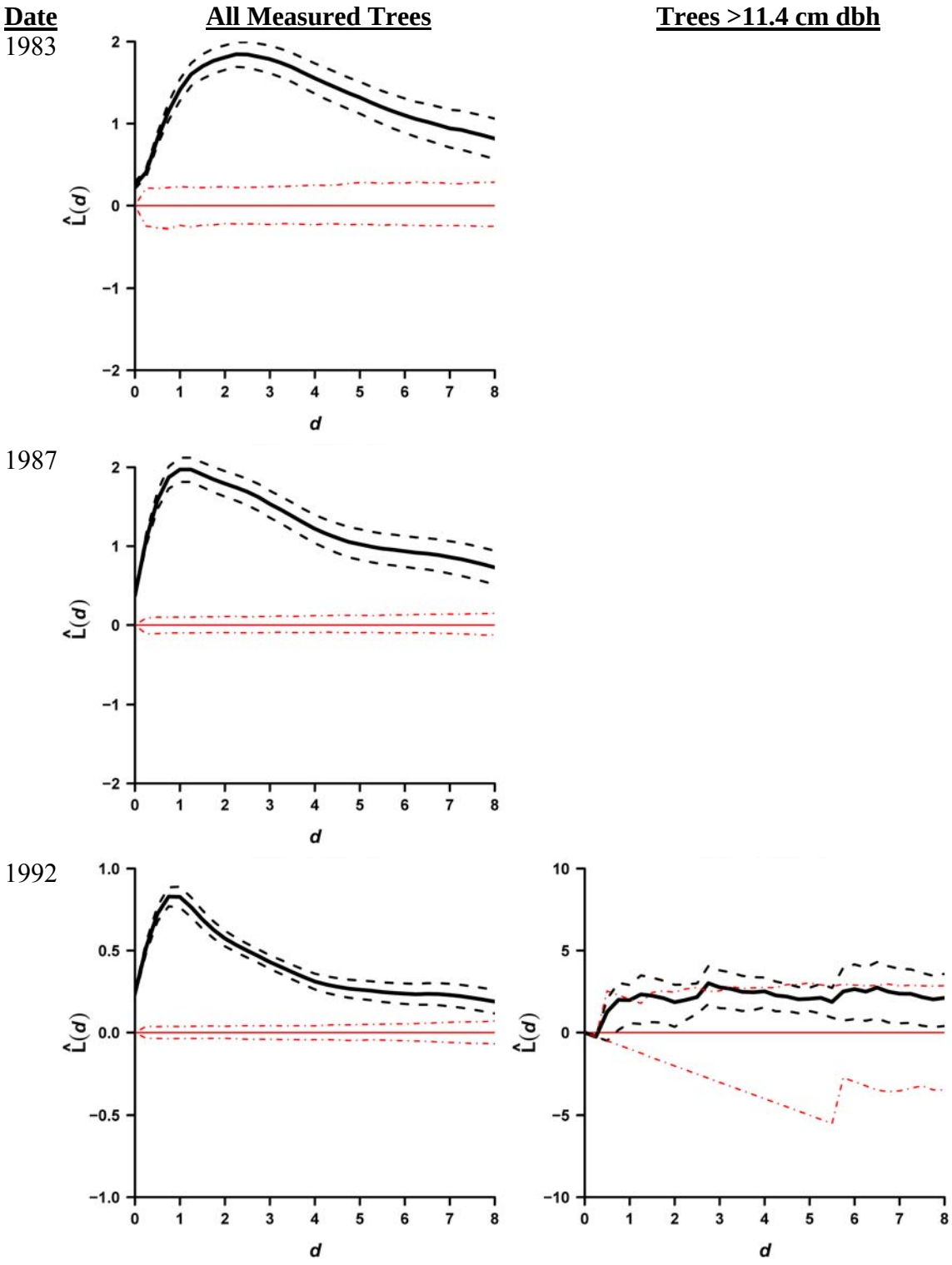

Figure C.1. Continued.

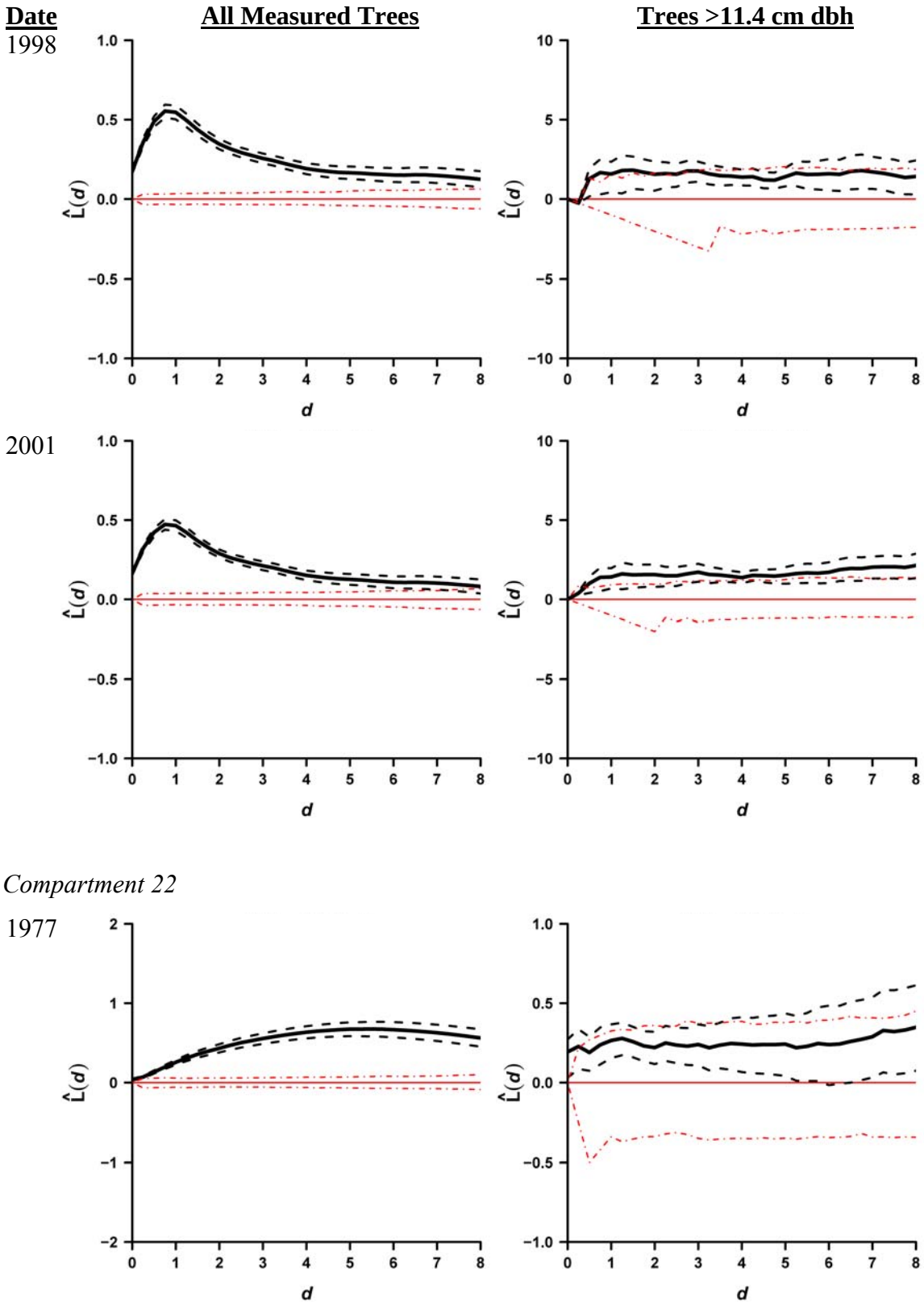

Figure C.1. Continued.

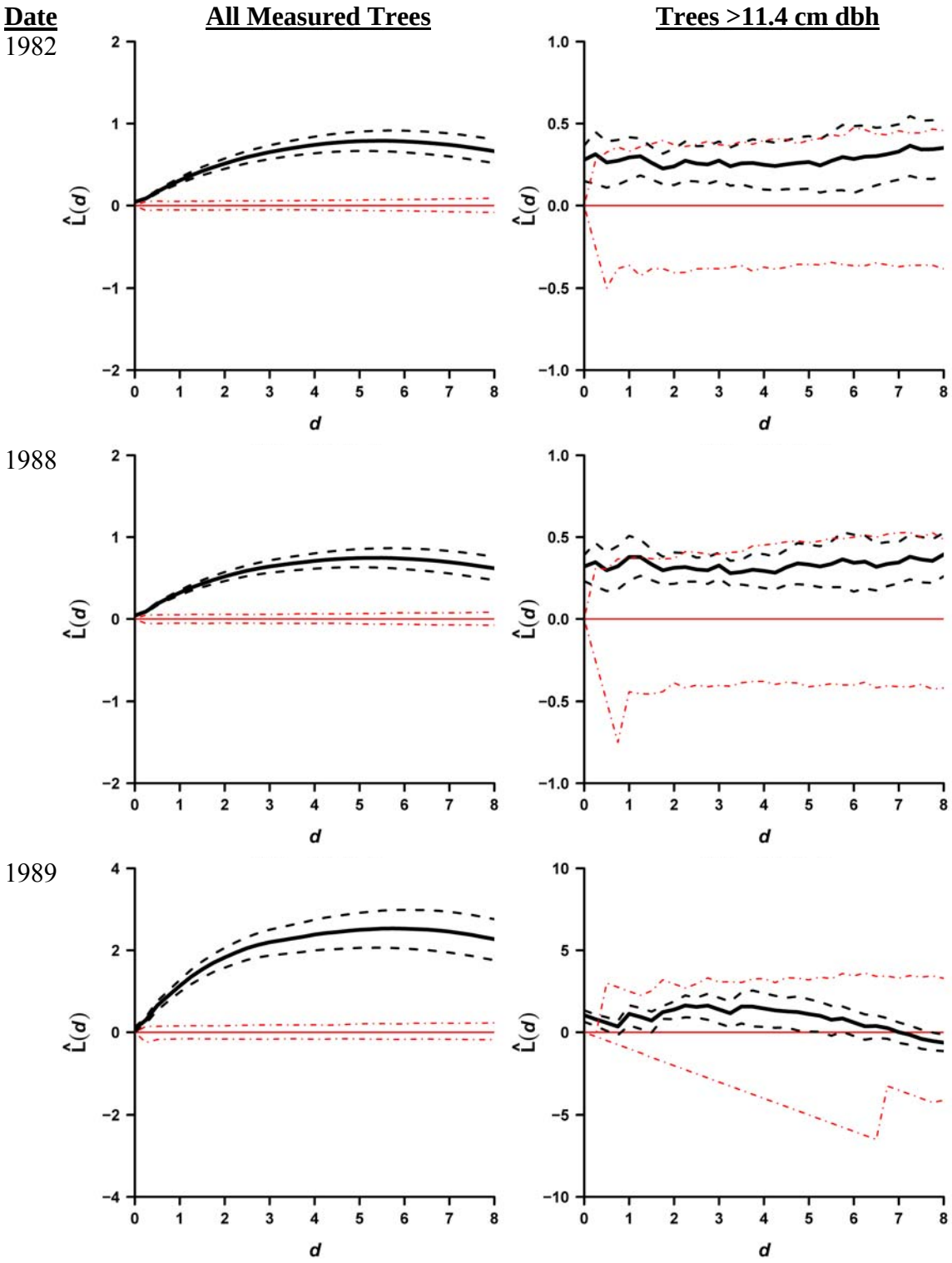

Figure C.1. Continued.

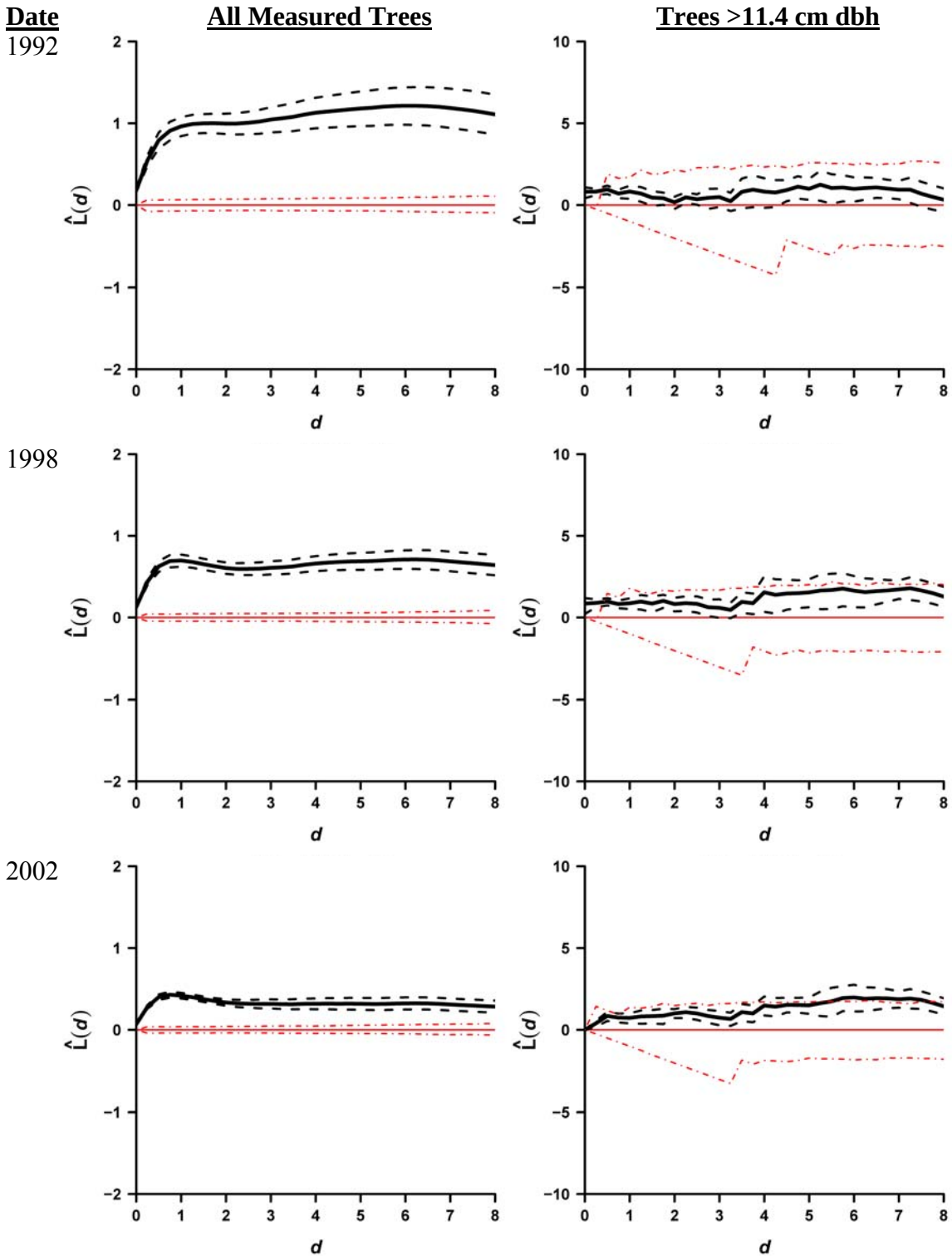

Figure C.1. Continued.

FIXED-DIAMETER LIMIT (DL)
Compartment 4

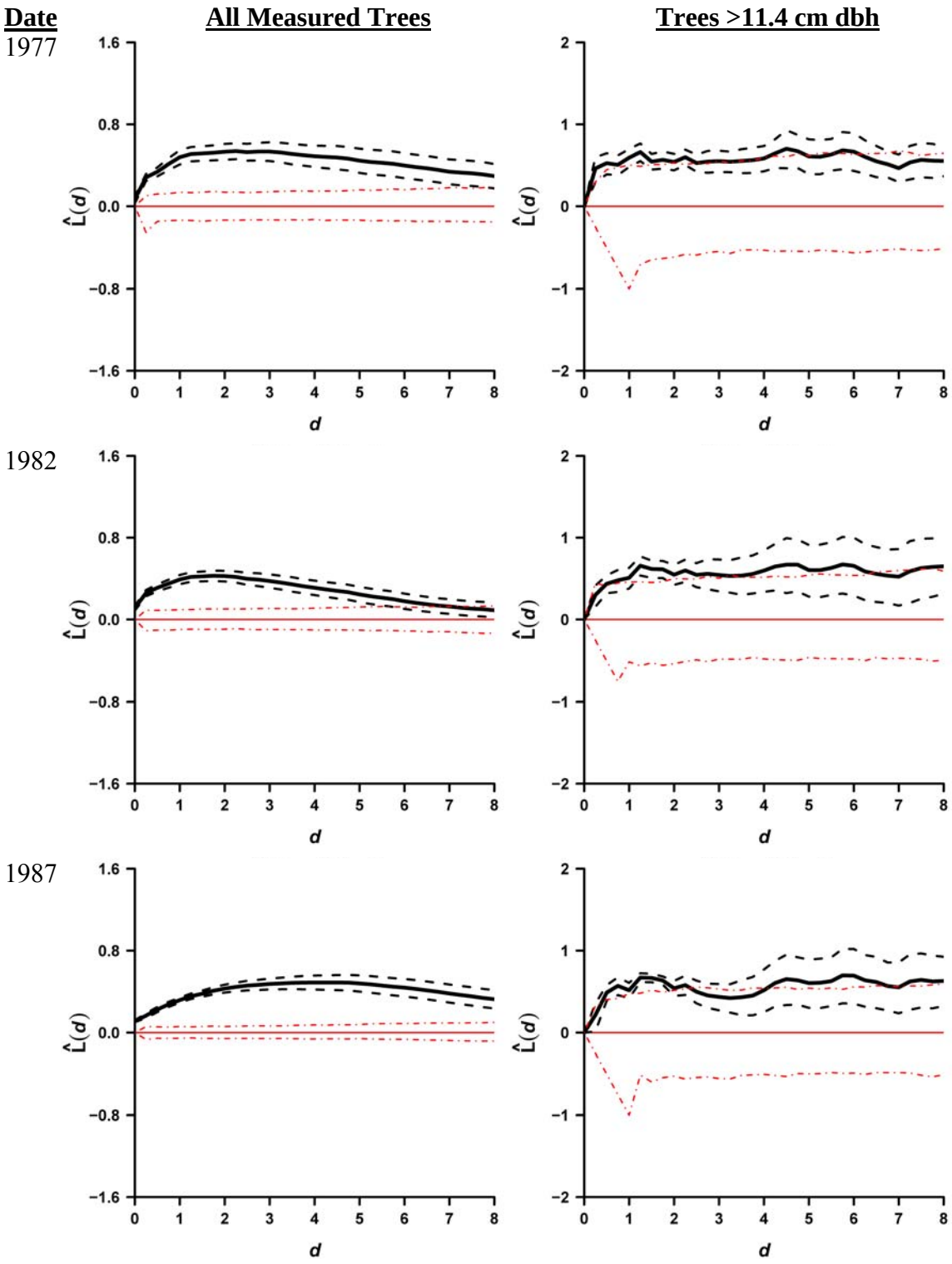

Figure C.1. Continued.

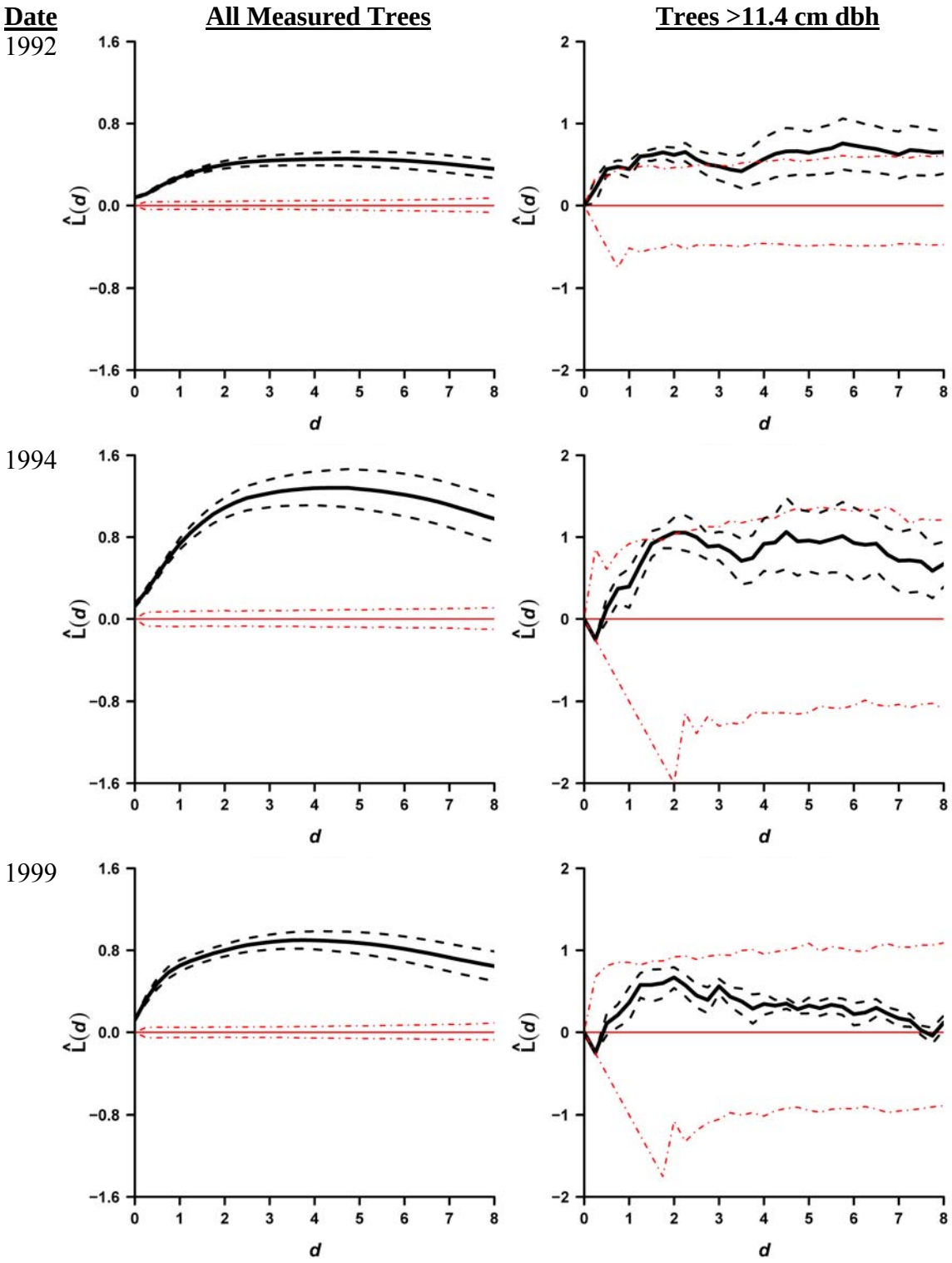

Figure C.1. Continued.

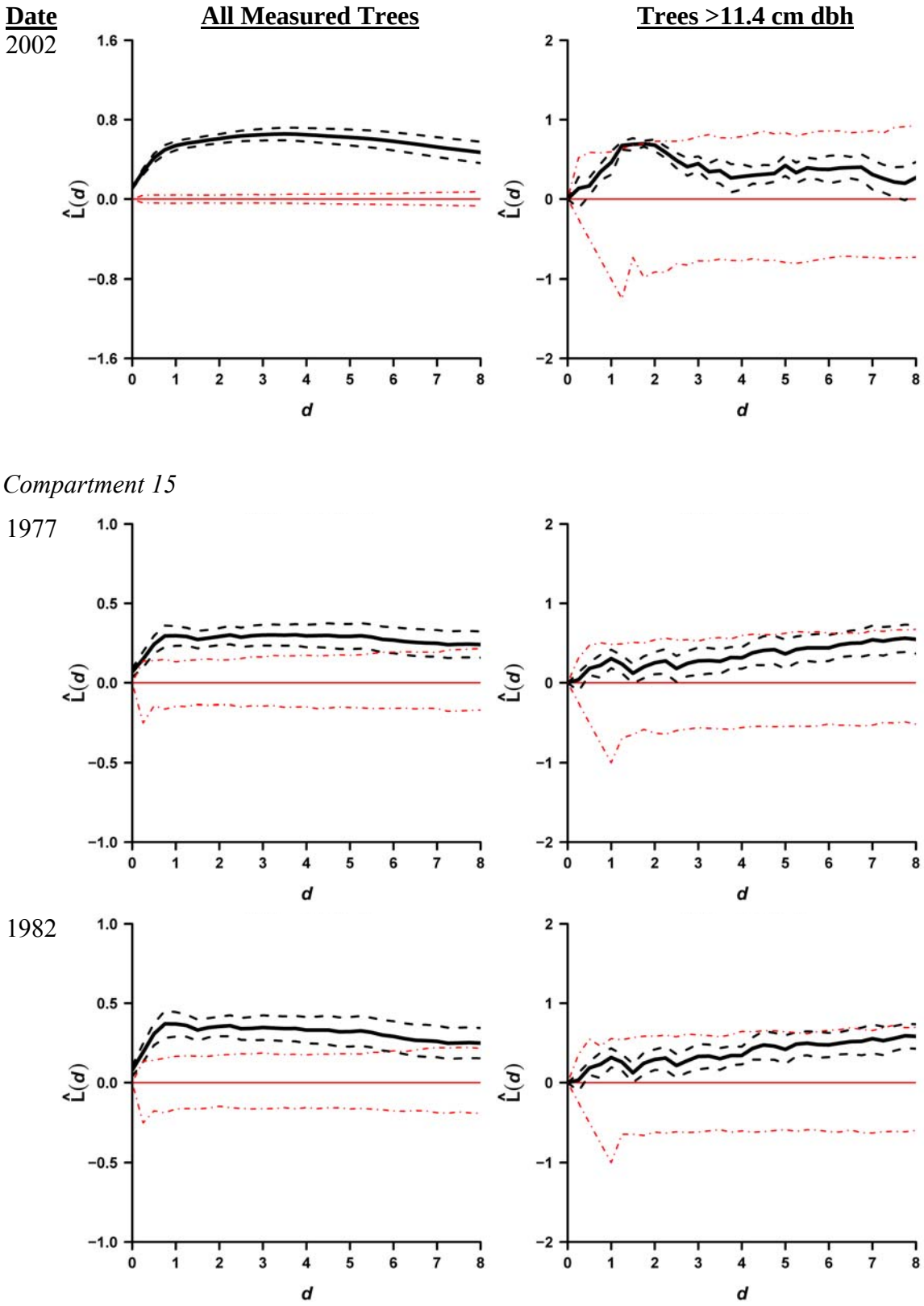

Figure C.1. Continued.

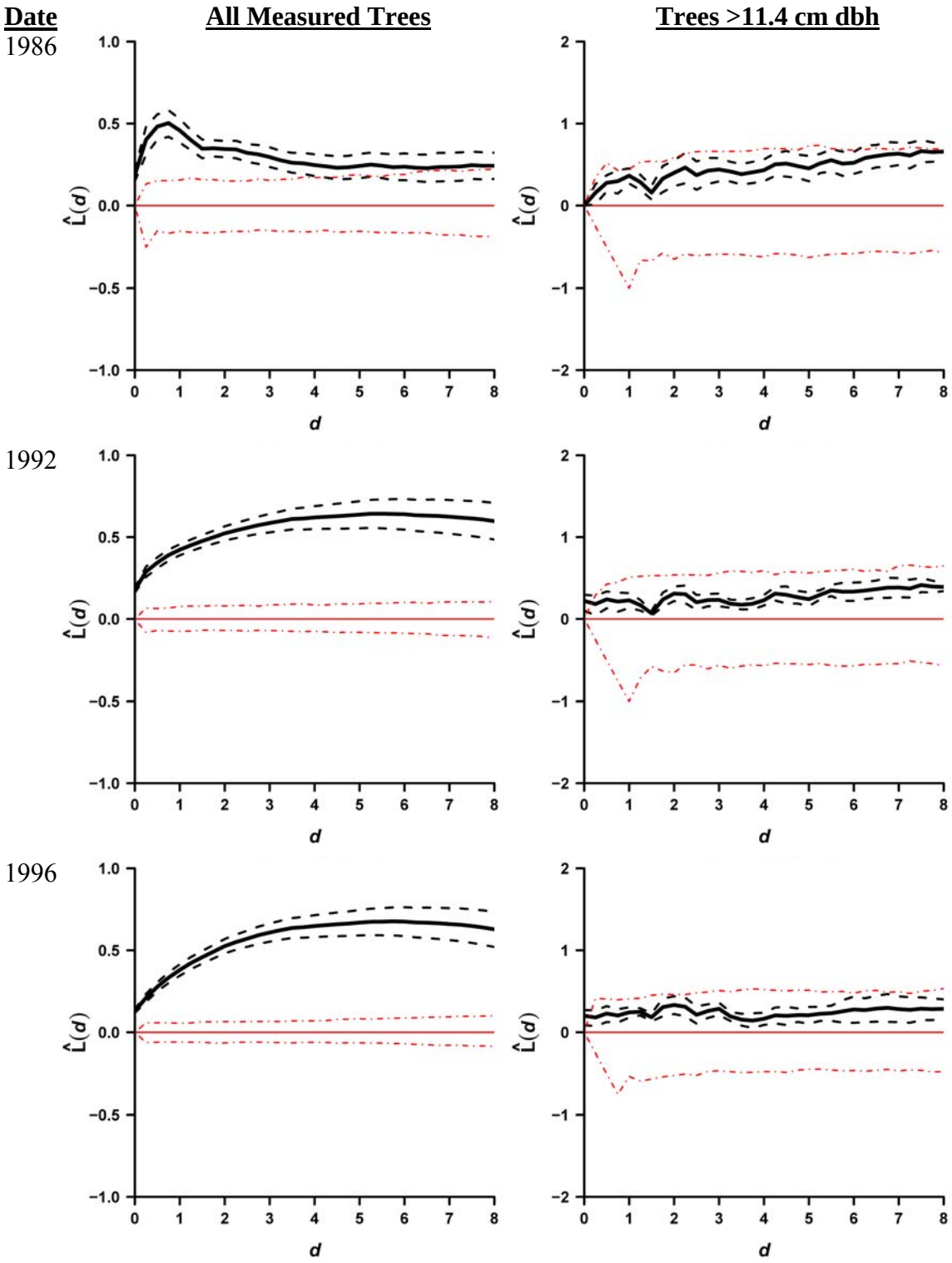

Figure C.1. Continued.

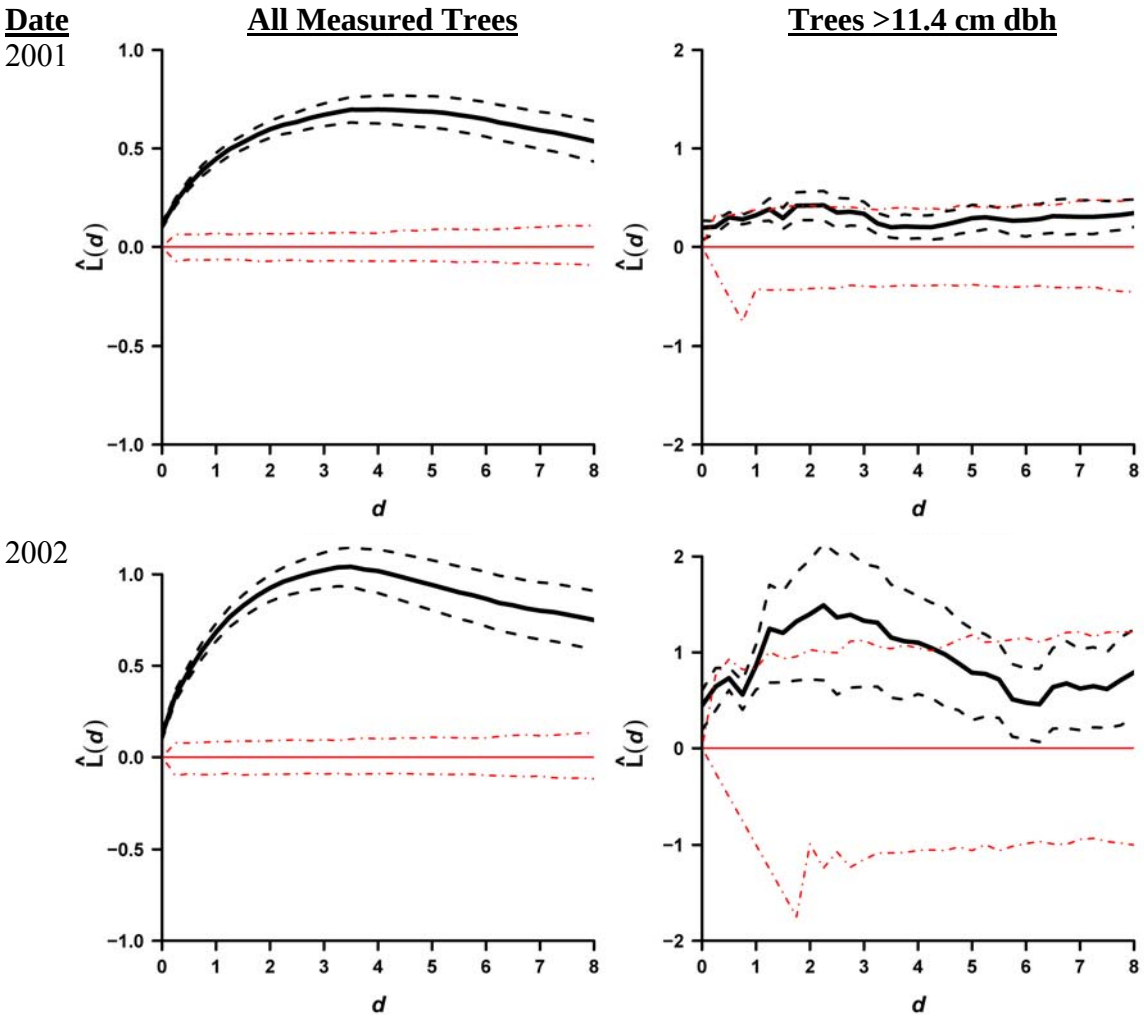

Figure C.1. Continued.

FIVE-YEAR SELECTION SYSTEM (5S)
Compartment 9

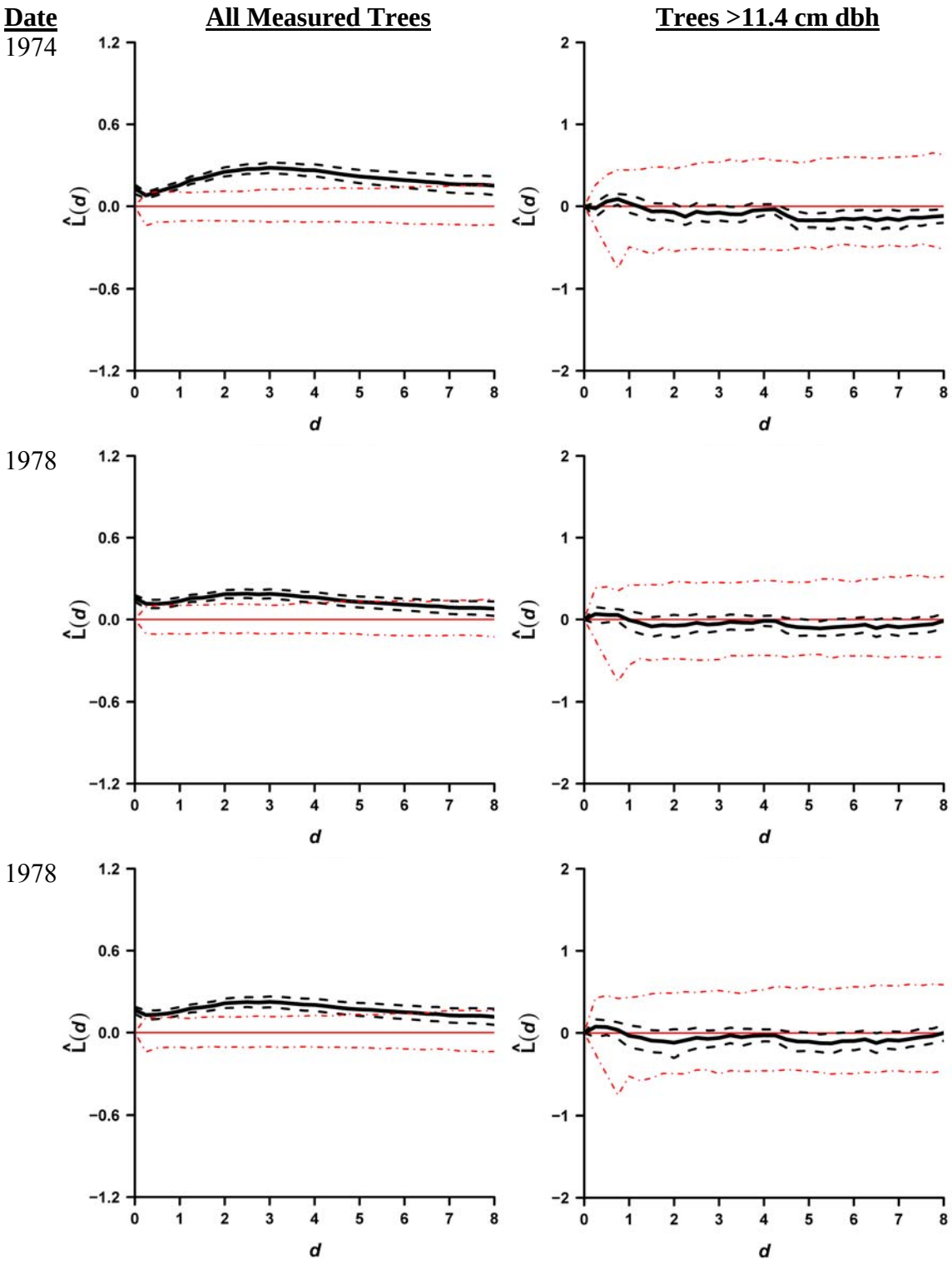

Figure C.1. Continued.

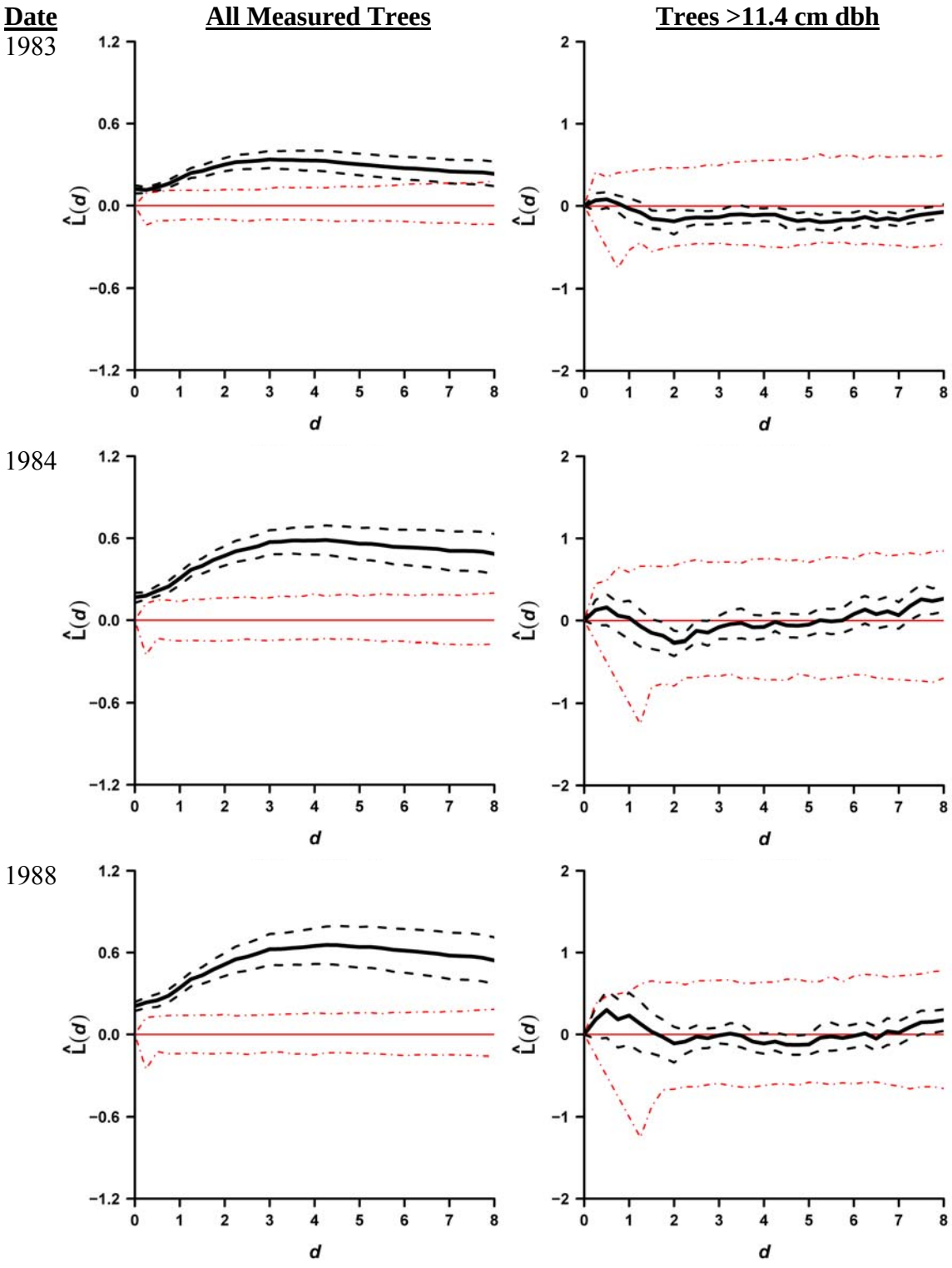

Figure C.1. Continued.

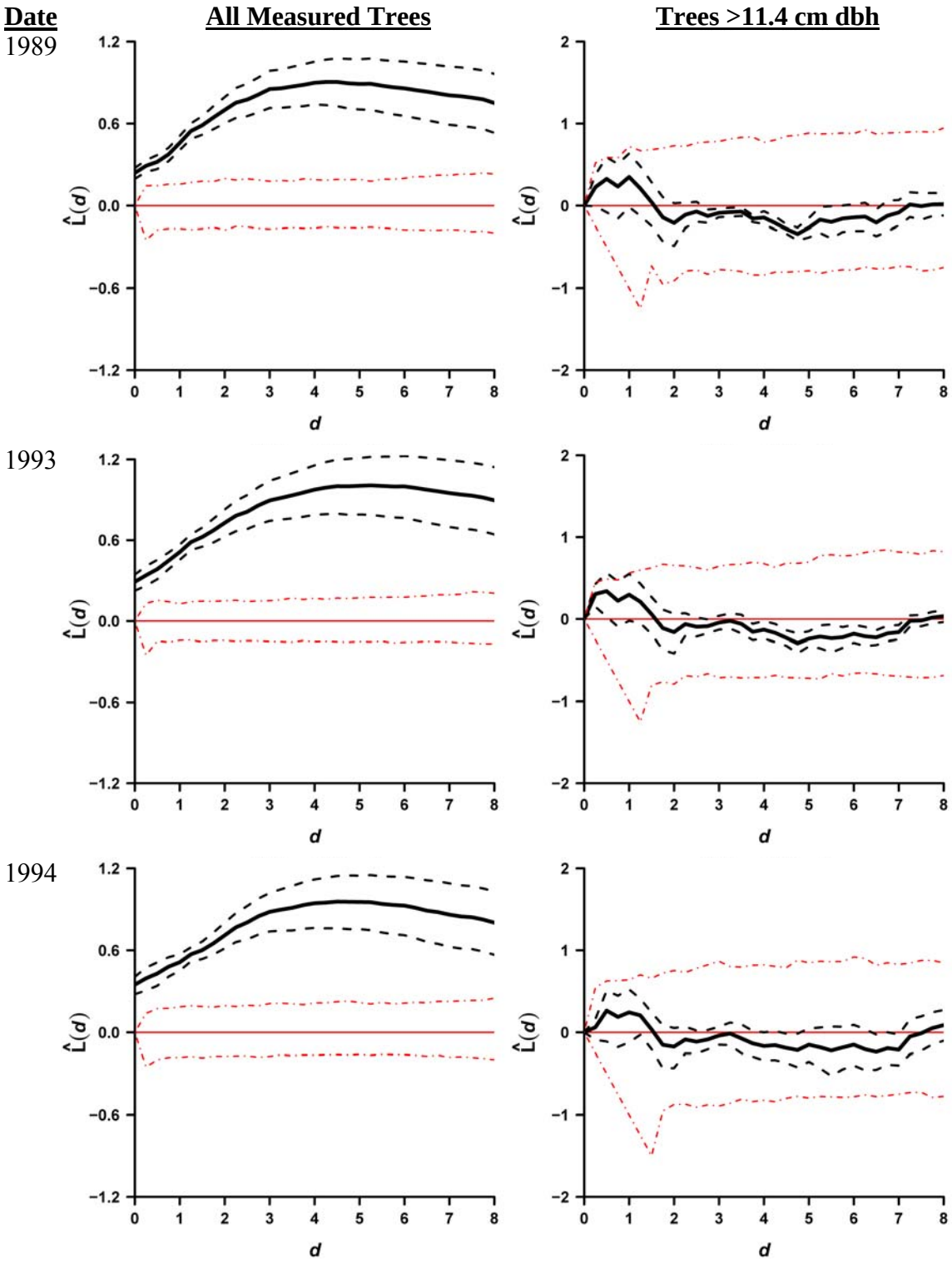

Figure C.1. Continued.

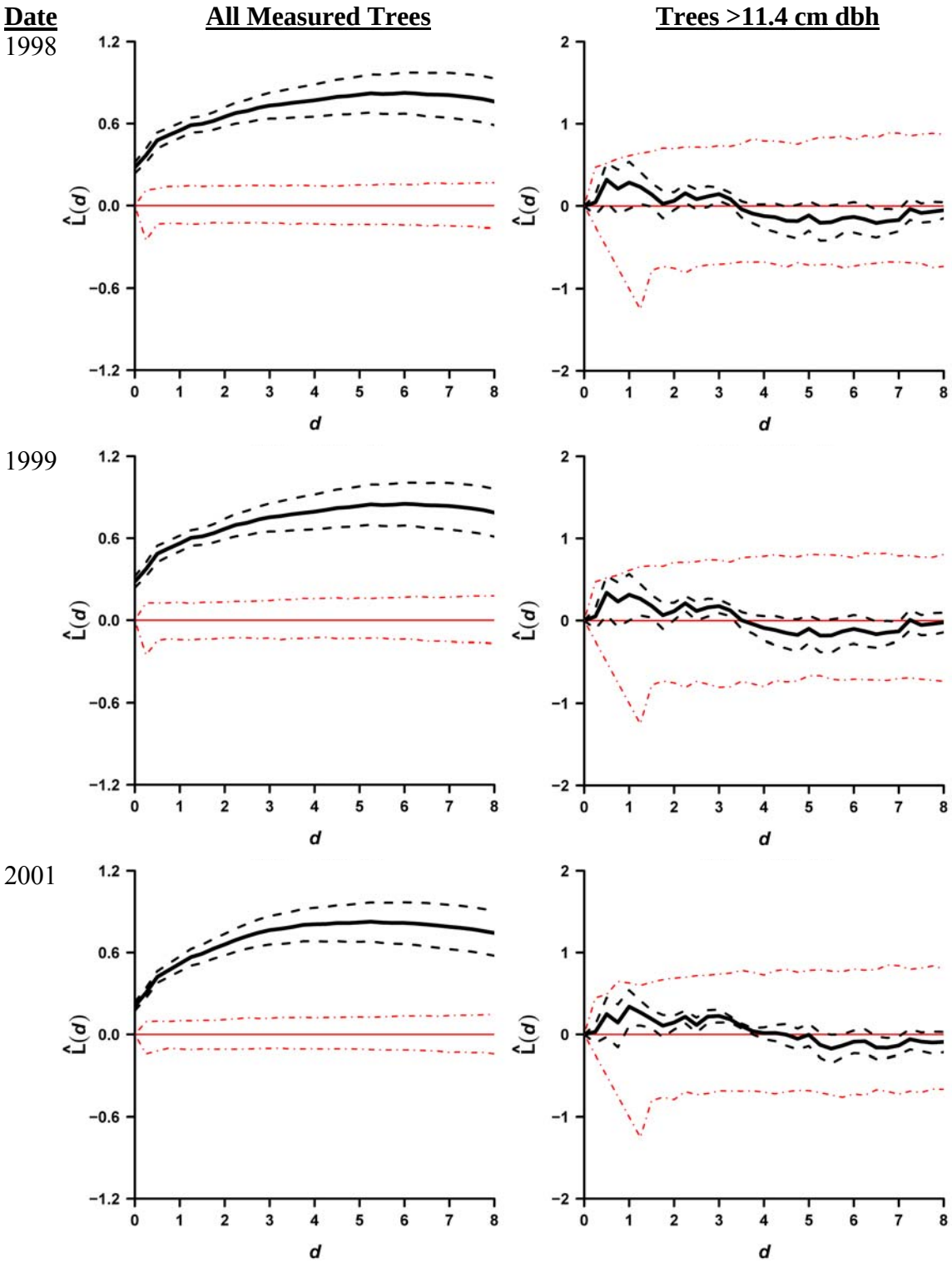

Figure C.1. Continued.

Compartment 16

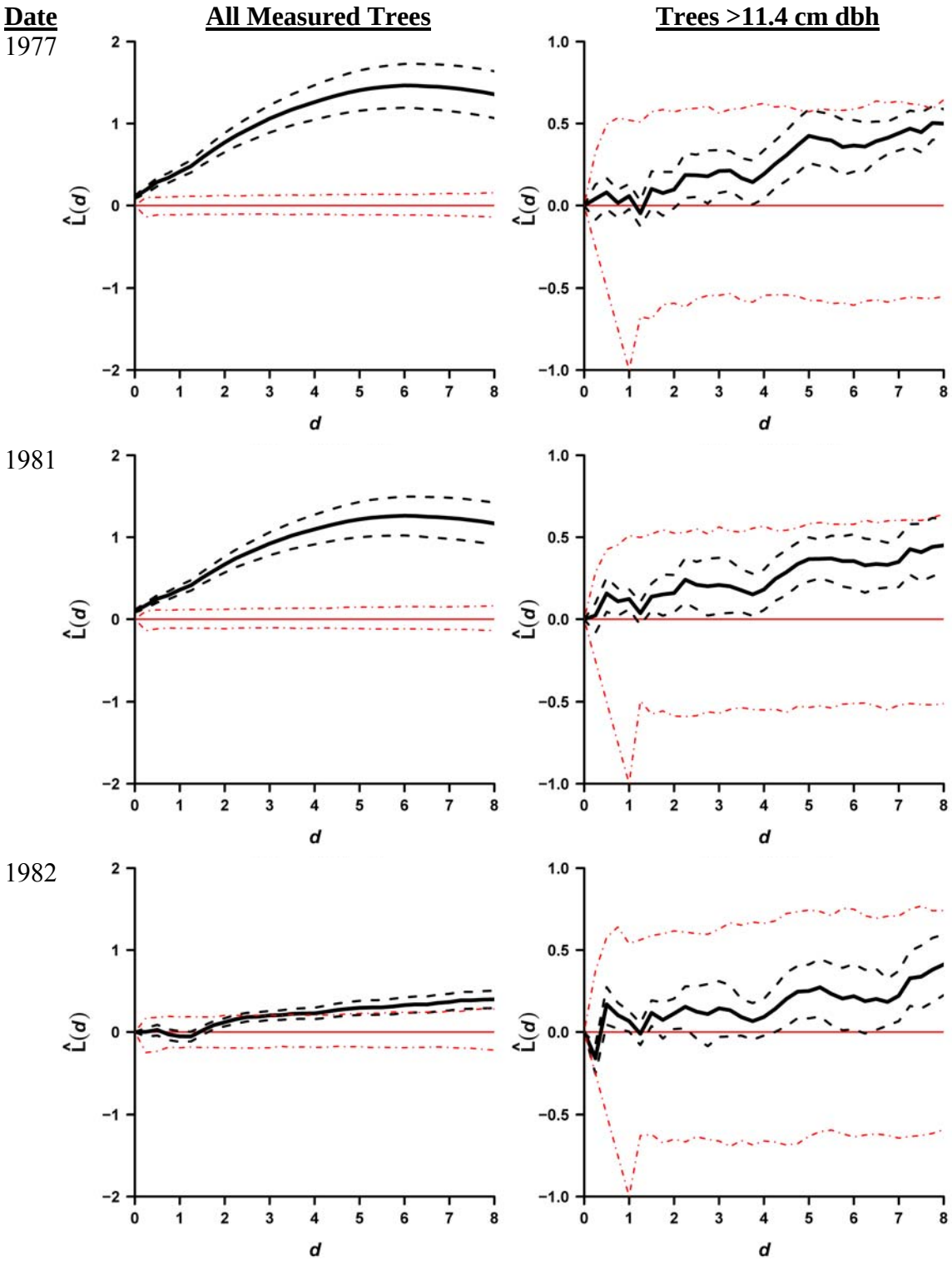

Figure C.1. Continued.

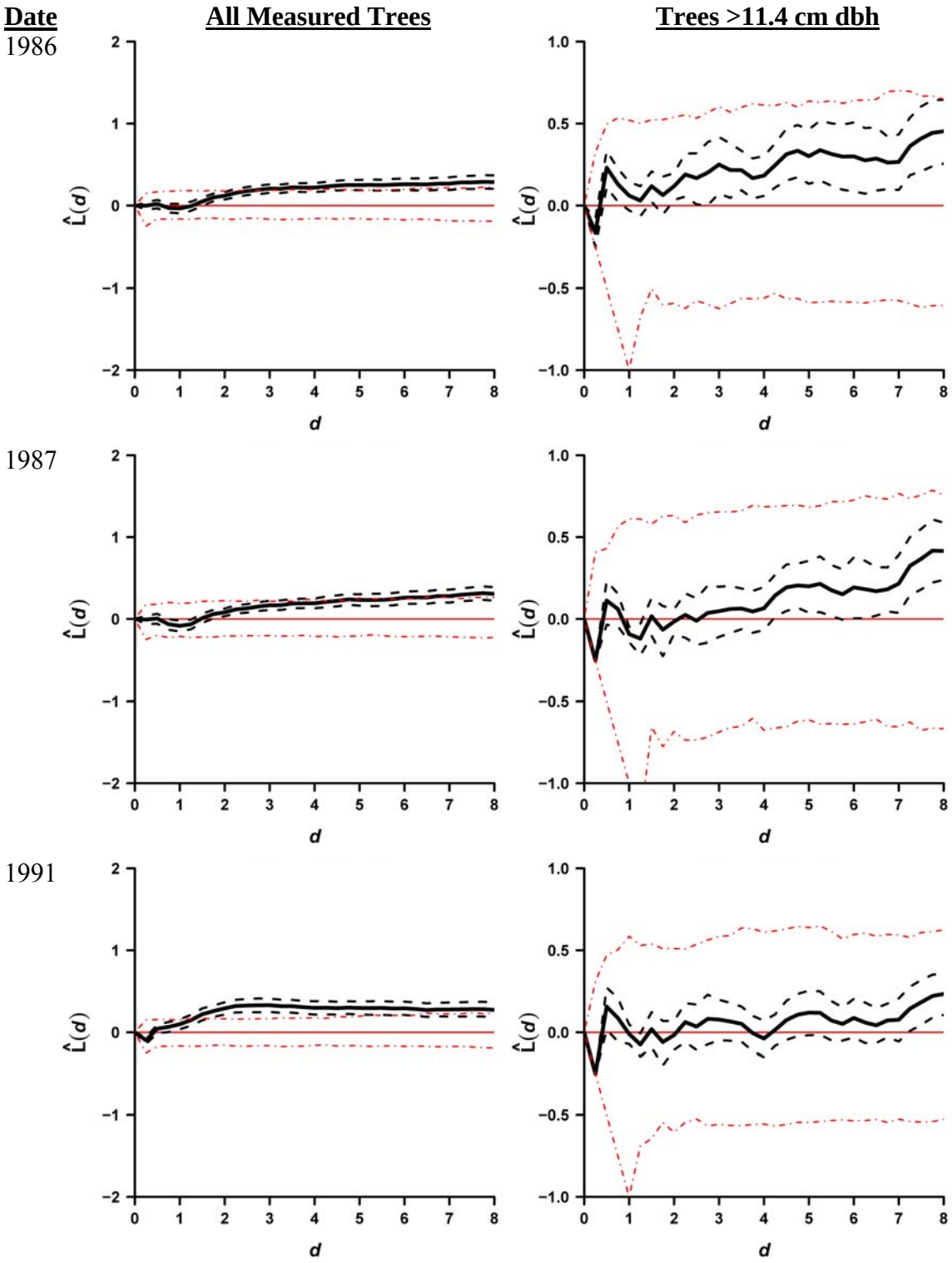

Figure C.1. Continued.

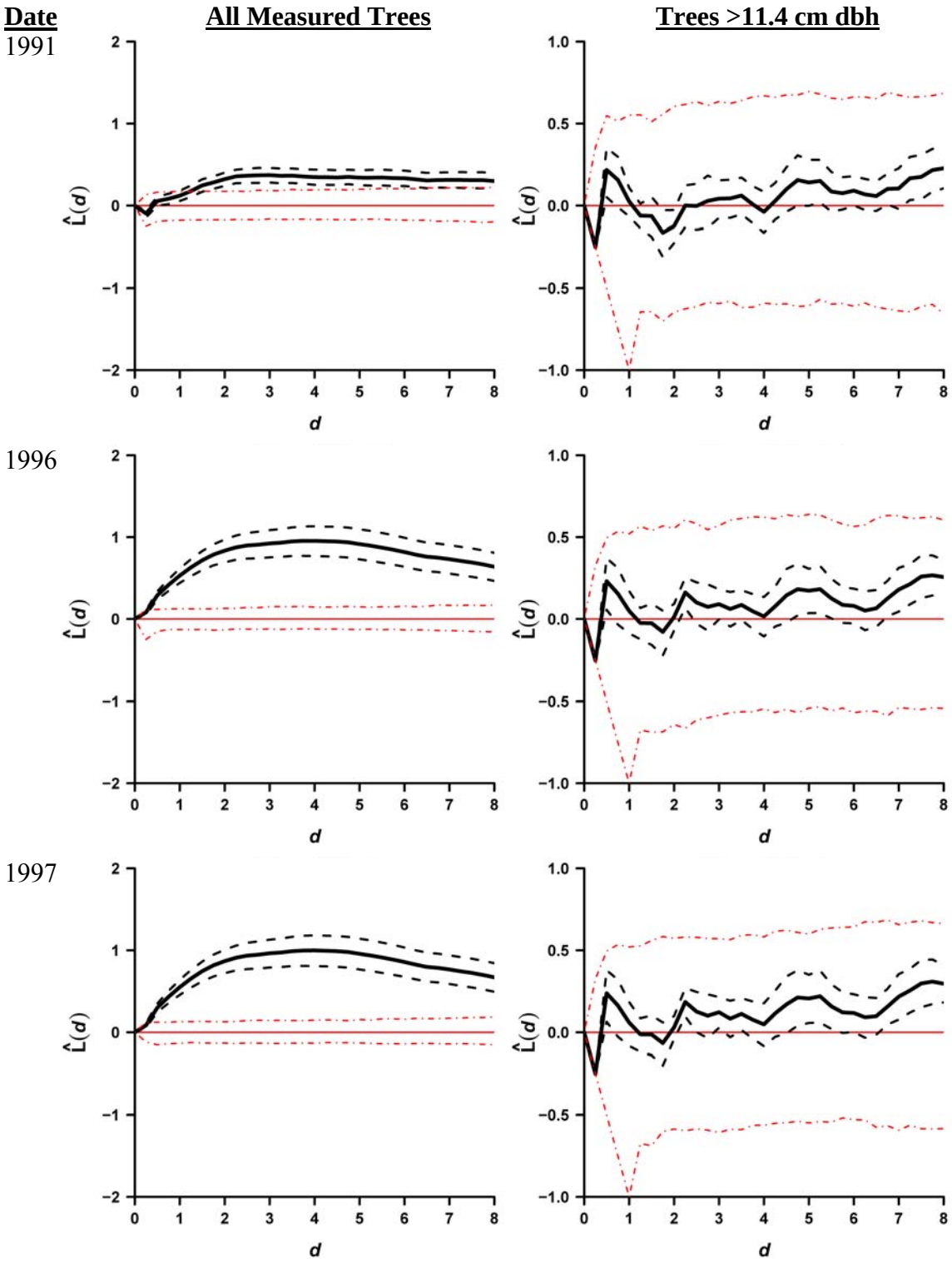

Figure C.1. Continued.

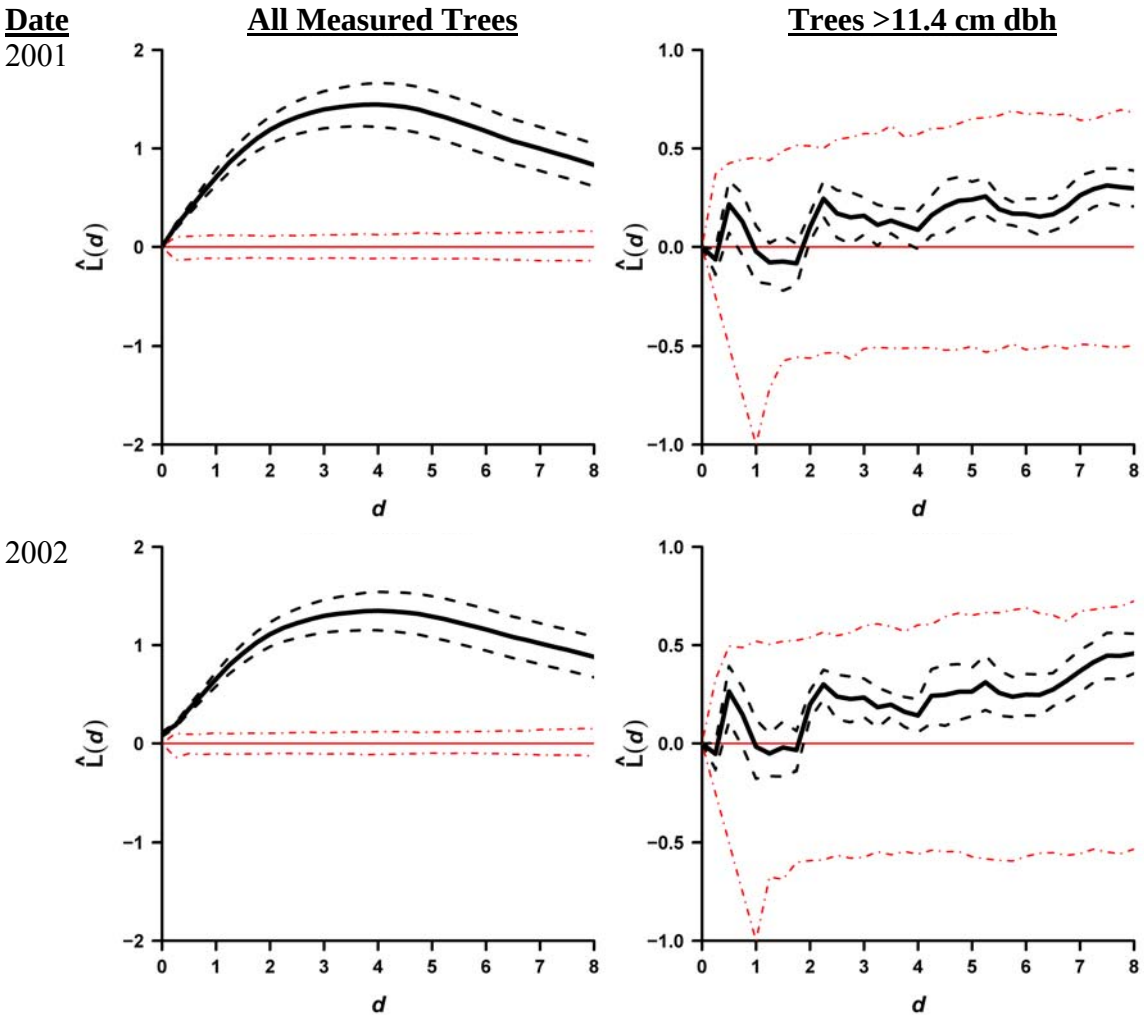

Figure C.1. Continued.

THREE-STAGE SHELTERWOOD (SW)
Compartment 29A (w/PCT)

Date | **All Measured Trees** | **Trees >11.4 cm dbh**

1975

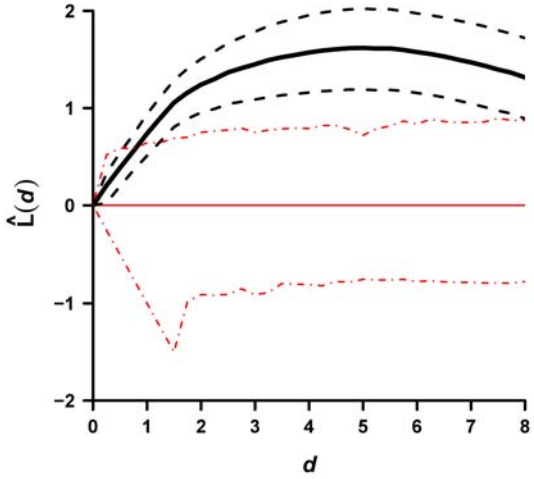

1977

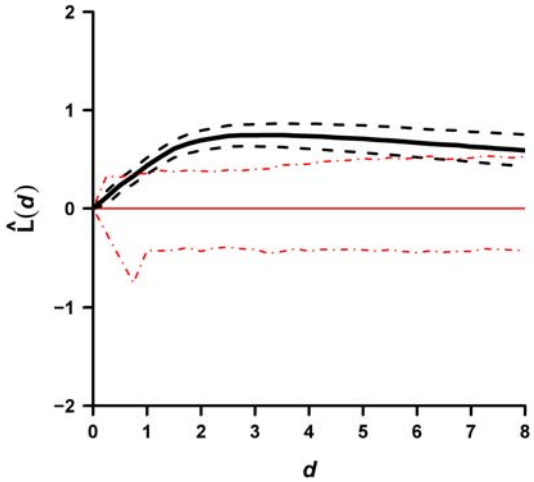

1982

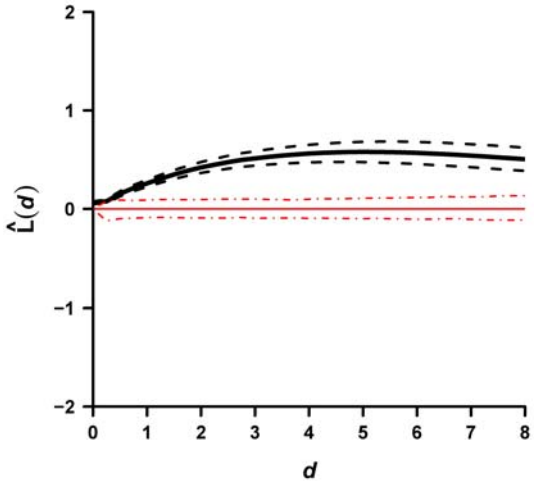

Figure C.1. Continued.

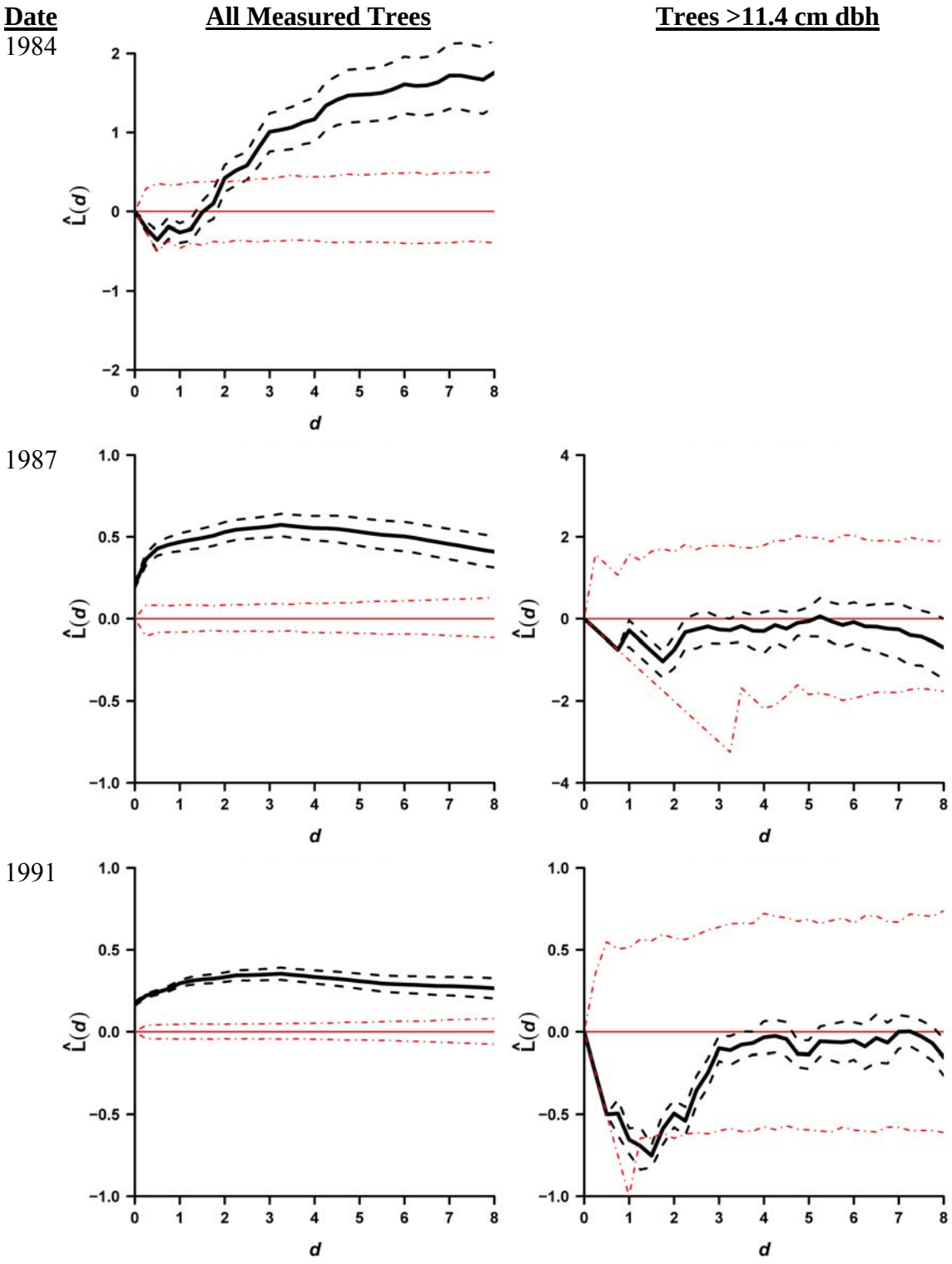

Figure C.1. Continued.

Date **All Measured Trees** **Trees >11.4 cm dbh**

2002

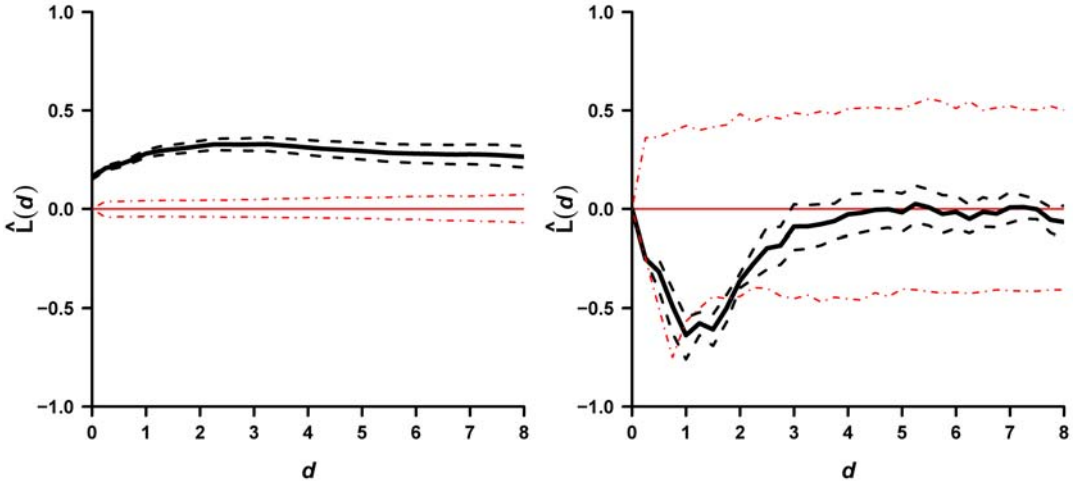

Compartment 29B (w/o PCT)

1975

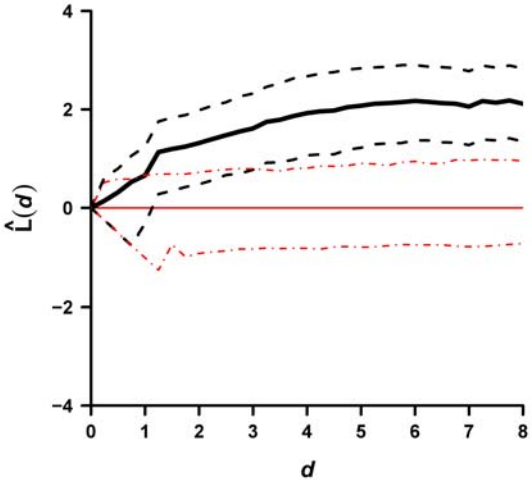

1977

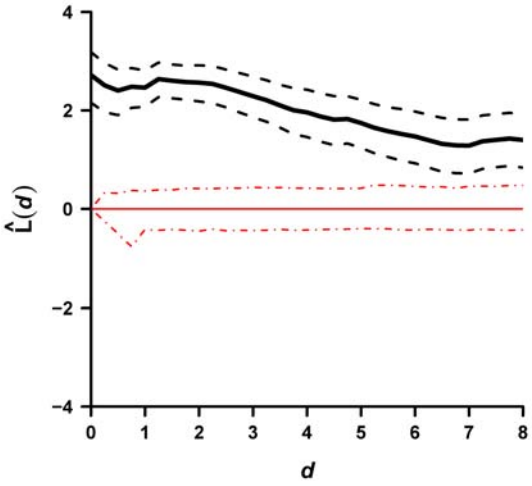

Figure C.1. Continued.

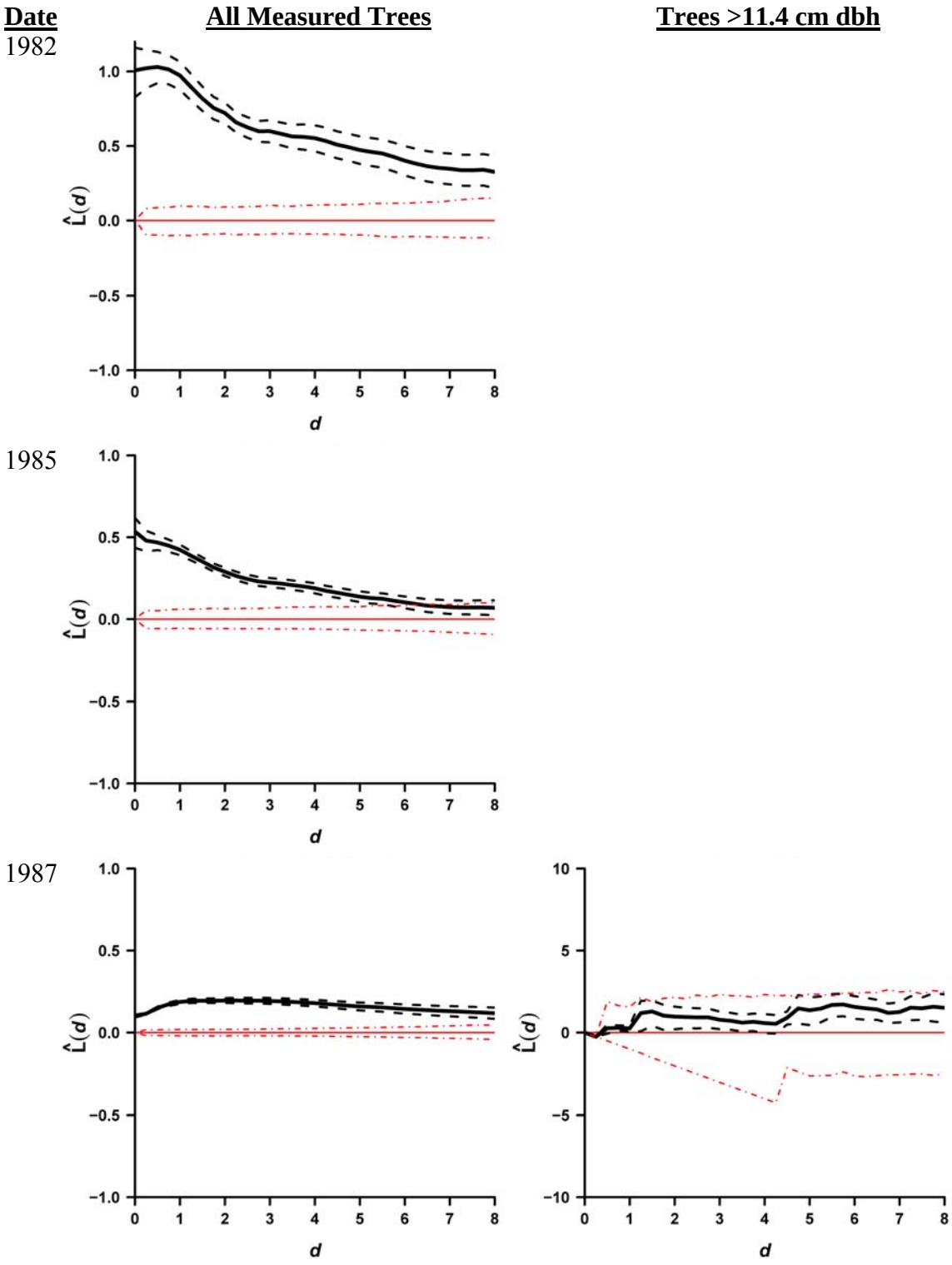

Figure C.1. Continued.

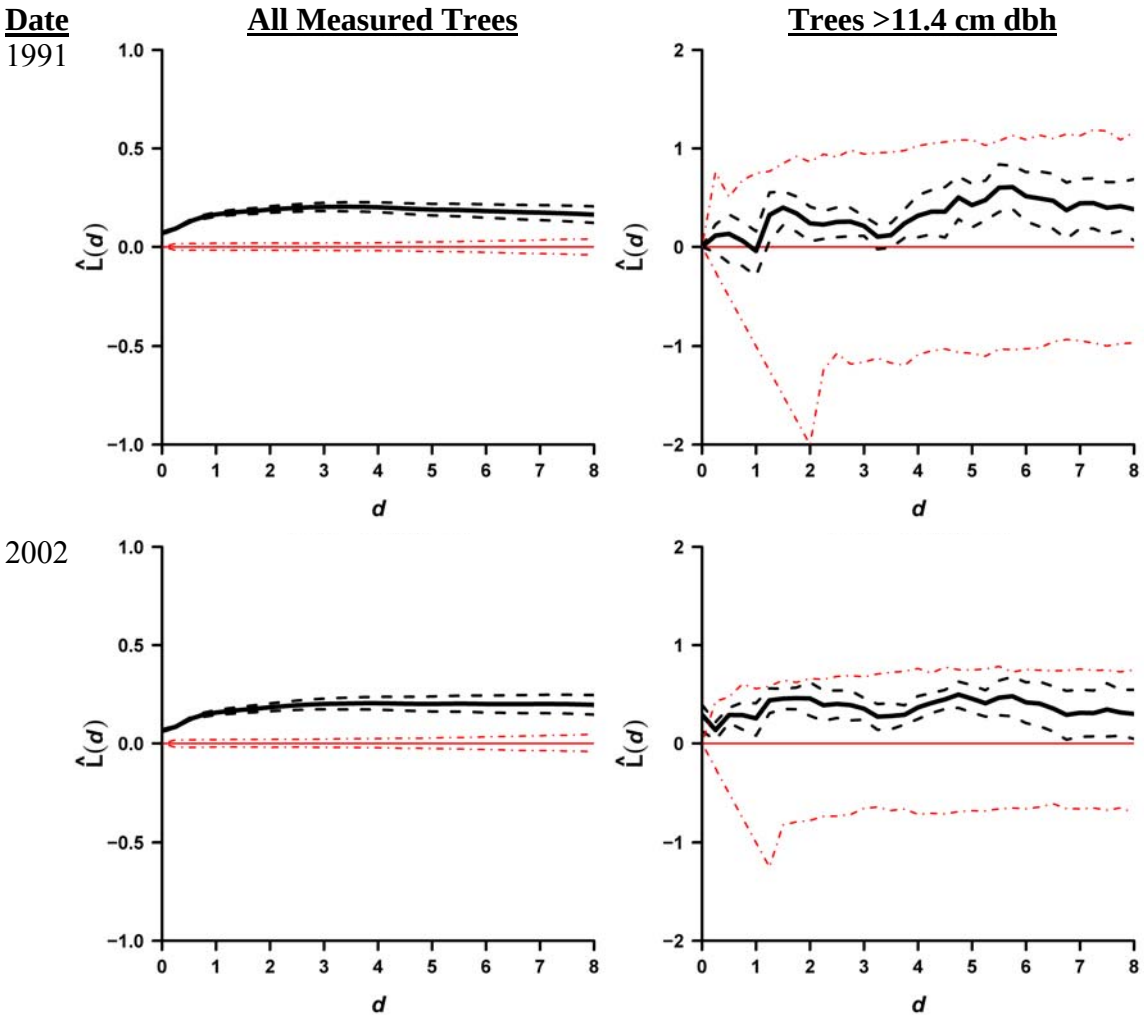

Figure C.1. Concluded.

BIOGRAPHY OF THE AUTHOR

Born in rural northeastern Iowa in 1971 (really flat, corn country), Mike knew early on that the outdoors was his calling. He attended Iowa State University and received two bachelor degrees, one in Forestry and one in Fisheries and Wildlife Biology, in May, 1994. Mike received numerous awards during his studies there, most notably Graduating Scholar as the valedictorian of the College of Agriculture.

In 1995, Mike attended the University of Minnesota to pursue an M.S. in silviculture. There he investigated the relationship between white pine seedling survival/growth and white-tailed deer (i.e., "forest rats") browsing pressure on several sites in northern Minnesota. Mike graduated in June, 1998, and continued to work at University of Minnesota as a Research Fellow until August, 2000.

At that time, Mike enrolled in a Ph.D. program at the University of Maine and was in charge of the day-to-day operations of the Acadian Forest Ecosystem Management Program. Mike also heavily became involved in the installation of the Agenda 2020 project, which looks at the effects of silvicultural intensity and compositional goals on development of cutover stands in Maine. In his spare time, Mike worked on this dissertation and sometimes could be found hiking one of the many trails in Maine with his wife, Dena, and daughter, Zylee.

Mike currently lives in a cramped (i.e., toy-infested) apartment in Hampden, Maine and is employed with the Cooperative Forest Research Unit at the University of Maine. He is a candidate for the Doctor of Philosophy degree in Forest Resources from The University of Maine in May, 2006.